The Use of ^{238}U and ^{232}Th Decay Series Radionuclides in Sediment Tracing

Jonathan Martin Olley

B.Sc. (Hons)

Australian National University

A thesis submitted for the degree of Doctor of Philosophy of the University of New South Wales

May 1994

Abstract

A variety of geochemical tracers, including natural radioactivity, can be used to trace the source of sediment, moving on hillslopes and in rivers. If the source of sediment is to be correctly determined, we need to understand the nature of the material being traced and why the parameter being used to 'fingerprint' the sediment varies. Previous studies using correlations between ^{238}U and ^{232}Th decay series nuclides to trace sediment have been empirically based. This thesis examines the mechanisms which cause variations in the concentrations and ratios of the decay series nuclides in modern sediments, and develops a mechanistic framework for the application of decay series nuclides to tracing sediment.

Fluvial transport produces changes in the material being transported both as a function of sorting (by shape, size and density) and by grain abrasion. Radionuclide concentrations and ratios have been examined in rocks, and soils from nine sites, the effects of grain abrasion and of sorting soil material by both density and particle-size have been investigated. It is shown that the different particle-size and density fractions from soil developed from a uniform lithology have a constant $^{230}Th/^{232}Th$ ratio, the same ratio as that in the rock from which the soil was formed. The $^{230}Th/^{232}Th$ ratio can therefore be used to distinguish between sediments derived from different lithologies within a catchment, providing that the lithologies have distinctive $^{230}Th/^{232}Th$ ratios. The application of $^{230}Th/^{232}Th$ ratio to the spatial sourcing of sediment is demonstrated in the McKeowns Valley catchment, New South Wales.

In contrast to the uniformity of the $^{230}Th/^{232}Th$ ratio in soils developed from a uniform rock type, the $^{226}Ra/^{232}Th$ ratio was found to be variable and in many cases significantly different to the U/Th ratio in the rock. This variability was due largely to the presence of a ^{226}Ra excess over ^{230}Th. The effects of processes such as grain abrasion and sorting by particle size and density on the $^{226}Ra/^{232}Th$ ratio were shown to be dependent on two factors (i) the degree to which the ^{226}Ra concentration was in excess of ^{230}Th and (ii) where, in relation to the thorium, the ^{226}Ra excess was bound on the particles. Where the ^{226}Ra and ^{232}Th were bound on similar sites on the soil grains and the ^{226}Ra excess over ^{230}Th varied throughout a catchment, it was found that the $^{226}Ra/^{232}Th$ could be used to distinguish sediments derived from different points in the catchment even if it had a uniform lithology, and hence a uniform $^{230}Th/^{232}Th$ ratio. The application of the $^{226}Ra/^{232}Th$ ratio to spatial sourcing problems in a catchment with a uniform lithology is demonstrated at the Geebung Creek catchment, New South Wales.

In circumstances where the ^{226}Ra excess on the soil grains was not held in similar sites to the ^{232}Th, then grain abrasion and sorting (by particle-size and density) were found to produce fractions which had variable $^{226}Ra/^{232}Th$ ratios. This suggests that fluvial transport of soil material in which concentrations of ^{226}Ra are in excess of ^{230}Th concentrations and the radium and thorium are held in different sites will result in sediments which have a variable $^{226}Ra/^{232}Th$ ratio which cannot easily be related back to that of the source. Consequently, under circumstances in which these processes are important, the $^{226}Ra/^{232}Th$ ratio is not likely to provide a stable 'fingerprint' unless the ^{226}Ra excess is small.

Concentrations of ^{228}Ra (half-life 5.75 years) in excess of ^{232}Th concentration were observed in both soils and sediments. It is suggested that this excess is developed on the hillslope and begins to decay back to equilibrium once the sediment is finally removed from contact with the groundwater. When combined with indicators of sediment source, such as $^{226}Ra/^{232}Th$ and $^{230}Th/^{232}Th$ ratios, observation of this excess should provide a useful new tool for examining the transport rates and residence times of bedload and suspended load sediments in streams and lakes on time scale of up to 30 years. An example of the application of the

^{228}Ra excess to determining sediment residence times is given for the Murrumbidgee arm of Lake Burrinjuck, New South Wales.

In addition to developing a framework for the application of decay series nuclides to tracing sediment, observations are reported which indicate that significant mobilisation of the decay series nuclides, including the thorium isotopes, occurs during pedogenesis. Differential mobilisation of the nuclides, particularly radium and thorium results in disequilibrium in the soils. However, the similarity of the parent rock and soil ^{230}Th/^{232}Th ratios indicates that no differential mobilisation of the thorium isotopes occurs. This implies that either uranium and thorium are behaving similarly during pedogenesis or that any disequilibrium between ^{230}Th and ^{238}U concentrations in the soils is young (<<80,000 years).

The results presented in this thesis provide an understanding of the mechanisms which cause variability in ^{238}U and ^{232}Th decay series nuclides in modern sediments and demonstrate the applicability of nuclide ratios to providing information on the spatial distribution of sediment sources, sediment transport rates and residence times. Radionuclide tracing techniques offer a significant addition to the methods available for investigating sediment movement in the landscape. Such methods can provide a better understanding of the source of sediment, and facilitate more informed decisions concerning catchment management and the allocation of soil conservation resources.

I certify that the substance of this thesis has not already been submitted for any degree and is not being currently submitted for any other degree.
I certify that any help received in preparing this thesis, and all sources used, have been acknowledged.

Jonathan M. Olley

Table of Contents

Part III Three Examples of the Application of ^{238}U and ^{232}Th Decay Series Nuclides to Sediment Tracing Problems

Chapter 9 : Identifying Sediment Sources in a Catchment with a Uniform Lithology

Chapter 10 : Sourcing Sediment in the McKeowns Valley Area NSW using $^{230}Th/^{232}Th$ ratios

Chapter 11 : Sediment Residence Times in the Murrumbidgee Arm of Burrinjuck Reservoir

Chapter 12 : Concluding remarks

Tables

Figures

Acknowledgments

I acknowledge the support given by CSIRO Division of Water Resources in terms of time and facilities. In particular, I would like to thank Mr N. Body and Dr. R.J. Wasson who look on most of my requests for both time and facilities favourably.

I would like to thank my supervisors Dr. Andrew Murray (CSIRO) and Dr Mike Melville (UNSW). Mike made sure that I jumped through all the right hoops for the university. Andrew provided feed back, comments, criticism (most of it constructive) and played devils advocate throughout the four years taken to complete this study. Many thanks to you both.

Of my colleagues at CSIRO I would like to thank : Gary Hancock for introducing me to the dark secrets of alpha spectrometry; Peter Wallbrink for help with the gamma spectrometry, some of the fieldwork, and for providing good company and many lively discussions over lunch; Jacquie Olley for providing some of the XRF and gamma analyses; Rob Sageman for much of the wet chemical work; Catriona Turley for technical support and company throughout the four years; Katrina Daniels for help with some of the alpha spectrometry and wet chemistry; Graham Chiles for some of the sieving; Daphne Mahon for preparing some of the maps; Dave MacKenzie for collecting the Whiteheads Creek samples; Gary Caitcheon for access to the Snowy River samples; and Craig Smith for helping with some of the gamma spectrometry samples.

I would also like to thank Mark and Tracey Weber for their support, use of their spare room, reading of the first draft and help with the typing.

Thanks to Mr. L. Olive of the University of New South Wales and Dr. R. Roberts of the Australian National University for providing comments on the first draft, and Jacquie and Geoff Olley for proof reading the final draft.

And lastly my wife Vanessa who typed most of this manuscript, edited, and generally kept me sane. Thank you.

This thesis is dedicated to my loving wife

Vanessa

and to our two sons

Christopher and Andrew

who

will not believe that it is

finished.

Boys, Dad's home!!

Chapter 1: Introduction

Land degradation is a critical environmental issue with significant implications for agriculture, pastoral and forest production, water quality and water storage. In Australia, the Murray-Darling Ministerial Council estimated the reduction in annual production due to land degradation for the Murray-Darling basin alone to be more than A$200 million for the 1987 year. This basin accounts for about half the nation's rural production, which is worth about A$15000 million annually (1985-86) [*Hawtrey*, 1987]. If the effects of land degradation are not reversed, production from our rural lands will continue to decline and costs will increase. Any measures which successfully reduce sediment movement are likely to have large long term financial benefits. Decisions on targeting soil conservation works are from necessity, often made on subjective grounds. A recent survey by New South Wales Soil Conservation Service found that 70% of the field officers made targeting decisions based solely on visual observations, and educated guesses (*K. Edwards,* pers. com. 1990). Obviously there is a need for a more objective methods of assessing conservation targets.

Tracing sediments and associated pollutants to their source offers a direct method of targeting soil conservation and reparation works. Sediment characteristics such as clay mineralogy, sediment colour, mineral magnetic properties, lithogenic radionuclide ratios and major element chemistry have all been used to successfully identify sediment source areas [*Woods*, 1978; *Grimshaw and Lewin*, 1980; *Walling and Cane*, 1984; *Caitcheon*, 1993; *Murray et al.*, 1993; *Olley et al.*, 1993]. However, no one tracer has proved to be universally applicable. If any confidence is to be placed in the results of a sediment sourcing study then we need to understand how variations in the 'signal' used to trace the sediment arise.

Studies using correlations between lithogenic radionuclides to characterise sediment sources have to date been based purely on empirical observations [*Meijer et al.*, 1987,1988; *Murray et al.*, 1991; *Murray et al.*, 1993; *Olley et al.*, 1993]. No explicit investigations into the mechanism controlling the variability and the constancy of ratios have been undertaken. A better understanding of the behaviour and distribution of the lithogenic radionuclide and the mechanisms by which these correlations develop is required. This thesis aims to provide an understanding of the mechanisms controlling the distribution of ^{238}U and ^{232}Th decay series

radionuclides (particularly ^{226}Ra and ^{232}Th) in soils and sediments. The study develops a model of the distribution and behaviour of lithogenic radionuclides in the erosion cycle based on observations carried out at a variety of catchment scales ranging from square metres to hundreds of square kilometres. This model is then used in three site studies to illustrate its application to the spatial sourcing of sediment.

1.1 Tracing Sediment Using ^{238}U and ^{232}Th Decay Series Radionuclides

The spatial sourcing of sediment involves the measurement of some parameter which provides a 'fingerprint' by which sediment from one source may be distinguished from sediment derived from another source. Correlations between nuclides from the ^{238}U and ^{232}Th decay series (Fig. 1a and 1b) have been found to provide distinctive 'fingerprints' for different source areas. For example *Meijer et al.*, [1987, 1988] determined the origins of Dutch coastal sands using the $^{238}U/^{232}Th$ ratio of the heavy mineral fraction in beach and dune deposits. Sands with a heavy mineral component U/Th activity ratio >1 were considered to have come from central Europe, those with a ratio of <1 were consistent with Scandinavian sands. Similarly, *Kamel and Johnson* [1963] used the radioactivity of the heavy mineral component of coastal sands to examine sand drift along the Californian coast.

Carpenter et al., [1984] interpreted the constant $^{230}Th/^{232}Th$ ratio in Puget Sound sediments as suggesting no change in the types of detritus being deposited within the Sound. The similarity of $^{230}Th/^{232}Th$ ratios in feruginous concretions and calcrete from Gilberts River were used by *Short et al.*, [1989] to indicate a common detrital component in these two distinct chemically precipitated phases. A constant $^{230}Th/^{232}Th$ ratio in the detrital component is often assumed in the uranium series dating of carbonates [see various authors in *Ivanovich and Harmon,* 1992]. While observations of uniform $^{230}Th/^{232}Th$ ratios have been widely used to infer a common or constant source of sedimentary material, application of variations in the ratio to spatial sourcing of material has only been done in exploration for uranium deposits [see *Levinson et al.*, 1982 for examples].

Murray et al., [1990, 1991] measured concentrations of ^{226}Ra and ^{232}Th in bulk sediment samples from a wide variety of terrestrial environments and demonstrated that in sediments derived from a single source area these radionuclides were linearly correlated and could be used to distinguish sediments derived from different source areas in which each source had a unique ^{226}Ra to ^{232}Th correlation (this is discussed further in section 2.1). They

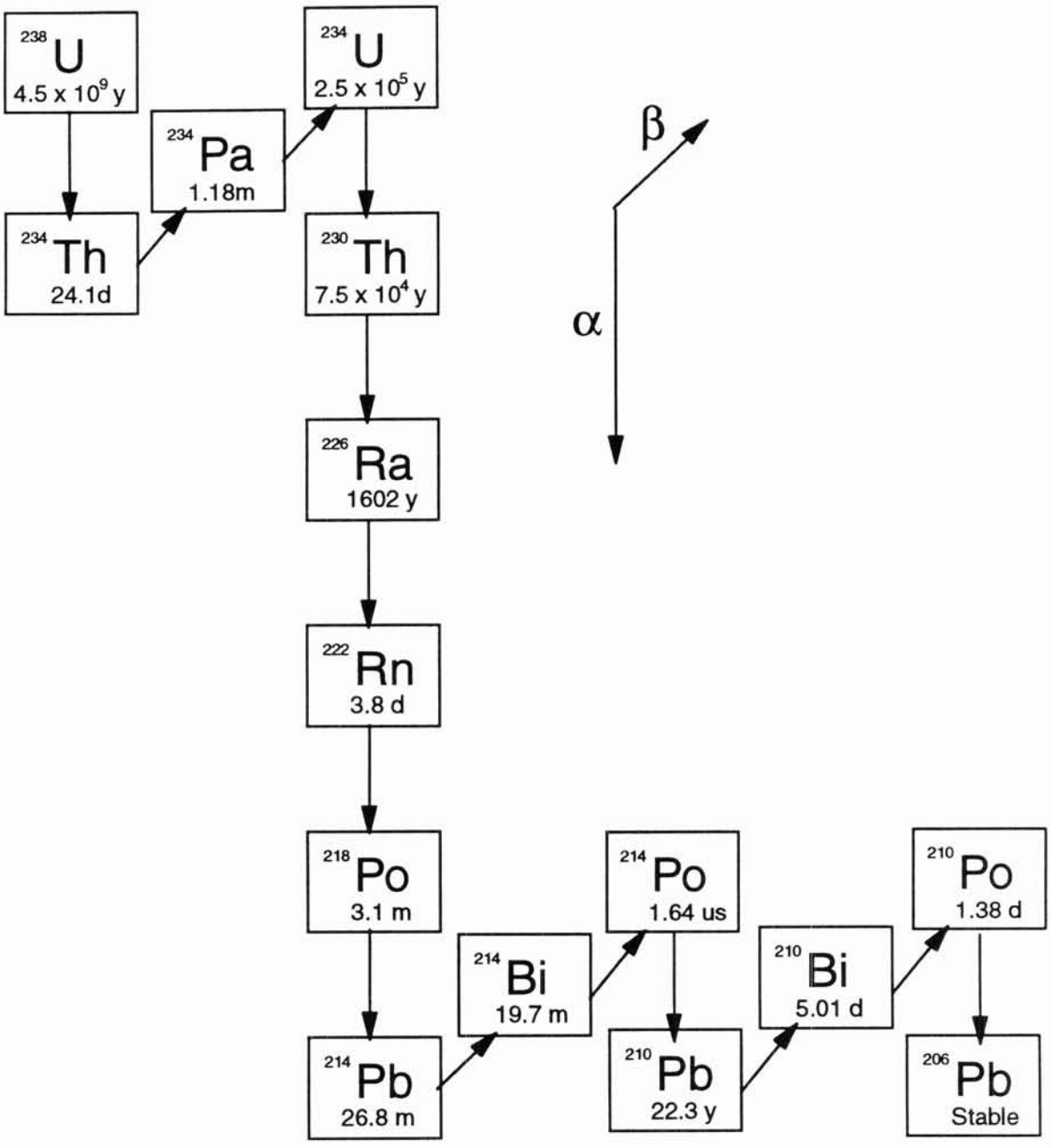

Figure 1.1 a: The ^{238}U decay series (after *Ivanovich and Harmon,* 1992)

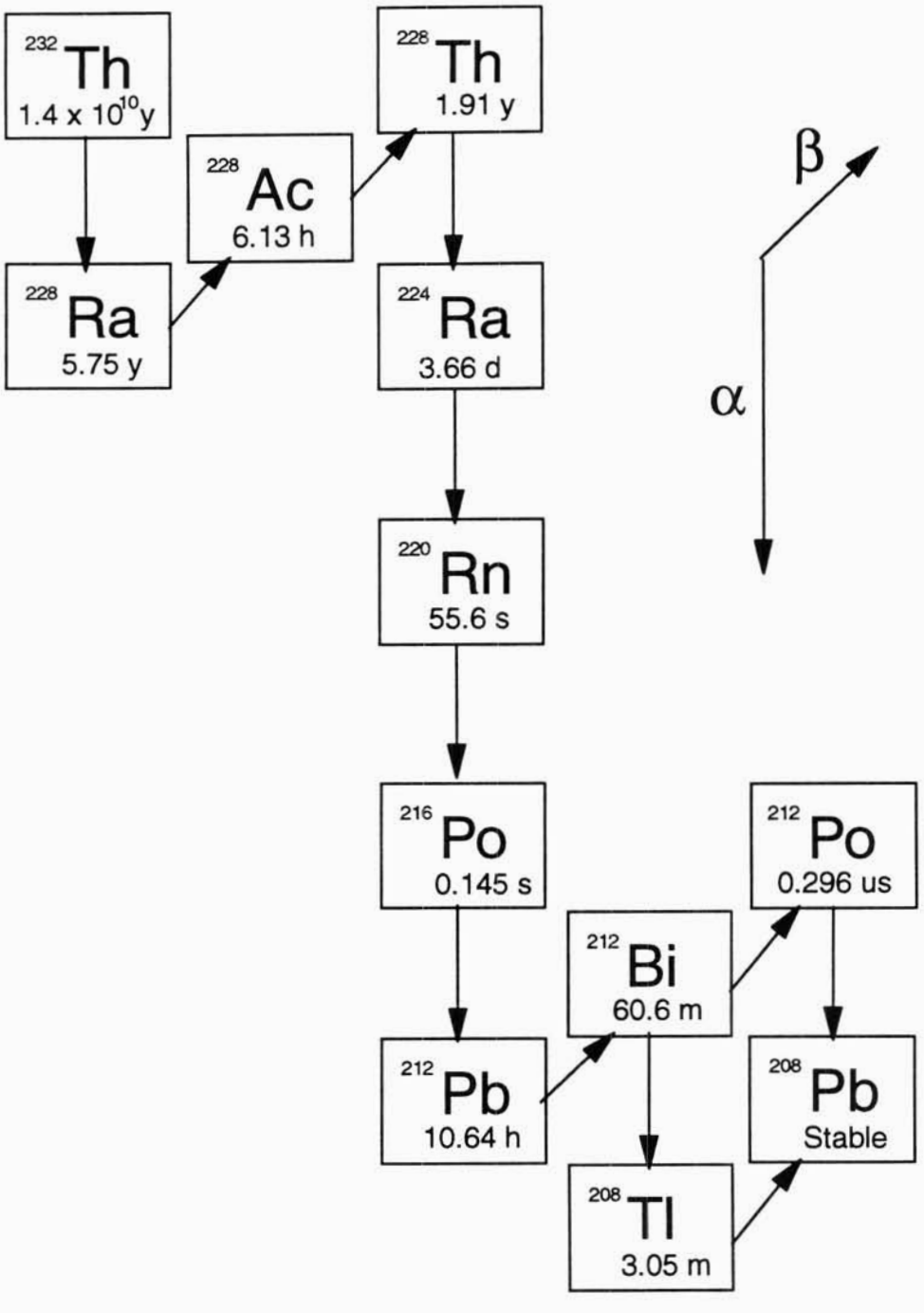

Figure 1.1 b: The ^{232}Th decay series (after *Ivanovich and Harmon,* 1992)

showed that the ^{226}Ra to ^{232}Th tracer signal was stable during both transport and storage following deposition. There are two published examples of the application of these correlations to the sourcing of sediment: *Olley et al.*, [1993] study of a gullied catchment at the head waters of Whiteheads Creek, NSW; and *Murray et al.*, [1993] sourcing of sediment in the Jenolan caves, NSW. These are the only reported applications of bulk sample radionuclide measurements to spatial sourcing of material. These studies were empirically based and the mechanisms which give rise to the correlations and to the heterogeneity across the landscape are at this stage poorly understood.

1.2 Thesis Aims and Outline

This study aims to provide an understanding of the behaviour and causes of variability in ^{238}U and ^{232}Th decay series nuclides concentrations and ratios in modern sediments.

The thesis is divided into three parts. Part I provides a review of the known environmental behaviour and distribution of ^{238}U and ^{232}Th decay series radionuclides relevant to their application in the spatial sourcing of sediment, and outlines in more detail the use of ^{226}Ra to ^{232}Th correlations in sediment sourcing. At the end of Part I the hypotheses to be examined in this thesis are proposed; and the methodology and analytical methods used to address these hypotheses are described.

Radionuclide data from rock, soil and sediment samples from a wide variety of sites are presented and discussed in Part II. The effects of weathering, soil formation, fluvial transport on the radionuclide distributions are examined, and a mechanistic framework for the environmental behaviour of lithogenic radionuclides is developed.

In Part III the understanding of the environmental behaviour of ^{238}U and ^{232}Th series nuclides gained from the work presented in Parts I and II is used to provide information on the spatial source of sediment in three catchments ranging in scale from 76 ha to 8000 km^2.

Part I

Background, Methodology and Analytical Methods

Chapter 2: Environmental Behaviour and Distribution of Lithogenic Radionuclides

To place the work described in this thesis in context, the sediment tracing technique based on radionuclide correlations [*Murray et al.,* 1991; *Olley et al.,* 1993; *Murray et al.,* 1993] is described first. Secondly, the phenomena of radioactive decay, secular equilibrium and the chemistry of uranium, thorium and radium are summarised. Thirdly, the reported natural distributions and behaviour of uranium, thorium and radium relevant to the development of the correlations used in the sediment tracing technique are discussed.

2.1 The Sediment Tracing Technique

This section introduces nuclide ratios, nuclide correlations, and outlines the sediment tracing technique. Examples of lithogenic radionuclide correlations are presented from a number of sites to enable an understanding of the empirically observed behaviour of the lithogenic radionuclides in modern sediments in Australia.

2.1.1 Nuclide ratios

Variations in the concentration of lithogenic radionuclides usually prevent the use of simple concentration information as a tool in sediment tracing [*Murray et al.,* 1991]. The probability of overlapping concentrations is generally too high. However, strong correlations have been observed between many radionuclide concentrations [*Murray et al.,* 1990], and it has been demonstrated that the use of activity ratios, in particular $^{226}Ra/^{232}Th$ can reduce the spread (compared with concentration data) often to within analytical uncertainties [*Murray et al.,* 1991] .

An example is given in Figure 2.1. These data come from a sediment core collected from the Jenolan caves, NSW. The activity concentrations of ^{226}Ra and ^{232}Th both vary by 40% (spread/mean value) down the core. However, these concentration variations are reduced to within analytical uncertainties of about 3% when the activity ratios are taken. Clearly the use of activity ratios reduces the variability, and therefore should increase the probability of distinguishing sediments from different sources, compared with using the concentration data alone.

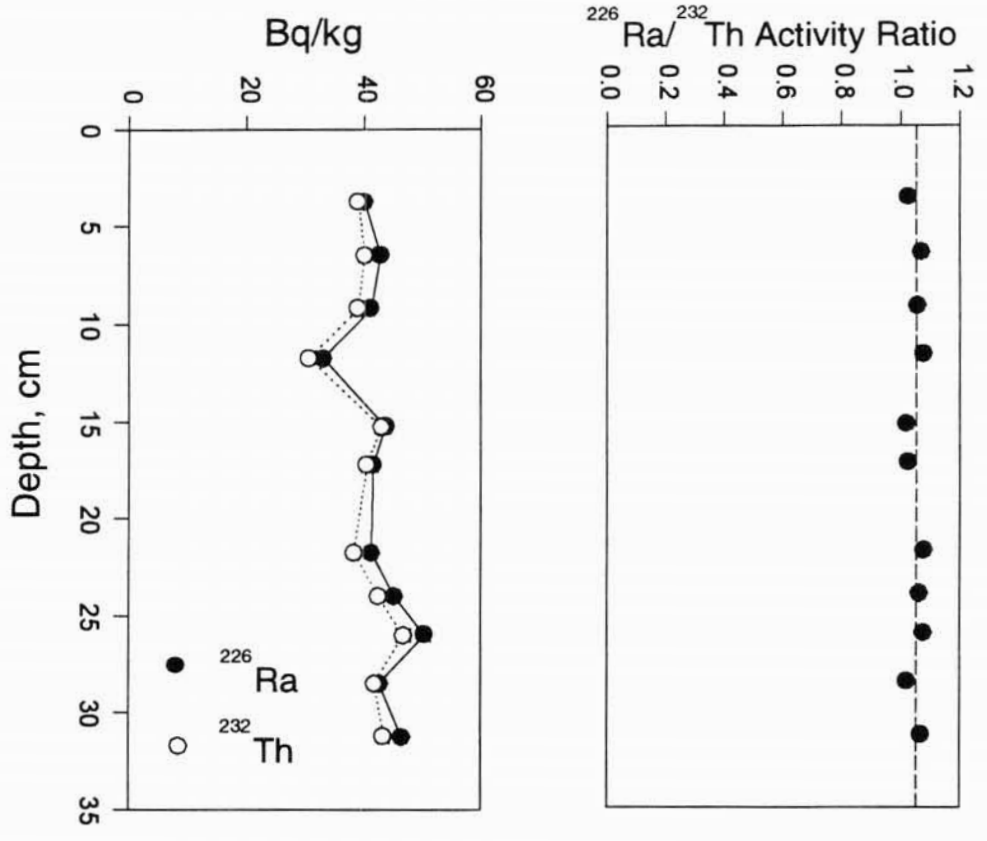

Figure 2.1: Data from the Jenolan caves area NSW [after *Murray et al.,* 1991]. Absolute concentration of ^{226}Ra and ^{232}Th (a), and the variation of the ^{226}Ra/^{232}Th ratio (b) with depth. Analytical uncertainties equivalent to one standard error on the mean are all smaller than the symbol size.

2.1.2 Nuclide correlations with non-zero intercepts

Constancy in ratio arises from a correlation with neglibile intercept on either the x or y axis. Other studies have demonstrated that this is not always the case. The data presented in Table 2.1 come from samples of the Woolgarlo sediment core, taken from the Yass River arm of the Burrinjuck Dam N.S.W (*Murray pers. comm. 1989*). The ratio data for ^{226}Ra/^{232}Th vary by 24%. However, a plot of the ^{226}Ra and ^{232}Th concentrations (Fig 2.2) reveals that the data are well correlated ($r^2 = 0.98$). The total spread in the data about the line is less than 6%, well within the analytical uncertainties of 3% (at 1 σ), but the line has a non-zero intercept. This explains the spread in the ratio data.

Table 2.1: Activity ratios for the bulk sediments from the Woolgarlo sediment core. (Murray pers. com .1989)

$^{226}Ra/^{232}Th$
0.706 ± 0.010
0.701 ± 0.012
0.725 ± 0.008
0.705 ± 0.009
0.683 ± 0.011
0.706 ± 0.011
0.692 ± 0.011
0.729 ± 0.012
0.718 ± 0.012
0.708 ± 0.012
0.669 ± 0.013
0.680 ± 0.011
0.671 ± 0.012
0.650 ± 0.008
0.655 ± 0.008
0.642 ± 0.008
0.567 ± 0.011

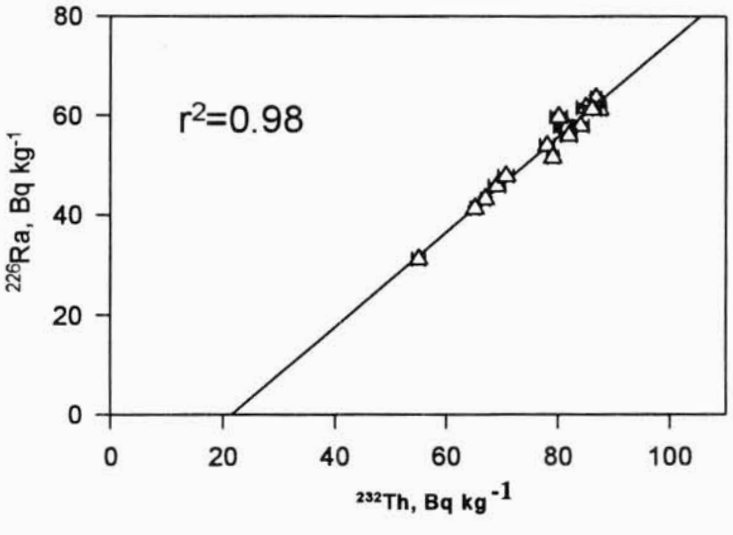

Figure 2.2: ^{226}Ra against ^{232}Th concentrations for samples from Woolgarlo core, from the Yass River arm of Lake Burrinjuck, NSW, Australia. The error bars represent uncertainties equivalent to one standard error on the mean.

2.1.3 Nuclide correlations distinguishing source areas

If nuclide correlations are to be useful in sediment tracing, different source areas need to give different correlations. That is, data from the different sources need to lie on lines of either different slope and/or intercepts. A number of studies conducted at a variety of sites have found this is often the case for ^{226}Ra and ^{232}Th correlations [*Murray et al.*, 1990, 1991; *Murray et al.*, 1993; *Olley et al.*, 1993].

2.1.4 Resolving sediment mixtures

The mixing of sediment derived from source areas with distinctive ^{226}Ra and ^{232}Th correlations result in the mixture displaying a ^{226}Ra and ^{232}Th correlation which lies between the two source correlations. By measuring the ^{226}Ra to ^{232}Th correlation for the two source areas and the sediment mixture, it is then possible to determine the relative contribution of the different source areas.

A good example of this technique is presented in a study of the Jenolan caves area NSW (Fig 2.3) [*Murray et al.*, 1993] . These data provide an example of the mixing of sediments derived from areas with distinctive ^{226}Ra/^{232}Th correlations. Two linked sediment

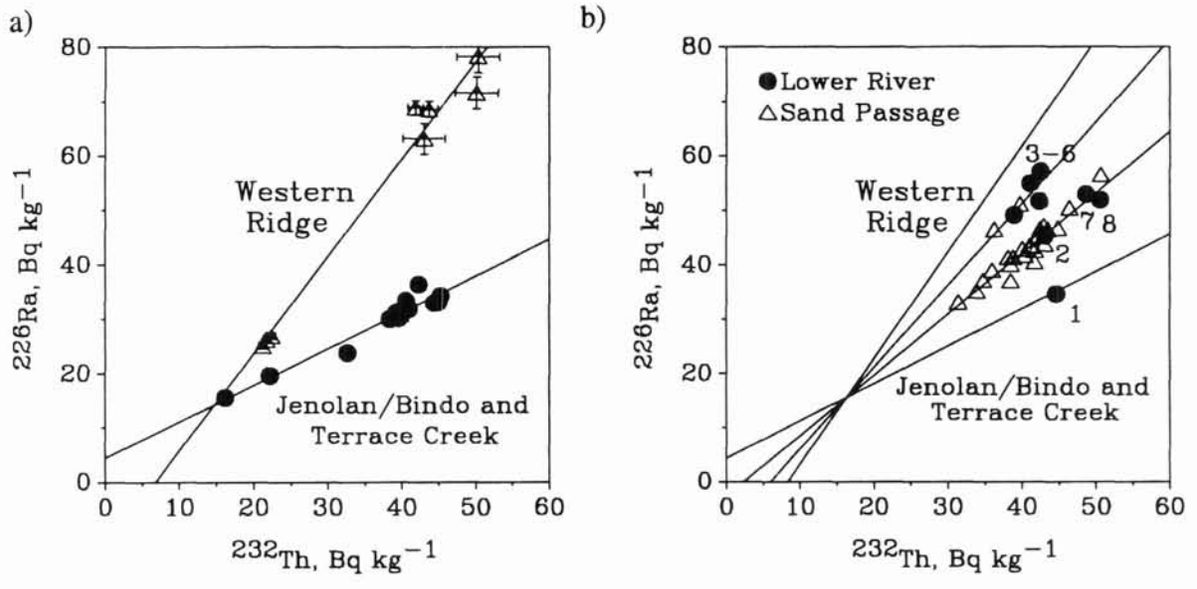

Figure 2.3: ^{226}Ra against ^{232}Th concentrations of samples from the Jenolan Caves Area, NSW, Australia. The error bars represent uncertainties equivalent to one standard error on the mean in most cases these are smaller than the symbol size [after *Murray et al.*, 1993] .

sinks (Sand Passage and Lower Creek) and the two major potential sediment source areas were sampled [Western Ridge (WR) and Jenolan Bindo Divide/Terrace creek (BD/Tck)]. The source area data lies on two distinct lines (Figure 2.3a) and the sources are clearly distinguishable using the ^{226}Ra to ^{232}Th correlations.

All of the sink data lie on two well defined lines between the two source lines. The numbers associated with the Lower Creek points (closed circles) in Figure 2.3b indicate sample progression from the base of the core to the top. This change in the ^{226}Ra/^{232}Th ratio through the core was interpreted as a change in the relative contributions from the two source areas with time. Initially sediment was being derived solely from the BD/Tck area (pt. 1), then a transition occurred (pt. 2) and then WR became the dominant source (pts 3-6); BD/Tck was still contributing sediment, but less than 15% of the total. Subsequently, BD/Tck again became a significant source contributing 60% of the sediment to the sinks (pts 7&8); this was the case at least up to the time of sampling.

Using the correlations between ^{226}Ra to ^{232}Th it was possible to characterize the major sources of sediment in the catchment, and to describe the changes in relative contribution from the two sources with time. This example clearly demonstrates the usefullness of ^{226}Ra to ^{232}Th correlations in sediment tracing studies.

2.1.5 Other radionuclide correlations

The above discussion has focused on the use of correlations between ^{226}Ra and ^{232}Th in sediment tracing. Only these correlations have been reported in the literature as being useful in the spatial sourcing of bulk sediment, although *Murray et al.*, [1991] report correlations between ^{238}U, ^{40}K and ^{232}Th in transported material. Correlation between these nuclides may also provide sediment tracing information.

It is also noted that in the examples given by *Murray et al.*, [1991] there is no significant disequilibrium between ^{238}U and ^{226}Ra. This suggests that the ^{238}U decay chain is in secular equilibrium at least down to ^{226}Ra (see Figure 1.1a) and that the ^{226}Ra and ^{232}Th correlations are in fact ^{238}U and ^{232}Th correlations.

2.1.6 Sediment tracing summary

The usefulness of ^{226}Ra and ^{232}Th concentration correlations in sediment tracing has been demonstrated in the literature. Correlations between these nuclides have been observed

in all sorted sediments examined to date. These correlations occur with both zero and non-zero intercepts, but the reasons for these differences are not known. Other lithogenic radionuclides correlations are also known to exist, but the value of these to sediment tracing studies is also unknown.

In the following sections the reported natural distributions and behaviour of uranium, thorium and radium relevant to the development of the correlations used in the sediment tracing technique are discussed, but firstly the phenomena of radioactive decay, secular equilibrium and the chemistry of uranium, thorium and radium are summarised.

2.2 Radioactivity and Secular Equilibrium

A full discussion of this topic is provided in *Ivanovich and Harmon* [1982, 1992]. A brief outline is provided here.

A radioactive nucleus is one which at any instant may change spontaneously into a different element by losing energy from the nucleus. This process is termed radioactive decay. The radioactivity of an unstable nuclide is by definition

$$\frac{dN}{dt} = a = -N\lambda \qquad (2.1)$$

where a is the activity in nuclear disintegrations per unit time, N is the number of atoms of the nuclide and λ is the decay constant, the probability of decay per unit time. The unit of activity is the Becquerel (Bq), which is defined as 1 nuclear disintegration per second. The solution to equation (2.1) can be expressed as

$$N = N_0 e^{-\lambda t} \qquad (2.2)$$

N_0 is the initial number of radioactive atoms at $t = 0$, and N is the number of remaining atoms at some later time t.

The half-life $t_{1/2}$, is the time interval over which the initial number of radioactive atoms N_0, is exactly halved i.e. $N = 0.5N_0$ at $t = t_{1/2}$. The half-life is related to the decay constant by

$$t_{1/2} = \ln 2/\lambda = 0.693/\lambda \qquad (2.3)$$

In the case where nuclide 1 is part of a decay chain in which it decays to a radioactive daughter nuclide 2, the nett rate of decay of the daughter nuclide is given by the difference between the decay rate and the production rate resulting from the decay of its parent.

$$dN_2/dt = N_1\lambda_1 - N_2\lambda_2 \qquad (2.4)$$

where N_1 and N_2 represent the number of atoms of the parent and daughter at any time t, and λ_1 and λ_2 are the respective decay constants.

In the cases examined in this study the daughter half-life is usually much shorter than that of the parent nuclide i.e. $\lambda_1 << \lambda_2$. Consequently the activity of the parent does not decrease markedly during many daughter half-lives. In this case the solution to eqn 2.4 simplifies to

$$N_2\lambda_2 = N_1\lambda_1(1-e^{-\lambda_2 t}) \qquad (2.5)$$

Then for values of t much greater than the daughter half-life

$$N_2\lambda_2 = N_1\lambda_1 \qquad (2.6)$$

This condition is termed secular equilibrium. For a decay series, where the series parent half-life is much longer than that of the longest lived daughter, secular equilibrium implies

$$N_1\lambda_1 = N_2\lambda_2 = N_3\lambda_3 = \ldots\ldots\ldots\ldots = N_n\lambda_n \qquad (2.7)$$

2.3 Mass and Activity Concentrations

While the activity concentrations of the nuclides in a decay series at secular equilibrium are approximately equal, mass concentrations are typically far from equal. The ratio of the number of atoms of nuclide 1 to the number of atoms of nuclide 2 is

$$N_1/N_2 = \lambda_2/\lambda_1$$

For example, in the case of secular equilibrium in the ^{238}U decay series using activity concentrations,

$^{238}\mathbf{U}$ ($t_{1/2}$= 4.5 x 10^9 y) = $^{234}\mathbf{U}$ ($t_{1/2}$= 2.5 x 10^5 y) = $^{230}\mathbf{Th}$ ($t_{1/2}$= 7.5 x 10^4 y) = $^{226}\mathbf{Ra}$ ($t_{1/2}$= 1.6 x 10^3 y)

but the mass concentrations decrease by many orders of magnitude down the chain. So, for an initial mass concentration of ^{238}U of 3ppm (crustal average *Wedepohl,* 1969), which corresponds to an activity concentration of ~40 Bq kg^{-1}, mass concentrations of the various nuclides along the chain are 3ppm, 0.167ppb, 0.050ppb and 0.00107ppb respectively.

This is important because while the radioactivity of the daughters is significant, gravimetrically the contribution of the daughter nuclides can be ignored. Furthermore, it has implications for the chemical behaviour of the daughter nuclides in the natural environment. For example, the activity concentrations of ^{226}Ra in natural waters range up to approximately 20 Bq l^{-1} in some saline environments [*Gascoyne,* 1989], this high concentration is equivalent to ~10^{-11}M radium. It is unlikely that ^{226}Ra even at this upper activity concentration would exceed any solubility products in natural waters. Therefore ^{226}Ra concentrations in solution are likely to be limited by sorbtion and co-precipitation [*Langmiur and Riese,* 1985] and not by precipitation reactions. Consequently, the environmental behaviour of ^{226}Ra (and the other daughter nuclides) is likely to be different than that which would be predicted from the element chemistry alone.

2.4. Chemistry

The environmental chemistry of uranium and thorium series nuclides have been summarised by various authors [see for example *Katzin,* 1954; *Wedepohl,* 1969; *Osmond and Cowart,* 1976, 1982; *Ivanovich and Harmon* 1982, 1992]. Only the salient features of the element chemistries relevant to this study are presented here.

2.4.1 Uranium

Chemically, uranium has two natural valency states 4+ and 6+. Under surficial oxidising conditions it is normally in the 6+ state. In the 4+ state uranium is considered immobile. However, the 6+ ion is far more soluble, largely because of its tendency to form uranyl complexes, particularly with carbonates and phosphates [*Gascoyne,* 1992]. The mobility of uranium is therefore dictated by the Eh-pH conditions.

Significant quantities of uranium may be transported by oxidised groundwaters. *Gascoyne* [1992] gives the typical range for uranium in groundwaters as 0.1 to 50 parts per billion (ppb), but notes that even in unmineralised areas they may get as high as 2000 ppb.

Transport of uranium as colloids, fine particulate phases and as absorbed ions provides another avenue for mobility [*Sheppard at al.,* 1980; *Borovec,* 1981; *Short et al.,* 1988; *Vilkes et al.,* 1988; *Moore,* 1992; *Tipping and Higgo,* 1992]. Studies show that generally less than 10% of the uranium load is associated with inorganic colloids [*Osmond and Ivanovich,* 1992], but that up to 80% of the load may be carried by organic colloids

[*Dearlove et al.,* 1991]. These organic colloids are highly stable in the groundwater environment [*Osmond and Ivanovich,* 1992].

Natural colloids are capable of transporting significant portions of the uranium load and may have the effect of increasing the mobility of uranium under reducing conditions. However, solution transport under oxidised conditions would appear to be the dominant mechanism for uranium mobility.

2.4.2 Thorium

In solution, thorium exists only as a 4+ ion, though it rarely occurs in significant concentrations as a dissolved ion. It is widely assumed that thorium is immobile in the aqueous environment. This assumption is based largely on thorium's high particle reactivity [*Moore,* 1992] and the low solubility of thorium oxide.

The solubility of thorium is greatly increased in the presence of anions with which it can form complexes. For example, it increases by 3 to 4 orders of magnitude in the presence of inorganic ligands such as sulphate, fluoride, phosphates [*Langmuir and Herman,* 1980] and carbonates [*Simpson et al.,* 1982; *Anderson et al,.* 1982; *LaFlamme and Murray,* 1987]. Organic ligands such as oxalate, citrate and ethylene diamine tetra acid (EDTA) are known to greatly increase the solubility of Th^{4+} (up to 10^7 for oxalate [*Langmuir and Herman,* 1980]). However, above pH7 thorium tends to adsorb almost completely onto clays and solid organic matter [*Gascoyne*, 1992]. While complexing increases thorium solubility, the thorium content of natural waters is nevertheless very low, largely due to its particle reactivity. *Krishnaswami et al.,* [1982] showed that sorption removes thorium from groundwater on a time scale of 3 minutes or less, demonstrating its particle reactive nature.

As with uranium, recent studies have shown that colloids and fine particulate phases are important in the transport of thorium [*Orlandini et al.,* 1990; *Gaffney et al.,* 1992; various authors in *Ivanovich and Harmon,* 1992; *Marley et al.,* 1993;]. Given thorium's generally low solubility, and its particle reactive nature, colloidal transport may be the predominant means of thorium migration in the environment.

2.4.3 Radium

Radium is the heaviest of the alkaline earth group. Chemically, it behaves similarly to barium and is present in the natural environment only as a 2+ species. ^{226}Ra

concentrations range from 0.1 $mBqL^{-1}$ in fresh surface waters, to over 20 Bq L^{-1} in some saline waters [*Gascoyne,* 1989]. *Moore* [1992] stated that in river water and non-saline groundwater radium strongly sorbed to particles; in seawater it is primarily dissolved. *Krishnaswami et al.,* [1982] noted that radium injected into fresh groundwater did not migrate far from the point of injection and was rapidly removed from solution by sorption. However, *Krishnaswami et al.,* [1991] also observed that it is much less particle reactive in brines.

Radium co-precipitates with hydrous oxides of Mn and Fe [*Kronfeld et al.,* 1991; *Levinson et al.,* 1982] and in soils, radium is mainly on exchangeable sites or associated with iron and/or iron oxides [*Frissel and Koster,* 1990]. As with thorium, particulate transport of radium is likely to be the dominant mechanism of mobility in the near surface low salinity environment.

2.5 Natural Distribution

In the natural environment rocks, soils and sediments can be viewed as linked compartments in the erosion cycle. This is shown diagrammatically in Figure 2.4. The primary mechanism of erosion is weathering [*Press and Siever*, 1978]. In weathering, chemical and mechanical processes act to break down rock mass. The residual product of rock weathering is soil. In detail, these pedogenic processes are complicated but the nett result is a loss of soluble elements such as Na, Ca and Mg, a consequential enrichment in the soil profile of less soluble elements (Al, Fe, Mn) [*Middelburg et al.*, 1988; *Paton* 1978] and the production of usually finer grained secondary minerals [*Moss and Walker*, 1978; *Press and Siever*, 1978].

Hydraulically most soils consist of an unstable mix of fine and coarse particles [*Moss and Walker*, 1978]. Clastic sediments are produced by the transportation of the residue produce of rock weathering (soils) [*Leeder*, 1982]. Sediment transport results in the sorting of the material being transported by particle size and to a lesser extent by density, and abrasion of the grains [*Krumbein and Sloss*, 1963]. Following deposition the sediments produced from the mobilisation of soil will re-enter the cycle either by being remobilised, undergoing soil formation [*Moss and Walker*, 1978] or by being indurated to form sedimentary rock [*Press and Siever,* 1978].

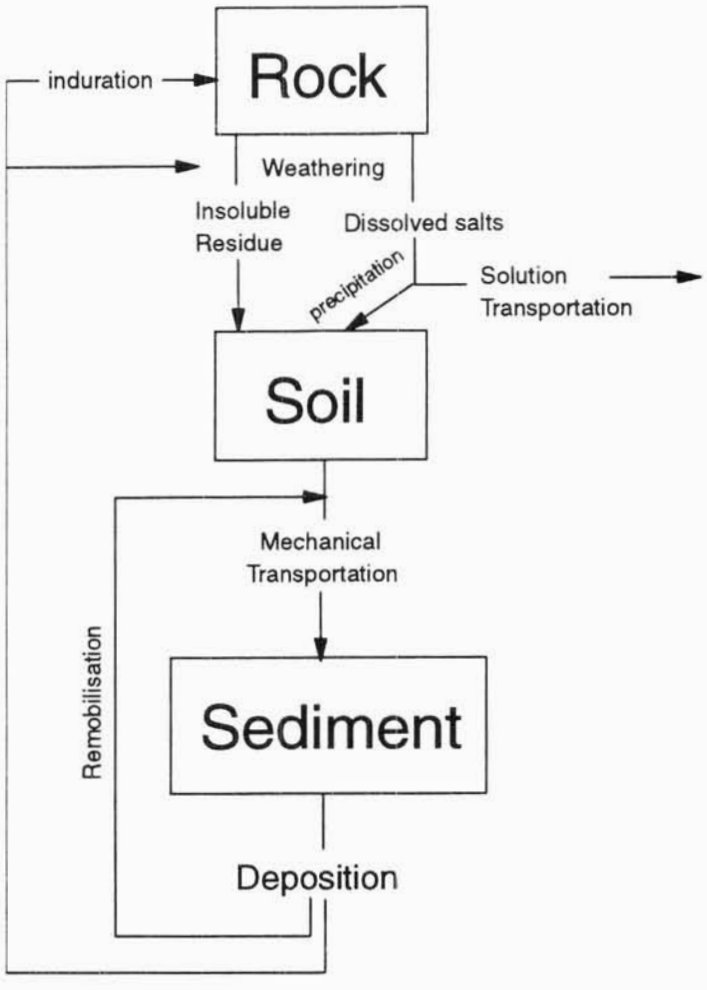

Figure 2.4: A diagrammatic representation of the erosion cycle, showing the links between rocks, soils and sediments (from discussions in *Leeder* [1982], *Krumbein and Sloss* [1963] and *Press and Siever* [1978]).

Section 2.1 presented distributions and showed that correlations exist between ^{238}U and ^{232}Th decay series nuclides in modern sediments. The following sections examine the distribution of ^{238}U and ^{232}Th in the other two compartments defined above, rocks and soils.

2.5.1 Distribution in rocks

2.5.1a Igneous rocks

Thorium and uranium are known to increase in abundance towards the more petrologically differentiated rock types. Typically, high uranium and thorium contents accompany high concentrations of SiO_2 and K_2O and low CaO [*Harmon and Rosholt,* 1982]. Enrichment of the residuum fluids in elements rejected by most rock forming minerals

appears to be the simplest explanation of the distribution of uranium and thorium in igneous rocks [*Lyons,* 1964]. The large ionic radii of uranium and thorium is presumably what precludes them from early crystallising silicates [*Goldschmidt,* 1954].

The concentrations of ^{232}Th appear to be more closely related to ^{238}U in mafic and intermediate rocks than in granitic rocks (correlation coefficients of 0.93 and 0.77 respectively) [*Clarke et al.,* 1966]. The mass ratio of ^{232}Th to ^{238}U in igneous rocks generally ranges from 3 to 5 [*Harmon and Rosholt*, 1982] with an average ratio of 3.5 [*Rogers and Adams,* 1969]. The constancy of this value among many igneous rock types indicates a lack of fractionation of the two elements during magmatic processes [*Gascoyne,* 1982]. However, many granites have higher thorium to uranium ratios, which *Harmon and Rosholt* [1982] have suggested is due to leaching of uranium subsequent to crystallisation.

While data are available on the general correlations between uranium, thorium and potassium in igneous rock, little specific data are available on the relationships of these nuclides in comagmatic suites. One of the few examples is the work of *Larsen and Gottfried* [1960] in which they examined the concentration of uranium and thorium in 199 rocks from a variety of petrographic provinces. *Larsen and Gottfried* [1960] plotted uranium, thorium and the thorium/uranium ratio against a differentiation index. They observed that in general uranium and thorium increased in concentration towards the more felsic members in each suite and that the thorium/uranium ratio was more or less constant for a given petrographic province. Given the importance of their observation to this study, their data have been converted to Bq kg^{-1}, using the conversion factors in Appendix A, and replotted as uranium to thorium plots (Fig 2.5 a to g).

The concentrations of uranium and thorium are strongly correlated in each of the rock suites, with r^2 values ranging from 0.75 to 0.99. These correlations all have intercepts at or near zero. The slopes range from 0.49 to 1.4 and many of the rock suites can be distinguished from one another on the basis of their uranium to thorium correlations. This is an important observation from the point of view of this study: petrographic provinces may be distinguished by distinctive uranium to thorium correlations. As the uranium and thorium decay series are commonly in secular equilibrium in most unexposed rocks [*Iyengar,* 1990], identical correlations would therefore be expected between other nuclides from the two decay chains, for example ^{230}Th to ^{232}Th or ^{226}Ra to ^{232}Th.

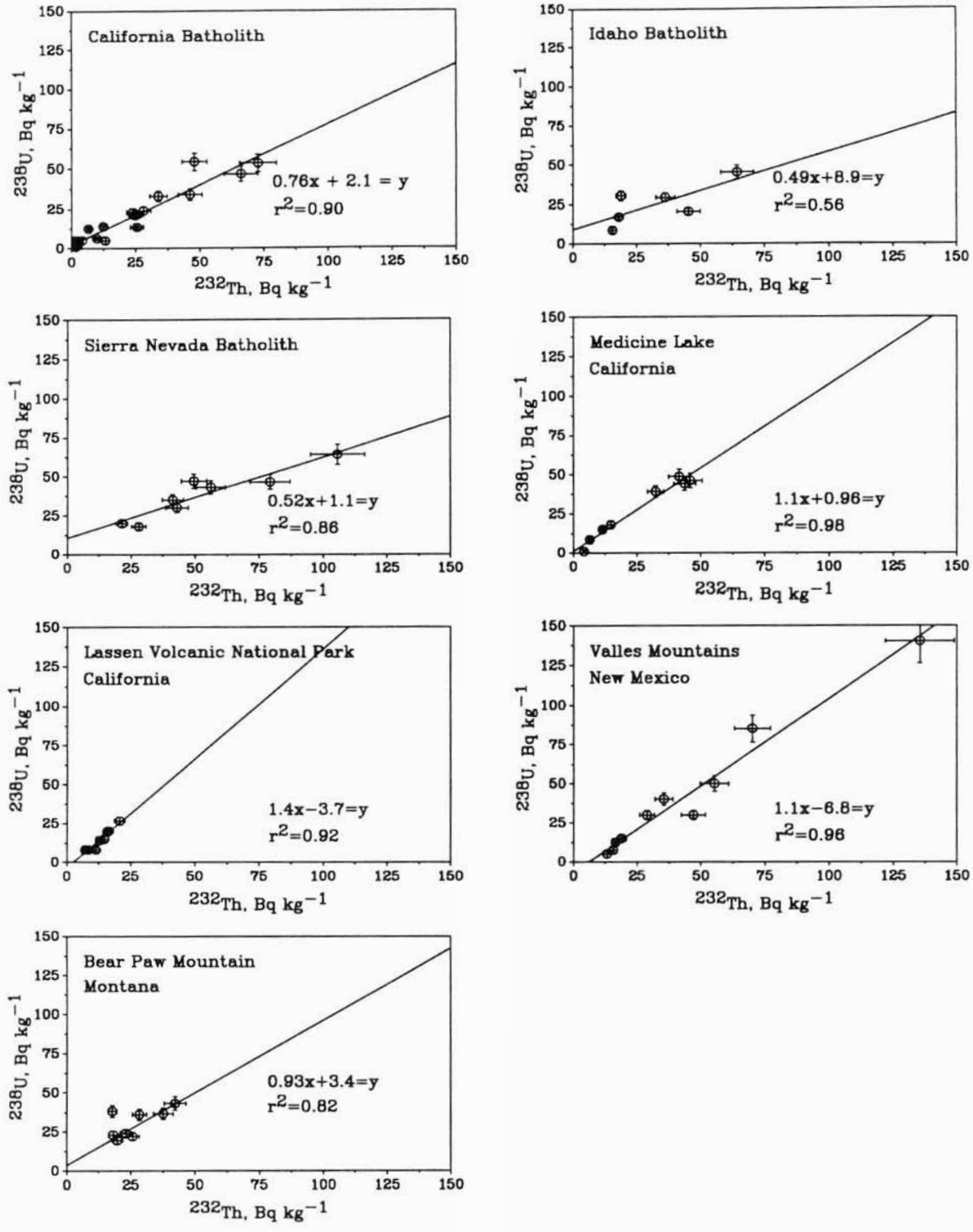

Figure 2.5: ^{238}U and ^{232}Th concentration data for selected igneous rock suites. Data from *Larson and Gottfried* [1960].

2.5.1b Sedimentary rocks

A large proportion of the earth's crust is covered by sediments. Continental sediments are dominated by clastic material. This material is derived from the erosion of soil material which is ultimately derived from rock weathering. Nuclide correlations in modern sediments were presented in chapter 1. This section briefly describes the evidence for the presence of nuclide correlations in sedimentary rocks.

Gascoyne [1982] states that clastic sediment deposits typically contain thorium in concentrations comparable to those in the source rock. *Wedepohl* [1969] notes that the Th/U mass ratio for shales (non black) is between 3.5-4. This is similar to the 3 to 5 range reported for igneous rocks [*Harmon and Rosholt*, 1982]. However, most of the published uranium and thorium analyses of sedimentary rocks are of individual samples collected from a variety of lithologies. While these results are of use in determining the general ranges and distribution of these elements, they provide no information on whether these elements are correlated in sedimentary rocks.

One exception to this is the *Plier and Adams* [1962a] study of the Mancos shale. These authors made 135 measurements of U and Th concentrations in samples, of this homogenous dark-grey-carbonaceous shale, collected from 16 sites along more than 500 kms of outcrop. Their data have been converted to Bq kg^{-1}, using the conversion factors in Appendix A, and are plotted in Figure 2.6.

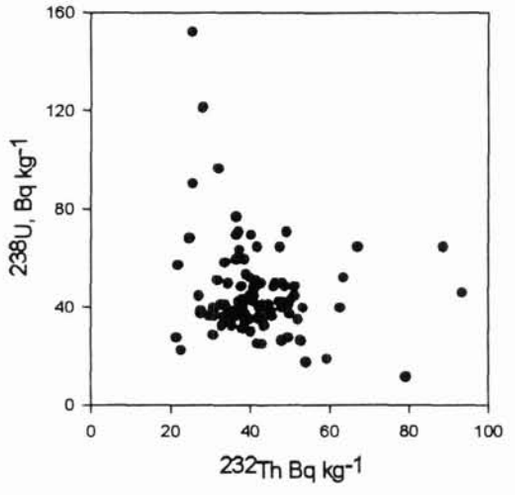

Figure 2.6: ^{238}U and ^{232}Th concentration data for samples from the Mancos Shale. Data from *Plier and Adams* [1962a].

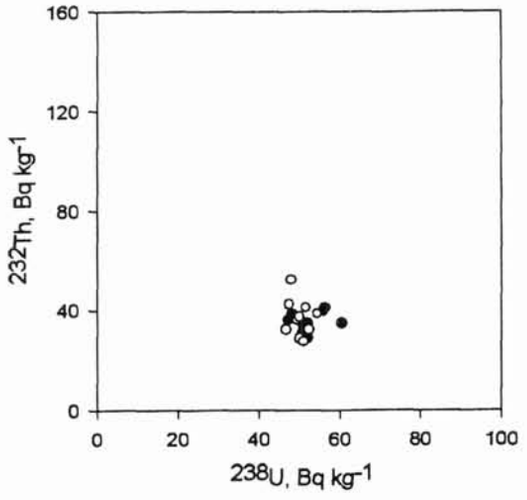

Figure 2.7: ^{238}U and ^{232}Th concentration data from vertical (open circle) and horizontal (closed circles) sampling at intervals of 6 ft at one outcrop of the Mancos Shale. The relative standard deviation of the U/Th ratio for these samples is 9.1%. Data from *Plier and Adams* [1962a].

The data from this regional sampling shows a wide scatter and there is no correlation evident between the U and Th concentrations. However, *Plier and Adams* [1962a] demonstrated that while the U/Th ratios in samples of the Mancos shale varied markedly on a regional scale, the local variations were small (Figure 2.7). From this and other evidence they attributed the spread in ^{238}U and ^{232}Th concentrations evident in regional data to changes in the depositional environment of the shale. This suggests that while ^{238}U and ^{232}Th may be poorly correlated in a sedimentary rock on a regional scale, locally uniform U/Th ratios may be expected. Given the absence of other comparable data it is not possible to state whether this is generally the case in all sedimentary rocks.

2.5.2 Distribution in soils

It is clear from the above discussion that correlations exist between uranium and thorium in igneous and sedimentary rocks. While these elements are correlated in the whole rock they are not uniformly distributed within most rock material. Uranium and thorium are predominantly concentrated in accessory minerals such as zircon, sphene and apatite [*Wedepohl,* 1969] or in poorly crystalline phases [*Levinson et al.,* 1982; *Gascoyne,* 1982] typically concentrated along grain boundaries [*Wedepohl,* 1969]. The decay series in deeply buried unweathered materials are generally in equilibrium [*Osmond and Cowart,* 1982].

Disequilibrium results from geochemical or geophysical sorting, whereby a process acts to move a parent or daughter into or out of a system at a rate which is significant, relative to the half-life of the daughter. It is the weathering processes that occur at or near the earth surface which occur on time scales fast enough to result in disequilibrium. As weathering processes break the rock down it would seem unlikely, given the differences in the distribution and chemistry of the elements, that the nuclide concentrations or correlations present in the rock would carry through to the soil.

In general the mobility of uranium and thorium is considered to be limited [*Harmsen and de Haan*, 1980; *Middelburg et al.,* 1988]. Similarly radium does not appear to migrate significantly through soils [*Frissel and Koster,* 1990; *Jesus et al.,* 1980]. A number of studies have demonstrated that the concentration of uranium, thorium and radium in soils is largely dictated by the concentration of these nuclides in the parent material [*Harmsen and de Haan,* 1980; *Megumi et al.,* 1988; *Frissel and Koster,* 1990]. The correlations present in rocks might therefore, be expected to exist in the soil profile developed from those rocks.

Megumi et al., [1988] found a general correlation between uranium and thorium series nuclides in soils collected from a variety of petrographic provinces. They explained the scatter in the correlations in terms of surface area effects. Uranium and thorium series nuclides have been shown to increase in concentration as particle size decreases [*Megumi and Maruro,* 1977; *Megumi et al.,* 1986; *Meriwether et al.,* 1988] and surface area increases [*Megumi et al.,* 1982; *Megumi et al.,* 1988]. The nuclides are dominantly present on the surface of soil particles either as sorbed ions or incorporated into Fe/Mn oxides [*Frissel and Koster,* 1980; *Megumi et al.*, 1982]. The spread in the correlations between uranium and thorium series nuclides in soils may be the result of minor differences in the relative mobility of the nuclides and differences in soil particle surface area. Therefore, it would seem probable that if correlations are present in the parent rocks, they are transferred to the soils with some degree of localised modification. This modification would be largely due to surface area effects and differences in nuclide chemistries, with the uranium and thorium series nuclides being primarily present on the surface of soil particles or in relicted heavy mineral phases.

In contrast to the observations of low nuclide mobility and the prevalence of secular equilibrium in soils discussed above, a number of studies have found evidence of significant nuclide mobility and distinct disequilibrium. For example, *Michel* [1984] observed up to 70% loss of ^{232}Th during granite weathering in Cayce, Southern Carolina, USA. She also

considered that a significant fraction of the uranium and radium had been removed and then added back to the profile. The ^{238}U decay series was not in equilibrium, with the $^{230}Th/^{234}U$ and $^{230}Th/^{226}Ra$ activity ratios being less than 1. Disequilibrium in the ^{238}U decay series has also been observed in soils by other workers [*Hansen and Stout,* 1968; *Megumi,* 1979; *Rosholt,* 1982; *Moreira-Nordemann,* 1980]. *Dickson and Wheller* [1992] stated that the activity ratios in many soils for $^{234}U/^{238}U$ were less than 1, and greater than 1 for $^{230}Th/^{238}U$ and $^{226}Ra/^{238}U$.

There is little literature available on the equilibrium conditions of the ^{232}Th decay series in soils. However, given the short half-lives of the longer lived daughters in the series, ^{228}Ra (5.75y) and ^{228}Th (1.91y), it would be expected that the decay series would be in secular equilibrium in most natural materials [*Murray et al.,* 1991]. *Murray et al.,* [1992] confirmed this in a number of samples of Australian soils and sediments.

Murray et al., [1991] presented ^{226}Ra and ^{238}U data from sediments collected from Australian catchments ranging in size from a few hectares to tens of thousands of km^2. These sediments would have been derived from the soils in those catchments. In each of the examples presented by *Murray et al.,* [1991] the activity ratio of $^{226}Ra/^{238}U$ was within analytical uncertainty of one. This suggests that the ^{238}U decay series is probably in equilibrium down to ^{226}Ra in these sediments, and presumably in the soils from which they are derived. Given the scale of the *Murray et al.,* [1991] study, secular equilibrium (at least down to ^{226}Ra) would seem to be the common condition in Australian soils.

2.6 Evidence for the Mobility of Thorium.

An interesting issue arises from the work of *Michel* [1984]. As discussed above thorium is generally considered to be immobile in the environment. The *Michel* [1984] study is a notable exception. She observed a loss of up to 70% of ^{232}Th during iso-volumetric weathering of granite. However, ^{238}U, ^{234}U and ^{226}Ra showed no significant loss. The concentration of ^{230}Th was generally found to be deficient relative to its parent ^{234}U and it daughter ^{226}Ra. *Michel* [1984] concluded that ^{226}Ra and ^{234}U had been lost during the intense weathering and then added to the profile in the last 10, 000 years. Interestingly the $^{226}Ra/^{234}U$ ratio for most points is close to 1 (Table 2.2). If the sample 8 is disregarded the mean is 1.05 ± 0.03. The mean $^{230}Th/^{234}U$ ratio is 0.88 ± 0.03.

Table 2.2: Concentration data and activity ratios for the weathered granite samples [after *Michel,* 1984].

No.	^{234}U	^{230}Th	^{226}Ra	$^{226}Ra/^{234}U$	$^{230}Th/^{234}U$
1	9.18	7.5	10.52	1.15	0.82
2	9.1	8.54	8.93	0.98	0.94
3	12.15	9.12	13.14	1.08	0.75
4	7.66	5.85	8.81	1.15	0.76
5	8.02	7.41	7.95	0.99	0.92
6	9.07	7.74	9.36	1.03	0.85
7	10.29	9.41	10.59	1.03	0.91
8	6.77	8.24	13.4	1.98	1.22
9	9.33	8.57			0.92
10	11.1	12.76	11.37	1.02	1.15
11	9.56	8.38	10.6	1.11	0.88
12	13.24	11.9	13.83	1.04	0.90
13	13.25	11.95	11.52	0.87	0.90
14	6.06	5.81	6.21	1.02	0.96
15	8.77	6.35	11.44	1.30	0.72
16	11.75	9.48	10.61	0.90	0.81
mean (not including sample 8) and standard error				1.05 0.03	0.88 0.03

If the addition hypothesis is correct the apparent equilibrium between ^{226}Ra and ^{234}U has to be regarded as coincidental. It is possible that ^{234}U and ^{226}Ra were added to the profile and that *Michel* [1984] sampled at a time when their activities were equal. However, given the 70% loss of ^{232}Th observed, an alternative explanation would be that ^{230}Th had been lost from the profile in the last 200 to 300 years and that ^{234}U and ^{226}Ra had been preferentially retained. This single step process has the attraction of simplicity, compared with the dual step and coincidence required by the Michel hypothesis. It suggests that under some conditions, thorium may be more mobile than either uranium or radium.

A possible mechanism for this is described in *Short et al.,* [1988]. They observed that uranium was largely present in soluble species, whereas thorium was present in the colloidal phase. In addition they also noted that ^{234}U sorbed on the colloids was lost back to solution, but that the relative mobility of ^{230}Th between phases was low. The uranium present in solution would be able to become involved in redox or co-precipitation reactions. The sorbed thorium would not be as chemically available. Under these circumstances, situations can be envisaged in which thorium could be more mobile than uranium and presumably radium.

As this thesis is examining equilibrium conditions in soils and sediments, the opportunity exists to address the relative mobility of the various nuclides in a variety of geomorphic settings.

2.7 Summary

The follow summarises the information on natural distribution and behaviour of uranium, thorium and radium relevant to the development of the correlations used in the sediment tracing technique described in chapters 1 and 2:

1. Correlations exist between uranium and thorium in igneous rocks. The ^{238}U and ^{232}Th decay series are in secular equilibrium in most igneous rocks so these correlations also apply to the daughters in the decay series. These correlations all have intercepts consistent with zero.
2. Petrogenic provinces may be distinguished on the basis of these nuclide relationships.
3. Lithogenic radionuclides may be poorly correlated in sedimentary rocks on a regional scale but well correlated at smaller scales.
4. Strong correlations exist between ^{238}U and ^{232}Th decay series in modern sediments. These correlations may be used to distinguish sediment derived from different sources. Correlations with non-zero intercepts do occur.
5. The correlations between lithogenic nuclides in soils are weaker than those observed in modern sediments. The uranium and thorium series nuclides are primarily present on the surface of soil particles or in relict heavy mineral phases.
6. In general the mobility of uranium, thorium and radium is limited and it is strongly suggested that secular equilibrium (at least down to ^{226}Ra and ^{228}Th) is the dominant condition in Australian soils.

Chapter 3: Hypotheses, Methodology and Analytical Methods

This chapter presents hypotheses which have been examined in this thesis in order to develop a mechanistic framework for the application of lithogenic radionuclides to sediment tracing. It also describes the methodology and analytical methods employed in addressing these hypotheses.

3.1 Statement of Hypotheses

Correlations between concentrations of ^{226}Ra and ^{232}Th have been widely observed in modern sediments (see chapter 2 for discussion). From the literature, two possible mechanisms by which the correlation between ^{238}U and ^{232}Th decay series nuclides in modern sediments arise can be proposed. Firstly, if secular equilibrium prevails in most soils and the mobility of the parent nuclides is in general limited, then the correlations observed in modern transported sediments have been directly inherited from the parent rock. From this Hypothesis 1 is proposed:-

1. Lithology is the dominant factor controlling the heterogeneity of ^{226}Ra and ^{232}Th across the landscape. Nuclide correlations present in the rock are carried through to the soils developed on them. The decay series are in secular equilibrium in soil material with the nuclides being present either on the grain surfaces or in primary resistate minerals. Erosion and sorting of the soil material results in sediments which have uranium to thorium series nuclide ratios equal to the uranium to thorium ratio of the parent material.

Conversely, if significant nuclide mobility occurs during soil formation, then the observed correlations must be a function of the nuclide redistribution on the soil particles and the transportation processes. In soils, radionuclides are known to be associated with grain surface coatings, such as iron/manganese oxides/hydroxides and organic coatings [*Frissel and Koster,* 1990; *Megumi et al.,* 1982; *Rosholt,* 1982]. These coatings probably develop radionuclide signatures through sorption and co-precipitation. Therefore, the average concentration of radionuclides in a grain will be dependant on the original grain diameter and the thickness of the coating compared with the diameter. In grains with varying coat thicknesses, the bulk concentration of a radionuclide should then correlate linearly with the

concentration of other nuclides. It is therefore possible that the correlations observed between nuclides, in transported sediments, could be due to different degrees of development and/or abrasion of these coatings [*Murray et al.,* 1991]. Concentrations would range between the low values in the core grain and the typically higher values in the surface coatings. From this a second hypothesis is proposed which contradicts hypotheis 1:-

2. The heterogeneity observed in ^{226}Ra and ^{232}Th across the landscape is the result of soil forming processes. The ^{238}U and ^{232}Th decay series nuclides are dominantly surface sorbed, either directly or in association with Fe/Mn oxide. Particle size separation during fluvial transport then results in the linear correlations observed in transported material. The $^{226}Ra/^{232}Th$ correlations in sediments are therefore related to soil formation effects, and secular equilibrium will not necessarily be observed in soils and sediments.

In addition to these two general hypotheses (above) an additional hypothesis related to ^{238}U and ^{232}Th decay series nuclides concentrations in sandy sediments has also been examined. Zircon, apatite and other heavy minerals are known to contain high concentrations of uranium and thorium [*Kamel and Johnson,* 1963; *Wedepohl,* 1969] and are resistant to weathering. *Adams et al.,* [1959] suggested that these resistate minerals are transferred intact to sediments. In samples with varying heavy mineral content, the bulk concentration of a radionuclide should then correlate linearly with the concentration of other nuclides. Concentrations would range between the low values in the gangue minerals and the much higher concentrations in the heavy minerals. The slope of the correlation would largely be dependant on the uranium to thorium ratio in the heavy mineral phases. The third hypothesis is therefore:-

3. In coarse grained material (sands) ^{226}Ra and ^{232}Th are primarily associated with resistate heavy minerals. Density separation of these minerals from the gangue results in the correlations observed in modern sediments.

3.2 Methodology

In order to test the hypotheses of Section 3.1, and to illustrate the complexities of applying natural decay series nuclides to sediment tracing problems the behaviour and distribution of radionuclides has been examined at nine distinct sites. These range in scale from $10m^2$ to 100,000 km^2. The thesis aims to establish the links between lithogenic radionuclide relationships in the three erosion cycle compartments defined in Figure 2.4 that is between rocks, soils and sediments, with particular emphasis on the links between radionuclide distribution in soils and those present in sediments derived from them. Each chapter in Part II of the thesis aims to contribute to the development of an overall model of the behaviour of lithogenic radionuclides pertaining to their use in sediment tracing studies.

In chapter 4 lithogenic radionuclide data from nine rock types and the soils developed from them are studied. Equilibrium conditions are discussed and relationships between ^{238}U and ^{232}Th decay series nuclides in the rocks and soils are examined. This chapter aims to determine effects of pedogenisis on ^{238}U and ^{232}Th decay series nuclides.

The effects of fluvial transport of soil material on the ^{238}U and ^{232}Th decay series nuclide concentrations are examined in chapter 5. Three main processes occur to soil material during fluvial transportation; (i) separation of the soil grains by particle size, (ii) separation by density, and (iii) grain abrasion [*Krumbein and Sloss,* 1963]. The effects of each of these processes on the concentration of radionuclides are determined by measuring radionuclide concentrations in artificially sorted and abraded soil fractions. At the end of this chapter the radionuclide concentrations in sediments derived from fluvial transportation of soil material are compared to the radionuclide correlations produced by artificial sorting of the same soil material by particle size and by density. The aim is to determine whether the two processes produce the similar correlations.

The dependance of lithogenic radionuclide concentrations in coarse-grained sediments on the heavy mineral content of the sediments are studied in chapter 6. This work was done at a single river confluence with the specific aim of testing hypothesis 3. In chapter 7 the effects of post-depositional alteration of sediments on the radionuclide concentrations and ratios are examined. This work was done at a site in which sediment showed evidence of having accumulated iron-manganese oxides following deposition.

In chapter 8 each of the hypotheses proposed are assessed against the observations made in chapters 4 to 7, and a model is developed of the mechanism controlling the

distribution of lithogenic radionuclides in modern sediments. This model is then applied to three sites in Part III of this thesis.

3.3 Analytical Methods

3.3.1 Techniques for the analysis of radionuclides

Radionuclide concentrations in samples were determined by a combination of gamma and alpha spectrometry. The analyses were done at the CSIROs Division of Water Resources Canberra laboratory; the analytical techniques used are described below.

3.3.1a Gamma spectrometry

High resolution gamma spectrometry has been used for analysis of ^{238}U, ^{226}Ra, ^{228}Th, ^{228}Ra, ^{210}Pb and ^{137}Cs in soil and sediment samples. The methods used are described in detail by *Murray et al.*, [1987]. The spectrometers are based on high purity, n-type and p-type, germanium detectors with pulses fed to a personal computer based multichannel analysis system. All sediment samples were dried and reduced to a particle size less than 100μm in a chrome steel ring grinder, then ashed at 450°C for 24 hours to remove the organic fraction. Depending on the amount of material available, either about 40g or 250g of sample was mixed with polyester resin and cast in one of two fixed geometries (disc or cup respectively) for counting [*Murray et al.*, 1987]. The samples were cast in polyester resin to efficiently retain the gaseous nuclide ^{222}Rn and to provide reproducible counting geometries. They were then stored for approximately 6 half-lives of ^{222}Rn (half-life 3.8 days) to ensure equilibrium with its parent ^{226}Ra, this enables concentrations of ^{226}Ra to be determined with higher sensitivity from the ^{222}Rn daughters. The samples were usually counted for 24 hours. Experimentally derived minimum detection limits for the two geometries are given in Table 3.1.

Table 3.1 Experimentally derived minimum detection limits for Gamma Spectrometry (after *Murray et al.*, 1987)

Nuclide	Disc, 33cm3	Cup, 201cm3
	Bq kg-1	Bq kg-1
^{238}U	15	5
^{226}Ra	2	0.4
^{210}Pb	14	10
^{228}Ra	5	1
^{228}Th	2	0.4

The spectrometers were calibrated using Canadian Centre for Mineral and Energy Technology (CANMET) uranium ore BL-5, thorium nitrate refined in 1906 (Amersham International), Analar grade potassium chloride, and absolutely standardised ^{137}Cs solution (Amersham International). Independent checks on calibration were performed using various U.S. National Bureau of Standards standards and IAEA intercomparisons.

3.3.1b Alpha - particle spectrometry

Alpha-particle spectrometry has been used to analyse; 1) ^{232}Th, ^{230}Th and ^{228}Th in soils and sediment samples from each of the sites; 2) thorium and radium isotopes in chemical extractions from soils and sediment from a number of the sites; 3) groundwaters from the Geebung Creek site. The procedures involved have been described in detail by *Hancock and Martin* [1991] and *Martin and Hancock* [1992]. A summary follows.

The chemical procedure followed was the same for each type of sample (groundwater, soil, sediment, or chemical extract) once the sample had been taken into solution.

Sample Dissolution

Sediment and Soil Samples: The absolute concentration of thorium isotopes in sediment and soil samples was determined either by using ^{229}Th tracer (Amersham International $\pm$ 1%) or by using the ^{228}Th activity determined by gamma spectrometry. In each case between 0.5-1g of dried finely-ground sediment was processed. Samples were processed either by acid digestion or pyro-sulphate fusion [Sill, 1987]. The latter technique was generally favoured.

Acid digestion of samples was done in high temperature teflon beakers. Samples were refluxed with HF for 8 hours. The solution was then taken to dryness and 2 ml of 5M HCl added. If all the sample went into solution it was then made up to 120 ml with deionized water. However, if the sample was not fully dissolved, the HF reflux was repeated and 5 mL of H_2Cl_2 was added. This solution was then taken to dryness and the 2 ml of HCl added again. Two grams of K_2SO_4 was then added to the 120 ml of solution and radium and thorium isotopes were coprecipitated with lead sulphate.

The pyro-sulphate fusion technique used is modified from *Sill* [1987]. A few mls of HF was added (samples with high organic contents were first refluxed with nitric acid). The slurry was evaporated to dryness. The residue was then solubilized by fusion with potassium fluoride. This was transposed to a pyro-sulphate cake. The cake was then readily dissolved

in 120ml of 0.1M HCl and the radium and thorium isotopes were coprecipitated with lead sulphate.

Groundwater: Water samples were filtered through 0.45μm membrane filters. The 2 L filtrate was then acidified with 1ml concentrated HCl per litre. After addition of the tracer, radium and thorium isotopes were concentrated by co-precipitation with manganese dioxide at pH 10. The precipitate was recovered by filtration, dissolved in a HCl/H_2O_2 solution and then evaporated to dryness. The residue was then dissolved in 2 ml of 5M HCl and the solution made up to 120 ml. Two grams of potassium sulphate (K_2SO_4) were added and the radium and thorium isotopes were then co-precipitated with lead sulphate.

Chemical Extracts: The chemical extracts described in section (3.3.8) were taken to total dryness in silica crucibles after the addition of ^{229}Th tracer. They were then ashed at 450 - 500 °C for 8hrs. The ashed residue was transferred to a platinum crucible and the samples were then processed as with the sediment and soil samples described above.

Chemical Separation of the Radioelements

After decanting, the precipitate from the above dissolution processes was washed and dissolved in an ammonical EDTA solution. The EDTA solution was then poured onto an anion exchange column. Radium passed through the column and was collected for further purification. The thorium which was retained on the column was washed with 8M nitric acid (H_2NO_3) and then eluted with 9M HCl. The solution was then evaporated to dryness and electrodeposited on to a stainless steel disc (20mm dia.) from a sulphate electrolyte. The radium fraction was transferred to a cation exchange column and the alkali earth cations were sequentially eluted from the column with 1.5 M ammonium acetate and 2.5 M HCl solutions. The radium was finally eluted with 6 M HNO_3. This solution was then evaporated to dryness and the radium was then electrodeposited onto a stainless steel disc from an aqueous/ethanol solution at pH 2.

Counting

The electroplated discs were counted using an alpha-particle detection system. Ortex silicon surface barrier detectors with 450mm^2 active areas were used. A negative charge was applied to the source and the chamber pressure adjusted to 10 torr to limit contamination of

the detector by recoiling daughter products (*Sill and Olsen,* 1970). Samples were typically counted for 1 to 2 days depending on the activity of the source. The concentration of a particular nuclide was calculated by integrating the counts for that nuclide over its peak area and comparing this activity with the known activity of the tracer nuclide. Recoveries were typically of the order of 70%.

3.3.1c Comparision of $^{228}Th(\alpha)$ to $^{228}Th(\gamma)$

This study involved the use and comparison of analyses from both gamma and alpha-particle spectrometry. It is therefore necessary to provide an intercomparison of radionuclide results from both techniques. Concentration of ^{228}Th in samples can be determined by either technique. Concentrations of ^{228}Th have been determined by both alpha and gamma spectrometry in 69 sediment and soil samples from 5 distinct sites. The $^{228}Th(\gamma)$ are plotted against $^{228}Th(\alpha)$ in Figure 3.1a. There is very good agreement between the two analytical techniques with $^{228}Th(\gamma)=1.01^{228}Th(\alpha)-1.4$ and $r^2=0.98$. The percentage difference between the two sets of analyses has been calculated using the formula

$$\left(\frac{^{228}Th(\gamma)-^{228}Th(\alpha)}{^{228}Th(m)}\right)\times 100$$

in which $^{228}Th(\gamma)$ and $^{228}Th(\alpha)$ are the concentrations of ^{228}Th determined by gamma and alpha spectrometry respectively, $^{228}Th(m)$ is the weighted mean. The percentage difference is plotted against the weighted mean value in Figure 3.1b. The average value is 0.76%, σ=3.5%. This is comparable with the typical individual uncertainty on each value of about 3%. The agreement between the two estimates of reproducibility confirm that there is no random variability in the analyses that cannot be explained entirely by the counting statistics.

The standard error on the ratio is 0.44% (n=69). There is no evidence that the mean value is statistically different from zero. i.e. there is no systematic difference between the gamma and alpha spectrometry determinations of ^{228}Th. It is concluded that both in terms of accuracy and precision the two sets of analyses were comparable and can be used interchangably.

a)

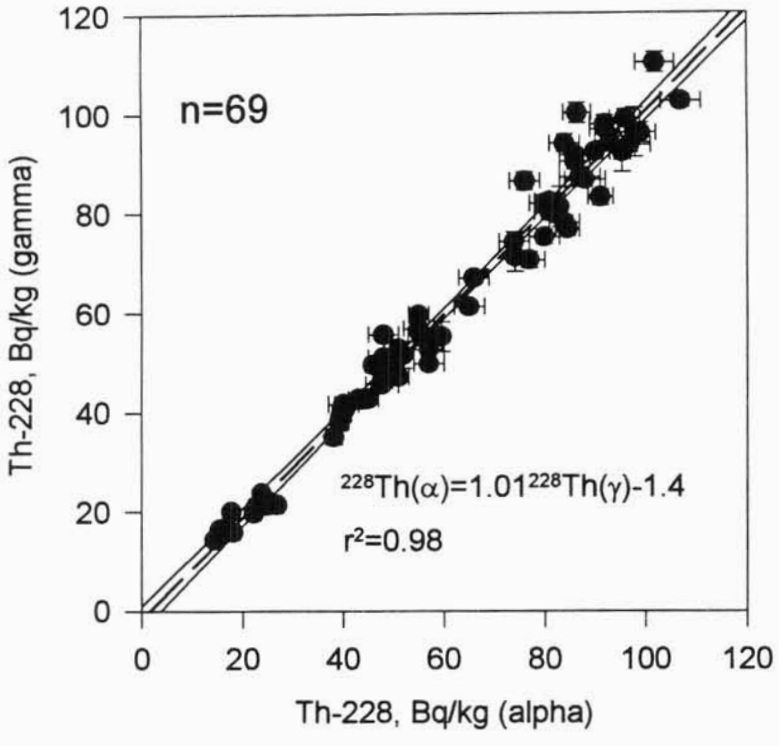

b)

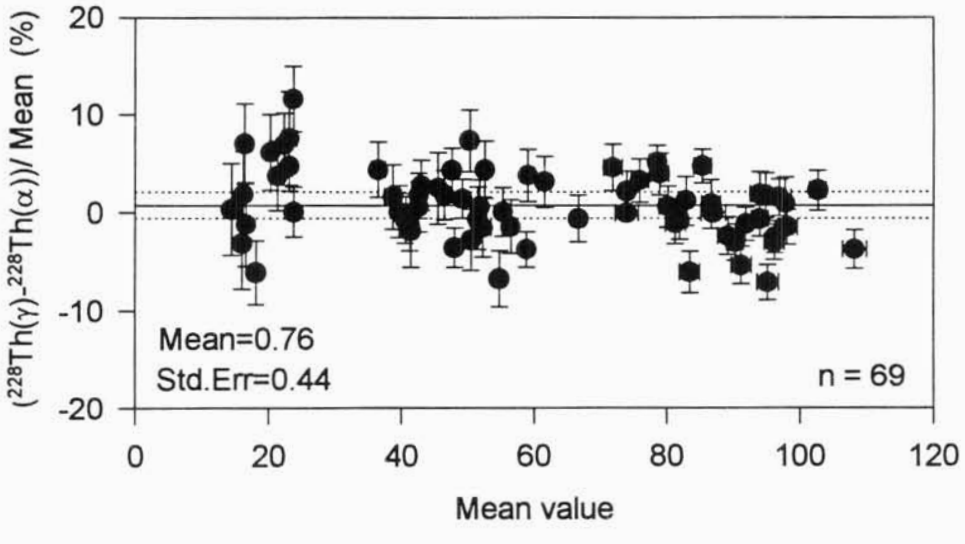

Figure 3.1: Comparison of ^{228}Th concentrations determined by Gamma and Alpha Spectrometry in 69 samples; a) ^{228}Th (gamma) against ^{228}Th (alpha). The regression line and the 95% confidence limits are shown; b) The percentage difference [(α)-(γ)] against the weighted mean value.

3.3.2 Major element analyses

The concentration of major elements in selected samples were determined by one of two methods depending on availability (i) Flame atomic absorption (AA) or (ii) X-ray Fluorescence (XRF).

3.3.2a Flame atomic absorption

After acid digestion by standard techniques [*Allen et al.,* 1974] concentrations of Al, Fe, Mn, Ca, Mg, Na, and K were determined by Atomic absorption analysis at the CSIROs Division of Water Resources Canberra laboratory. An air-acetylene flame was used, and samples were aspirated directly into the flame.

3.3.2b X-ray fluorescent spectrography

Major element concentrations were determined in soil, rock and sediment samples on a Phillips PW1404 spectrometer at CSIRO's Division of Plant Industry's Canberra laboratory. Samples were prepared for analysis by fusing 0.4g of fine ground sample in a lithium borate glass at 1000^{0}C [*Norrish and Hutton,* 1969; *Norrish and Chappell,* 1977].

3.3.3 Mineral determinations

Sample mineralogy was determined by a combination of Microscopic examination and X-ray diffraction analysis (XRD). The X-ray diffraction work was done on fine ground samples prepared on glass slides. The X-ray diffraction instrument was a Siemen D-501 with a Cu tube.

3.3.4 Sample fractionation and abrasion

In chapter 5 the effects of fluvial transport of soil material on the ^{238}U and ^{232}Th decay series nuclide concentrations are examined. Three main processes occur to soil material during fluvial transportation; (i) separation of the soil grains by particle size and (ii) separation by density and (iii) grain abrasion. In order to investigate the effects of these processes soil samples were artificially sorted by both density and particle size, and abraded. The methods used are described below.

3.3.4a Density separation

Heavy mineral separation was done using sodium polytungstate. This inorganic salt supplied by SOMETU (West Germany) forms an aqueous neutral solution, stable in the pH

range of 2-14. The density of the solution is adjustable by dilution between 1 and 3.1 g cm^{-3}. One of the main advantages of sodium polytungstate is that it is non-toxic and reusable. This compound has gained favour in a number of areas where heavy liquids such as TBE, bromoform etc. have traditionally been used for mineral separation [*Callahan*, 1987], conodont extraction [*Merrill,* 1987] and biogenic silicate separation [*Hart,* 1988].

A 30-100g of dried sample was placed in the bottom of a 250ml centrifuge tube and the tube was filled with sodium polytungstate solution with a density adjusted to 2.95 g cm^{-3}. Separation was done at this density to separate the quartz, feldspar and clays from the primary heavy minerals (zircon, rutile etc) and the secondary iron and manganese oxides. The sample was then centrifuged at 3000rpm for 20 minutes. Minerals with densities >2.95g/cm^3 remain on the bottom of the tube while all others floated to the surface. The mineral separates were then washed in deionised water to enable the sodium polytungstate to be recovered. Recovery simply involved drying the wash solution down. The >2.95g cm^{-3} were analysed by a combination of alpha and gamma spectrometry. The mineralogy was determined by XRD.

3.3.4b Particle size separation

Particle size separation was carried out by wet sieving. Samples were first slaked with water then added to the top of a stack of 6 or 7 sieves (2mm, 1.4mm, 500μm, 250μm, 125μm, 63μm and occasionally 38μm). The stack was continuously flushed with water and shaken mechanically. All the fractions produced were then dried in an oven at 45^{0}C, and weighed. The various particle size fractions were then analysed by a combination of AA, XRF, XRD and alpha and gamma spectrometry.

3.3.4c Grain abrasion

Sub-samples of three of the soil samples (A1, D9 and I1) were used to examine the effects of grain abrasion on the radionuclide concentrations. Samples were first wet sieved to remove the <38μm fraction. This was done because the <38μm fraction is normally carried in suspension during fluvial transport and therefore probably does not undergo significant abrasion. 300 g of the >38 μm fraction of each sample was placed in a 1l thick walled plastic bottle with ~600 ml of distilled water. The bottles were then agitated for 62 hrs on a mechanical shaker. After shaking, the samples were particle sized by wet sieving and the particle size distributions compared to those prior to abrasion. A subsample of the >38μm

fraction prior to abrasion and the <38 μm and > 38 μm fractions after abrasion were then analysed by XRF, alpha and gamma spectrometry.

3.3.5 Chemical extraction

In chapter 4 the effects of soil development on lithogenic radionuclide concentrations are examined. Secondary iron and manganese oxides are formed during pedogenesis. The ability of these oxides to trap radionuclides has already been discussed. In this study citrate-dithionite extraction [*Coffin*, 1963] has been used to investigate the role of these oxides in controlling the distribution of radionuclides in soils. This is a standard reagent commonly used in soil science for selectively dissolving Fe oxides/oxyhydroxides, it will not dissolve clay etc, and has been widely used in the study of trace metal associated with these oxides. Citrate-dithionite is a strong complexing agent and is effective in preventing the readsorption of particle reactive elements such as Th onto the residue of extraction [*Short et al.*, 1989].

In this study typically 4 g of sample was extracted at 25°C for 24 hours with intermittent shaking. Iron and manganese concentrations in the extract were determined by Atomic Absorbtion analysis (AA). The proportion of extract remaining after the AA analysis was retained for radionuclide analyses by alpha spectrometry.

Part II

Rock, Soil and Sediment

Chapter 4: ^{238}U and ^{232}Th Decay Series Nuclides in Rocks and Soils

4.1 Introduction

Soils result from the weathering of rocks. Rock weathering involves the destruction of rock forming minerals, the loss of soluble elements such as Na, Ca and Mg and the creation of new secondary minerals such as clays and iron-manganese oxides. These secondary minerals are invariably finer-grained and more poorly crystalline than the original rock forming minerals. These pedogenic processes are complicated, involving many solution, carbonation and oxidation reactions [*Krumbein and Sloss,* 1963].

Hypothesis 1 (Section 3.1) proposed that the radionuclide ratios ($^{226}Ra/^{232}Th$ in particular) in sediments were inherited directly from the parent rock and that lithology was the dominant factor controlling the heterogeneity of ^{226}Ra and ^{232}Th across the landscape. For this hypothesis to be true the following statements must hold:

1. No differential mobilisation of ^{226}Ra with respect to its parent nuclides ^{238}U, ^{234}U and ^{230}Th or to ^{232}Th has to occur during the weathering process.

2. Secular equilibrium which is assumed to exist in the parent rock has to be preserved in the soil.

3. Nuclide ratios in the rock and soil have to be the same but concentrations may vary due to loss of soluble elements. This loss to solution would tend to increase the concentration of the radionuclide in the soil relative to the rock.

Each of these statements are tested in this chapter by examining radionuclide concentrations and ratios in rock and soil samples from nine sites. If these statements are proved correct, then the ^{226}Ra to ^{232}Th correlations in sediments are inherited from the parent rock, as proposed in hypothesis 1. However, if these statements are shown to be false then, as proposed in hypothesis 2, the correlations in sediments must be related to the weathering process.

4.2 Sampling and Sample Treatment

Parent rock and soil samples were collected from nine sites (A to I). The site locations are shown in Figure 4.1. Details of the sampling at each of the sites are presented in Appendix B and summarised in Table 4.1 along with site and sample codes. In further discussion sites and samples will be referred to by their code. As only one rock analysis was done for each site, rocks are referred to by their site code; i.e. rock A comes from site A. The number of samples collected and the area sampled varied from site to site (Table 4.1). However, in each case the groups of soil samples were collected from above a known uniform lithology. The rock samples analysed from each of the sites consisted of a number of fresh (unweathered) sub-samples which were combined to provide one well averaged sample of the site lithology.

Radionuclide concentrations in the soil samples were determined by alpha and gamma spectrometry (section 3.3.1). The rock samples were analysed by alpha spectrometry (section 3.3.1b). Major element concentrations in all the soil samples were determined by either XRF (section 3.3.2b) or AA (section 3.3.2a). The concentrations of radionuclides associated with the secondary iron oxides were determined by citrate-dithonite extraction followed by alpha particle spectrometry on the extract. This was done for samples A1 to A17, C8 to C12 and D1 to D6.

In addition to the rock and soil samples four 2L water samples (Aw1 to Aw4) were collected from site A. These samples were filtered through 0.45μm membrane filters, and the filtrate acidified with 2ml concentrated HCl. In one of the samples the concentration of colloids was sufficiently high that these precipitated/flocculated after the filtering. This sample was taken to dryness and processed as a solid sample. The concentrations of radionuclides in the water samples were determined by alpha particle spectrometry (Section 3.3.1).

4.3 Results and Discussion

The following sections examine (i) the equilibrium conditions in the soils at each site, (ii) the ^{230}Th and ^{232}Th and ^{226}Ra and ^{232}Th correlations in the soils and rock samples, (iii) the association of radionuclides with secondary iron-manganese oxides. The radionuclide analyses for all the rock, bulk soil and extraction samples are presented in Appendix C Tables C1, C2 and C3. Major element analyses are presented in Appendix D.

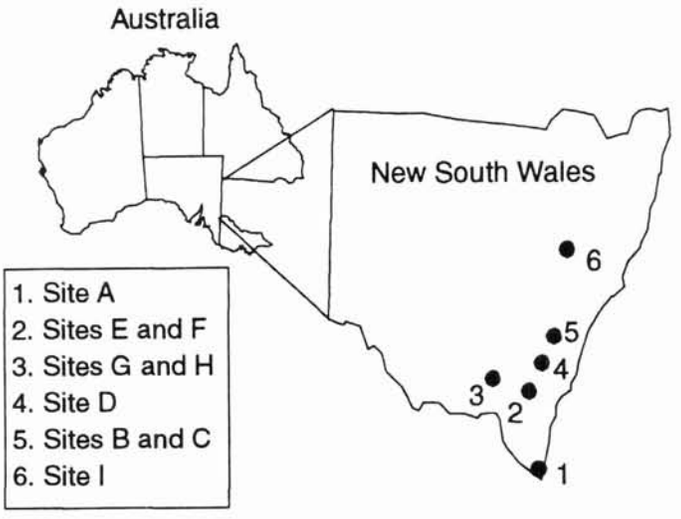

Figure 4.1: A map showing the study site locations

Table 4.1: Summary of the rock and soil sampling, details are presented in Appendix B

Code	Site Name	Lithology	Sampled Area	N	Sample Codes
A	Geebung Creek	Granite	800m Downslope transect including 4 depth profiles	19	A1 to A19
B	McKeowns Valley	Basalt	Soils from an area of ~30 km^2 each sample being made up of ~20 sub-samples	13	B1 to B13
C	McKeowns Valley	Mixed Sediments	Soils from an area of ~100 km^2 each sample being made up of ~20 sub-samples	13	C1 to C13
D	Whiteheads Creek	Granite	Soil depth profile Bulk soil profile	8 1	D1 to D8 D9
E	Yarramundi Reach	Dacite	100 x 100m area sampled on a 10 x 10 grid every second sample analysed	50	E1 to E50
F	Black Mountain	Sandstone	Soil depth profile Soil sample consisting of 20 sub samples collected over a 12 x 12 m area.	8 1	F1 to F8 F9
G	Killimacat Creek	Sandstone	Bulked soil profile	1	G1
H	Killimacat Creek	Rhyolite	Bulked soil profile	1	H1
I	Chaffey Dam	Basalt	Bulked soil profile	1	I1

4.3.1. Soil equilibrium conditions

^{238}U and ^{230}Th: The ^{230}Th and ^{238}U concentrations in soil samples from sites A to F are plotted in Figure 4.2a to f. In each plot the dashed line represents secular equilibrium (^{230}Th/^{238}U = 1). The ^{230}Th/^{238}U activity ratios for the individual samples from sites G and H are presented in Table 4.2. There was no ^{238}U analysis for sample I1.

Table 4.2: Daughter/parent activity ratios for the samples collected from sites G, H and I. Uncertainties are equivalent to one standard error on the mean.

Sample	^{230}Th/^{238}U	^{226}Ra/^{238}U	^{226}Ra/^{230}Th	^{228}Ra/^{232}Th	^{228}Th/^{228}Ra
G1	1.04 ± 0.09	1.03 ± 0.09	0.99 ± 0.02	0.99 ± 0.03	1.01 ± 0.02
H1	1.00 ± 0.14	0.95 ± 0.13	0.96 ± 0.05	1.08 ± 0.10	0.92 ± 0.05
I1			0.92 ± 0.05	1.04 ± 0.05	0.98 ± 0.03

Four of the samples from site A show significant excesses of ^{238}U over ^{230}Th. An excess of ^{238}U over ^{230}Th is also evident in one of the samples from site D. In all other cases ^{238}U and ^{232}Th concentrations are within analytical uncertainty of equilibrium though there is systematic evidence of a ^{230}Th excess over ^{238}U in sites B and E.

^{226}Ra and ^{238}U: The ^{226}Ra and ^{238}U concentrations in soil samples from sites A to F are plotted in Figure 4.3a to f. Note the change of scale (from Figure 4.2a and d) in Figure 4.3a and 4.3d. The ^{226}Ra/^{238}U activity ratios have been calculated for the samples from sites G and H and are presented in Table 4.2. Concentrations of ^{226}Ra in excess of ^{238}U occur in samples from sites A, B and D. There is also systematic evidence for an excess of ^{226}Ra over ^{238}U in the samples from site C. ^{238}U concentrations in excess of ^{226}Ra occur in two of the samples from site A. In all the samples from the remaining six sites the concentrations ^{238}U and ^{226}Ra concentrations are within analytical uncertainty of equilibrium and there is no systematic evidence of disequilibrium.

^{226}Ra and ^{230}Th: Concentrations of ^{226}Ra and ^{230}Th from sites A to F are plotted in Figure 4.4 and the ^{226}Ra/^{230}Th activity ratios for the samples from sites G, H and I are in Table 4.2. Significant excesses of ^{226}Ra over its parent ^{230}Th occur in a number of samples from sites A and B, and in all but two of the samples from site D. There is also a systematic tendency for ^{226}Ra to be in excess in many samples from site C. All the samples from site A, except one, show evidence of a small excess of ^{226}Ra over ^{230}Th. In site E there is clear evidence of a ^{230}Th excess over ^{226}Ra. Figure 4.4f and the ^{226}Ra/^{230}Th activity ratios in Table 4.2 indicate that the concentrations of ^{226}Ra and ^{230}Th are within analytical uncertainty of equilibrium in the samples from sites F, G, H and I.

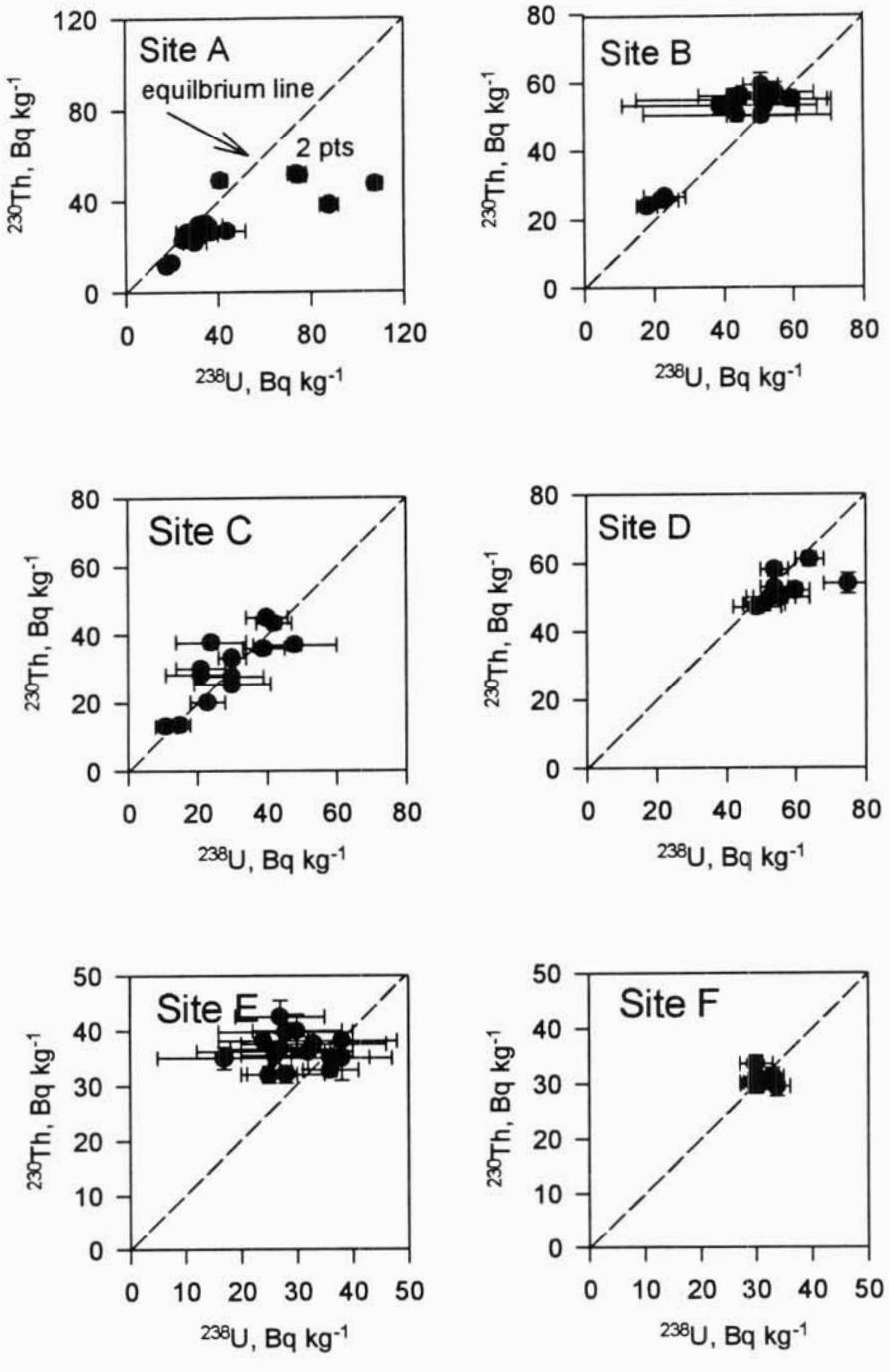

Figure 4.2: ^{230}Th to ^{238}U equilibrium plots for the soil samples from sites A to F. In each figure the dashed line represents secular equilibrium. The error bars represent the analytical uncertainty equivalent to one standard error on the mean.

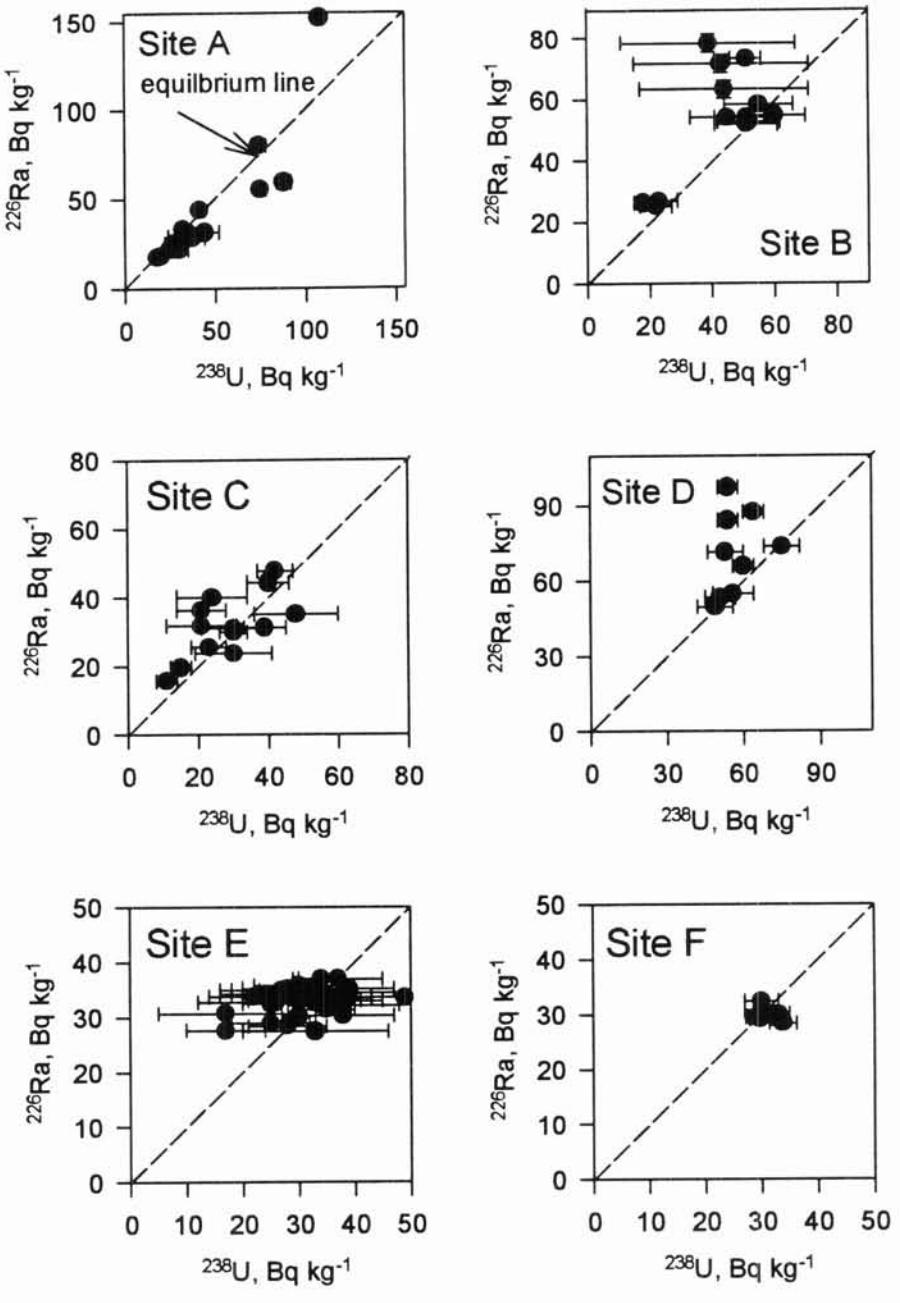

Figure 4.3: ^{226}Ra to ^{238}U equilibrium plots for the soil samples from sites A to F. In each figure the dashed line represents secular equilibrium. The error bars represent the analytical uncertainty equivalent to one standard error on the mean.

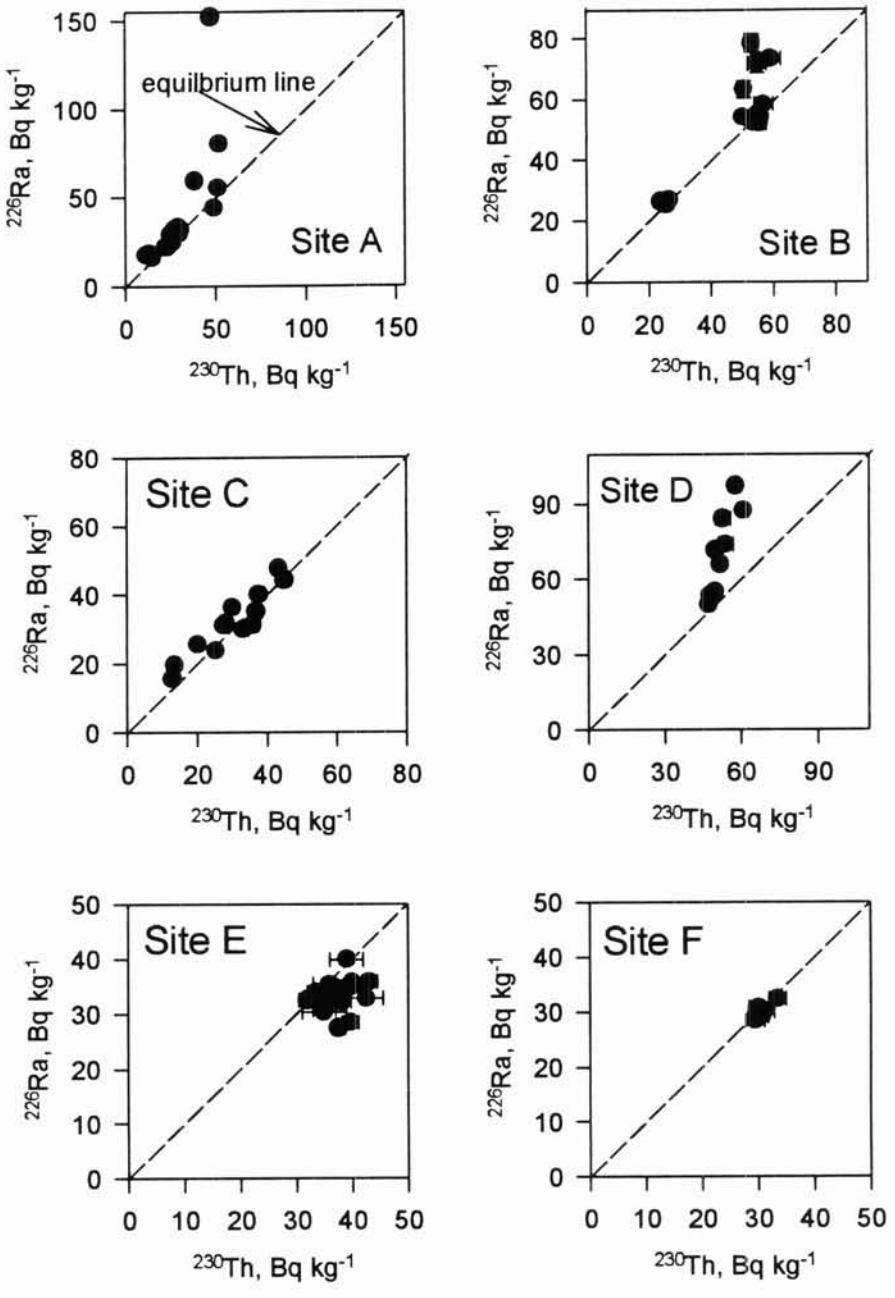

Figure 4.4: ^{226}Ra to ^{230}Th equilibrium plots for the soil samples from sites A to F. In each figure the dashed line represents secular equilibrium. The error bars represent the analytical uncertainty equivalent to one standard error on the mean, in many instances these are smaller than the symbol size.

^{228}Ra and ^{232}Th: Concentrations of ^{228}Ra are within analytical uncertainty of equilibrium with ^{232}Th concentrations at most of the sites examined [Figure 4.6 (a to f) and Table 4.2]. However, concentrations of ^{228}Ra are in excess of ^{232}Th by 24 $\pm$ 7% in one of the samples from site A, and ^{228}Ra excesses are evident in a number of samples from sites B and C.

^{228}Th and ^{228}Ra: The concentrations of ^{228}Th and ^{228}Ra in all the samples [Figure 4.6 (a to f) and Table 4.2] are with analytical uncertainty of equilibrium, although there is some sign of an excess of ^{228}Ra over ^{228}Th in two of the samples from site B.

It is clear from the above that the ^{238}U decay series is not in secular equilibrium in most of the soil samples examined. This observation of disequilibrium in the ^{238}U decay series in soils is in agreement with those of other workers [*Hansen and Stout*, 1968; *Megumi*, 1979; *Rosholt*, 1982]. As both decay chains are presumed to be in secular equilibrium in the rocks from which these soils have formed. This disequilibrium implies that nuclides in the ^{238}U decay series are being differentially redistributed during the soil forming process.

In general, because of the large uncertainties on many of the ^{238}U analyses, the ^{226}Ra to ^{230}Th equilibrium conditions were better defined. Significant excess of ^{226}Ra over ^{230}Th were observed in samples from sites A, B, and D. These ^{226}Ra excesses over ^{230}Th are plotted against Mn_2O_3 concentration in Figure 4.7. At each site there is a tendency for samples with the higher Mn_2O_3 contents to have the higher ^{226}Ra excess. This is consistent with the suggestion that the redistribution of the ^{238}U decay series radionuclides is associated with deposition of the secondary oxides. This is examined further in sections 4.3.3 and 4.3.4.

The ^{232}Th decay series was in equilibrium in most of the soil samples examined. However, there were samples in which concentrations of ^{228}Ra were clearly in excess of ^{232}Th concentrations. This suggests that ^{232}Th decay series nuclides are also being differentially mobilised within the soils. This result is somewhat surprising given the short half-life of ^{228}Ra (5.75 years) and implies that this redistribution is occurring on a time scale of <30 years. The presence of this excess has implications for dating sediment movement. This is examined later.

In summary the proposal in hypothesis 1 that "the decay series are in secular equilibrium in soils" is not supported by the evidence presented above.

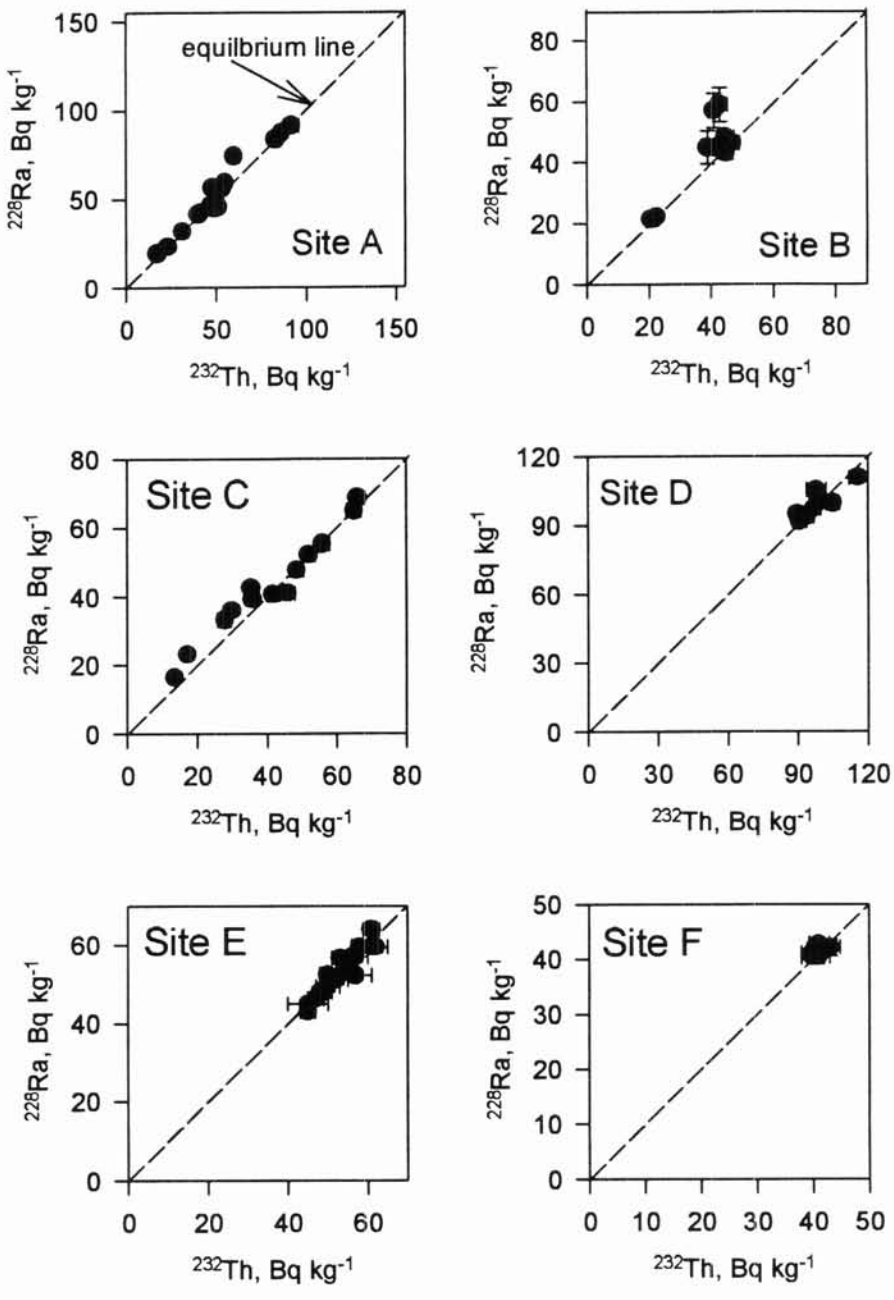

Figure 4.5: ^{228}Ra to ^{232}Th equilibrium plots for the soil samples from sites A to F. In each figure the dashed line represents secular equilibrium. The error bars represent the analytical uncertainty equivalent to one standard error on the mean, in many instances these are smaller than the symbol size.

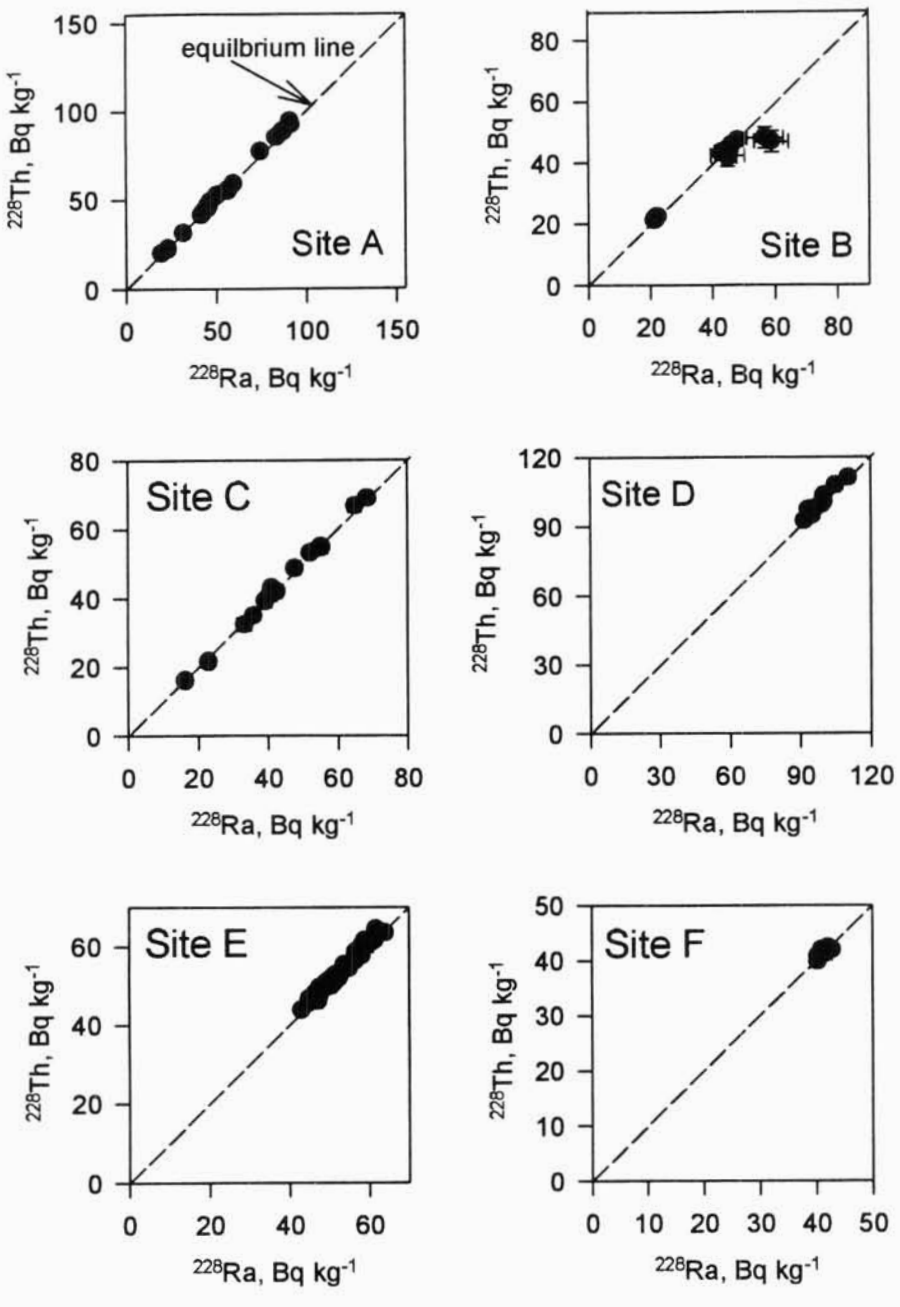

Figure 4.6: ^{228}Th to ^{228}Ra equilibrium plots for the soil samples from sites A to F. In each figure the dashed line represents secular equilibrium. The error bars represent the analytical uncertainty equivalent to one standard error on the mean, in many instances these are smaller than the symbol size.

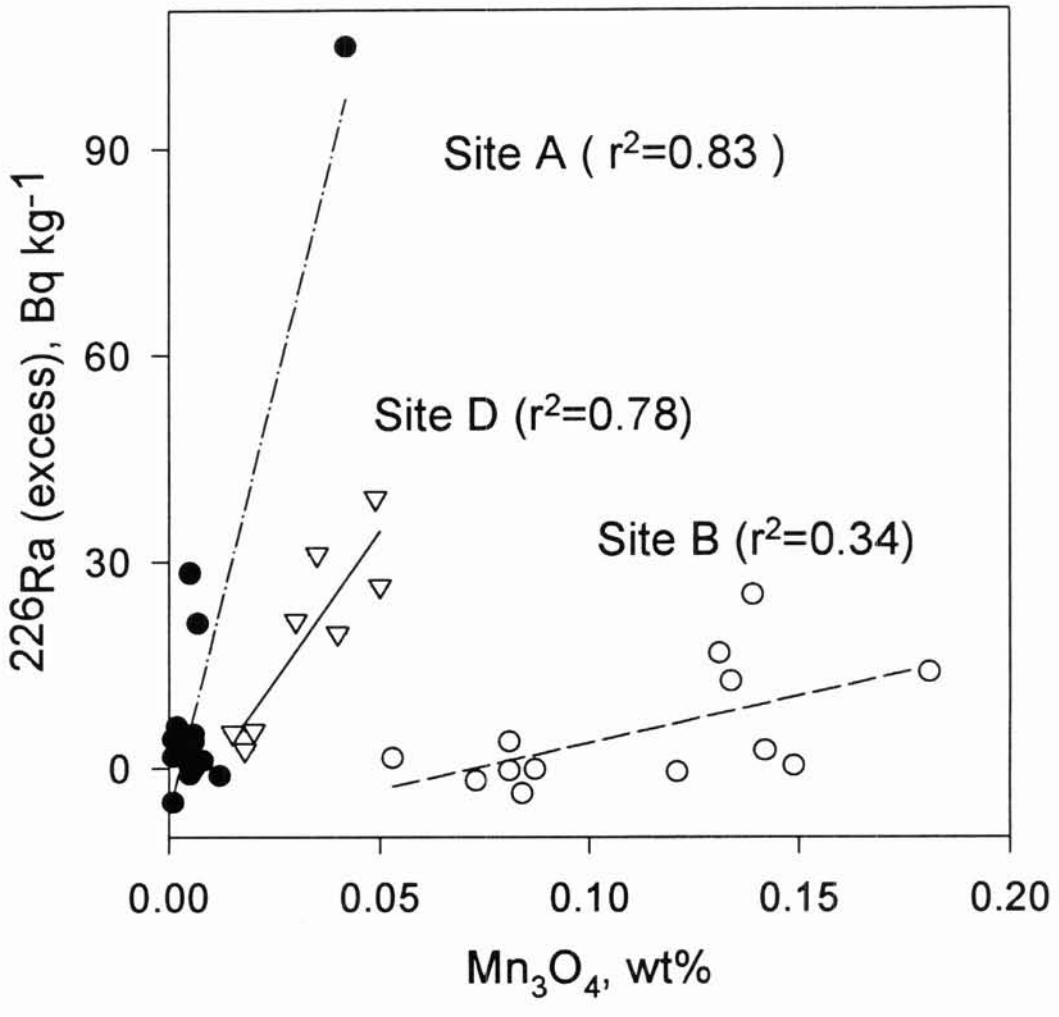

Figure 4.7: Concentrations of ^{226}Ra in excess of its parent ^{230}Th against Mn_3O_4 concentrations in soil samples from sites A, B and D. In each case the regression line and correlation coefficient is shown. The analytical uncertainty equivalent to one standard error on the mean for the calculated ^{226}Ra excess are all smaller than the symbol sizes.

4.3.2 ^{238}U and ^{232}Th decay series nuclide correlations in soils

As many of the ^{238}U analyses had large (>10%) uncertainties, the following discussion of correlations between ^{238}U and ^{232}Th decay series nuclides is confined to the relationships of ^{230}Th to ^{232}Th and ^{226}Ra to ^{232}Th. These nuclides were typically determined with random uncertainties of <3% at one standard error.

4.3.2a ^{230}Th and ^{232}Th in soils

The concentrations of ^{230}Th in the soil and rock samples are plotted against the ^{232}Th concentration for sites A to F in Figure 4.8 (a to f).

In each case the soil data (closed circles) are consistent with a single regression line passing through the origin. The data from each site represent soil material developed on a single rock type. The data therefore indicate that soils developed on a uniform rock type have a uniform $^{230}Th/^{232}Th$ ratio. The ^{230}Th and ^{232}Th data for the rock samples from each of the sample groups are all consistent with the regression line fitted through the soil data, and there is, in each case, good agreement between the ratio in the rock samples and that in the soil samples. This suggests that the $^{230}Th/^{232}Th$ ratio in the soils is likely to be inherited directly from the parent rock material

The rock and mean soil $^{230}Th/^{232}Th$ activity ratios for each of the sample groups are shown in Table 4.3.

Table 4.3 : The mean soil and parent rock $^{230}Th/^{232}Th$ ratios for each of the sample groups and the range of $^{226}Ra/^{232}Th$ ratios in the soil. Uncertainties are equivalent to one standard error on the mean.

Site	Rock type	Soil $^{230}Th/^{232}Th$	Soil $^{226}Ra/^{232}Th$	Rock $^{230}Th/^{232}Th$
A	Granite	0.571± 0.010	0.52 ± 0.02 to 1.83 ± 0.07	0.56 ± 0.06
B	Basalt	1.25 ± 0.02	1.17 ± 0.05 to 1.91 ± 0.11	1.30 ± 0.09
C	Mix sediments	0.76 ± 0.03	0.60 ± 0.02 to 1.15 ± 0.06	0.70 ± 0.03
D	Granite	0.532 ± 0.009	0.55 ± 0.02 to 0.98 ± 0.03	0.55 ± 0.04
E	Dacite	0.694 ± 0.009	0.52 ± 0.02 to 0.70 ± 0.03	0.70 ± 0.04
F	Sandstone	0.744 ± 0.003	0.73 ± 0.01	0.80 ± 0.04
G	Sandstone	0.66 ± 0.02	0.65 ± 0.01	0.64 ± 0.02
H	Rhyolite	0.95 ± 0.06	1.10 ± 0.05	0.96 ± 0.05
I	Basalt	0.91 ± 0.06	0.84 ± 0.04	0.84 ± 0.04

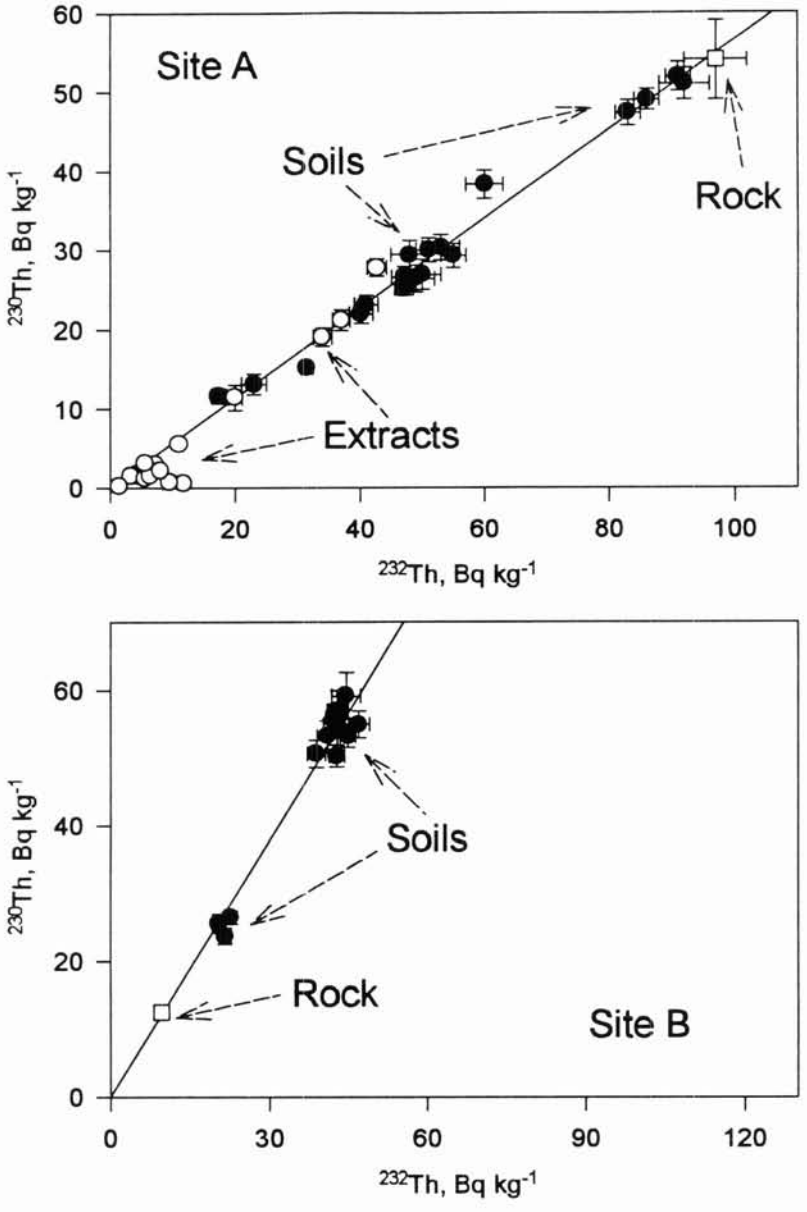

Figure 4.8 a and b: Concentrations of ^{230}Th against ^{232} Th concentrations in the rock samples (open squares) and soil samples (closed circles) from Site A (Figure 4.8a) and Site B (Figure 4.8b). Data from the Citrate-Dithionite extracts of selected soils from site A are also shown (open circles). In each figure the regression line has been fitted through the soil data and the origin. The error bars represent the analytical uncertainty equivalent to one standard error on the mean, in many cases these are smaller than the symbol size.

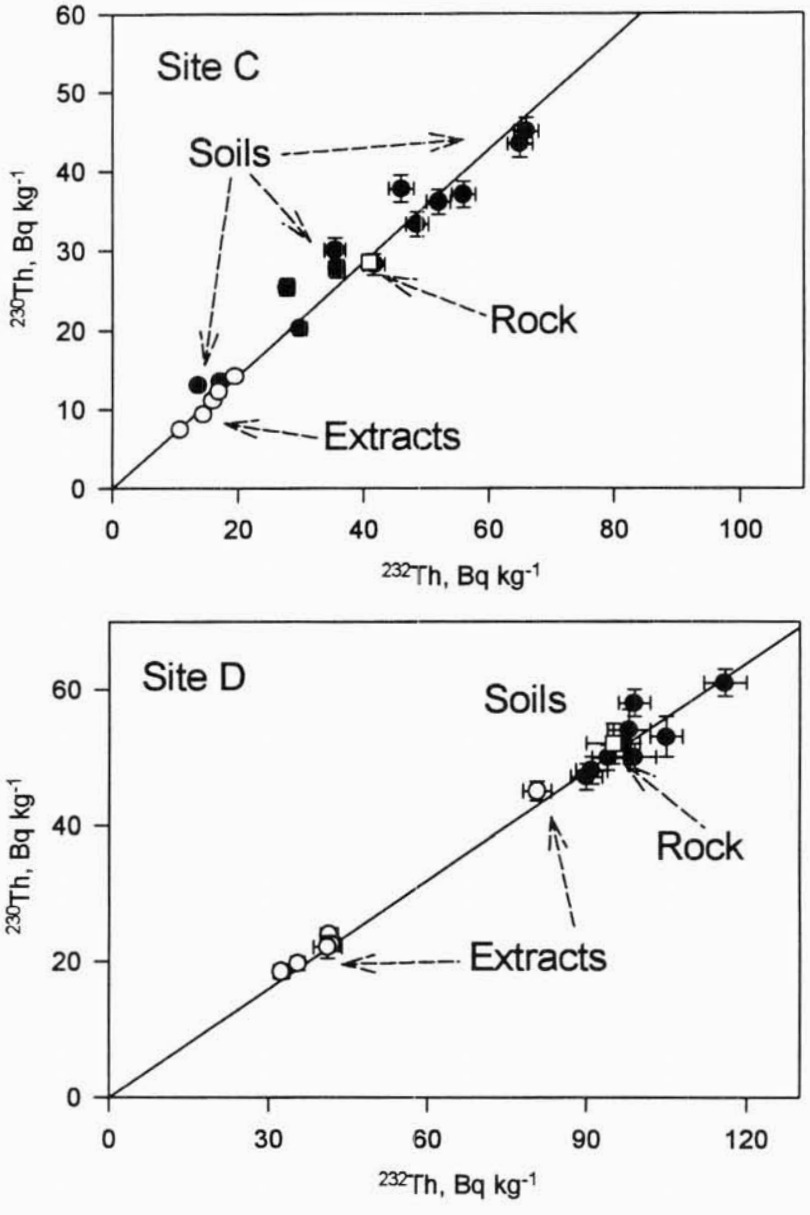

Figure 4.8 c and d: Concentrations of ^{230}Th against ^{232} Th concentrations in the rock samples (open squares), soil samples (closed circles) and in the Citrate-Dithionite extracts of selected soils (open circles) samples from Site C (Figure 4.8c) and Site D (Figure 4.8b). In each figure the regression line has been fitted through the soil data and the origin. The error bars represent the analytical uncertainty equivalent to one standard error on the mean, in many cases these are smaller than the symbol size.

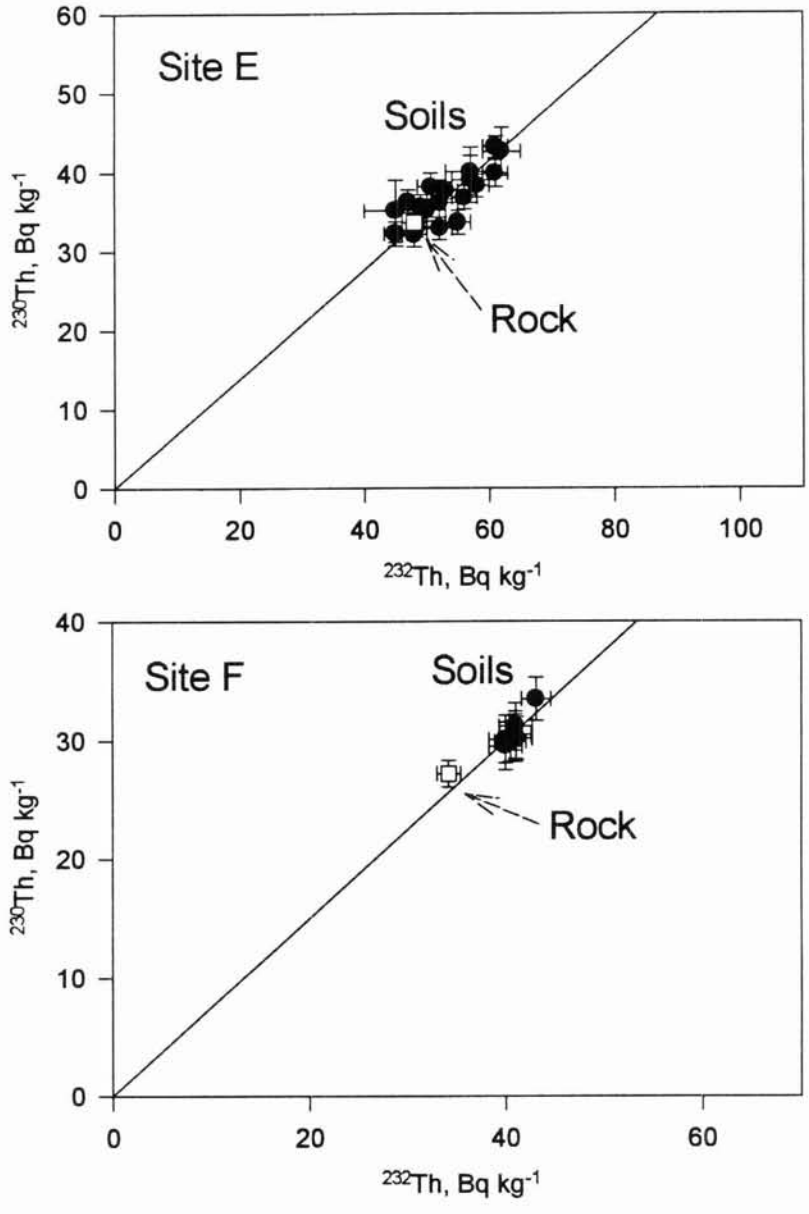

Figure 4.8 e and f: Concentrations of ^{230}Th against ^{232} Th concentrations in the rock samples (open squares) and soil samples (closed circles) from Site E (Figure 4.8e) and Site F (Figure 4.8f). In each figure the regression line has been fitted through the soil data and the origin. The error bars represent the analytical uncertainty equivalent to one standard error on the mean, in many cases these are smaller than the symbol size.

This table also includes the three rock-soil pairs from sites G, H and I. In each case the $^{230}Th/^{232}Th$ activity ratios in the soil and parent rock pairs from these three sites are also within analytical uncertainty of each other. The data in Table 4.3 show that, at all the sites studied, soils and the rock from which the soils formed have $^{230}Th/^{232}Th$ ratios within analytical uncertainty. It is therefore concluded that the lithology is the dominant factor controlling the heterogeneity of $^{230}Th/^{232}Th$ ratio in soils.

The $^{230}Th/^{232}Th$ activity ratio in the soil samples ranges from 1.25 ± 0.02 for the samples from site B to 0.532 ± 0.009 in samples from site D (Table 4.3). While soils developed for a single uniform rock type have a uniform ratio, soils developed on different rock types can have distinctive $^{230}Th/^{232}Th$ ratios, suggesting that the $^{230}Th/^{232}Th$ activity ratio may be useful in distinguishing material derived from different lithologies.

4.3.2b Correlations between ^{226}Ra and ^{232}Th

The concentrations of ^{226}Ra and ^{232}Th in the soil and rock samples from sites A to F are plotted in Figure 4.9 a to f. The regression lines from Figure 4.8 (a to f) are also shown together with the rock values. These regression lines should be equivalent to the parent rock $^{226}Ra/^{232}Th$ ratio (if secular equilibrium in the rock samples is assumed).

The ^{226}Ra and ^{232}Th data from sites A to E are, in general, more weakly correlated and are not completely consistent with the regression lines from the ^{230}Th and ^{232}Th data. The $^{226}Ra/^{232}Th$ activity ratios have been calculated for the samples from all nine sites and maximum and minimum values are shown in Table 4.3. In the samples from sites F, G, H and I the ^{238}U decay series was shown to be in secular equilibrium, consequently, there is good agreement between the soil ^{226}Ra $/^{232}Th$ and $^{230}Th/^{232}Th$ ratios at these sites. At the other sites the $^{226}Ra/^{232}Th$ ratio is highly variable and often not the same as the $^{230}Th/^{232}Th$ ratio of the rock from which the soils are derived. As it is reasonable to assume that the two decay series are in secular equilibrium in the rocks this indicates that the ^{226}Ra to ^{232}Th relationships are not directly inherited from the parent material but probably results from secondary processes (weathering).

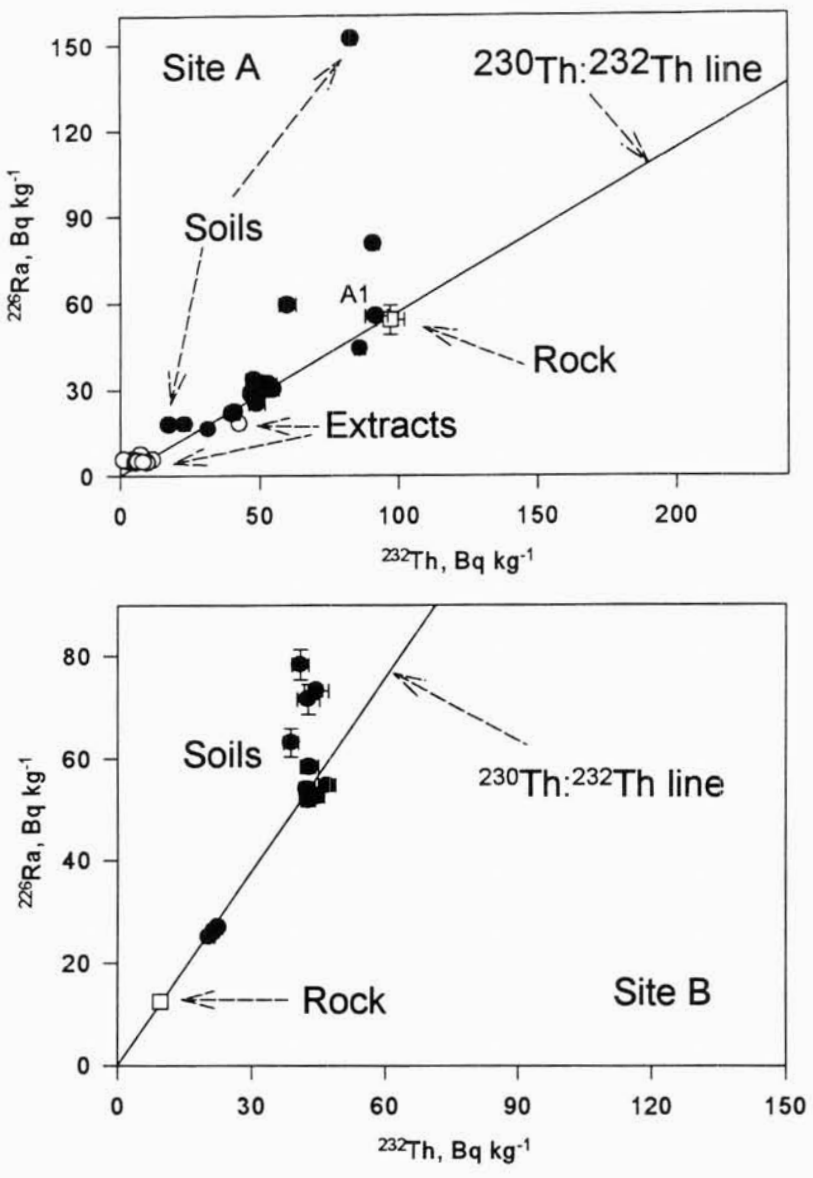

Figure 4.9 a and b: Concentrations of ^{226}Ra against ^{232} Th concentrations in the soil samples (closed circles) from Site A (Figure 4.9a) and Site B (Figure 4.9b). Data from the Citrate-Dithionite extracts of selected soils (open circles) samples from Site A are also plotted in Figure 9a. In each figure the regression line fitted through the soil thorium data and the origin is shown. Rock values (open squares) have been plotted assuming secular equilibrium. The error bars represent the analytical uncertainty equivalent to one standard error on the mean, in many cases these are smaller than the symbol size.

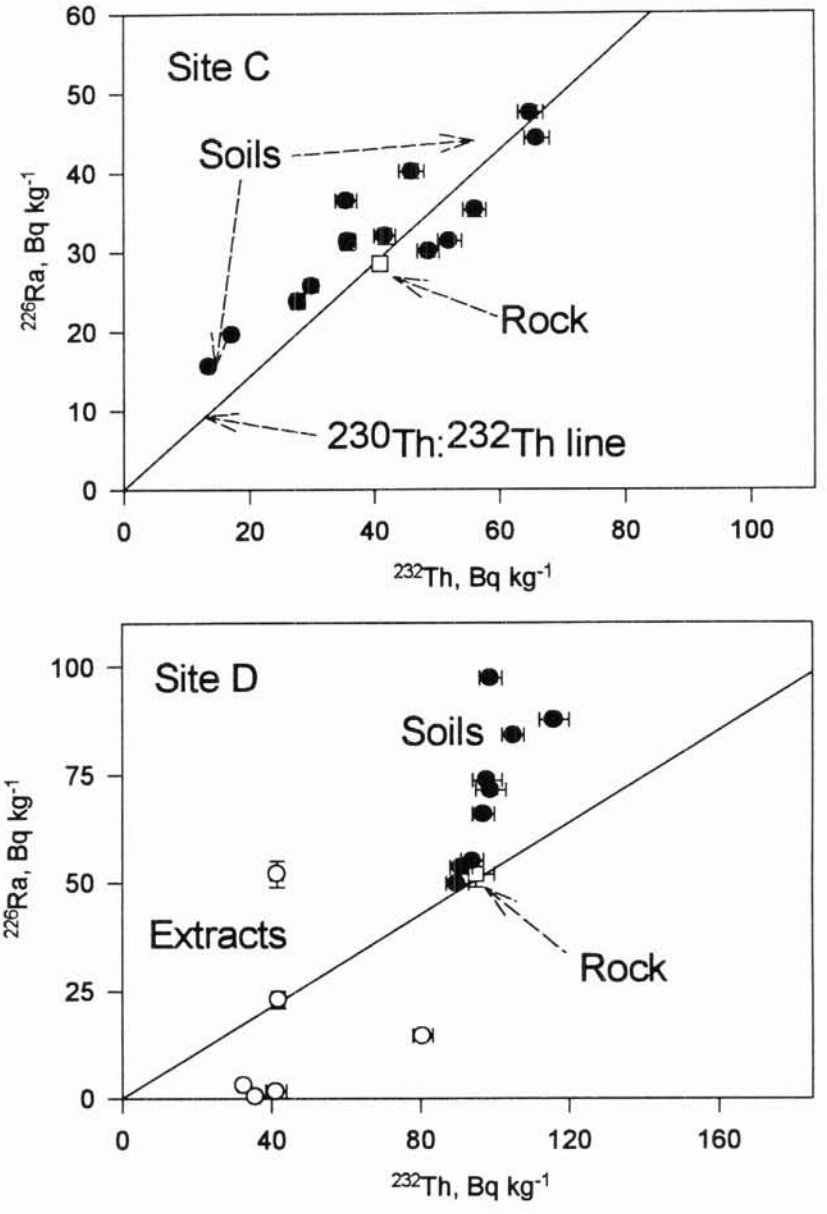

Figure 4.9 c and d: Concentrations of ^{226}Ra against ^{232}Th concentrations in the soil samples (closed circles) from Site C (Figure 4.9c) and Site D (Figure 4.9d). Data from the Citrate-Dithionite extracts of selected soils (open circles) samples from Site D are also plotted in Figure 9d. In each figure the regression line fitted through the soil thorium data and the origin is shown. Rock values (open squares) have been plotted assuming secular equilibrium. The error bars represent the analytical uncertainty equivalent to one standard error on the mean, in many cases these are smaller than the symbol size.

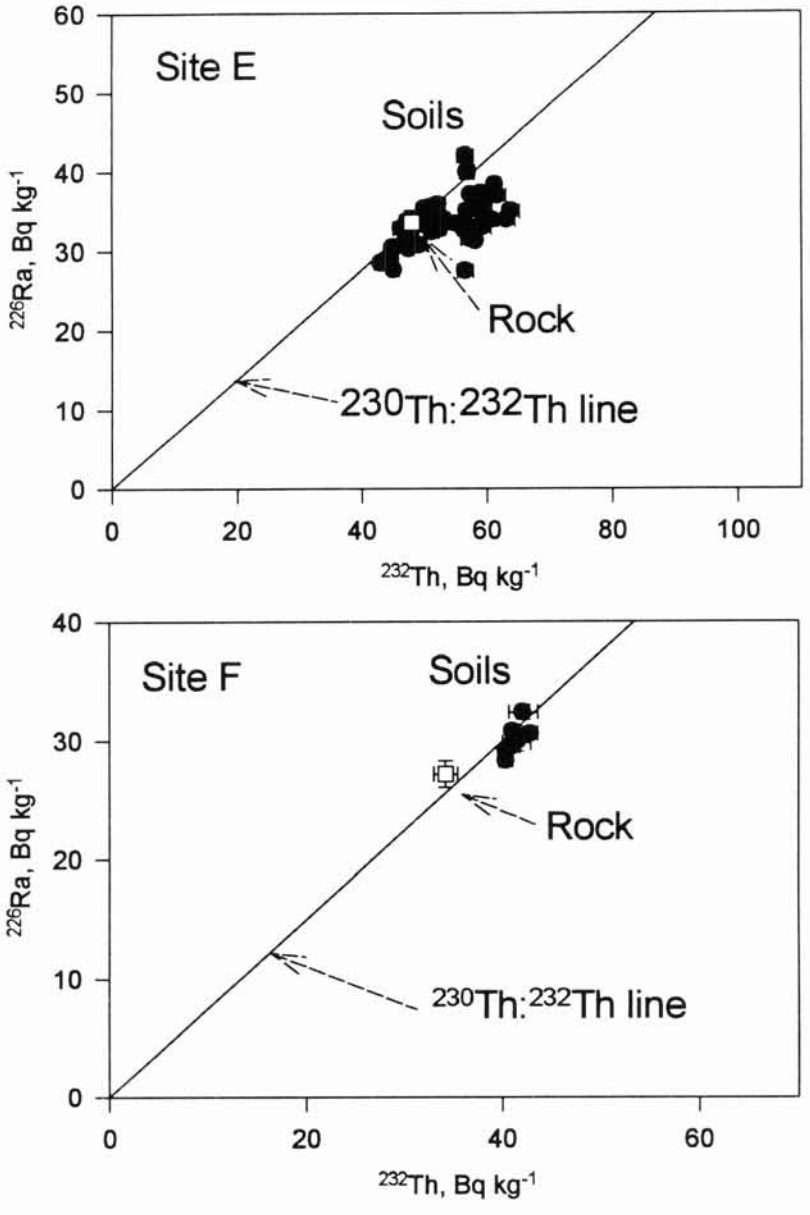

Figure 4.9 e and f: Concentrations of ^{226}Ra against ^{232}Th concentrations in the soil samples (closed circles) from Site E (Figure 4.9e) and Site F (Figure 4.9f). In each figure the regression line fitted through the soil thorium data and the origin is shown. Rock values (open squares) have been plotted assuming secular equilibrium. The error bars represent the analytical uncertainty equivalent to one standard error on the mean, in many cases these are smaller than the symbol size.

4.3.3 The effects of weathering on thorium

While the $^{230}Th/^{232}Th$ ratios in the soils are the same as those in the parent rock, the absolute concentration of these nuclides varies between the soil and rock samples. Thorium concentrations in the soil are invariably either higher or lower than those in the parent rock (see Figures 4.8a to f). This implies that thorium is being mobilised during the weathering process but that no differential mobilisation of the thorium isotopes is occurring. *Scott* [1968] also observed that extensive redistribution of thorium occurred during the weathering process with no significant fractionation of the thorium isotopes. *Sarin et al.*, [1990] also made similar observations.

The ^{230}Th and ^{232}Th concentrations in the citrate-dithionite extractions from samples from sites A, C and D (with the exception of some of the lower concentration samples from site A) are also consistent with the regression line fitted through the soil data and the origin (Figures 4.8a, c and d). This indicates that the $^{230}Th/^{232}Th$ ratio in the poorly crystalline iron and manganese oxides is the same as that in the bulk soil samples.

The secondary iron and manganese oxides (which are extracted by the citrate-dithionite solution) are formed as the result of redox reactions in the soil profile. Iron and manganese are both deposited from solution (in the groundwater) onto the soil particles. The association of up to 80% of the thorium (in the case of samples from site D) with these secondary precipitated mineral phases indicates that the thorium must also have been present in the groundwater. The concentration of thorium in solution as an ionic species is usually very low (see section 2.4.2). Transport of thorium by groundwater may involve the thorium isotopes being carried by colloids [*Short et al.*, 1988]. As the $^{230}Th/^{232}Th$ ratio in the extracts is the same as that of the bulk material this suggests that the $^{230}Th/^{232}Th$ ratio on these colloids must be the same as the parent rock material. This has been investigated at site A.

4.3.3a Transport of thorium by groundwater at Site A

Four 20L groundwater samples were collected from the downslope transect at site A (see Appendix B for details). The pH and electrical-conductivity data for the waters at the time of collection are presented in Table 4.4. The groundwaters are acid with pH ranging from 4.2 - 5.6 and have low electrical-conductivity.

Water samples were filtered through 0.45μm membrane filters. The 2L filtrate was then acidified. In one of the samples (Aw1) the concentration of dissolved colloids was

Table 4.4: Groundwater electrical-conductivity and pH at the time of sampling, Geebung Creek catchment.

	EC (mS cm^{-1})	pH
Aw1	122	4.26
Aw2	160	4.50
Aw3	171	5.60
Aw4	175	6.05

sufficiently high that these precipitated/flocculated immediately after the filtering, and prior to the acidification.

The concentrations of ^{230}Th and ^{232}Th in the water samples are plotted in Figure 4.10. The soil $^{230}Th/^{232}Th$ ratio line is also shown. The ^{230}Th and ^{232}Th concentration data for the four water samples are all consistent with the soil $^{230}Th/^{232}Th$ ratio line. The low solubility of thorium [*Langmuir and Herman,* 1980] and the precipitation/flocculation reaction which occurred after filtering of sample Aw1 (which had the highest thorium concentrations) strongly suggests that the thorium in these 0.45µm filtered waters is associated with colloids. These colloids have the same $^{230}Th/^{232}Th$ ratio as the parent rock, and so trapping of these

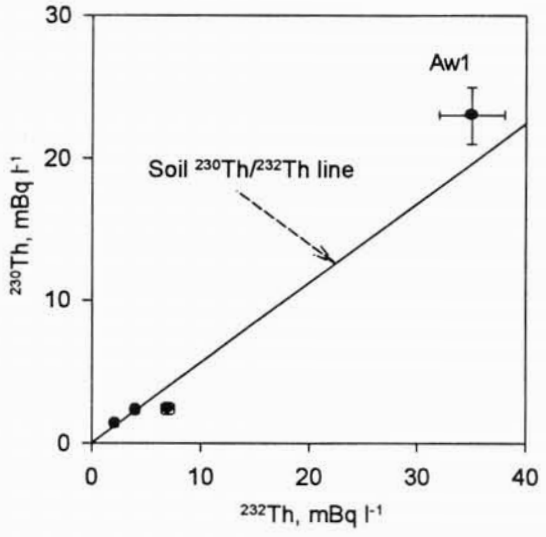

Figure 4.10: Concentrations of ^{230}Th against ^{232}Th concentrations in the groundwater samples from Site A. The line shown is the soil $^{230}Th/^{232}Th$ ratio line. The error bars represent the analytical uncertainty equivalent to one standard error on the mean.

colloids by iron and manganese oxide in the soil profile would result in the oxides having the same $^{230}Th/^{232}Th$ ratio as the parent rock, as was observed above.

4.3.4 The effects of weathering on radium

In section 4.3.1 it was shown that soil samples which had high ^{226}Ra excess over ^{230}Th were generally those which had the higher Mn_2O_3 contents. This was particularly evident for the samples from site D. The ^{226}Ra and ^{232}Th data from the citrate-dithonite extractions of soil samples from sites A and D are plotted in Figures 4.9 (a and d) respectively.

Unfortunately, none of the extracts of samples from site A which had a large ^{226}Ra excess were analysed for ^{226}Ra. The ^{226}Ra and ^{232}Th concentrations in the citrate-dithionite extractions in the other samples (A1 to A12) are generally consistent with the regression line fitted through the soil data and the origin (Figures 4.9a). This indicates that, in these samples with small excesses of ^{226}Ra, the $^{226}Ra/^{232}Th$ ratio in the secondary iron and manganese oxides is similar to that in the parent rock.

The ^{226}Ra and ^{232}Th concentrations in the citrate-dithionite extracts from the samples from Site D (Figure 4.9d) shows that with one exception more thorium was extracted than ^{226}Ra. In samples with low ^{226}Ra excess, little of the radium was extractable by the citrate-dithonite solution, even though in some cases a large fraction of the ^{230}Th was extractable. For example, in sample D1 the $^{226}Ra/^{230}Th$ ratio was 1.06 ± 0.05 indicating that these nuclides were in equilibrium in the bulk sample. However, $30 \pm 2\%$ of the ^{230}Th and only $6.0 \pm 0.6\%$ of the ^{226}Ra was extractable. This implies that these nuclides are present in very different sites on the grains. The thorium is associated with more easily reduced sites than the supported radium. Similar observations have been made by *Short et al.*, [1988] in ferricretions.

The citrate-dithonite extracted a large proportion of the excess ^{226}Ra (Figure 4.11) present in samples from site D. This confirms that the excess radium is associated with the iron and manganese secondary oxides as was suggested in section 4.3.1, and indicates that the variations in the $^{226}Ra/^{232}Th$ ratio evident in soils developed on a uniform rock type probably result from the sorbtion/co-precipitation of radium with the iron and manganese oxides.

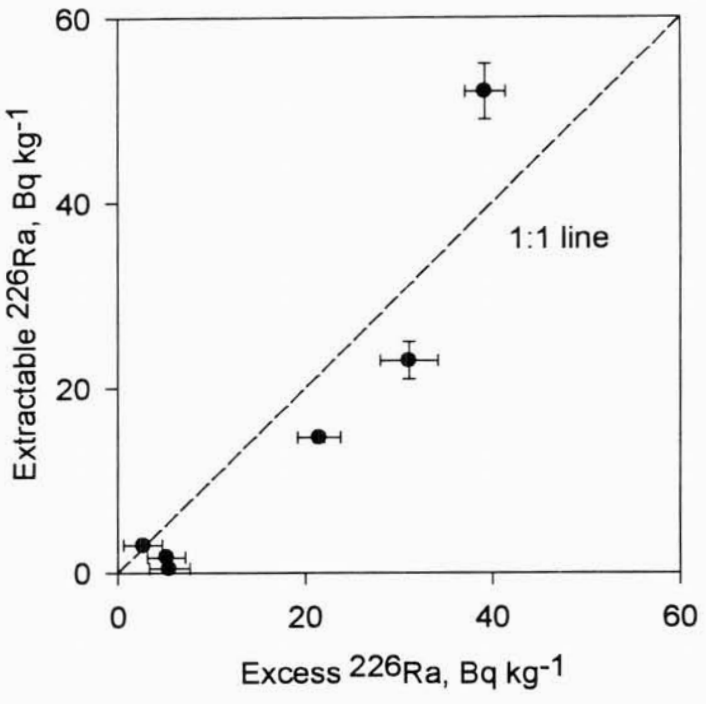

Figure 4.11: Citrate-dithionite extractable ^{226}Ra against excess ^{226}Ra in samples from site D. Error bars represent uncertainties equivalent to one standard error on the mean.

4.4 Summary

Soil and rock samples from nine sites have been studied, and the radionuclide equilibrium conditions and the relationships between the ^{238}U and ^{232}Th decay series nuclides, particularly those between ^{230}Th and ^{232}Th, and ^{226}Ra and ^{232}Th, were examined at each of the sites. It was shown that:

1. The proposal in hypothesis 1 that "the decay series are in secular equilibrium in soil material" was not supported by the evidence presented in this chapter. The ^{238}U decay series was not in secular equilibrium in most of the soil samples examined. While the ^{232}Th decay series was usually in equilibrium, concentrations of ^{228}Ra were in excess of ^{232}Th concentrations in a number of samples. As both decay chains are expected to be in secular equilibrium in the rocks from which these soils have formed, the observed disequilibrium implies that nuclides in this decay series are being redistributed during

the soil forming process. The short half-life of ^{228}Ra (5.75 years) means that in some instances this redistribution is occurring on a time scale of <30 years .

2. Soils developed on a uniform rock type have a uniform $^{230}Th/^{232}Th$ ratio. This ratio may vary from one rock type to another and so soils developed from different rock types can have distinctive $^{230}Th/^{232}Th$ ratios. It is concluded that the lithology is probably the dominant factor controlling the heterogeneity of $^{230}Th/^{232}Th$ ratio across the landscape.

3. The $^{226}Ra/^{232}Th$ ratio in soils was found to be highly variable and typically not the same as the $^{230}Th/^{232}Th$ ratio of the rock from which the soils were derived. As it is reasonable to assume that the two decay series are in secular equilibrium in the rocks this indicates that the ^{226}Ra to ^{232}Th relationships are not directly inherited from the parent material but probably result from secondary processes (weathering).

4. While the $^{230}Th/^{232}Th$ ratios in the soils were the same as the parent rock ratio, absolute concentration of these nuclides varied between the soils and rock samples. This implies that thorium is being mobilised during the weathering process but that no differential mobilisation of the isotopes is occurring. Citrate-dithionite extraction showed that a large proportion (up to 80%) of the thorium may be associated with the secondary iron and manganese oxides. Iron and manganese are both deposited from solution (in the groundwater) on to the soil particles. The association of the thorium with these secondary precipitated mineral phases indicates that the thorium must also have been present in the groundwater. The concentration of thorium in solution as ionic species are usually very low and it is suggested that colloid transport of the thorium was probably the dominant mechanism. As the $^{230}Th/^{232}Th$ ratio in the extracts was mainly the same as that of the bulk material this suggests that the $^{230}Th/^{232}Th$ ratio on these colloids must be the same as the parent rock material. This was shown by direct measurement to be the case at site A.

5. Soil samples which had high ^{226}Ra excess over ^{230}Th were generally those which had the higher Mn_2O_3 content. This was particularly evident for the samples from site D. Citrate-dithionite extracted a large proportion of the excess ^{226}Ra present in samples from this site. This indicates that the excess radium was predominantly associated with

the iron and manganese secondary oxides and that the variations in the $^{226}Ra/^{232}Th$ ratio, evident in soils developed from a uniform rock type, may result from the deposition of radium in association with the iron and manganese oxides in excess of its parent ^{230}Th.

Chapter 5: The Effects of Fluvial Processes on ^{238}U and ^{232}Th Decay Series Nuclides

In the previous chapter the links between the rock and soil compartments in the erosion cycle were investigated. It was shown that the $^{230}Th/^{232}Th$ activity ratio of soils developed from a uniform rock type were the same as the $^{230}Th/^{232}Th$ ratio of the parent rock. The $^{226}Ra/^{232}Th$ ratio was found to be more variable and commonly not the same as the rock ratio. The variability of the $^{226}Ra/^{232}Th$ ratio in soils was in general due to the presence of an excess of ^{226}Ra over its parent ^{230}Th. This excess was considered to be primarily associated with the secondary iron-manganese oxides. This chapter investigates the effects of fluvial transport, defined here as the movement of material by water, on the radionuclide concentrations and correlations present in soil, in order to develop an understanding of the links between the soil and sediment compartments in the erosion cycle.

5.1 Fluvial Transport

Fluvial transport produces changes in the characteristics of the material being transported (Figure 5.1). In general, the average size of particles decrease, while the degree of sorting and the average roundness increase with distance travelled. These changes result from a combination of selective transportation and particle abrasion [*Krumbein and Sloss*, 1963; *Moss et al.*, 1973]. These processes act over the entire landscape; overland flow and rivers transport solids by the same mechanisms [*Moss and Walker,* 1978]. For simplification all of these processes will be considered to be fluvial in the remainder of this thesis.

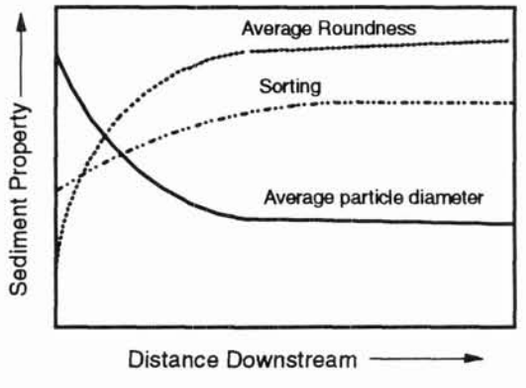

Figure 5.1: Diagram showing changes in the average size of particles, degree of sorting and the average roundness with distance travelled (after *Krumbein and Sloss*, 1963).

Krumbein and Sloss [1963] suggest that selective transportation is the most important mechanism by which these changes occur, with grain abrasion perhaps contributing only about 10%. Selective transportation result in the separation of sediment grains by particle size, shape and density. Of these three sorting parameters particle size is considered to be the most important.

In this chapter the effects of fluvial transport on the nuclide concentrations and correlations present in soils have been investigated by measuring radionuclide concentrations in artificially sorted (by both particle size and by density) and abraded soil material from the sites discussed in Chapter 4. At the end of the chapter radionuclide concentrations in sediments derived from fluvial transport of soil material are compared to those produced by artificial sorting of soil from the same site.

5.2 Samples and Sample Treatment

5.2.1 Particle size sorting

A subsample of selected samples from each of the sites (except site E) examined in Chapter 4 was separated into various size fractions by wet sieving (Section 3.3.4b). The details of the samples used in this part of the study and the fractions analyses are presented in Table 5.1. All of the particles size fractions were analysed by gamma spectrometry (Section 3.3.1.a) and all the particle size fractions from at least one sample from each site were analysed by alpha spectrometry (Section 3.3.1b).

5.2.2 Sorting by density

The effects of sorting by density were investigated by examining radionuclide concentrations in the heavy mineral fraction from selected soil samples (A13, A18, B12 C13, D1, D9, F8, and H1). Separation was done at a density of 2.95g cm^{-3} (Section 3.3.4a). This separates the primary and secondary heavy minerals from the major soil minerals (quartz, feldspar and clay). This separation produces the most marked contrast in mineralogy and consequently any effects of density sorting on the lithogenic radionuclides should be apparent in the fractions produced by this separation.

All of the density separates were analysed by alpha spectrometry for thorium isotopes. Concentrations of ^{226}Ra were determined by alpha spectrometry in samples A13(1) and A18, all other ^{226}Ra analyses were done by gamma spectrometry. The mineralogy of the heavy

Table 5.1: Details of samples used to determine the effects of sorting by particle size on ^{238}U and ^{232}Th decay series nuclides.

Site	Sample Code	Size Fractions Separated
A	A1, A18	<63μm, 63 - 125μm, 125-250μm, 250-500μm, 0.5-1.4mm, 1.4-2.0mm and >2mm.
	A13, A16	<38μm, 38 - 63μm, 63 - 125μm, 125-250μm, 250-500μm, 0.5-1.4mm, 1.4-2.0mm >2mm.
B	B8 to B13	<63μm, 63-250μm, 250-500μm, 0.5-1.4mm, 1.4-2.0mm, >2mm.
C	C13	<63μm, 63 - 125μm, 125-250μm, 250-500μm, > 0.5mm.
D	D1	<63μm, 63 - 125μm, 125-250mm, 250-500μm, > 0.5mm.
	D9	<38μm, 250-500μm, 0.5-1.4mm, 1.4-2.0mm, >2mm.
F	F8	<63μm, 63 - 125μm, 125-250mm, 250-500μm, > 0.5mm.
G	G1	<2μm, 2-63μm, 63 - 125μm, 125-250μm, 250-500μm, > 0.5mm.
H	H1	<2μm, 63 - 125μm, 125-250μm, 250-500μm, > 0.5mm.
I	I1	2-10μm, 10-20μm, 20-38mm, 38-63μm, 63 - 125μm, 125-250mm, 250-500mm, >0.5mm.

mineral separates was determined by a combination of XRD and microscopy examination (Section 3.3.3).

5.2.3 Grain abrasion

Three contrasting soil samples were used to examine the effects of grain abrasion on radionuclide concentrations;

Sample A1: a quartz-rich granitic soil which showed little evidence of the development of secondary iron oxides, and consisted predominantly of quartz and feldspar.

Sample D9: This is also a granitic soil but shows significant iron oxide formation evident in the presence of iron-manganese concretions. Sample mineralogy consists of clay, quartz, feldspar and secondary Fe-Mn oxides.

Sample I1: Fine grained basaltic soil which consisted mainly of clay and iron oxides.

The samples were first wet sieved to remove the <38 μm fraction. This fraction is normally separated from the bulk material during the initial stages of fluvial transport and is mainly carried in suspension, consequently it is probably not subjected to significant abrasion effects. The samples minus the <38μm fraction were then abraded (as described in Section

3.3.4c). The abraded sample was then wet sieved and the <38μm fraction was again separated; as there was no <38μm material in the samples prior to abrasion this fraction must have been produced by the abrasion of the coarser grains. The <38μm and >38μm fractions produced by the abrasion were analysed by both alpha spectrometry and gamma spectrometry. Particle size distribution both before and after abrasion were determined by wet sieving of subsamples of the bulk material.

5.2.4 Comparison of the effects of fluvial transport and artificial mixing and sorting

Sediment was detached and transported from a 12m x 12m plot at site F (described in Appendix B) by artificial rainfall of controlled distribution and intensity, both suspended and bedload sediment samples were collected. The radionuclide data from these fluvial sorted sediments were then compared to those of the particle size and density fractions from Sample F8. (Sample F8 consists of 20 subsamples collected from 1cm deep 20 x 20 cm surface scrapes from within the 12m x 12m area.)

Run-off from the site was directed by means of plastic lined channels through a discharge measuring flume into a plastic pond. Water from the pond was then pumped into a continuous flow centrifuge (Alpha-Laval, model no. MAB103b) (from now on referred to as CFC). In this way, sediment of particle size greater than about 1μm was collected from the water. A total of 18 samples were collected over a period of 260 minutes. Samples were prepared by oven drying at 50°C. The sample size was generally small (<10g) and all of the material was used for analysis by gamma spectrometry. A total of three coarse grained samples were collected at the end of the run from sediment fans developing in front of the flume. These were bulked into 1 sample and subsamples of this were prepared for analysis as above.

5.3 Results and Discussion

The following sections examine the radionuclide concentrations in soil fractions produced by:

(i) sorting by particle size

(ii) sorting by density

(iii) grain abrasion followed by sorting by particle size

in order to determine the relationships between ^{238}U and ^{232}Th decay series nuclides likely to be present in sediments derived from soils from the various sites. The correlations and concentration ranges produced by artificial sorting are then compared to those produced by fluvial transportation at site F.

5.3.1 The effects of sorting by particle size

The gamma and alpha spectrometry analyses of the particle size fractions are presented in Appendix C, Table C4. The XRF analyses of selected samples are presented in Appendix D.

5.3.1a ^{230}Th and ^{232}Th

The ^{230}Th and ^{232}Th concentrations in the various size fractions from soils from site A are plotted against median particle size in Figures 5.2 (a) and (b). The ^{230}Th concentrations are plotted against ^{232}Th concentrations in these fractions in Figure 5.2c. This is repeated for sites B to I (except E) in Figures 5.3 to 5.9. In each of the ^{230}Th to ^{232}Th figure, the rock $^{230}Th/^{232}Th$ ratio line is shown (solid line) together with the 66% (1σ) confidence limits (dashed lines). The data from each site are discussed in turn.

Site A (bedrock = granite): The concentrations of ^{230}Th and ^{232}Th in the various size fractions from the samples from site A vary markedly with particle size, the finer fractions having the higher concentrations (Figures 5.2 a and b). The ^{230}Th and ^{232}Th data in these various particle size fractions are all consistent with the rock $^{230}Th/^{232}Th$ line with all the data lying within the 66% confidence limits. The data spread along the line in order of particle size.

Site B (basalt): There is not a strong dependence in the concentration of ^{230}Th or ^{232}Th on particle size in this basaltic soil sample [Figure 5.3 (a) and (b)] and the >2mm fraction has the highest ^{230}Th and ^{232}Th concentration. The data are however all consistent with the rock $^{230}Th/^{232}Th$ line (within 2 σ) [Figure 5.3c].

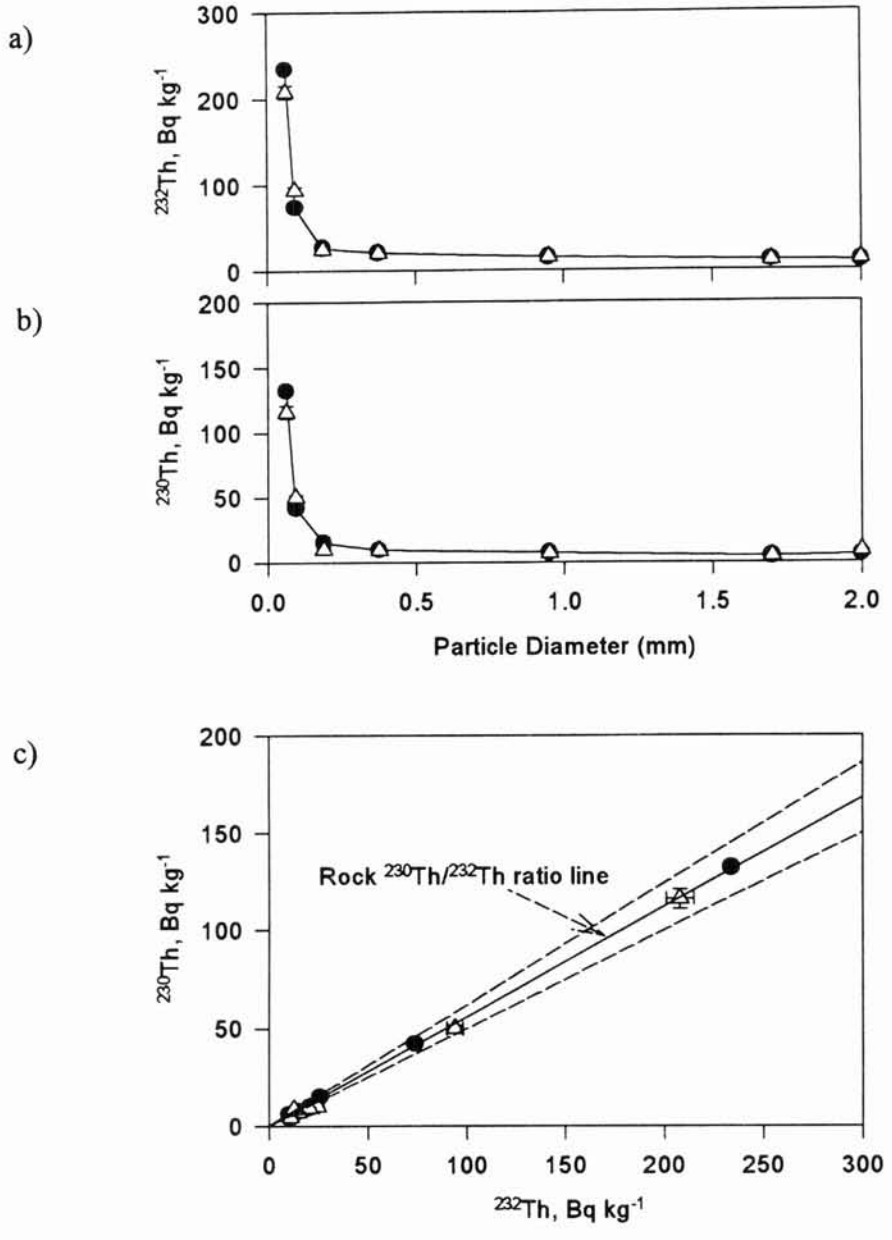

Figure 5.2: Concentrations of ^{230}Th (a) and ^{232}Th (b) against median particle size in the fractions from soil samples A1 (closed circles) and A18 (open triangles). Concentrations of ^{230}Th against ^{232}Th (c) in the various particle size fractions. The solid line represents the rock ^{230}Th/^{232}Th ratio and the dashed lines are the 66% confidence limits on this ratio. The error bars represent the analytical uncertainty equivalent to one standard error on the mean, in many cases these are smaller than the symbol size.

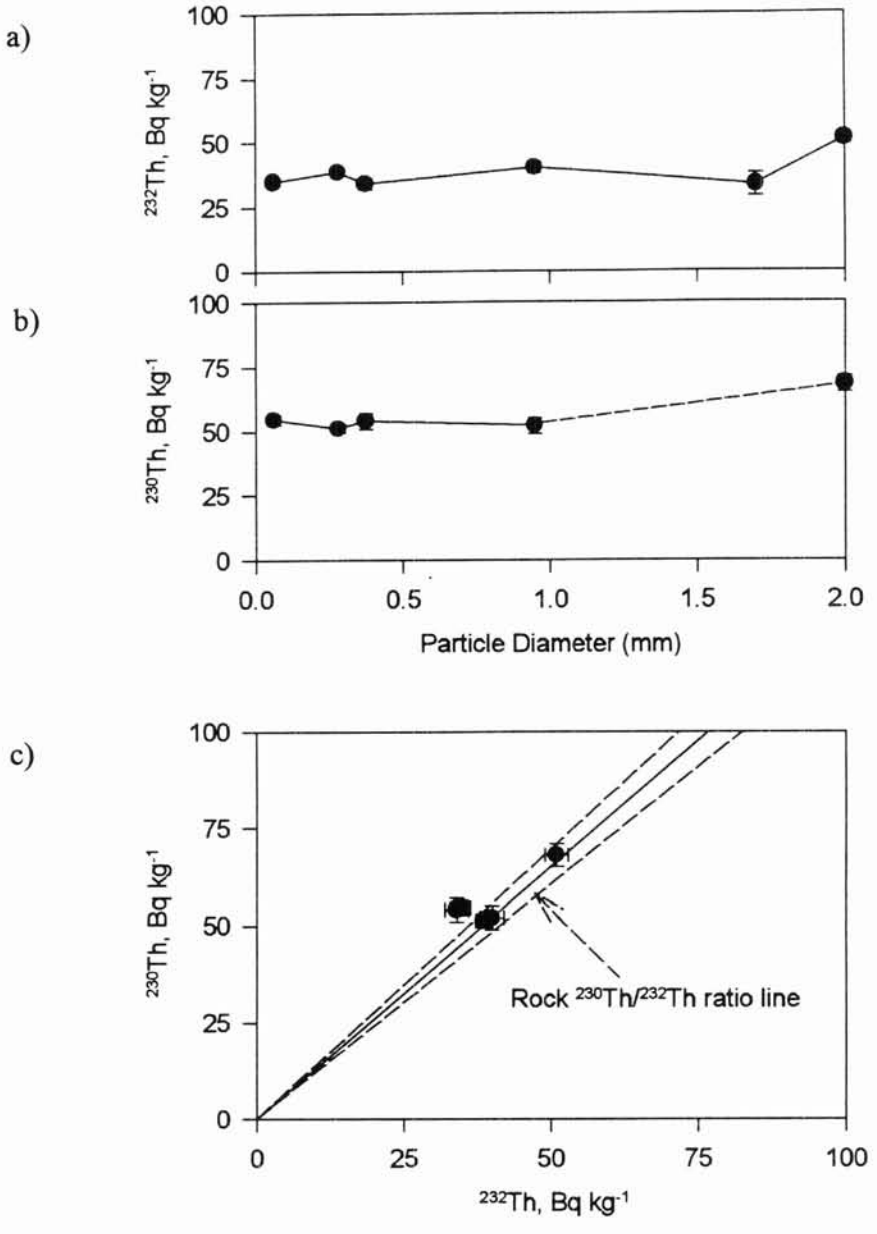

Figure 5.3: Concentrations of ^{230}Th (a) and ^{232}Th (b) against median particle size in the fractions from soil sample B13. Concentrations of ^{230}Th against ^{232}Th (c) in the various particle size fractions. The solid line represents the rock ^{230}Th/^{232}Th ratio and the dashed lines are the 66% confidence limits on this ratio. The error bars represent the analytical uncertainty equivalent to one standard error on the mean, in many cases these are smaller than the symbol size.

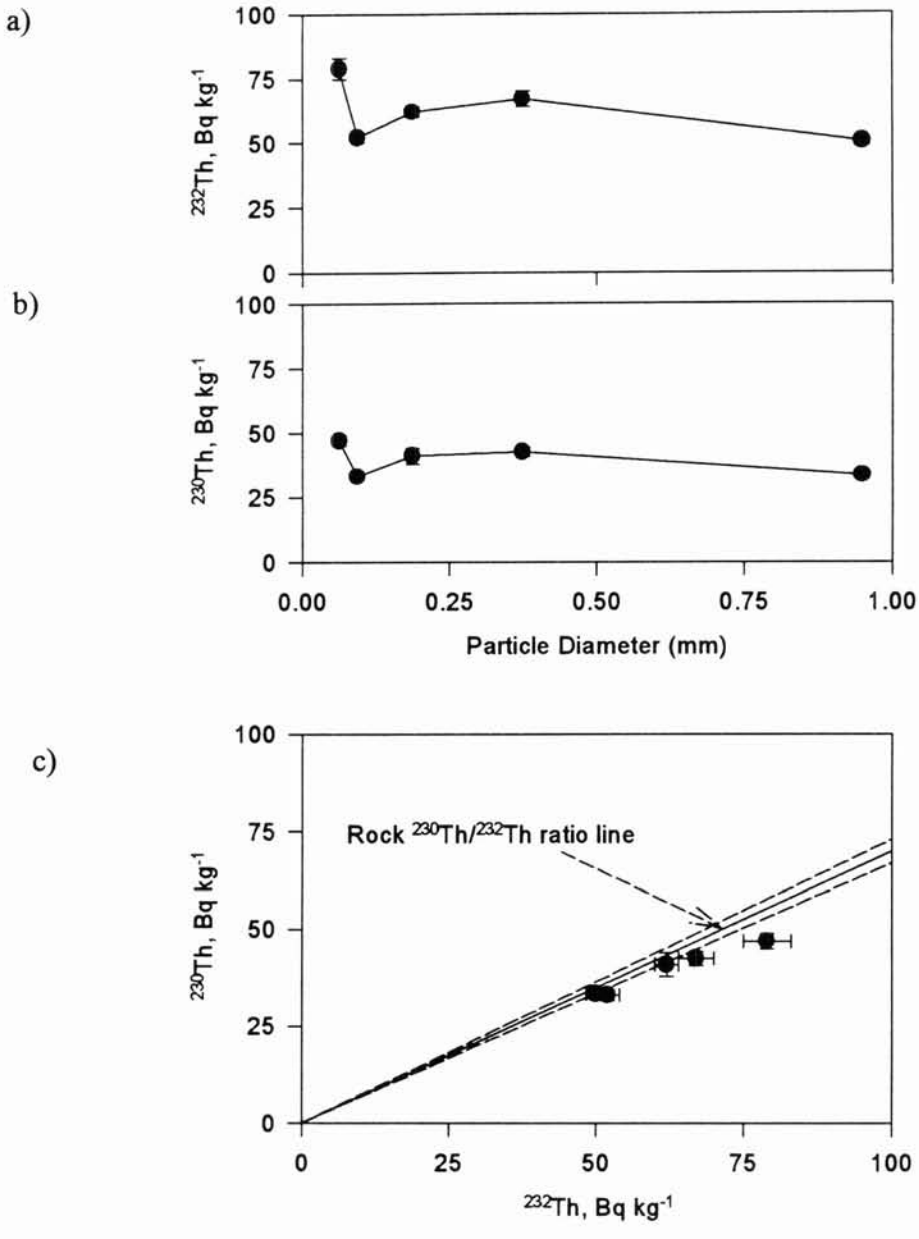

Figure 5.4: Concentrations of ^{230}Th (a) and ^{232}Th (b) against median particle size in the fractions from soil sample C13. Concentrations of ^{230}Th against ^{232}Th (c) in the various particle size fractions. The solid line represents the rock ^{230}Th/^{232}Th ratio and the dashed lines are the 66% confidence limits on this ratio. The error bars represent the analytical uncertainty equivalent to one standard error on the mean, in many cases these are smaller than the symbol size.

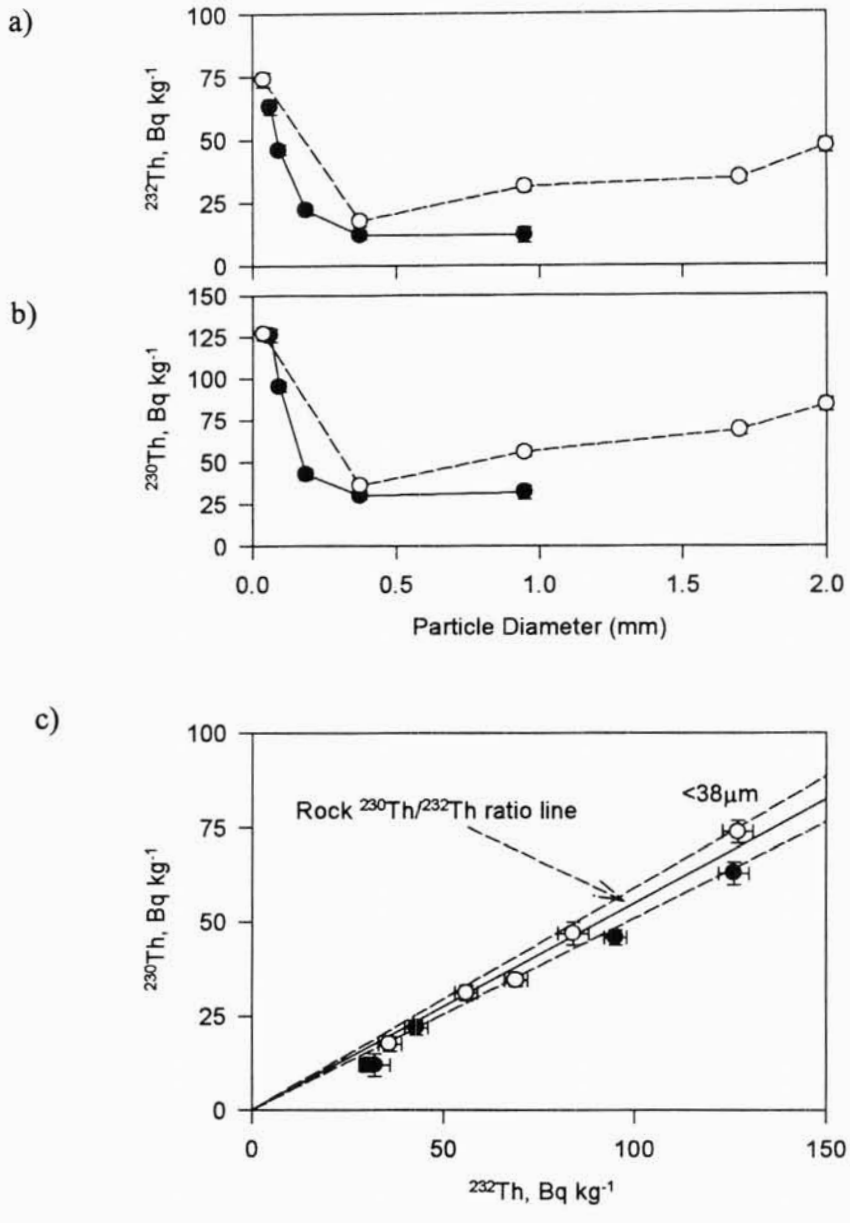

Figure 5.5: Concentrations of ^{230}Th (a) and ^{232}Th (b) against particle size in the fractions from soil samples D1 (closed circles) and D9 (open circles). Concentrations of ^{230}Th against ^{232}Th (c) in the various particle size fractions. The solid line represents the rock ^{230}Th/^{232}Th ratio and the dashed lines are the 66% confidence limits on this ratio. The error bars represent the analytical uncertainty equivalent to one standard error on the mean, in many cases these are smaller than the symbol size.

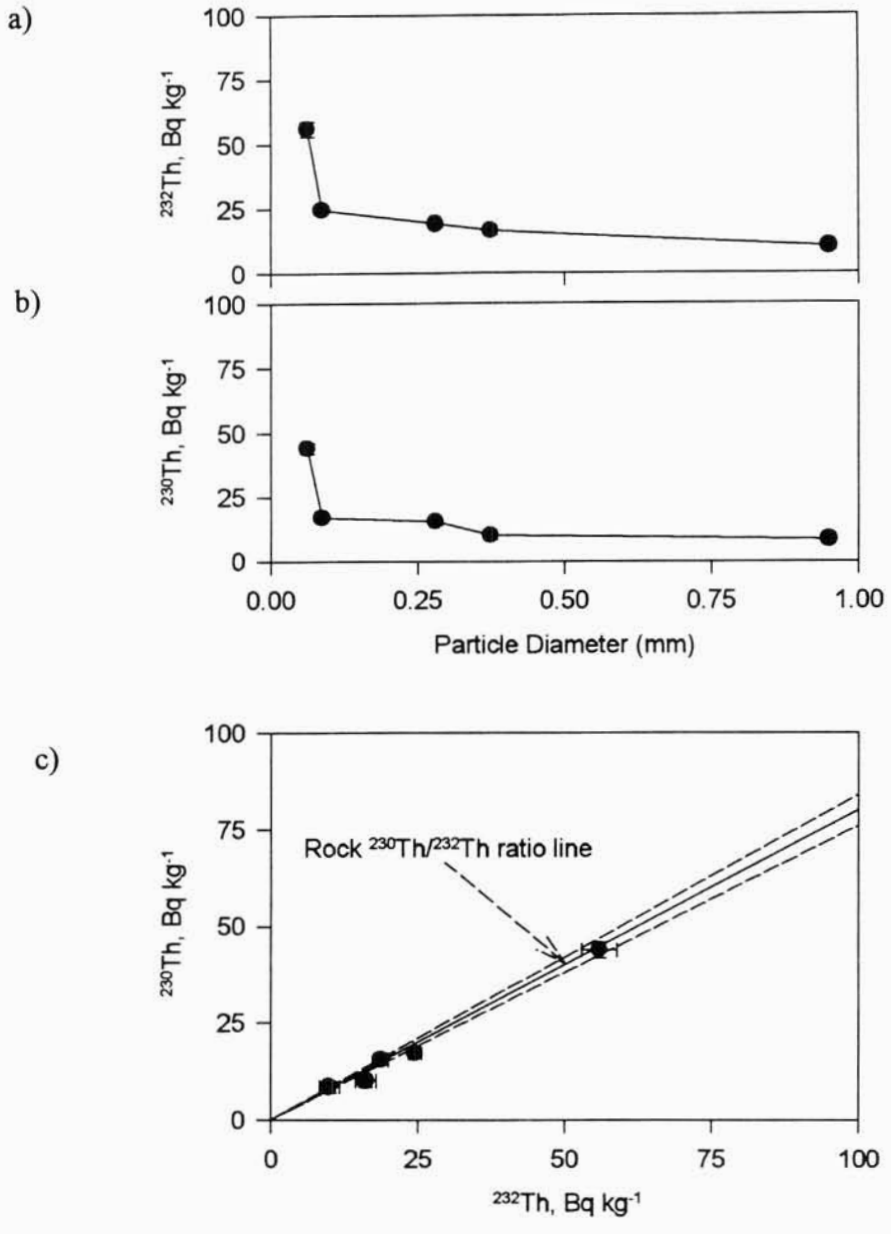

Figure 5.6: Concentrations of ^{230}Th (a) and ^{232}Th (b) against particle size in the fractions from soil sample F8. Concentrations of ^{230}Th against ^{232}Th (c) in the various particle size fractions. The solid line represents the rock ^{230}Th/^{232}Th ratio and the dashed lines are the 66% confidence limits on this ratio. The error bars represent the analytical uncertainty equivalent to one standard error on the mean, in many cases these are smaller than the symbol size.

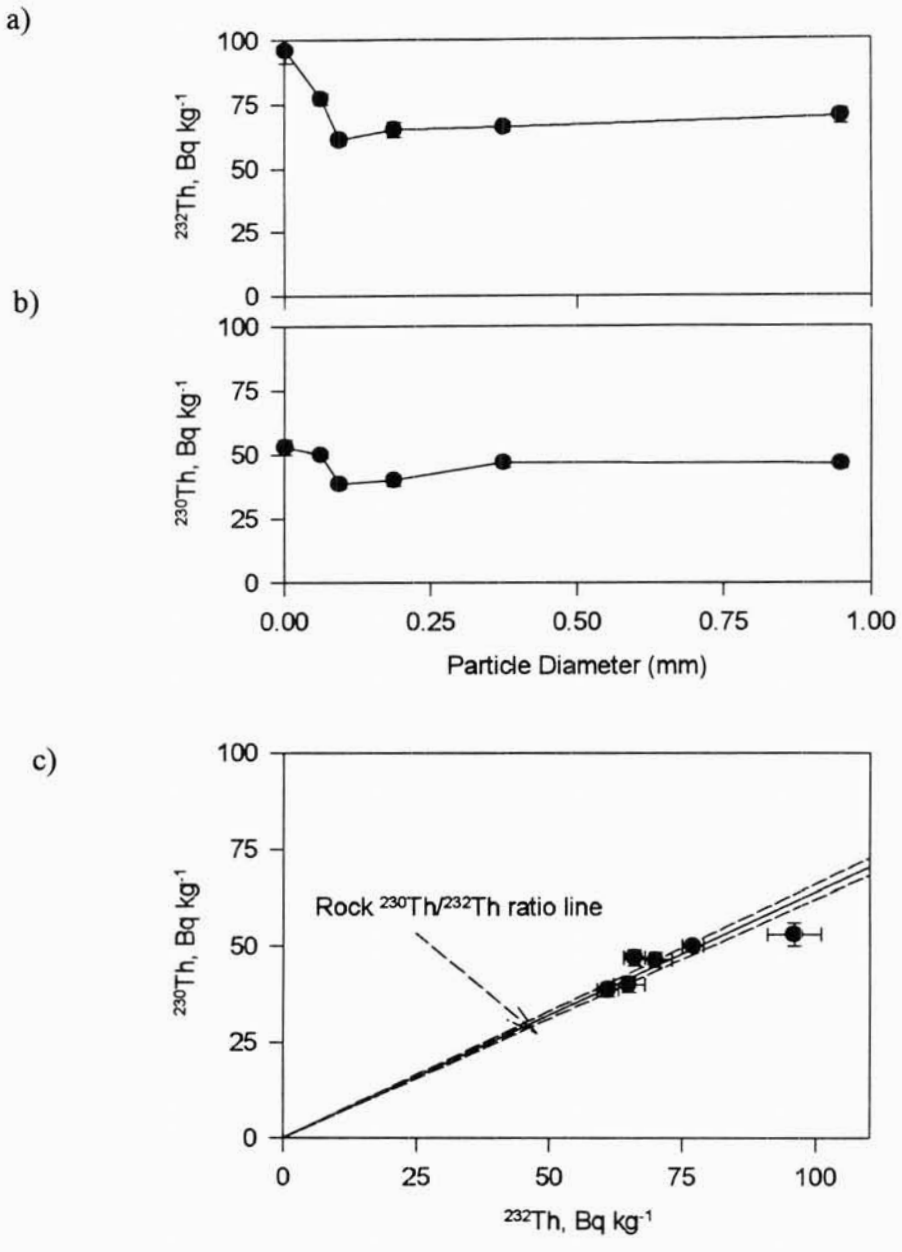

Figure 5.7: Concentrations of ^{230}Th (a) and ^{232}Th (b) against median particle size in the fractions from soil sample G1. Concentrations of ^{230}Th against ^{232}Th (c) in the various particle size fractions. The solid line represents the rock ^{230}Th/^{232}Th ratio and the dashed lines are the 66% confidence limits on this ratio. The error bars represent the analytical uncertainty equivalent to one standard error on the mean, in many cases these are smaller than the symbol size.

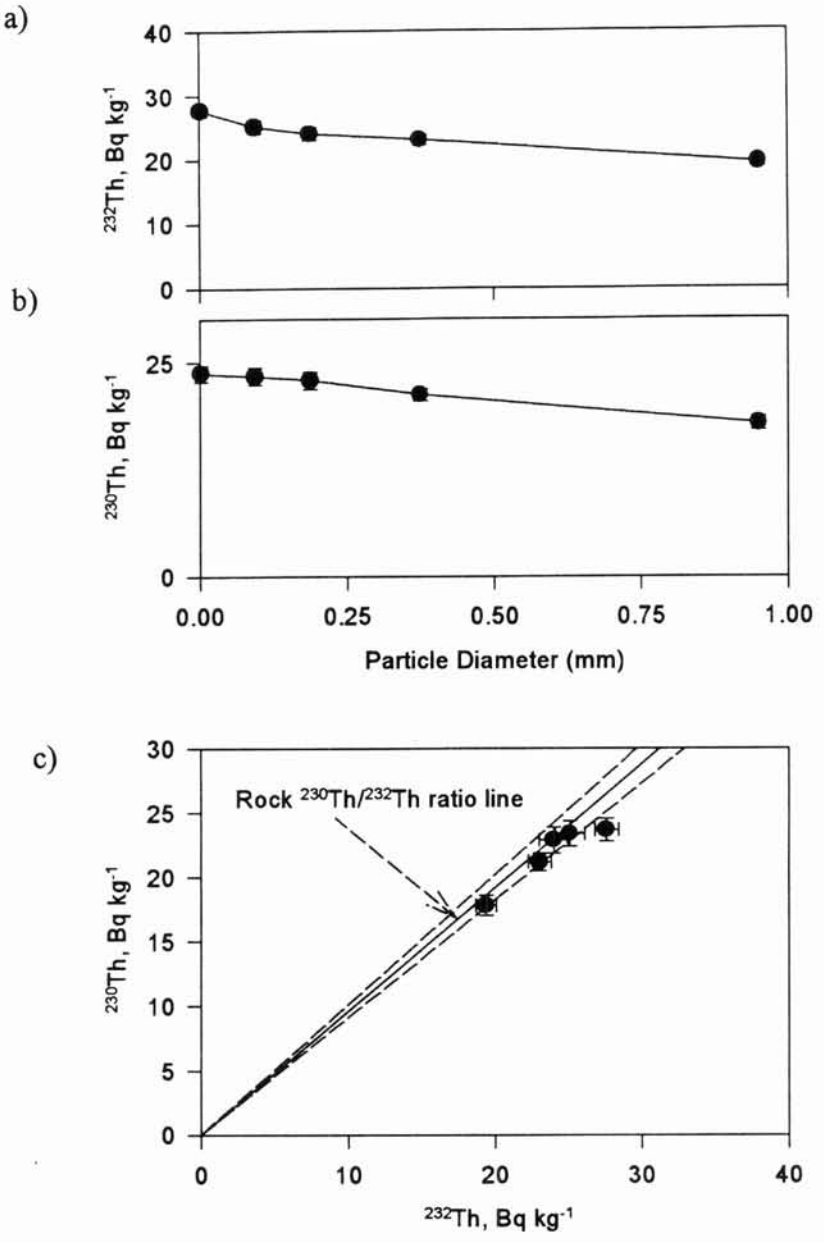

Figure 5.8: Concentrations of ^{230}Th (a) and ^{232}Th (b) against median particle size in the fractions from soil sample H1. Concentrations of ^{230}Th against ^{232}Th (c) in the various particle size fractions. The solid line represents the rock ^{230}Th/^{232}Th ratio and the dashed lines are the 66% confidence limits on this ratio. The error bars represent the analytical uncertainty equivalent to one standard error on the mean, in many cases these are smaller than the symbol size.

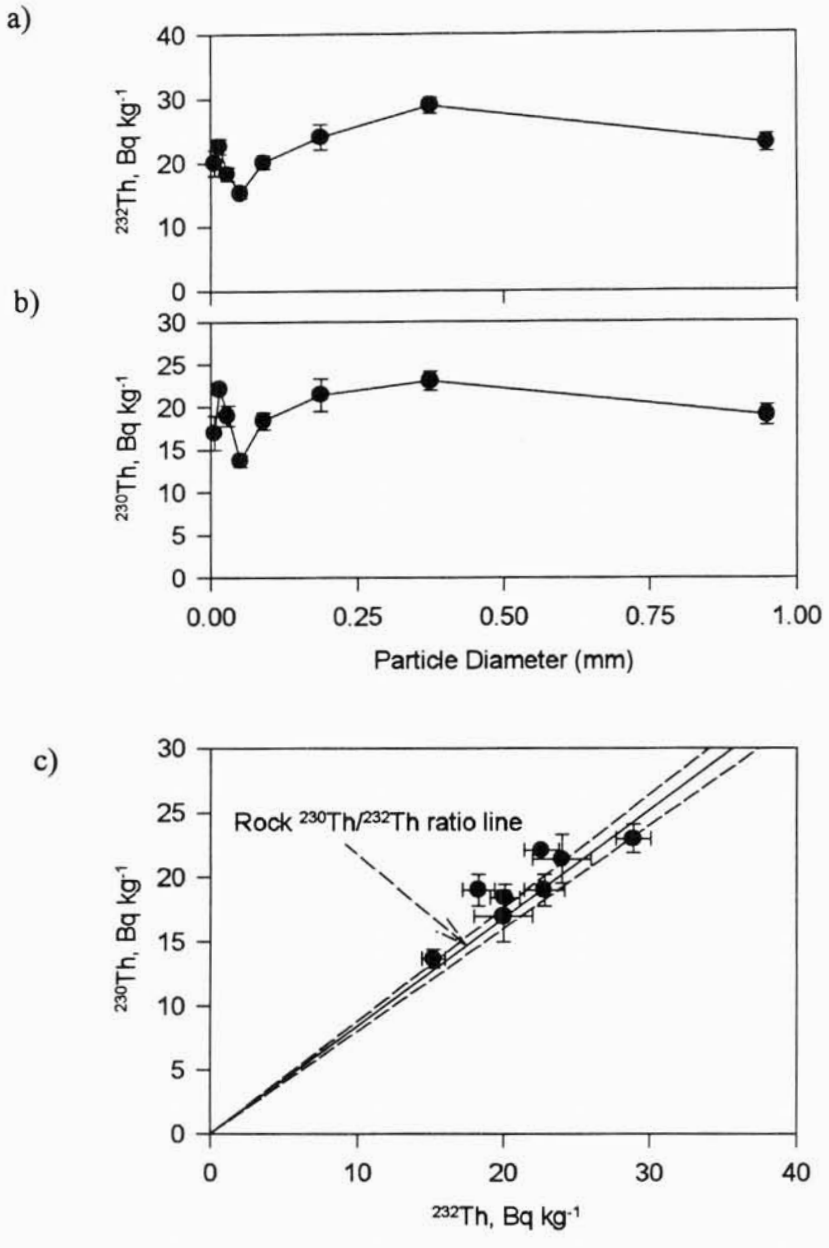

Figure 5.9: Concentrations of ^{230}Th (a) and ^{232}Th (b) against median particle size in the fractions from soil sample I1. Concentrations of ^{230}Th against ^{232}Th (c) in the various particle size fractions. The solid line represents the rock ^{230}Th/^{232}Th ratio and the dashed lines are the 66% confidence limits on this ratio. The error bars represent the analytical uncertainty equivalent to one standard error on the mean, in many cases these are smaller than the symbol size.

Site C (mixed sediments): The ^{230}Th and ^{232}Th concentrations do not vary systematically with particle size in the fractions from soil sample C13 (Figure 5.4 a and b). Though the <63μm fraction does have the highest concentration of both nuclides and the >500μm the lowest. The ^{230}Th and ^{232}Th data are again consistent with the rock $^{230}Th/^{232}Th$ ratio line from this site (4 point within 1 σ, 1 point within 2 σ), although there is a slight systematic tendency for the particle size data to lie below the average rock ratio line.

Site D (granite): The ^{230}Th and ^{232}Th concentrations in the fractions from sample D1 do vary, increasing systematically as particle size decreases (Figure 5.5 a and b). The concentrations in fractions from the coarser grained, more iron-rich sample D9 do not vary monotonically with particle size, being highest in the finer fraction, lowest in the 250-500μm fraction, and then increasing as particle size increase.

The ^{230}Th concentrations are plotted against ^{232}Th concentration in Figure 5.5c. These nuclides are correlated and all the size fractions from both samples are within analytical uncertainty of the rock $^{230}Th/^{232}Th$ ratio line.

Site F (sandstone): The concentrations of ^{230}Th and ^{232}Th vary systematically with particle size with the finer fractions having the highest concentration of both nuclides (Figure 5.6 a and b). The ^{230}Th and ^{232}Th data are again consistent with the rock $^{230}Th/^{232}Th$ ratio line with all the data within 1σ of the line.

Site G (sandstone): The finest fraction (<2μm) contains the highest $^{230}Th/^{232}Th$ concentration (Figure 5.7 a and b), but there is only a weak systematic variation in concentration with particle size in this soil. As at previous sites the ^{230}Th and ^{232}Th concentrations in all of the particle size fractions are within analytical uncertainty of the parent rock $^{230}Th/^{232}Th$ ratio line (Figure 5.7c).

Site H (rhyolite): In this sample (H1) the ^{230}Th and ^{232}Th concentrations vary systematically with particle size (Figure 5.8a and b) with the finer fractions having the higher concentrations. The ^{230}Th and ^{232}Th data are all consistent with the rock $^{230}Th/^{232}Th$ ratio line, with all the points within 1 σ (Figure 5.8c).

Site I (basalt): Concentration of ^{230}Th and ^{232}Th do not vary systematically with particle size in this basaltic soil (Figure 5.9 a and b). The data are however all consistent with the rock $^{230}Th/^{232}Th$ line (5 data points within 1σ, 3 within 2σ).

In each of the above cases, all the particle size fractions had $^{230}Th/^{232}Th$ within 2 σ of the rock ratio line with 47 of the 57 (82%) fractions measured, falling within 1 σ of the rock ratio. It is therefore concluded that sorting by particle size of soil derived from a uniform rock type will produce size fractions in which the concentration of ^{230}Th and ^{232}Th may vary, but the $^{230}Th/^{232}Th$ ratio will be the same as that of the parent rock.

5.3.1b ^{226}Ra and ^{232}Th

Site A (granite): The ^{226}Ra concentrations in the various size fractions from the four samples (A1, A13, A16 and A18) are plotted against median particle size in Figure 5.10 (a). In each case the ^{226}Ra concentrations vary systematically with particle size, with the finer fractions having the higher concentrations. The only exception to this is the >2mm fraction from sample A13. This fraction contained several large blocks (2 x 2 cm) of well indurated iron concretion.

The ^{226}Ra concentration are plotted against ^{232}Th concentration in Figure 5.10 (b). The concentrations of ^{232}Th were not explicitly measured in the fractions from samples A13 and A16. However, they have been estimated from the ^{228}Ra and ^{228}Th concentrations and the bulk soil $^{228}Ra/^{232}Th$ ratios by assuming that this ratio is constant for all the size fractions. If the >2mm fraction from A13 is excluded, the ^{226}Ra data from the particle size from each of the samples are linearly correlated with ^{232}Th concentrations. Regression lines fitted through each of the data sets all pass through the origin. However, the slopes of the regressions are distinct (0.586 ± 0.005, 0.937 ± 0.008, 1.78 ± 0.04 and 0.529 ± 0.004 for samples A1, A13, A16,A18 respectively).

The above data indicate that separation by particle size of soil material from a point in the Site A catchment will produce particle size fractions with a uniform $^{226}Ra/^{232}Th$ ratio but that this ratio may vary from one sampling point to another in the catchment. The correlation between ^{226}Ra and ^{232}Th suggests that these nuclides are being held in similar sites on the soil grains. This is discussed further in section 5.3.1c.

Site B (basalt): While the ^{226}Ra concentrations in the size fractions from these soils vary systematically with particle size, with the finer fractions having the higher ^{226}Ra concentrations (Figure 5.11a), they are only weakly correlated with ^{232}Th concentrations (Figure 5.11b). (Note : In this plot the ^{232}Th concentrations in the size fractions from samples B8 to B11 and B13 have been calculated from the ^{228}Ra and ^{228}Th data assuming secular equilibrium. This is a reasonable assumption as (i) the ^{232}Th decay series was found to be in secular equilibrium in all

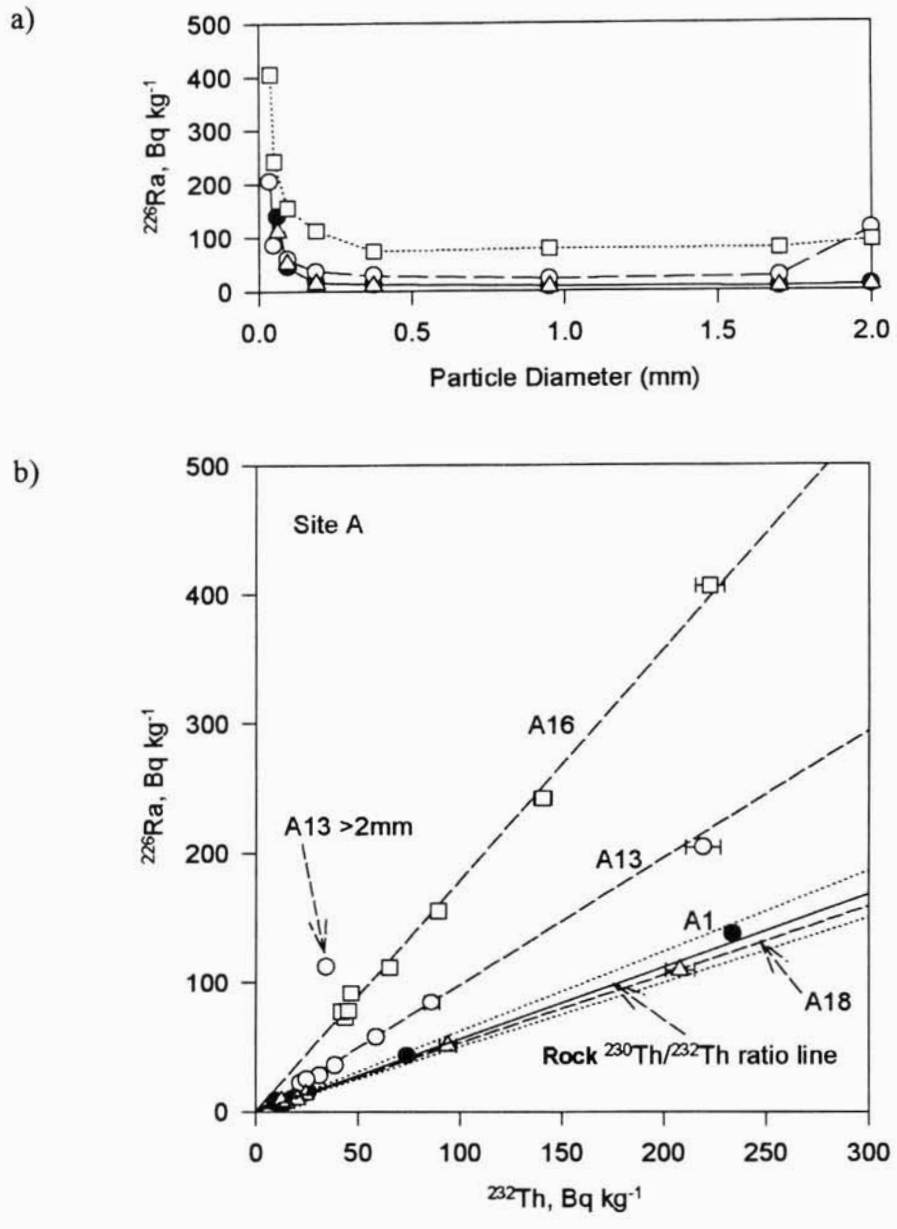

Figure 5.10: Concentrations of ^{226}Ra (a) against median particle size in the fractions from soil samples A1 (closed circles), A13 (open circles), A16 (open squares) and A18 (open triangles). Concentrations of ^{226}Ra against ^{232}Th (b) in the various particle size fractions from these samples. The solid line represents the rock ^{230}Th/^{232}Th ratio and the dotted lines are the 66% confidence limits on this ratio. Regression lines (dashed) have been fitted through each of the data sets. The error bars represent the analytical uncertainty equivalent to one standard error on the mean, in many cases these are smaller than the symbol size.

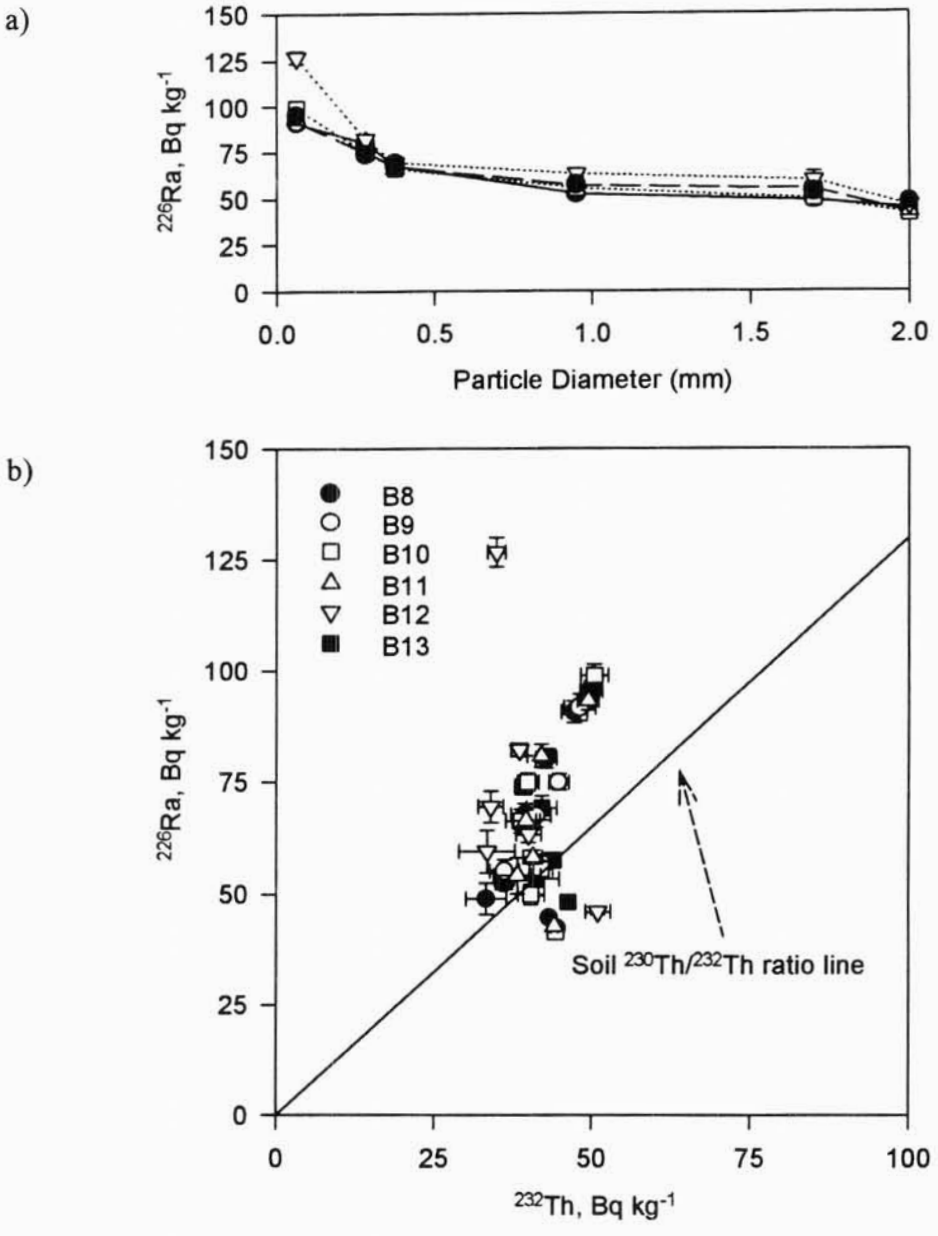

Figure 5.11: Concentrations of ^{226}Ra (a) against median particle size in the fractions from soil samples B8 to B13. Concentrations of ^{226}Ra against ^{232}Th (b) in the various particle size fractions from these samples. The solid line represents the rock ^{230}Th/^{232}Th ratio. The error bars represent the analytical uncertainty equivalent to one standard error on the mean, in many cases these are smaller than the symbol size.

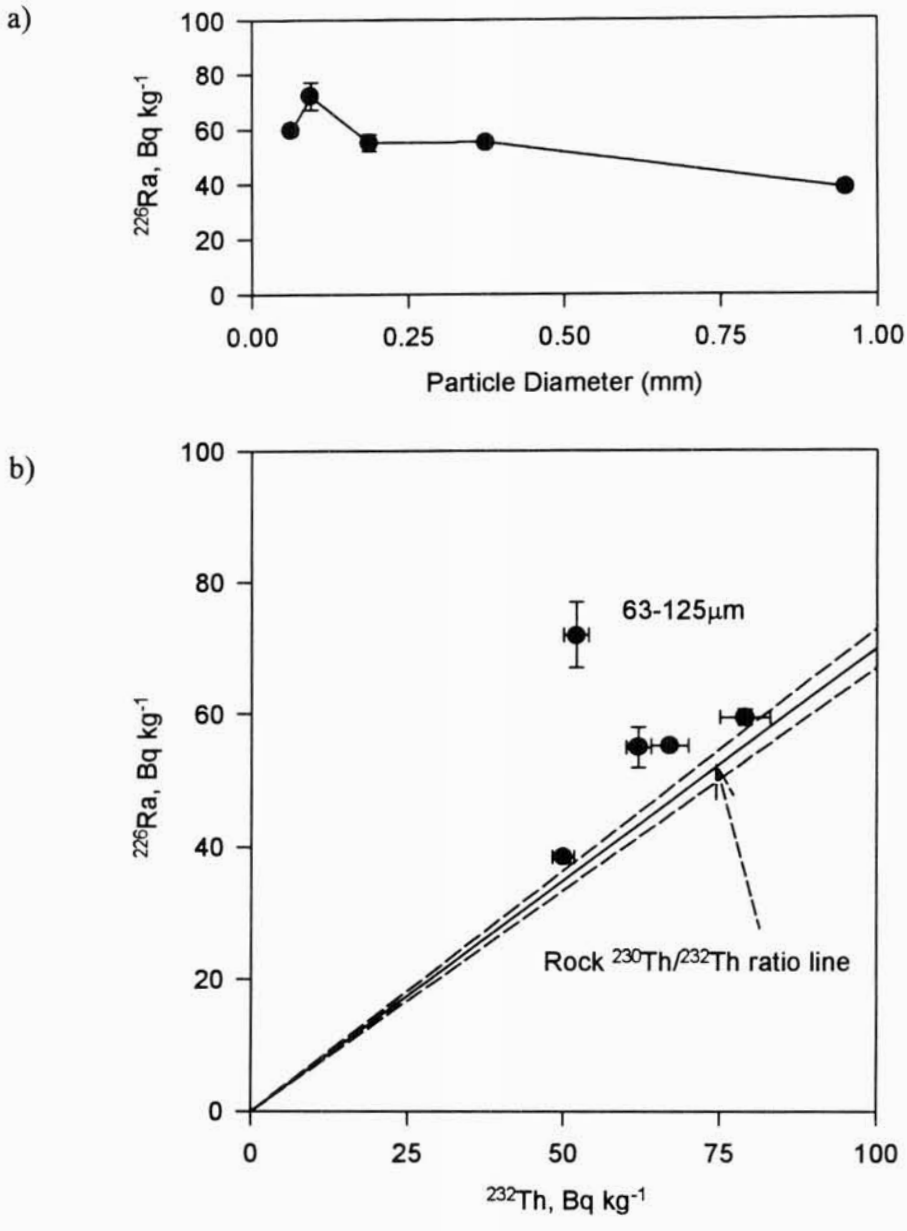

Figure 5.12: Concentrations of ^{226}Ra (a) against median particle size in the fractions from soil sample C3. Concentrations of ^{226}Ra against ^{232}Th (b) in the various particle size fractions from these samples. The solid line represents the rock ^{230}Th/^{232}Th ratio, and the dashed lines are the 66% confidence limits on this ratio. The error bars represent the analytical uncertainty equivalent to one standard error on the mean, in many cases these are smaller than the symbol size.

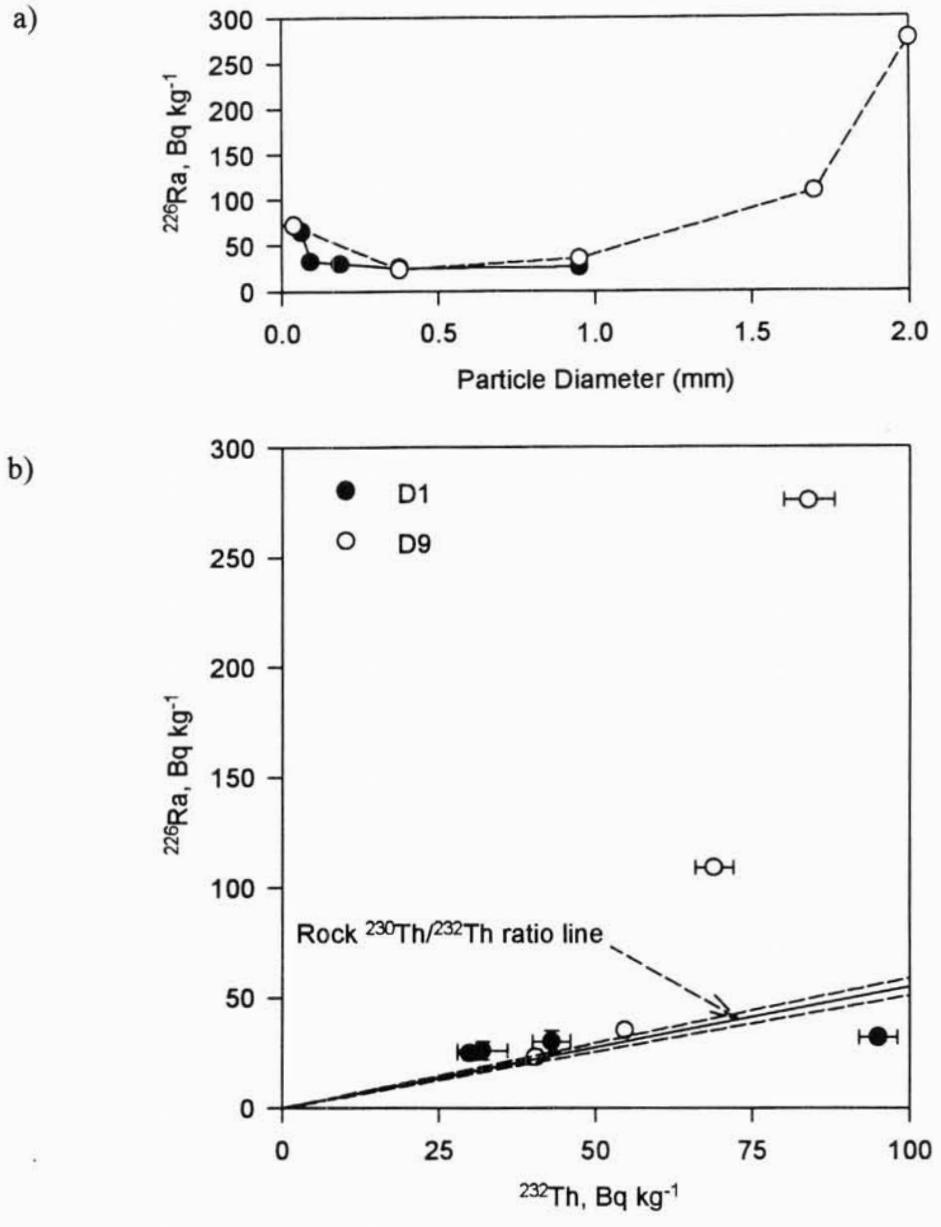

Figure 5.13: Concentrations of ^{226}Ra (a) against median particle size in the fractions from soil samples D1 and D9. Concentrations of ^{226}Ra against ^{232}Th (b) in the various particle size fractions from these samples. The solid line represents the rock ^{230}Th/^{232}Th ratio, and the dashed lines are the 66% confidence limits on this ratio. The error bars represent the analytical uncertainty equivalent to one standard error on the mean, in many cases these are smaller than the symbol size.

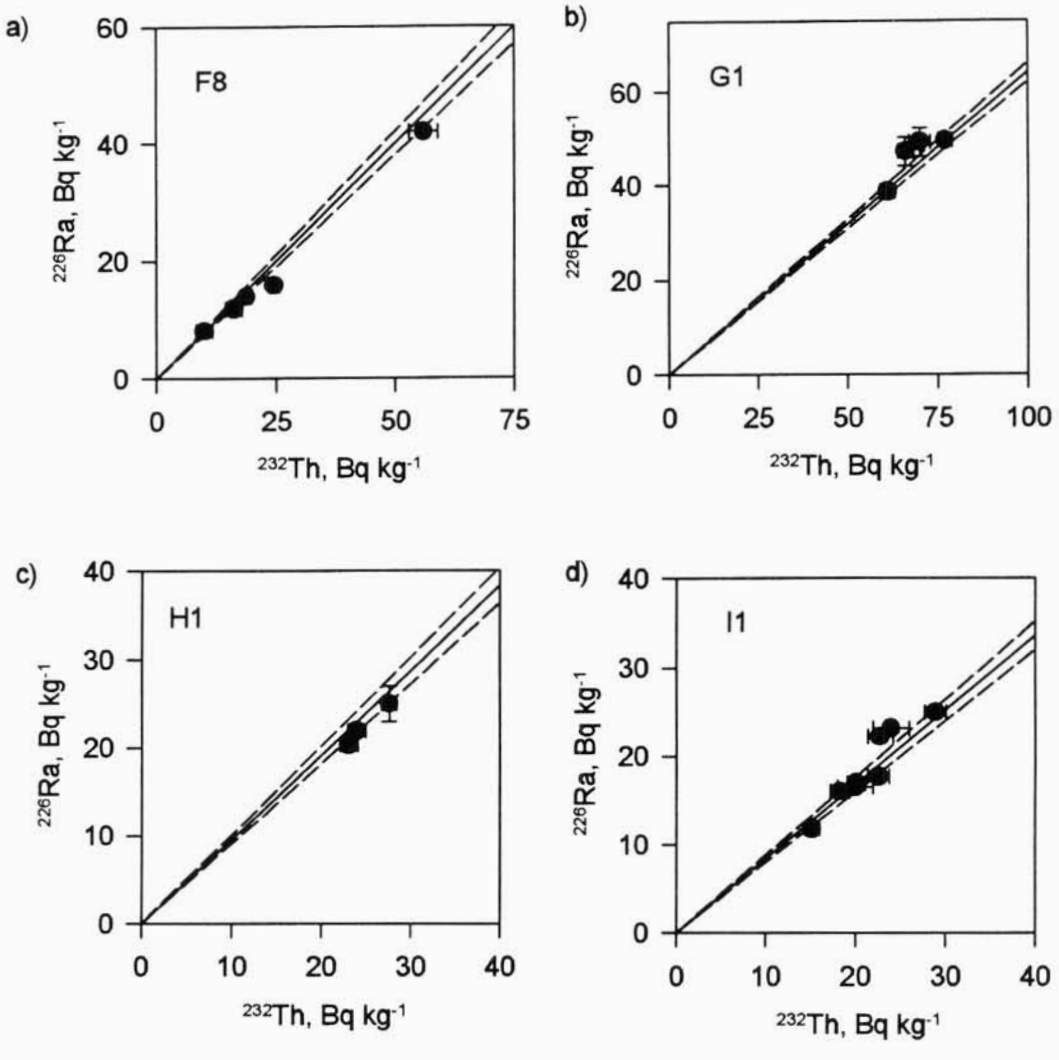

Figure 5.14: Concentrations of ^{226}Ra against ^{232}Th concentrations in the various particle size fractions from samples (a) F8, (b) G1, (c) H1 and (d) I1. The solid line represents the rock ^{230}Th/^{232}Th ratio, and the dashed lines are the 66% confidence limits on this ratio. The error bars represent the analytical uncertainty equivalent to one standard error on the mean, in many cases these are smaller than the symbol size.

the bulk samples used here, and (ii) in all the size fractions from sample B13). The poor correlation between the ^{226}Ra and ^{232}Th concentrations suggests that these nuclides are not bound in similar sites in each of the soil particle size fractions. This is examined further in section 5.3.1c.

Site C (mixed sediments): The ^{226}Ra concentrations in the size fraction from sample C13 do not vary systematically with particle size with the highest concentration being in the 63-125μm fraction (Figure 5.12a). The concentrations of ^{226}Ra and ^{232}Th are poorly correlated in the particle size fractions from this soil (Figure 5.12b).

Site D (granite): Again the concentrations of ^{226}Ra do not vary systematically with particle size in soil fractions from this site (Figure 5.13 (a)). The highest concentrations occur in the >2mm and 2-1.4mm fractions. The ^{226}Ra and ^{232}Th concentrations are poorly correlated with $^{226}Ra/^{232}Th$ ratio ranging from 0.34 ± 0.02 to 3.28 ± 0.16.

Sites F (sandstone), **G** (sandstone), **H** (rhyolite) **and I** (basalt): Concentrations of ^{230}Th and ^{226}Ra were within analytical uncertainty of equilibrium in the bulk samples from these sites. The $^{226}Ra/^{230}Th$, $^{228}Ra/^{232}Th$ and $^{228}Th/^{228}Ra$ activity ratios for the various particle size fractions from the samples from each of these sites are presented in Table 5.2. In each case the parent-daughter concentrations are within analytical uncertainty of equilibrium (with the exception of the $^{226}Ra/^{230}Th$ ratio for 10-20mm fraction from I1). Consequently the ^{226}Ra to ^{232}Th plots (Figure 5.14 a, b, c and d) are comparable to the ^{230}Th to ^{232}Th plots and the ^{226}Ra to ^{232}Th data are largely consistent with the parent rock $^{230}Th/^{232}Th$ ratio lines.

The above data from eight sites and 17 soil samples indicated that separation of soil material in which the ^{226}Ra and ^{230}Th concentrations were in equilibrium will produce size fractions with a uniform $^{226}Ra/^{232}Th$ ratio which is the same as the parent rock ratio. In soil samples in which the concentration of ^{226}Ra was in excess of ^{230}Th the various particle size fractions generally had variable $^{226}Ra/^{232}Th$ ratios. The one exception to this was the data from the four soils from Site A, in which each sample produced size fractions which had a uniform $^{226}Ra/^{232}Th$ ratio (with the exception of the >2mm fraction from A13) but this ratio varied from soil sample to soil sample. This indicates that at this site ^{226}Ra and ^{232}Th are present on similar sites on the soil grains. In order to understand why Site A soils were generally different from those of the other sites which had a ^{226}Ra excess, the mechanism controlling the distribution of the radionuclides in the soil particle size fractions from Sites A, B and D have been examined further.

Table 5.2: The $^{226}Ra/^{230}Th$, $^{228}Ra/^{232}Th$ and $^{228}Th/^{228}Ra$ activity ratios for the various particle size fractions from the samples from sites F,G,H and I

Fraction	$^{226}Ra/^{230}Th$	$^{228}Ra/^{232}Th$	$^{228}Th/^{228}Ra$
Sample F8			
<63 μm	0.95±0.07	0.96±0.05	1.06±0.02
63-125 μm	0.92±0.05	0.85±0.05	1.03±0.04
125-250 μm	0.90±0.07	0.97±0.10	1.08±0.09
250-500 μm	1.17±0.18	1.08±0.14	0.91±0.08
>500 μm	0.95±0.19	1.12±0.20	0.83±0.07
Sample G1			
2-63 μm		1.00±0.03	1.01±0.02
63-125 μm	1.00±0.06	1.00±0.07	1.03±0.07
250-500 μm	1.00±0.08	1.00±0.12	1.00±0.13
0.5-1.4 mm	1.05±0.08	1.17±0.12	0.85±0.09
Sample H1			
<2 μm	1.05±0.09		
125-250 μm	0.96±0.05	1.00±0.07	0.96±0.05
250-500 μm	0.96±0.05	1.02±0.08	0.95±0.07
Sample I1			
2-10 μm	0.97±0.12	1.00±0.11	1.05±0.06
10-20 μm	0.80±0.05	0.99±0.07	0.97±0.05
20-38 μm	0.84±0.06	1.01±0.07	0.99±0.03
38-63 μm	0.86±0.05	0.97±0.06	0.99±0.04
63-125 μm	0.92±0.05	1.03±0.06	1.01±0.03
125-250 μm	1.08±0.10	1.11±0.10	0.98±0.03
250-500 μm	1.08±0.05	1.01±0.05	0.98±0.02

5.3.1c Mechanism controlling the distribution of radionuclides in the soil particle size fractions

Site A : The concentrations of ^{226}Ra, ^{230}Th and ^{232}Th in the soil particle size fractions from the four soil samples from this site were strongly dependent on particle size with the finer fractions having the higher concentrations. The concentration of all these nuclides decreased as particle size increased. The systematic variation in nuclide concentrations with particle size suggests that the nuclide concentrations are dependent on some parameter associated with particle diameter. *Megumi et al.*, [1982] found that the lithogenic radionuclides were primarily surface sorbed in the granite soils they examined. This may be the case for the soils from Site A.

The surface areas of the various particle size fractions have not been explicitly measured. However, sample A18 contained concentrations of the fallout nuclide ^{137}Cs. This nuclide is a product of nuclear weapons testing and consequently has only been present in the environment for the last 40 years. It is reasonable to assume that this fallout nuclide is

primarily bound on the surface of the soil particles. The concentrations of ^{226}Ra, ^{230}Th and ^{232}Th in the various particle size fractions from sample A18 have been plotted against ^{137}Cs concentration in Figure 5.15. Concentrations of all of these lithogenic nuclides are correlated with the ^{137}Cs concentration with $r^2 > 0.95$. This correlation suggests that the lithogenic radionuclides are primarily surface bound in the particle size fractions from this soil sample.

Significant concentrations of ^{137}Cs were not present in the other soil samples from this site, and so another method of estimating the relative surface area of the different size fractions is required in order to determine whether the nuclides are also correlated with surface area in these other samples. The relative surface area (surface area per kg) of the different particle size fractions can be defined as :

$$\text{Relative Surface Area} = \frac{\text{Surface Area}}{\text{Volume}} \times \frac{1}{\text{Density}} (m^2/kg)$$

If it is assumed that the particles are spherical and have a uniform density then the surface area ratio (SAR) of one particle size to another may be calculated as:

$$SAR_n = \frac{S_f}{S_n} = \frac{r_n}{r_f}$$

S_f and S_n are the relative surface areas of particle size fractions f and n respectively and r_n and r_f are the radii of the two size fractions. If we let r_n = 1mm then

$$SAR_{2mm} = \frac{1}{r_f}$$

in which r_f is the radius of size fraction f in millimetres. Using this formula it can be seen that a 1mm diameter particle has a relative surface area twice that of a 2mm particle. So a 1mm (dia) particle has a $SAR_{2mm} = 2$; a 0.5mm (dia) particle $SAR_{2mm} = 4$ and so forth. The SAR_{2mm} has been calculated for each of the size fractions from the sample A18, using the median diameter of each fraction. This calculated parameter is plotted against ^{137}Cs concentration from the various size fractions in Figure 5.16. There is a good correlation evident between this fallout nuclide and the calculated SAR_{2mm}, suggesting that the SAR_{2mm} provides a reasonable approximation of the relative surface areas of each of the size fractions.

Concentrations of ^{230}Th and ^{232}Th in the various particle size fractions from samples A1, A13, and A16 are plotted against calculated SAR_{2mm} in Figure 5.17. There is a good correlation between these nuclides and the SAR_{2mm} (both $r^2 > 0.95$). This strongly suggests that these nuclides are all primarily surface bound in these Site A soils. Similarly, concentrations of ^{226}Ra in the size fractions from each of the samples are also correlated with

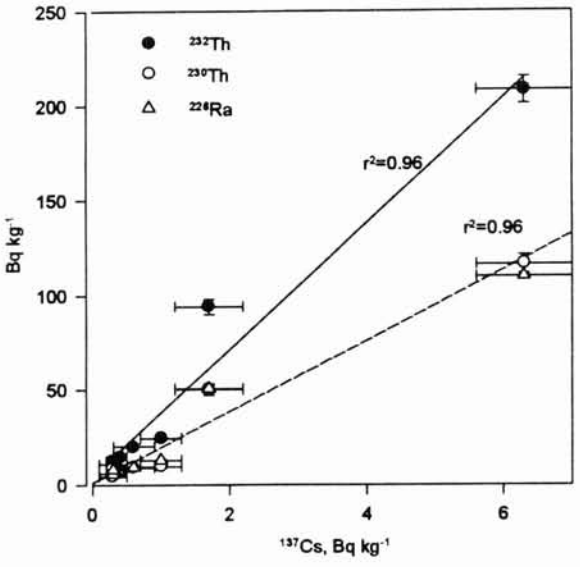

Figure 5.15: Concentrations of ^{226}Ra, ^{230}Th and ^{232}Th against ^{137}Cs concentrations in the various particle size fractions from sample A18. The error bars represent the analytical uncertainty equivalent to one standard error on the mean, in many cases these are smaller than the symbol size. Regression lines are shown.

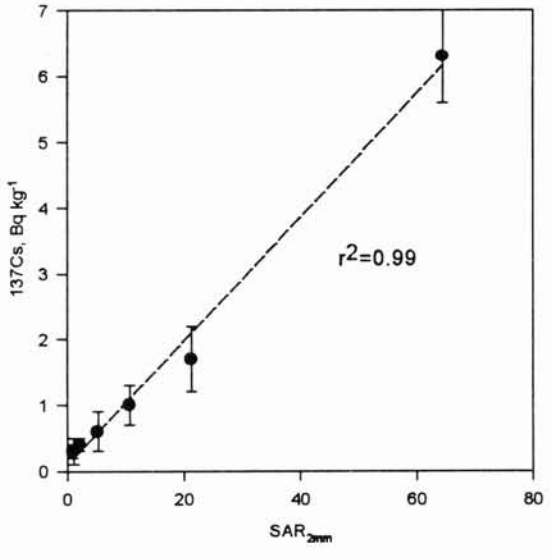

Figure 5.16: Concentrations of ^{137}Cs against calculated surface area relative to the 2mm fraction (SAR_{2mm}) for the various particle size fractions from sample A18. The error bars represent the analytical uncertainty equivalent to one standard error on the mean, in some cases these are smaller than the symbol size. Regression line (dashed) is shown.

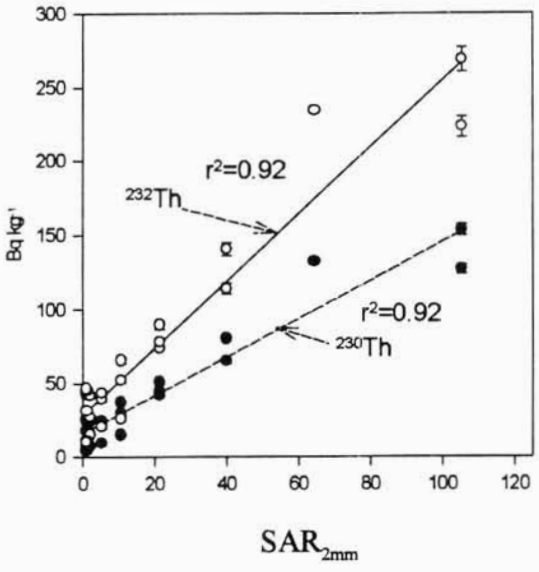

Figure 5.17: Concentrations of ^{230}Th (closed circles) and ^{232}Th (open circles) against calculated SAR_{2mm} in the various particle size fractions from samples A1, A13 and A16. The error bars represent the analytical uncertainty equivalent to one standard error on the mean, in some cases these are smaller than the symbol size. Lines represent regressions fitted through each of the data sets.

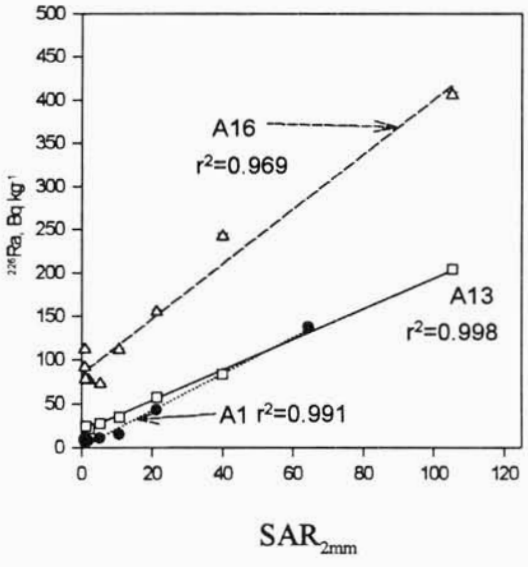

Figure 5.18: Concentrations of ^{226}Ra against calculated SAR_{2mm} in the various particle size fractions from samples A1, A13 and A16. The error bars represent the analytical uncertainty equivalent to one standard error on the mean, in many cases these are smaller than the symbol size. Lines represent regressions fitted through each of the data sets.

the calculated SAR_{2mm}, but the correlation is different for each of the samples, suggesting that the concentration of ^{226}Ra per unit area differs from sample to sample.

Site B: In contrast to the large change in ^{230}Th and ^{232}Th concentrations with particle size in samples from Site A, there was little dependence of thorium concentrations on particle size in the fractions from soil sample B12. The ^{230}Th and ^{232}Th concentration in the various size fractions from this sample are more or less constant. This suggests that these nuclides are not primarily surface bound in this basaltic soil but are probably uniformly distributed throughout the soil grains.

The concentrations of ^{226}Ra did vary systematically with particle size, being highest in the finest fraction in these samples. The difference between the thorium and radium particle size dependency results from the presence of a ^{226}Ra excess (up to 144%) in the samples. The excess ^{226}Ra has been calculated for all the particle size fractions from sample B8 to B13 by assuming a constant $^{230}Th/^{232}Th$ ratio. This excess ^{226}Ra is plotted against ^{137}Cs concentrations in Figure 5.19.

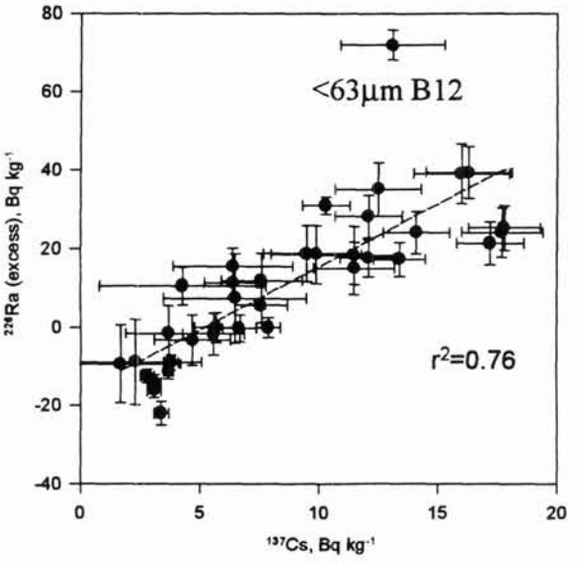

Figure 5.19: Concentrations of ^{226}Ra excess against ^{137}Cs in the various particle size fractions from samples B8 to B13. The error bars represent the analytical uncertainty equivalent to one standard error on the mean, in some cases these are smaller than the symbol size. The dashed line represent the regression fitted through all the data except the one outlier (<63µm fraction from sample B12).

These two parameters are well correlated ($r^2 = 0.76$, ignoring the <63μm fraction from sample B12) suggesting that the ^{226}Ra excess is predominantly surface bound in these soils. The poor correlations evident between ^{226}Ra and ^{232}Th in the particle size fractions (Figure 5.12b) presumably arises from most of the thorium isotope concentrations being distributed through the grains while a significant fraction of the ^{226}Ra (up to 60%) is present on the surfaces.

Site D: The concentrations of ^{230}Th and ^{232}Th in the particle size fractions from sample D1 decreased systematically with increasing particle size, suggesting that these thorium isotopes may be correlated with surface area. The correlation (r^2=0.85) between the concentrations of ^{232}Th and the calculated SAR_{2mm} of the particle size fractions (Figure 5.20) would tend to support this idea. Conversely, the data from sample D9 (Figure 5.20) would suggest that the thorium isotopes were not correlated with surface area in the fractions from this sample.

It was shown in chapter 4 that a large fraction (up to 80%) of the thorium isotopes are present in the secondary iron and manganese oxides in the soils from this site, and that ^{230}Th and ^{232}Th concentrations are well correlated in these oxides. The concentrations of ^{232}Th in particle size fractions from sample D9 are plotted against total Fe_2O_3 contents in Figure 5.21. There is a good correlation between total iron content and ^{232}Th concentrations in the coarser fractions (r^2=0.93). However, the <38μm fraction does not lie on this regression (as the thorium isotopes are correlated this is also the case for ^{230}Th concentrations).

These data suggest that thorium concentrations in the different size fractions in soils from this site may be dependent on both grain surface area and iron content. However, there is insufficient data to clearly resolve these relationships, although it is very likely that the distribution of both ^{230}Th and ^{232}Th are controlled by the same mechanisms (see Fig. 5.5).

The concentrations of ^{226}Ra in excess of its parent ^{230}Th in the soils from this site were shown in chapter 4 to be primarily associated with the secondary manganese oxides. The ^{226}Ra excess concentration in the particle size fractions from samples D1 and D9 are plotted against Mn_3O_4 contents in Figure 5.22. There is a good correlation between total Mn_3O_4 content and excess ^{226}Ra concentrations in the particle size fractions from both D1 and D9 (r^2=0.78 and 0.93 respectively), suggesting the ^{226}Ra excess in the individual size fractions is also primarily associated with the secondary manganese oxides. It was suggested above that the thorium isotopes are also to some extent associated with the secondary oxide. It is therefore surprising that ^{226}Ra and ^{232}Th are poorly correlated in the different size fractions. Citrate-dithionite

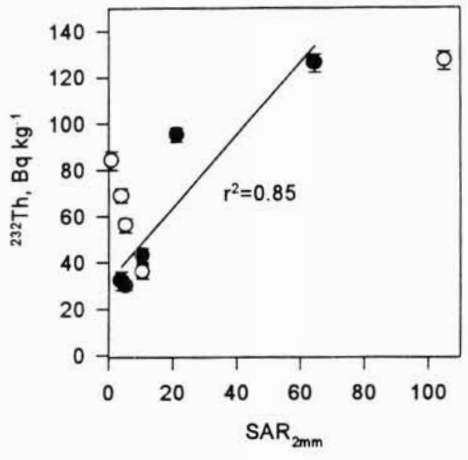

Figure 5.20: Concentrations of ^{232}Th against calculated SAR_{2mm} in the various particle size fractions from samples D1(closed circles) and D9 (open circles). The error bars represent the analytical uncertainty equivalent to one standard error on the mean, in some cases these are smaller than the symbol size. The line represents the regression fitted through the D1 data set.

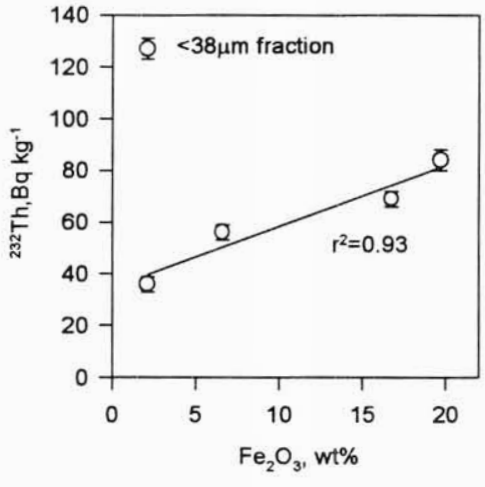

Figure 5.21: Concentrations of ^{232}Th against Fe_2O_3 contents in the various particle size fractions from sample D9. The error bars represent the analytical uncertainty equivalent to one standard error on the mean. The line represents the regression fitted through the data (except the <38μm fraction).

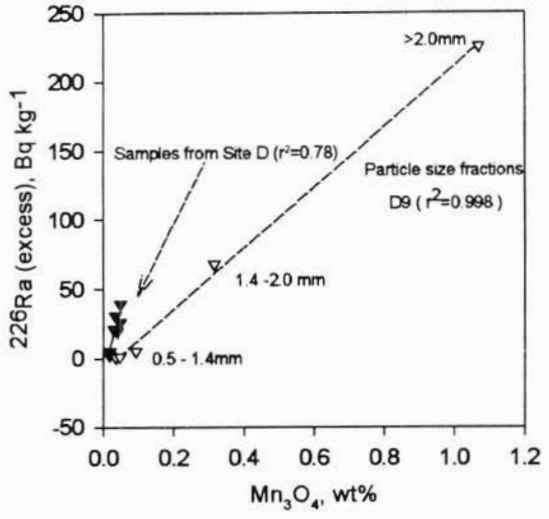

Figure 5.22: Concentrations ^{226}Ra excess against Mn_3O_4 in the various particle size fractions from samples D1(closed triangles) and D9 (open triangles). The error bars represent the analytical uncertainty equivalent to one standard error on the mean, in most cases these are smaller than the symbol size. The lines represent regressions fitted through each of the data sets.

extraction data from the bulk soils presented in chapter 4 showed that while the $^{230}Th/^{232}Th$ ratio in the poorly crystalline oxides was constant, $^{226}Ra/^{232}Th$ ratio in these oxides was variable. It is likely that the generally poor correlation evident between ^{226}Ra and ^{232}Th in the particle size fractions (particular in sample D9) result from the excess radium being distributed differently from the thorium isotopes in secondary oxides.

The data from the three sites examined above suggest that the reason the concentrations of ^{226}Ra and ^{232}Th were correlated in the size fractions from the Site A soils, and not in those from other sites which had large ^{226}Ra excess, was that in the site A soils the excess ^{226}Ra was bound to similar sites as the thorium isotopes. Whereas in the soils from the other sites, the distribution of the thorium isotopes and the ^{226}Ra excess were controlled by different mechanisms. At Site A the radionuclides are mainly surface bound; at Site B the thorium isotope data suggests that these nuclides are predominantly present in the grain matrix whereas the ^{226}Ra excess is surface bound; and at Site D, although the ^{226}Ra excess and a proportion of the thorium isotopes are associated with the secondary iron and manganese oxides, these oxides had variable $^{226}Ra/^{232}Th$ ratios indicating that the nuclides were not

uniformly distributed in the oxides. This variability may have arisen as a result of non-uniform deposition, or as a result of varying times since deposition of the ^{226}Ra excess.

5.3.2 The effects of sorting by density

In this section the radionuclide concentrations in the >2.95 g cm^{-3} density fractions from selected soil samples are examined. The mineralogy and radionuclide analyses of the >2.95 g cm^{-3} fractions are presented in Table 5.3, together with the relevant weight percent of the total sample. The $^{230}Th/^{232}Th$ and $^{226}Ra/^{232}Th$ activity ratios have been calculated for the >2.95 g cm^{-3} and are presented in Table 5.4. The bulk soil $^{226}Ra/^{232}Th$ and parent rock $^{230}Th/^{232}Th$ ratios are also presented in Table 5.4. From the activities and the percentage of the total sample (wt%) of heavy fractions (>2.95 g cm^{-3}) it can be seen that removal of this fraction will not significantly alter the nuclide ratio in the lighter fraction (<2.95 g cm^{-3}), consequently this fraction will have the ratios indistinguishable from those of the bulk soil.

5.3.2a ^{230}Th to ^{232}Th

The $^{230}Th/^{232}Th$ activity ratio in the heavy fraction from all the samples are consistent with the parent rock $^{230}Th/^{232}Th$ ratio. This is irrespective of whether the separates are primary or secondary minerals. This suggests that sorting soil material by density will produce fractions in which the $^{230}Th/^{232}Th$ ratio is the same as the parent rock.

5.3.2b ^{226}Ra to ^{232}Th

In the primary heavy minerals separated from samples A13 and A18 the concentrations of ^{226}Ra and ^{230}Th are within analytical uncertainty and are indistinguishable from equilibrium. This not surprising given that these are primary rock forming minerals. Consequently the $^{226}Ra/^{232}Th$ ratios are the same as the parent rock (within analytical uncertainties).

In the secondary heavy minerals analysed for ^{226}Ra, the concentrations of ^{226}Ra and ^{230}Th are clearly not in equilibrium (Table 5.3) with ^{226}Ra concentration in each case in excess of ^{230}Th. The more indurated iron oxides (A13iii) hand-picked from the A13 heavy fraction have $^{226}Ra/^{232}Th$ ratios within analytical uncertainty of the bulk soil ratio. This is however not the case for the more poorly crystalline iron oxides from this sample (A13ii) or the iron-manganese oxides separated from samples D1 and D2. This suggests that sorting of soil material by density may produce fractions in which the $^{226}Ra/^{232}Th$ ratio is variable.

Table 5.3: The radionuclide concentrations, mineralogy and the calculated percentage of the total sample for the >2.95g cm^{-3} fractions from selected soil samples. All radionuclide activities are reported as Bq kg^{-1}. Uncertainties are equivalent to one standard error on the mean.

Sample	Description	^{230}Th	^{226}Ra	^{232}Th	wt%
A13i	Anatase,rutile,biotite	257±3	260±10	455±5	0.2
A13ii	Secondary Fe Oxides	61±3	93±4	116±4	0.5
A13iii	Haematite	30.6±1.3	53±3	58±2	1.3
A18	Anatase,rutile,magnetite,biotite	269±5	270±20	470±8	0.2
B12	Secondary iron oxides	85±3		67±3	2.5
C13	Secondary Fe-Mn Oxides	60±3		80±5	0.4
D1	Secondary Fe-Mn Oxides	39.0±1.8	105±10	71±2	0.5
D9	Secondary Fe-Mn Oxides	54±2	280±15	97±3	2.0
F8	Haematite	46±2		60±3	0.3
H1	Secondary Fe Oxides	64±3		74±3	0.5

Table 5.4: The $^{226}Ra/^{232}Th$ and $^{230}Th/^{232}Th$ ratios in the >2.95g cm^{-3} fractions from selected soil samples. The relevant rock and soil ratios are included for comparison. Uncertainties are equivalent to one standard error on the mean.

	>2.95 g cm^{-3}		Rock	Soil
	$^{226}Ra/^{232}Th$	$^{230}Th/^{232}Th$	$^{230}Th/^{232}Th$	$^{226}Ra/^{232}Th$
A13i	0.57±0.02	0.565±0.009	0.56±0.06	0.99±0.05
A13ii	0.80±0.04	0.53±0.03	0.56±0.06	
A13iii	0.91±0.06	0.53±0.03	0.56±0.06	
A18	0.57±0.04	0.572±0.014	0.56±0.06	0.52±0.02
B12		1.30±0.07	1.30±0.09	1.36±0.07
C13		0.75±0.06	0.70±0.03	0.73±0.03
D1	1.48±0.15	0.55±0.03	0.55±0.04	0.55±0.02
D9	2.89±0.18	0.56±0.03	0.55±0.04	0.68±0.02
F8		0.77±0.05	0.80±0.04	0.75±0.03
H1		0.86±0.05	0.88±0.03	0.84±0.04

5.3.3 The effects of grain abrasion

Three soil samples have been used to examine the effects of grain abrasion on radionuclide concentrations and ratios:

Sample A1: a quartz-rich granitic soil which showed little evidence of the development of secondary iron oxides, and consisted predominantly of quartz and feldspar.

Sample D9: This is also a granitic soil but shows significant iron oxide formation evident in the presence of iron-manganese concretions. Sample mineralogy consists of clay, quartz, feldspar and secondary Fe-Mn oxides.

Sample I1: Fine grained basaltic soil which consisted mainly of clay and iron oxides.

The samples were first wet sieved to remove the <38μm fraction and then were shaken in water for a period of 62 hours (section 3.3.4c). The samples were again wet sieved following the abrasion and the radionuclide analyses of the <38μm and >38μm fractions after abrasion, and the weight % (of the total) of each fraction are presented in Table 5.5. As there were no <38μm grains in the samples prior to the abrasion, this fraction must consist of grain fragments produced by the abrasion of the >38μm fractions.

The weight % data indicate that 90% of sample I1, 70% of sample D9 and only 14% of sample A1 were reduced to grains <38μm in diameter. This is as would be expected from

Table 5.5: Radionuclide analyses of the <38μm and >38μm fractions after grain abrasion, and weight% of the total sample abraded. All radionuclide activities are reported as Bq kg^{-1}. Uncertainties are equivalent to one standard error on the mean.

	^{230}Th	^{226}Ra	^{232}Th	^{228}Ra	^{228}Th	wt%
			Abraded Fractions from Sample A1			
>38 μm	46.7±1.5	50.8±0.8	84±2	83.2±1.4	84.3±1.3	86%
<38 μm	45.0±1.5	47.8±0.8	81±2	81.3±1.6	82.3±1.4	14%
			Abraded Fractions from Sample D9			
>38 μm	18.6±1.2	165±2	37.0±1.5	42.1±2.5	42.4±1.1	30%
<38 μm	76±3	94.9±1.6	130±4	137±4	133±3	70%
			Abraded Fractions from Sample I1			
>38 μm	24±2	23±2	28±2	31±8	27±6	10%
<38 μm	19.1±1.5	17.2±0.7	22.5±1.9	23.8±1.6	22.9±0.6	90%

Table 5.6: Calculated Radionuclide ratios of the <38μm and >38μm fractions after grain abrasion. The relevant rock and soil ratios are included for comparison. Uncertainties are equivalent to one standard error on the mean.

	$^{230}Th/^{232}Th$	$^{226}Ra/^{232}Th$	Rock $^{230}Th/^{232}Th$	Soil $^{228}Ra/^{232}Th$
	Sample A1			
>38 μm	0.56 ± 0.02	0.60 ± 0.02	0.56 ± 0.06	0.60 ± 0.03
<38 μm	0.56 ± 0.02	0.59 ± 0.02		
	Sample D9			
>38 μm	0.50 ± 0.04	4.47 ± 0.19	0.55 ± 0.04	0.68 ±0.02
<38 μm	0.59 ± 0.03	0.73 ± 0.03		
	Sample I1			
>38 μm	0.86 ± 0.09	0.82 ± 0.09	0.84 ± 0.04	0.84 ± 0.04
<38 μm	0.85 ± 0.10	0.76 ± 0.07		

the mineralogy of the samples. Sample A1 consisted largely of quartz and feldspar grains which are likely to be more resistant to abrasion than the iron oxide and clay composite grains which are present in sample I1 and the secondary oxides in D9.

The concentration of the various nuclides in <38μm and >38μm fractions produced by abrasion of sample A1 are comparable (Table 5.5). The concentrations are also similar in the fractions from sample I1. However, comparison of the fractions from sample D9 shows that the thorium isotopes are present in higher concentrations in the fine fraction, whereas the ^{226}Ra is higher in the residual (>38μm) fraction.

The $^{230}Th/^{232}Th$ and $^{226}Ra/^{232}Th$ ratios are presented in Table 5.6. The parent rock $^{230}Th/^{232}Th$ and bulk soil $^{226}Ra/^{232}Th$ ratios are also presented for comparison. In each case the fractions produced by abrasion have $^{230}Th/^{232}Th$ ratios within analytical uncertainty of the parent rock ratios, suggesting that this ratio is not affected by grain abrasion during sediment transport. Similarly the $^{226}Ra/^{232}Th$ ratios in the fractions from A1 and I1 are comparable to the parent rock ratio (assuming secular equilibrium in the rock). The concentrations of ^{230}Th and ^{226}Ra were within analytical uncertainty of equilibrium in the A1 and I1 bulk soils, this is also the case in the fractions produced by abrasion (compare figures in Table 5.5). This suggests that abrasion of soil material in which concentrations of ^{226}Ra and ^{230}Th are in secular equilibrium will produce fractions with a uniform $^{226}Ra/^{232}Th$ ratio which will be within analytical uncertainty of that in the parent rock.

The concentration of ^{226}Ra in sample D9 was shown to be in excess of its parent ^{230}Th in section 4.3.1. This is also the case in the fractions produced from this sample by the

abrasion experiment (Table 5.5). The $^{226}Ra/^{232}Th$ ratios in these fractions (Table 5.6) differ from each other and from the ratio in the bulk soil, suggesting that abrasion of soil material in which concentrations of ^{226}Ra and ^{230}Th not in secular equilibrium may produce fractions with variable $^{266}Ra/^{232}Th$ ratios. The ^{226}Ra excess is greatest in the residual fraction. These data are consistent with the citrate-dithionite data which showed that more thorium was extractable from this sample than ^{226}Ra, and suggests that the radium was more tightly bound to the grains than the thorium. The data from the abrasion experiment indicate that the excess radium is held largely on or in the core of the grains, and not in the surface iron-oxide coating.

5.3.4 Comparison of fluvial and artificial mixing and sorting

The effects on the lithogenic radionuclide correlation of sorting soil material by particle size and density have been discussed above. In this section these effects are compared to those of natural sorting produced by fluvial transport. This work was done at Site F. Both of the decay series were considered to be in secular equilibrium at this site (Chapter 4 section 4.3.1)

A representative sample of the surface material F8 was made by combining 20 (1cm deep) subsamples from within a 12m x 12m plot. Sorting by particle size and density of this sample (discussed above) was shown to produce fractions with a uniform $^{226}Ra/^{232}Th$ ratio consistent with that of the parent rock. The plot was then subjected to rainfall of controlled intensity and volume. Sediment washed from the site was collected as described in section 5.2.4. Radionuclide concentration and ratios in these sediment samples are presented in Appendix C, Table C.5.

The ^{226}Ra and ^{232}Th data from the sediments (CFC and bedload) collected from the site are plotted in Figure 5.23. (The mean $^{228}Th/^{228}Ra$ ratio has been calculated and is 0.99 ± 0.05. The concentration of ^{232}Th has been calculated from the weighted mean of the ^{228}Th and ^{228}Ra concentrations for all samples assuming secular equilibrium. This assumption is reasonable at this site given the data presented in section 4.3.1). The rock $^{226}Ra/^{232}Th$ ratio line and the concentration data from the fractions produced by the sorting of sample F8 are also shown in this figure. The CFC sediment data are generally consistent with the rock ratio line, as is the bedload sample. The spread in the concentration data in these samples is similar to that in the artificially produced fractions. Consequently, it is concluded that both artificial and fluvial

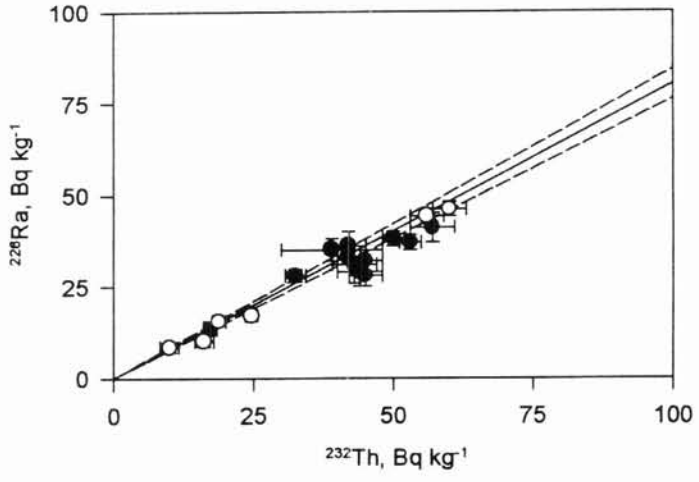

Figure 5.23: Concentrations of ^{226}Ra against ^{232}Th in the CFC (closed circles) and bedload (closed square) sediment samples from site F, and in the fractions produced by artificial sorting of sample F8 (open circles). The error bars represent the analytical uncertainty equivalent to one standard error on the mean, in some cases these are smaller than the symbol size. The solid line represents the parent rock $^{226}Ra/^{232}Th$ ratio. The dashed lines correspond to uncertainties of one standard error on this ratio.

sorting of material from this site have had a comparable effect on the radionuclide concentrations and ratios in the fractions and sediments produced.

5.4 Summary

Fluvial transport results in the sorting by particle size and density and in abrasion of the material being transported. In this chapter it has been shown that:

1. The particle size and density fractions of soil samples have constant $^{230}Th/^{232}Th$ activity ratios. This ratio is unaffected by grain abrasion and is consistent with the parent rock $^{230}Th/^{232}Th$ ratio. It is confidently predicted that fluvial transport of soil material will result in sediments which have a uniform $^{230}Th/^{232}Th$ ratio, independent of which particle sizes or densities are sampled. The value of this ratio will be dependent on U/Th ratio of the rock from which the soil was formed.

2. In soils in which the concentrations of ^{226}Ra and ^{230}Th were in secular equilibrium the $^{226}Ra/^{232}Th$ ratio behaved similarly to that of $^{230}Th/^{232}Th$, and the $^{226}Ra/^{232}Th$ ratios in

sediments derived from these soils are also expected to be the same as the parent rock U/Th ratio.

3. In soils which had large ^{226}Ra excess over ^{230}Th concentrations sorting (by both particle size and density) and grain abrasion produced fractions which had variable $^{226}Ra/^{232}Th$ ratios. This was shown at two of the sites examined to be due to the thorium isotopes and the ^{226}Ra excess being differentially distributed on or in the soil grains. Sediments derived from these soils are expected to have highly variable $^{226}Ra/^{232}Th$ ratios which would not easily be related to those of the bulk soils, or those of the parent rock.

4. An exception to (3) above was observed in the soils from site A. The ^{226}Ra excess in these soil samples was shown to be correlated with surface area. The thorium isotopes were distributed similarly. Sorting by particle size of individual soil samples from this site produced fractions which generally had a uniform $^{226}Ra/^{232}Th$ ratio. This ratio varied from soil sample to soil sample. While sorting by density was shown to produce heavy mineral fractions with variable $^{226}Ra/^{232}Th$ ratios, these fractions were only a small percentage of the total soil and are therefore unlikely to dominate the radionuclide signature of the sediments derived from these soils. Consequently it is expected that fluvial transport of soils from point sources in this catchment will produce sediments with constant $^{226}Ra/^{232}Th$ ratios but this ratio may vary from one point to another depending on the degree of ^{226}Ra excess at that location in the catchment.

5. Sorting by particle size and density of bulked surface soil from Site F produced fractions in which concentrations of ^{226}Ra and ^{232}Th were correlated. Sediments eroded from the same site by fluvial process had ^{226}Ra and ^{232}Th concentrations which were consistent with this correlation and had a comparable spread. It is concluded that particle size and density separation during transport are mechanisms by which the correlation observed between lithogenic radionuclides in transported sediment may originate.

Chapter 6: Lithogenic Radionuclides in Coarse Grained Sediments

The previous chapters have focused on lithogenic radionuclides in fine grained material. This chapter studies the behaviour and distribution of lithogenic radionuclide concentrations in coarse grained sediment (0.5-1 mm), in order to specifically address the third hypothesis proposed in chapter 3:

> In coarse grained material (sands) ^{226}Ra and ^{232}Th are primarily associated with resistate heavy minerals. Density separation of these minerals from the gangue results in the correlations observed in modern sediments.

The junction of the Snowy River and Wullwye Creek was chosen for this study. Sediment sample mineralogy, particle size range and chemistry, are all examined in an effort to test the above hypothesis and to determine what mechanism controls the distribution of radionuclides in these coarse grained sediments. At the end of the chapter the use of the radionuclide data in providing sediment source information in these coarse grained sediments at this site is also assessed.

6.1 Site Description

The Snowy River was dammed near its head waters to form Lake Jindabyne in the 1967. Wullwye Creek, the first major tributary below the dam, joins the Snowy River 20km downstream of the structure (Fig 6.1). The dam provides an effective trap for 0.5-1mm sand particles; however in-channel storage (in the river below the dam) of material derived from above the dam prior to its construction is probable.

The geology of the region is reported on the Berridale 1:100 000 geological sheet [*White et al.,* 1976]. Wullwye Creek drains the Dalgety Granodiorite, an S-type biotite-granodiorite of Silurian age, which outcrops over about 300 km^2. This granite is part of the Berridale Batholith.

The geology of the Snowy River upstream from the Wullwye Creek junction is dominated by three major granites: (i) Kalkite Adamellite, (ii) Mowamba Granodiorite (iii) Bullenbalong Granodiorite. These are all large (>300 km^2) biotite rich S-type granites of the Kosciusko Batholith [*Chappell et al.,* 1991]. The river channel also passes through minor

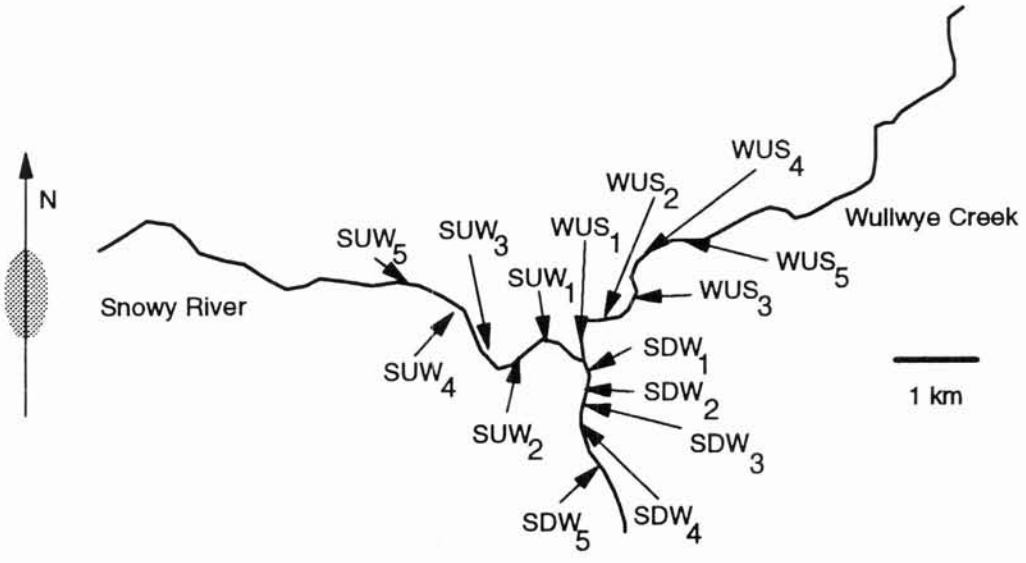

Figure 6.1: A sketch map of the Snowy River-Wullwye Creek Junction showing sampling locations and sample codes.

sections of Hornblende-biotite tonalite and short sections of Ordovician sandstones and shales.

6.2 Sampling and Sample Treatment

The field sampling was carried out by *Caitcheon et al.,* [1991] as part of a sediment sourcing study on the Snowy River. Sampling of the Wullwye Creek /Snowy River junction consisted of taking 5 grab samples of sediments in the active beds of the streams, from 500m long reaches upstream and downstream of the confluence. Sampling locations and sample numbers are shown in Figure 6.1. Each grab sample included up to 50 sub-samples (bulked in the field) to ensure a representative collection. These samples were wet sieved to obtain the 0.5-1mm fraction, which was then analysed for mineral magnetics and radionuclide content (by gamma spectrometry).

In this study the samples collected by *Caitcheon et al.,* [1991] have been analysed by alpha spectrometry to determine the concentrations of the thorium isotopes (Section 3.3.1b). Major element concentrations have been determined by XRF (Section 3.3.2b). Detailed sample mineralogy has been determined by a combination of microscopic examination, XRD analysis (Section 3.3.3) and heavy mineral separation (Section 3.3.4a). The fractions produced by heavy mineral separation have been bulked to provide 3 samples (1 from each arm) and these have been analysed by alpha spectrometry.

6.3 Results and Discussion

The radionuclide and major element analyses are presented in Appendix E, Tables E1 and E2 respectively. The following sections first describe (i) sample mineralogy (ii) the radionuclide equilibrium conditions (iii) concentration ranges (iv) correlations between ^{238}U and ^{232}Th decay series nuclides. Then radionuclide analyses of the heavy mineral fractions and major element analyses of the sediment samples are used to determine which mechanisms control the distribution of the radionuclides in these coarse grained sediments. Finally, both the radionuclide and chemical data are used to provide information on the sources of the sediment.

6.3.1 Sediment mineralogy

The mineralogy of the sediment samples was all very similar. They consist predominantly of a two component mixture of quartz and feldspar with minor biotite, apatite and magnetite. In general the grains were sharp and angular, though some round grains of feldspar were present. The samples from the Snowy River, both upstream and downstream of the junction, were darker in appearance than those from Wullwye Creek, probably due to the presence of heavier iron staining on the grains. This was the only mineralogical difference detected between sediments from the two arms.

Microscopic examination of the heavy mineral separates indicated that many of the biotite grains had partial oxide coating, as did many of the magnetite grains. Most of the biotite grains were well preserved. As biotite is a well cleaved mineral which is easily broken, this suggests that they had not been transported a great distance.

The sediments are dominated by primary minerals with only very minor secondary minerals present (mainly Fe oxides).

6.3.2 Equilibrium conditions

The relevant parent/daughter plots are presented in Figure 6.2 (a-d).

Concentrations of ^{238}U and ^{230}Th in the individual samples (Fig 6.2a) are within analytical uncertainty of equilibrium, although there is a tendency for ^{238}U to be in excess of ^{230}Th in most of the samples. The concentration of ^{226}Ra are in excess of ^{230}Th in 8 out of 15 samples (Fig. 6.2b); this is independent of the sampling locality.

Concentrations of ^{228}Ra and ^{228}Th are within analytical uncertainty of equilibrium (Fig.6.2 d). The ^{228}Ra concentrations are in excess of ^{232}Th in most of the samples collected

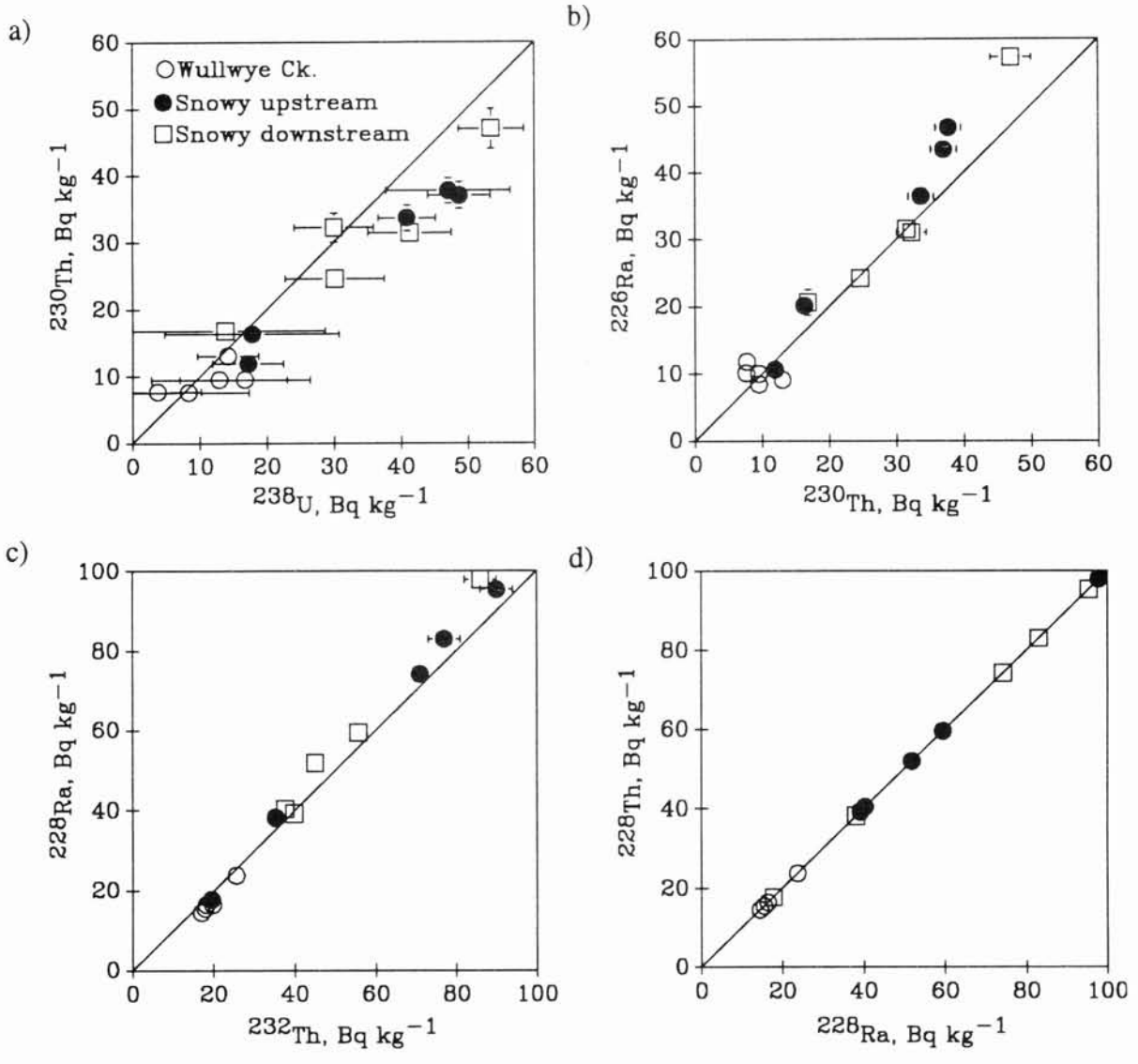

Figure 6.2: Radionuclide daughter to parent concentration plots for the Snowy River-Wullwye Creek confluence samples, a) ^{230}Th against ^{238}U, b) ^{226}Ra against ^{230}Th, c) ^{228}Ra against ^{232}Th and d) ^{228}Th against ^{228}Ra. In each case the solid line represents secular equilibrium. Error bars represent uncertainties equivalent to one standard error on the mean.

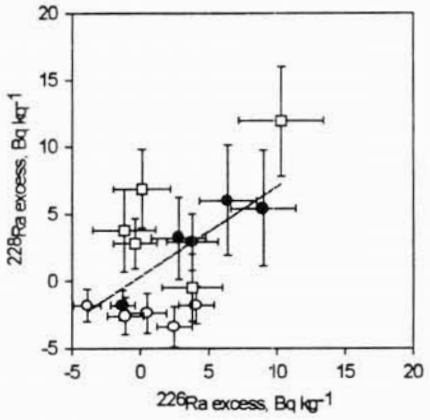

Figure 6.3: Concentrations of ^{228}Ra excess over ^{232}Th against ^{226}Ra excess over ^{230}Th for the samples from the Snowy River-Wullwye Creek confluence. Symbol are as in Figure 6.2. Error bars represent uncertainties equivalent to one standard error on the mean.

from the Snowy River both upstream and downstream of the confluence (Fig 6.2c). In the samples collected from Wullwye Creek there is a tendency for ^{232}Th to be in excess of ^{228}Ra.

The ^{226}Ra and ^{228}Ra excess have been calculated and are plotted in Figure 6.3. The ^{226}Ra and ^{228}Ra excesses are generally weakly correlated (r^2 = 0.37) with an intercept consistent with zero (0 $\pm$ 4). The correlation between these nuclides' excesses is better defined in the data from the Snowy river upstream of the junction (r^2 = 0.86) . The presence of the ^{226}Ra and ^{228}Ra excesses suggest that both nuclides have been deposited on the sediments either in the soil profile prior to transportation or from the river. Given that the concentrations of ^{228}Ra are in equilibrium with ^{228}Th, that is the ^{228}Ra excess is old compared to the half-life of ^{228}Th (1.8 years), it is unlikely that the excess ^{228}Ra has been recently sorbed. This implies that ^{228}Ra is not being deposited on to the sediment from the river water, and that the ^{228}Ra excess probably developed in the soil profile. If this is the case the excess could be expected to begin to decay back to equilibrium following transportation. Thus, the presence of a ^{228}Ra excess in the Snowy River samples probably indicates that these sediments have been in transport for a relatively short time, probably less than 4 half-lives of ^{228}Ra (~20 years).

6.3.3 ^{238}U and ^{232}Th series nuclides concentration ranges and correlations

The radionuclide concentration ranges, relative standard deviations (ie. standard deviation/mean value) and the ratio of maximum/minimum concentrations are presented in Table 6.1. The spread in concentration in the samples collected from the Snowy River, both

Table 6.1: Radionuclide concentration ranges and the relative standard deviations (ie. standard deviation/mean value) and max/min ratio for samples collected from the Snowy River-Wullwye Creek confluence. The least significant figures represent uncertainties equivalent to one standard error.

	Range	Mean	Relative StD	Max/Min
Wullwye Creek				
^{230}Th	7.6_7 - 13.0_7	9.5_9	21%	1.71 ± 0.18
^{226}Ra	8.4_{12} - 11.8_{10}	9.9_5	12%	1.4 ± 0.2
^{232}Th	17.9_{10} - 25.6_{10}	19.7_{14}	16%	1.43 ± 0.10
^{228}Ra	14.5_{11} - 23.8_7	17.3_{15}	19%	1.64 ± 0.13
Snowy River Upstream				
^{230}Th	11.9_8 - 37.7_{19}	27_5	40%	3.2 ± 0.3
^{226}Ra	10.6_4 - 47.7_{14}	31_6	44%	4.5 ± 0.2
^{232}Th	19.6_{10} - 90_4	59_{11}	45%	4.6 ± 0.3
^{228}Ra	17.8_4 - 95.4_{16}	62_{13}	47%	5.36 ± 0.15
Snowy River Downstream				
^{230}Th	16.8_{11} - 47_3	30_4	33%	2.8 ± 0.3
^{226}Ra	20.6_{19} - 57.3_7	33_6	39%	2.8 ± 0.3
^{232}Th	37.6_{15} - 86_4	53_8	34%	2.29 ± 0.14
^{228}Ra	39.3_{18} - 97.9_9	58_{10}	37%	2.49 ± 0.12

upstream and downstream of the junction is much greater than that present in the samples collected from the Wullwye Creek. Samples from Wullwye Creek also have the lowest absolute concentrations. The max/min concentration ratios for the Wullwye Creek samples are all <1.8 This ratio ranges from 2.29 to 5.36 in the samples from the Snowy River.

The concentrations of ^{230}Th and ^{232}Th are plotted in Figure 6.4a. Concentrations of these nuclides are correlated in the samples from the Snowy River upstream of the junction (r^2=0.976). The regression line fitted through these data has a slope of 0.40 ± 0.04 and an intercept close to zero (3 ± 2). Similarly the nuclides are correlated in the sample collected from the Snowy River downstream of the junction (r^2= 0.84); The regression line is within uncertainty of the upstream data (slope of 0.52 ± 0.12 and intercept of 3 ± 5). As expected from the concentration data the Wullwye Creek samples plot as a tight cluster, and the data are consistent with both regression lines.

The ^{226}Ra and ^{232}Th concentration are plotted in Figure 6.4b. These nuclides are also correlated in the Snowy River samples. However, the slopes of the correlations (0.52 ± 0.03 and 0.70 ± 0.10 upstream and downstream respectively) are greater than those of the ^{230}Th to ^{232}Th correlations. This is because of the presence of the ^{226}Ra excess in the samples. The intercepts for both the regression lines fitted through the ^{226}Ra to ^{232}Th data are consistent with zero (1 ± 2 and -4 ± 4 respectively). The data from the samples collected from

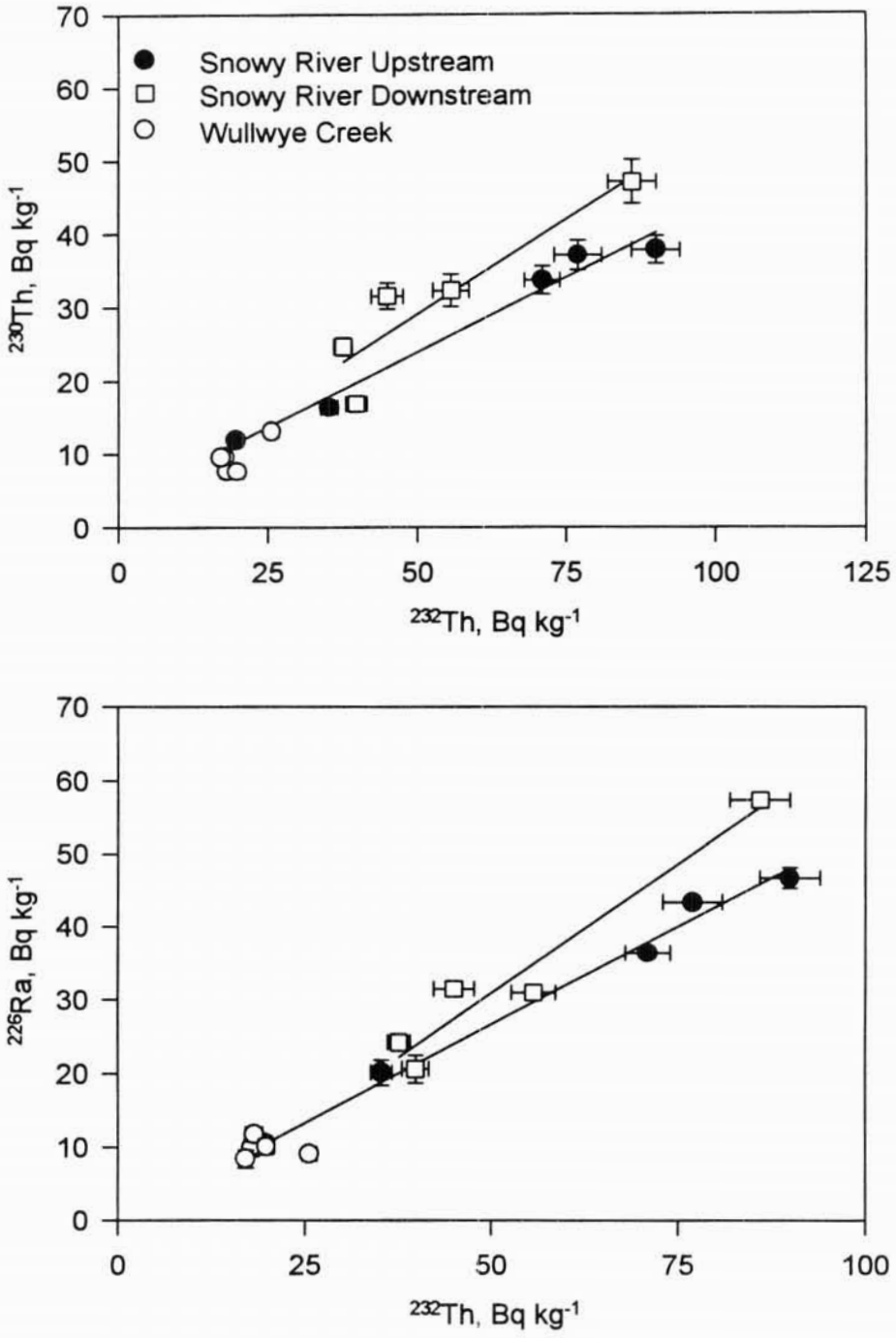

Figure 6.4: Concentrations of ^{230}Th (a) and ^{226}Ra (b) against ^{232}Th concentrations in samples from the Snowy River-Wullwye Creek junction. The lines shown are regressions fitted through the respective data groups. Error bars represent uncertainties equivalent to one standard error on the mean, in some cases these are smaller than the symbol size.

Wullwye Creek are again consistent with both regression lines.

6.3.4 Controlling mechanisms

In chapter 5 it was shown that correlations between ^{238}U and ^{232}Th decay series nuclides similar to those in Figure 6.3 (a and b) could be generated by sorting soil material by both particle size and/or density. Each of these sorting mechanisms also resulted in separation of mineral fractions, for instance: sorting by particle size concentrates the clay minerals in the finest fraction; separation by density sorts the heavy minerals such as apatite and rutile from the lighter quartz and feldspar. In the following sections an attempt is made to consider particle size separation and mineral sorting separately.

6.3.4a Particle size separation

In order to assess whether the correlations and spread in radionuclide concentrations result solely from differences in particle size distributions of the sediment samples, the sediment mineralogy has to be ignored. Consequently in this section the sediments are considered to consist of particles which differ from one another only by particle size and the radionuclides are considered to be primarily surface sorbed. Finer fractions consequently have higher concentrations because they have greater relative surface area (RSA as defined in chapter 5, section 5.3.1c).

The samples from the Snowy River - Wullwye Creek junction have a narrow particle size range of 0.5-1 mm (diameter). A 0.5 mm diameter particle has a RSA of only twice that of a 1.0 mm diameter particle (assuming uniform geometries and roughness). If particle size was the main factor controlling the spread in the radionuclide concentrations, then the ratio of maximum concentration to minimum concentration would not be expected to exceed ~2.

The max/min concentration ratios for the Wullwye Creek samples are all <1.8 (Table 6.1) it is therefore possible that particle size variations control the spread in concentrations in these samples. However, in the samples from the Snowy River this ratio ranges from ~2.3 to ~5.4, this suggest that another parameter such as mineralogy is the main controlling mechanism in these samples.

6.3.4b Mineral separation

If the correlation and spread in radionuclide concentrations evident in Figure 6.3 (a and b) results from differences in the mineralogy of the sediment samples then the radionuclides should be primarily associated with mineral fractions which can be separated by fluvial transport. The hypothesis proposed at the beginning of this chapter stated that the ^{226}Ra and ^{232}Th are primarily associated with resistate heavy minerals which may be fluvially separated because of density difference.

Density separations (section 3.3.7b) were undertaken on each sample to separate the quartz and feldspar from the minor heavy minerals (biotite, apatite and magnetite). The heavy minerals were then combined to give 3 samples (one from each of the arms). These were analysed by alpha spectrometry and the thorium results are presented in Table 6.2.

Table 6.2: The thorium isotope concentrations (Bq kg^{-1}) in the heavy mineral fractions of the samples collected from the three arms at junction of the Snowy River and Wullwye Creek.

	^{230}Th	^{232}Th
Wullwye Creek	119 ± 4	144 ± 4
Snowy upstream	77 ± 3	166 ± 5
Snowy downstream	137 ± 4	188 ± 5

The fraction of heavy minerals required to account for all the activity in the bulk samples is calculated to be between 10 - 57% in the samples from the Snowy River upstream of the junction, 10 - 16% for samples from the Wullwye Creek and 20 - 52 % for samples from the Snowy River downstream. The maximum percentage of heavy minerals extracted from any sample was 4.5% (after two extractions). While it was noted that a large number of biotite grains in particular remained in the light residue, due to rafting on lighter grains, none of the samples were considered to have heavy mineral content >6%. It is therefore unlikely that the heavy minerals are the dominant source of activity in the samples.

Obtaining pure separations of the other mineral phases present in the samples would require sorting by hand, which is both difficult and time consuming. Consequently another indirect method has been used to determine which of the mineral phases control the radioactivity in the samples. As the sediment samples consist predominantly of primary minerals which in general have well defined stoichiometries it is possible to calculate the sample mineralogy from its major element analysis. (A number of methods exist for calculating the mineralogy from a chemical analysis see Wedepohl [1969] for examples). An

adaptation of the CIPW norm method has been used here. The sample mineral assemblage (section 6.3.1) has been used with two additions; pyrite (FeS_2) and corundum (Al_2O_3) have been included to account for the S and excess Al respectively. It is recognised that these minerals probably do not occur in the samples and that the S, excess Al and some of the Fe (and other elements) are likely to be present as poorly crystalline oxides/hydroxides. However, this method should provide good quantitative estimates of the major components quartz and feldspar (K-feldspar and plagioclase). The mineral assemblage and the idealised chemical formulas used are presented in Table 6.3.

Table 6.3: Mineral assemblage and the idealised chemical formulas used in calculating mineral percentages.

Mineral	Symbol	Formula	Stoichiometric Weight
Quartz	Qz	SiO_2	60.06
K-Feldspar	Or	$KAlSi_2O_3$	278.25
Plagioclase	Ab	$Na[AlSi_3O_8]$	262.15
	An	$Ca[Al_2Si_2O_8]$	278.14
Apatite	Ap	$Ca_5(PO_4)_3OH$	502.35
Ilmenite	il	$FeTiO_2$	151.75
Magnetite	Mt	Fe_3O_4	231.55
Pyrite	Py	FeS_2	119.98
Corundum	Cor	Al_2O_3	101.94
Biotite	Bi	$KMg_2Fe[AlSi_3O_{10}]$	430.76

Table 6.4: An example of the calculation of the sample mineralogy from the chemical data for sample WUS_1

	moles/100g	**Qz**	**Or**	**Ab**	**An**	**Ap**	**Bi**	**Il**	**Mt**	**Py**	**Cor**
Na	0.0430			0.043							
Mg	0.0064						0.0064				
Al	0.1663		0.0718	0.0430	0.0184		0.0032				0.0299
Si	1.4023	1.1017	0.1436	0.1290	0.0184		0.0096				
P	0.0008					0.008					
S	0.0001									0.0001	
K	0.0750		0.0718				0.0032				
Ca	0.0105				0.0092	0.0013					
Ti	0.0011							0.0011			
Mn	0.0003								0.0003		
Fe	0.0175						0.0032	0.0011	0.0132	0.00005	
Mineral wt		66.76	19.98	11.27	2.56	0.13	1.43	0.17	1.019	0.006	1.51
Mineral %		63.64	19.08	10.76	2.46	0.12	1.36	0.17	0.97	0.006	1.43

An example calculation is given in Table 6.4. The wt% oxide is first converted to moles of cation per 100g . Na is only contained in Albite plagioclase (Ab) which has a molecular formula of $Na[AlSi_3O_8]$. The molar portion of Ab is therefore equal to the molar concentration of Na. In the case of sample WUS_1, a Na_2O concentration of 1.334 wt% converts to 0.0430 moles of Na per 100g, implying there is 0.0430 moles of Ab in 100g of this sample. Multiplying this by the molecular wt of Ab given in Table 6.4, this gives 11.3g Ab per 100g of sediment or 11.3(wt)% Ab. Al and Si are assigned in molar proportions (ie. Na:Al 1:1 and Na:Si 1:3). The percentage of the other mineral phases are then calculated in the order Ap, An, Bi, Or, il, Py; the remaining iron has been calculated as Mt; the remaining Si as Qz; and remaining Al as Cor. The calculated mineral assemblages are presented in Table 6.5.

The heavy mineral content has been calculated by summing all the components other than feldspar and quartz. The range of these estimates for each group is broadly consistent with the observed values, and is very much lower than required for the heavy minerals to account for the total activity present in the bulk samples.

Table 6.5: Percentage normative mineral fractions calculated from the chemical analyses of the samples collected from the Snowy River-Wullwye Creek Junction.

	Qz	Or	Ab	An	Ap	Py	Il	Cor	Bi	Mt	%heavy
WUS_1	63.64	19.08	10.76	2.46	0.12	0.01	0.17	1.43	1.36	0.97	4.1
WUS_2	62.14	21.58	10.49	2.36	0.13	0.04	0.24	1.03	1.16	0.83	3.4
WUS_3	64.73	18.50	10.45	2.40	0.11	0.01	0.25	1.48	1.21	0.85	3.9
WUS_4	64.62	18.88	10.00	2.48	0.14	0.01	0.20	1.58	1.08	1.01	4.0
WUS_5	60.93	21.14	11.38	2.47	0.12	0.01	0.18	1.51	1.40	0.87	4.1
SUW_1	56.52	15.93	10.86	3.60	0.31	0.03	0.99	5.34	4.36	2.05	13.1
SUW_2	59.89	18.27	10.68	2.80	0.22	0.02	0.56	3.60	2.64	1.33	8.4
SUW_3	69.86	14.13	9.50	2.21	0.10	0.01	0.21	1.85	1.44	0.68	4.3
SUW_4	56.96	17.30	10.02	3.37	0.29	0.03	0.84	5.01	4.18	2.02	12.4
SUW_5	56.57	15.11	10.32	3.75	0.28	0.06	1.06	5.89	4.97	1.99	14.3
SDW_1	57.25	17.20	11.73	3.91	0.24	0.03	0.75	3.73	3.52	1.65	9.9
SDW_2	59.26	16.13	10.14	3.63	0.32	0.05	0.81	4.42	3.42	1.82	10.8
SDW_3	53.80	12.62	11.08	3.85	0.44	0.06	1.63	7.79	6.10	2.64	18.7
SDW_4	60.72	15.84	11.02	3.03	0.29	0.04	0.68	3.82	2.75	1.81	9.4
SWD_5	63.53	16.22	10.54	3.11	0.17	0.02	0.44	2.44	2.13	1.40	6.6

Using the calculated mineralogy, it is now possible to determine with which mineral phases the radionuclides are primarily associated by successively removing mineral phases which dilute the concentrations of the radionuclides. As each non-causal component is removed, there should be a reduction in the relative standard deviation of the radionuclide data (ie. standard deviation/mean value).

An example calculation of the removal of a mineral component follows. The sum of all the mineral percentages is 100. Therefore in order to recalculate the concentration of the mineral components in the absence of a particular mineral phase, the initial concentrations of the remaining mineral phases is divided by the percentage remaining and multiplied by 100. For example, the concentration of orthoclase in the absence of quartz is given by :

$$\frac{Or}{(100-Qz)} \times 100 = Or_{Qz}$$

in which Or is the percentage of orthoclase in the sample, Qz is the percentage of quartz and Or_{Qz} is the percentage of orthoclase in the sample if all the quartz is removed. Similar calculation can be done for each of the mineral phases and for the radionuclide concentrations. The sum of the new weight percentages of the mineral fractions should also equal 100. This process is repeated following the same steps successively removing mineral phases.

The relative standard deviation (as percentages) for the radionuclide data on the total (i) sample, (ii) the sample - Qz (iii) sample - (Qz and feldspar) are presented in Table 6.6 for

Table 6.6: The Relative Standard Deviations (as percentages) for the Radionuclide data on the Total sample, Sample - Quartz and Sample -Quartz and Feldspar, for each of the sample groups

	^{230}Th	^{226}Ra	^{232}Th	^{228}Ra	^{228}Th
			Wullwye Creek		
initial	23	13	17	21	21
Qz	20	12	14	17	17
Qz+Feld	20	20	15	20	18
			Snowy River Upstream		
initial	45	49	51	53	52
Qz	36	42	43	46	44
Qz+Feld	14	16	20	22	20
			Snowy River Downstream		
initial	37	44	38	41	41
Qz	28	34	28	32	32
Qz+Feld	11	8	18	14	11

each of the sample groups. The Wullwye Creek radionuclide data had initial relative standards of the radionuclide data range from 13% to 23%. The removal of the quartz and quartz + feldspar did not significantly effect this. However, the relative standard deviations of the data of samples from the Snowy River both upstream and downstream of the junction were all significantly decreased by the removal of both the quartz and quartz + feldspar components. Removal of any of the remaining components did not significantly decrease the relative spread in the data. This data manipulation demonstrates that the quartz and feldspar do not contain significant activity. The radionuclides are therefore predominantly contained in the other mineral fractions in the samples. These minerals are biotite, apatite, magnetite and secondary iron oxides. The radionuclide analyses of the heavy mineral separation presented at the being of this section shows that biotite, apatite and magnetite did not contain sufficient activity and were not present in significant enough quantities to control the radionuclide concentrations of the sediments. This implies that the secondary oxides are the main mineral phase controlling the radionuclide concentrations in the samples from the Snowy River. This may also be the case for the samples from Wullwye Creek, although particle size variations could account for all the variability in radionuclide concentrations in these samples.

6.3.5 Source of the sediments

In chapter 4 it was found that the $^{230}Th/^{232}Th$ ratios in soils formed on a uniform rock type were identical to the U/Th ratio of the rock. Evidence presented in chapter 5 showed that various particle size and density fractions derived from the soils have a constant $^{230}Th/^{232}Th$ activity ratio. This ratio was also shown to be largely unaffected by grain abrasion, suggesting that fluvial transport of material derived from a soil formed from a uniform rock type should result in sediments which have a uniform $^{230}Th/^{232}Th$ ratio, independent of which particle sizes or densities are sampled. In this section the radionuclide and chemical data are interpreted to provide information on the nature of the sources of these sediments and to determine the relative contribution of Wullwye Creek to the sediment in the Snowy River down stream of the junction.

6.3.5a Uranium and thorium in the source rocks

The Snowy River and the Wullwye Creek drain granites which belong to different suites. The Snowy River drains granites of the Kosciusko Batholith from the Bullenbalong Supersuite, while Wullwye Creek drains a single granite of the Berridale Batholith from the Dalgety suite [*Chappell et al.*, 1991]. The work of *Larsen and Gottfried* [1960] (presented in chapter 2) would suggest that these suites could be expected to have distinctive U to Th ratios. From the geology of the catchments it would therefore be expected that the ^{238}U and ^{232}Th decay series nuclides ratios should have provided distinctive signatures for the two river tributaries.

Chemical analyses of the granites have been done by XRF by Dr. B.W. Chappell of the Australian National University. These U and Th concentrations are reported in Appendix E, Table E3. The analyses have been converted to Bq kg^{-1} using the conversion factors in Appendix A and are plotted in Figure 6.5. Analyses from the Dalgety Granodiorite, which is drained by Wullwye Creek, are shown as filled squares. The granites drained by the Snowy River are shown as open squares. There is no apparent correlation between U and Th

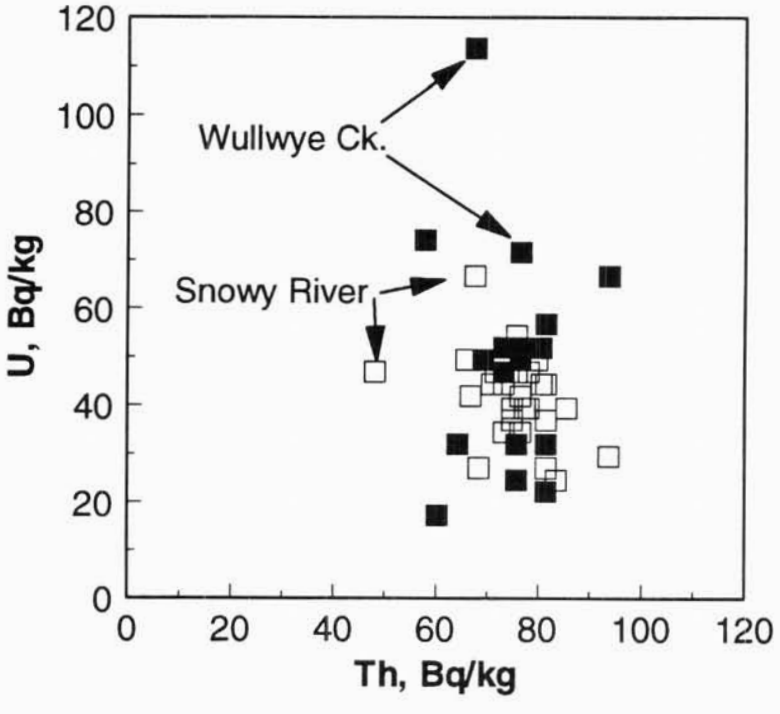

Figure 6.5: Concentration of uranium and thorium in the granite from the Snowy River-Wullwye Creek source areas (unpublished data B.W. Chappell).

concentration in the granite samples from either group. The data from both groups shows significant scatter and considerable overlap. The U/Th ratios range from 1.70 to 0.27 and 1.00 to 0.30 for the Dalgety Granodiorite and the Kosciusko batholith respectively with means of 0.68±0.08 and 0.57±0.03. These are within one standard error of each other. The U/Th ratios of the source area rocks are clearly highly variable and are not distinctive. This contrasts with the observations of *Larsen and Gottfried* [1960] of well defined correlations between U and Th in rocks from the same petrographic suite, and suggests that these nuclides are not uniformly distributed in these granites. *Rosholt,* [1983] observed similar non-uniform distribution of U and Th in granites which he attributed to redistribution of the nuclides due to rock/water interactions.

While a side issue at this point the variability of the U/Th ratio in these source rocks has implications for the work presented in chapters 4 and 5. In those chapters the soil samples were presumed to be derived from bedrock with a uniform U/Th ratio. In most cases only one representative sample of the parent rock was analysed. However the soils at each of the sites were found to have $^{230}Th/^{232}Th$ ratios consistent with that of the parent rock analysis. There are two possible mechanisms by which this can occur, either (i) the assumption of a uniform U/Th distribution in the bedrock of the areas described in Chapter 4 is correct and the soil directly inherited the $^{230}Th/^{232}Th$ ratio from the rock, or (ii) the U/Th ratio in the bedrock is variable about some mean value and the process of forming the soils in some way averages out this variability.

The difference between the work presented in chapter 4 and these data is probably related to the scale of the areas sampled. The largest area sampled in chapter 4 was ~38 km^2. The smallest of the granites described above was ~300 km^2. *Plier and Adams* [1962] showed that while the U/Th ratio in the Mancos shale, a single sedimentary unit, varied widely on a regional scale, on a local scale this ratio was relatively uniform (see discussion in chapter 2). This scale effect could also apply to other rock types.

6.3.5b ^{238}U and ^{232}Th decay series nuclide ratios in the sediments

The $^{230}Th/^{232}Th$, $^{226}Ra/^{232}Th$ and the $^{226}Ra/^{228}Ra$ activity ratios have been calculated for each of the 15 samples and are presented in Table 6.7.

The $^{230}Th/^{232}Th$ ratio for Wullwye Creek ranges from 0.38±0.04 to 0.56±0.04. Similarly, the $^{230}Th/^{232}Th$ ratio for the samples collected from the Snowy River upstream of the confluence ranges from 0.42±0.03 to 0.61±0.05. In each case the $^{230}Th/^{232}Th$ ratio falls

Table 6.7: ^{238}U and ^{232}Th series nuclide ratios for the samples collected from the Snowy River-Wullwye Creek confluence.

	$^{230}Th/^{232}Th$	$^{226}Ra/^{232}Th$	$^{226}Ra/^{228}Ra$
WUS1	0.53±0.05	0.56±0.07	0.65±0.14
WUS2	0.42±0.05	0.65±0.07	0.72±0.10
WUS3	0.56±0.04	0.49±0.07	0.58±0.16
WUS4	0.38±0.04	0.51±0.06	0.62±0.12
WUS5	0.51±0.03	0.36±0.03	0.38±0.08
Mean	0.48±0.03	0.51±0.04	0.59±0.05
SUW1	0.42±0.03	0.52±0.03	0.49±0.03
SUW2	0.46±0.03	0.57±0.05	0.53±0.09
SUW3	0.61±0.05	0.54±0.03	0.60±0.04
SUW4	0.47±0.03	0.51±0.02	0.49±0.02
SUW5	0.48±0.04	0.56±0.03	0.52±0.02
Mean	0.49±0.03	0.54±0.01	0.52±0.02
SDW1	0.58±0.05	0.56±0.03	0.52±0.03
SDW2	0.70±0.06	0.70±0.05	0.61±0.04
SDW3	0.55±0.04	0.67±0.03	0.59±0.02
SDW4	0.65±0.04	0.64±0.04	0.60±0.05
SDW5	0.42±0.03	0.52±0.05	0.52±0.10
Mean	0.58±0.04	0.62±0.03	0.57±0.02

well within the range of the U/Th ratios reported from the granites in the source areas. Clearly the thorium ratios in the sediments from the two arms overlap and do not provide distinctive signatures. Consequently, they cannot be used to determine the relative contribution of each arm to the stream. This is also the case for the $^{226}Ra/^{232}Th$ ratio and for the $^{226}Ra/^{228}Ra$ ratio. In addition the $^{230}Th/^{232}Th$ and $^{226}Ra/^{232}Th$ in the downstream sediments are on average higher than those in the upstream samples, although still within the range of the U/Th ratios of the granite source rocks. It is clear that the radionuclide data cannot be used to determine the relative contribution of Wullwye Creek to the Snowy River. However, the variability in the radionuclide ratios in both arms does indicate that sediments are being derived from a number of sources in each catchment and that these sediments are poorly mixed in the channel.

6.3.5c Normative mineralogy and sediment chemistry

The calculated mineral assemblage (section 6.3.4b) offers another means of determining the relative contribution of the two arms to the trunk stream. Quartz and feldspar are the dominant mineral components in the samples making up an average of 95% of the samples by weight. These components have very similar transport characteristics. Accordingly any signal which provides a trace on either of these components would effectively be tracing the bulk sediment. The feldspar component consists of 3 fractions; orthoclase (Or), and two plagioclases, albite (Ab) and anorthite (An). In Table 6.8 the relative concentration of Or as fraction of the total feldspar present has been calculated using the formula:

$$Or\% = \frac{Or}{Or+Ab+An} \times 100$$

Similarly, the percentage Ab in the plagioclase phase has been determined by:

$$Ab\% = \frac{Ab}{Ab+An} \times 100$$

The percentage contribution of Wullwye Creek to the sediments (0.5 - 1.4mm fraction) in the Snowy River has been calculated using a two component mixing model

$$AX + BY = C$$

where X and Y are the relative contributions from the two sources, so that X + Y=1 and A, B and C are the feldspar ratios of the two inputs and the output mix respectively. The results are presented at the bottom of Table 6.8. In each case the calculations indicate that the contribution from Wullwye Creek is negligible. These results differs markedly from the *Caitcheon et al.,* [1991] estimate of 87±8%, based on the mineral magnetic data. Given the mineralogy of the samples it is unlikely that the mineral magnetic parameters used in that study were tracing the bulk of the sediment.

Table 6.8: Feldspar concentrations used to estimate the percentage contribution of Wullwye Creek to sediments in the Snowy River downstream of the Junction.

	Or/(An+Ab+Or)	Ab/(An+Ab)
WUS1	59.1	81.4
WUS2	62.7	81.7
WUS3	59.0	81.3
WUS4	60.2	80.1
WUS5	60.4	82.2
Mean	60.3±0.6	81.3±0.3
SUW1	52.4	75.1
SUW2	57.5	79.2
SUW3	54.7	81.2
SUW4	56.4	74.8
SUW5	51.8	73.3
Mean	54.6±1.0	76.7±1.3
SDW1	52.4	75.0
SDW2	53.9	73.7
SDW3	45.8	74.2
SDW4	53.0	78.4
SDW5	54.3	77.2
Mean	51.9±1.4	75.7±0.8
	Calculated Contribution from Wullwye Creek using the above data	
	-47%±36%	-22%±38%

6.4 Summary

1. The major element and radionuclide analyses combined with mineralogical data and radionuclide analyses of the heavy mineral fractions indicates that the concentration of radionuclides in the samples are not dominated by the resistate heavy mineral contents of the samples. The data also indicates that the radionuclides are not associated with the major mineral components (quartz and feldspar) and implies that they are primarily associated with the secondary oxides. The hypothesis proposed at the beginning of the chapter is therefore not supported by the data presented here.

2. The variability of the ^{238}U to ^{232}Th series nuclide ratios in the sediments is consistent with that of the granite sources and indicates that the sediment is not derived from point sources within the catchment but come from a number of diverse source areas.

3. The lack of uniformity in the $^{238}U/^{232}Th$ series ratios in sediment from single arms must mean that they are poorly mixed. (This is particularly so considering the effort which went into the sampling in an attempt to get well averaged samples.)

4. Concentration of both ^{226}Ra and ^{228}Ra were in excess of their respective parent ^{230}Th and ^{232}Th in many of the samples examined. This was particularly the case for samples collected from the Snowy River. The radium excesses were generally correlated. This correlation was very evident in the samples collected from the Snowy River upstream of the junction. The presence of ^{228}Ra excess on many of the samples suggests that these samples have been in transport for a relatively short period of time (<20 years). This is supported by the presence of euhedral biotite in the samples.

Chapter 7: Post Depositional Changes

The previous chapters have studied the distribution and behaviour of radionuclides in rock, soil and sediments, and have examined the links between radionuclide concentrations and ratios in each of these compartments of the erosion cycle (Figure 2.4). Following deposition sediments all undergo some form of diagenesis [*Leeder* 1982], i.e. post depositional geophysical/chemical alteration. The effects of diagenesis range from simple dewatering of the newly deposited material to the formation of new secondary minerals and the lithification of the sediment. This chapter examines the effects of post-depositional alteration on radionuclide concentrations and ratios at one site (Whiteheads Creek) by studying an alluvial sedimentary deposit which shows evidence of post-depositional accumulation of secondary iron-manganese oxides. This deposit overlies the site D soil profile discussed in Chapter 4. It was shown in chapters 4 and 5 that in some soils a large proportion of the lithogenic radionuclide activity was associated with the secondary iron-manganese oxides. Therefore, redistribution and deposition of these oxides in sediments may also significantly effect the radionuclide concentrations and ratios.

Major element and radionuclide concentrations have been measured down through the alluvial sedimentary layers and citrate-dithionate extraction has been used to determine the radionuclides associated with the poorly crystalline iron oxides. These results were compared to those from the soil profile which the sediments overlie and are interpreted to provide an understanding of the effects of post-depositional alteration at this site.

7.1 Sample Description

An 800mm deep block of soil of cross-section 200 by 300 mm was cut from a valley fill deposit exposed in the gully wall at Site D (Chapter 4). Sampling locations are given in Appendix B. Examination of this soil monolith revealed three well defined units (0-160mm, 160-360mm and 360-800mm). The upper two, Units 1 and 2, are sedimentary. The basal unit is a duplex soil [*Talsma,* 1989](site D, Chapter 4). A field photograph and sampling points are shown in Figure 7.1. A total of twenty seven 1cm slices were analysed from the monolith, nine from Unit 1 (S1 to S9), ten from Unit 2 (S10 to S19) and eight from the duplex soil (D1 to D8).

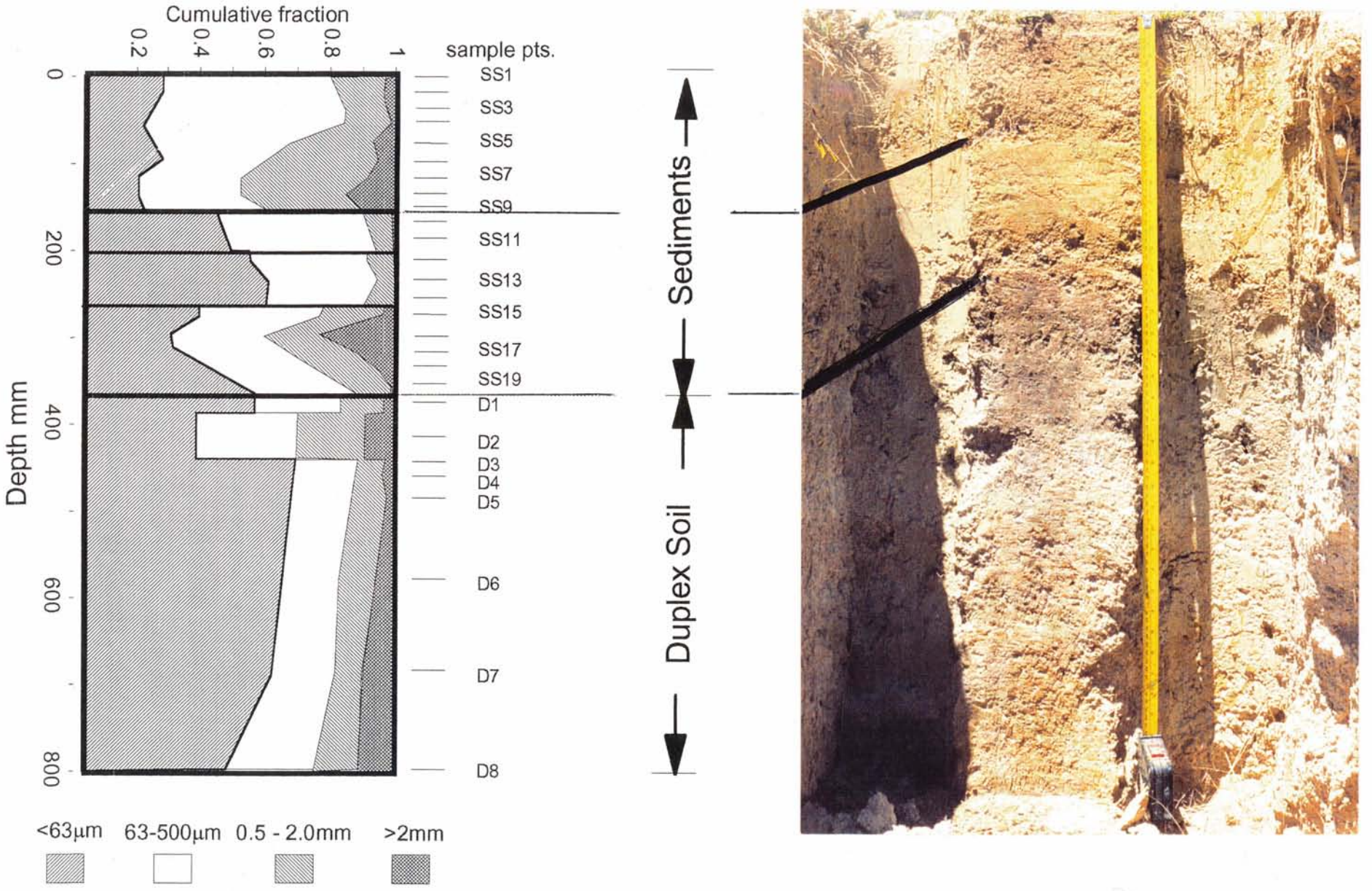

Figure 7.1:Diagram and field photograph of the Whiteheads Creek soil profile showing particle size profile and sampling points

The upper two units (Units 1 and 2), consist mainly of sand with well defined depositional structures (graded bedding and laminations). Unit 1 consists of a single bed which grades from fine sand at the surface to coarser sand at 160mm. The contact with Unit 2 is marked by an abrupt change to fine sand. Three bands were identified in Unit 2. The upper of these consists of fine sand. The middle band is a mixture of fine and coarse sand. The lower band consists of coarse sand and shows evidence of prior waterlogging and the development of iron staining. Each of these bands is clearly separated but the contacts are not as well defined as those between the units. The sedimentary units are evident on both sides of the gully, and so must have been deposited prior to the formation of the gully. These layers have been dated by optically stimulated luminescence (OSL)[*Aiken*; 1992] to circa 500 years old [*A.S. Murray pers. comm.*1994]. This date should be regarded as an upper limit because of uncertainties as to the efficacy of the bleaching process.

7.1.1 Sample treatment

Gamma and alpha spectrometry (section 3.3.1a and b) were used to determine the concentration of radionuclides in each of the samples. Major element determinations were conducted on all the samples by wet chemical techniques (section 3.3.2a). A sub sample of each sample was wet sieved to determine the particle size distributions.

The proportion of Fe and Mn associated with poorly crystalline phases was determined by citrate-dithionite extractions (section 3.3.5) in all of the samples. Alpha spectrometry was used to determine the concentration of ^{226}Ra and the thorium isotopes in 13 of these extracts - three from Unit 1, four from Unit 2 and six from the duplex soil.

X-ray diffraction mineralogical analysis was undertaken on all the bulk samples and on the <63μm fraction from 7 of the samples - one from Unit 1, one from each of the three bands in Unit 2 and one from each of the soil horizons A1, A2 and B.

7.2 Results and Discussion

The results of the various analyses of the Whiteheads Creek monolith samples are presented in the following sections. The mineralogy, particle size distribution and major element chemistry are examined first in order to provide a framework for interpreting the radionuclide data.

7.2.1 Mineralogy and particle size distribution

The X-ray diffraction spectra of the bulk samples and the <63μm fraction were dominated by quartz and feldspar (albite). Visual inspection showed that oxide coatings on the grains were present in all of the samples, but these were particularly evident in the samples from the A2 horizon in the duplex soil and in the samples from below 270mm in Unit 2. Clay was present in samples from the B horizon from the duplex soil. These phases were not detected in the XRD scans.

The particle size distributions are presented in Appendix F, Table F1, and plotted in Figure 7.1. Unit 1 is dominated by fine to coarse sand, with more than 70% of the particles in the samples from this unit >63μm in diameter. Samples from Unit 2 typically contain finer sediment than those from Unit 1 with ~50% of the grains <63μm in diameter. Samples from the lower band in this unit also contain more >2mm particles than were present in any of the Unit 1 samples. The particle size data from the duplex soil indicate that the A1 horizon is finer than A2 and the contact with the B horizon is marked by a sharp increase in the <63μm fraction. The B horizon coarsens slightly with depth.

7.2.2 Chemistry

The wet chemical analysis of the sediment samples are presented in Appendix F, Table F2, and are plotted in Figure 7.2 (after calculation of the organic free concentrations).

Al_2O_3 and SiO_2: The Al_2O_3 and SiO_2 data are presented in Figure 7.2a. The mineralogical analyses indicated that the samples were dominated by a two component mixture of quartz and feldspar. This is supported by these data. There is a strong negative correlation between Al_2O_3 and SiO_2 in the samples from Units 1 and 3 indicative of a simple two component mix. This correlation is also present in the samples from Unit 2, but the data show greater spread, suggesting that a third component may be important in this unit.

Regression lines have been fitted through the data from Unit 1 and the soil (Unit 3). The regressions have differing slopes. This suggests that the Al rich component in the soil may be different to that in Unit 1. The data from Unit 2 are largely consistent with the regression fitted through the Unit 1 data.

K_2O, Na_2O, CaO and Al_2O_3: The concentrations of K_2O, CaO and Na_2O have been added and plotted against Al_2O_3 in Figure 7.2b. Correlation between this summed component and

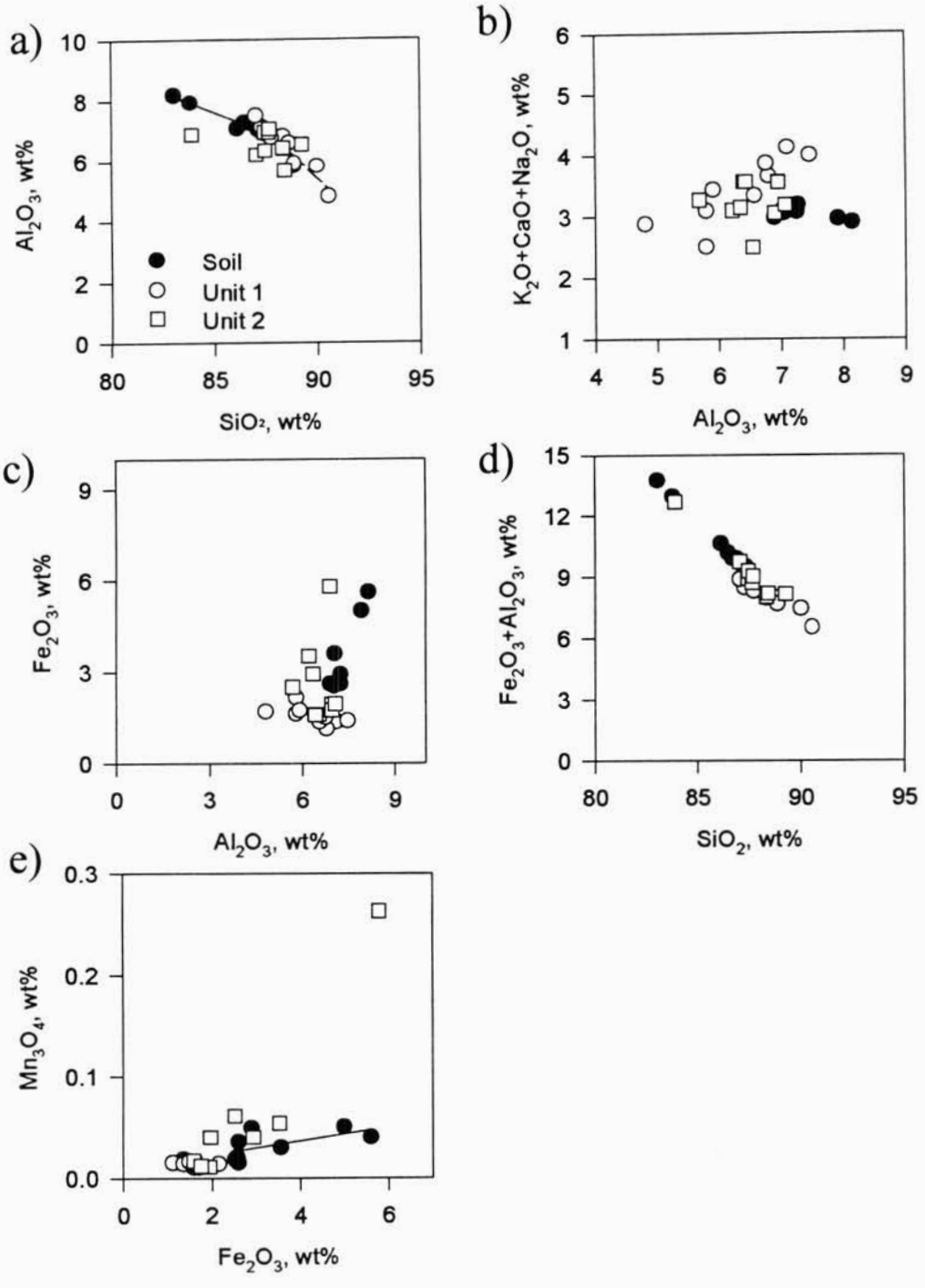

Figure 7.2: Various plots of the major element data from samples collected from the Whiteheads Creek Profile.

Al_2O_3 concentrations would be expected if the dominant Al-rich mineral is feldspar. There is a moderate correlation (r^2=0.69) between these components in the samples from Unit 1. The data from the Unit 2 samples are largely consistent with this correlation. From this, Units 1 and 2 are deduced to consist largely of quartz and feldspar, confirming the XRD analysis.

There is no correlation between these components in the data from the soil samples. This suggests that the Al-rich component in this unit is not dominated by feldspar as was indicated by the XRD analysis, but probably consists of a mixture of clay and feldspar. This is not surprising because the simplified XRD analytical technique used here favours the more crystalline mineral phases. The clay fraction requires separation followed by the preparation of orientated slides to be clearly detected by XRD analysis.

Fe_2O_3 and Mn_3O_4: There is no correlation apparent between Al_2O_3 and Fe_2O_3 in the samples from this site (Fig 7.2c). However, the summed concentrations of Al_2O_3, Fe_2O_3 and SiO_2 account for an average of 96.64 $\pm$ 0.07% of the samples by weight, and while Fe_2O_3 and Al_2O_3 are not correlated, the summed concentrations of Al_2O_3 and Fe_2O_3 are very strongly correlated (r^2=0.96) with SiO_2 (Figure 7.2d). This confirms that the samples from the profile are dominated by a three component mix of a Si rich phase (quartz), an Al rich phase (clay and feldspar) and a Fe_2O_3 rich component, presumably iron oxides.

The concentrations of Mn_3O_4 and Fe_2O_3 weakly correlated (r^2=0.36) in the samples from the soil (Figure 7.2e). Samples from Unit 1 and the the upper section of Unit 2 are generally consistent with this correlation. However, all the samples collected from Unit 2 below 270mm plot above this correlation.

The total and extractable manganese and iron concentrations are plotted against depth in Figures 7.3a and 7.3b respectively. Between 30 and 100% of the total iron and the total manganese in the samples was extracted by citrate-dithionite solution. The concentrations of both Fe and Mn generally increase with depth. However, a number of peaks in concentration do occur down the profile. The first at a depth of 135cm is marked by a sharp increase in the absolute iron concentration and also a peak in the extractable iron fraction (to 100%). There is only a minor peak in the total fraction of Mn at this depth but a marked increase in the fraction of extractable Mn (76% compared to 56% and 48% on either side of the peak) (Figure 7.4c). This peak occurs just above the junction between Units 1 and 2.

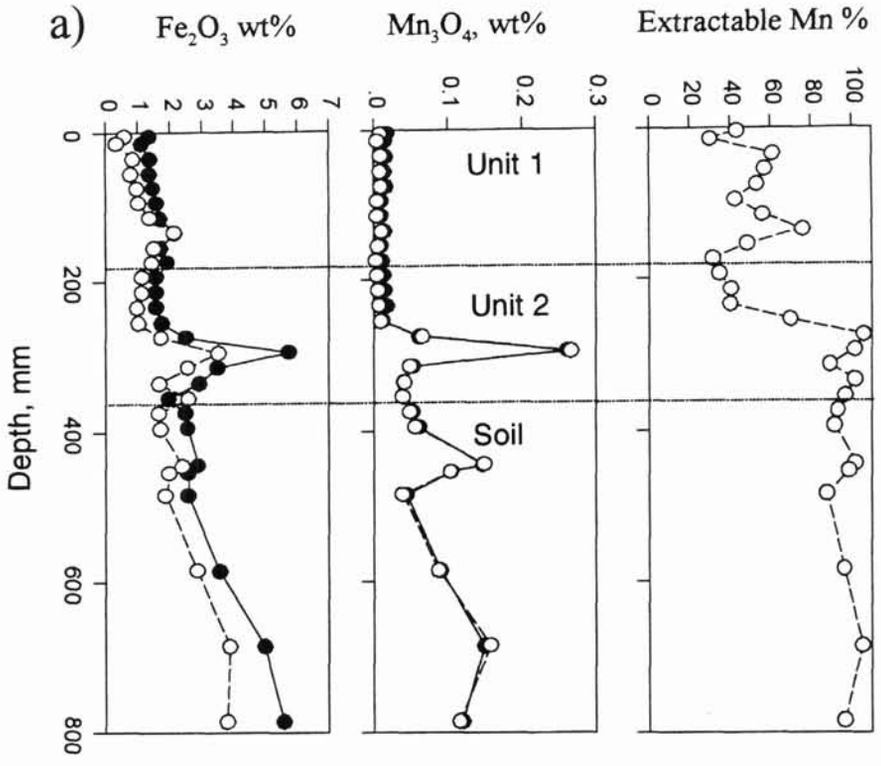

Figure 7.3: Total (closed symbols) and extractable (open symbols) iron (a) and managanese (b) concentrations, and percentage extractable Mn_3O_4 (c) against depth in samples from the Whiteheads Creek profile. The dashed lines show the boundaries between the units.

The second peak in the Fe and Mn concentration occurs between 270 and 320mm and is marked by a sharp increase in both the Fe and Mn concentrations and a marked increase in the extractable Mn concentrations (to 100%). From this depth down, most of the Mn is in an extractable form (Figure 7.3c), indicating that it is largely associated with poorly crystalline oxides. The percentage of total Fe associated with these poorly crystalline oxides ranges between 60 and 80%. This second peak is coincident with the iron stain observed in Unit 2.

Two further peaks in the Mn concentration occur at depths of 440-450mm and 680-690mm. The 440-450mm peak occurs at the junction between the A_2 and B horizons of the duplex soil. The 680-690mm peak occurs in an area where the texture of the B horizon is coarsening. These are not as marked as the peak at 270-320mm, although this may be a product of the greater sampling interval used in duplex soil. These peaks are associated with much less pronounced peaks in the Fe concentration.

The distribution of iron and manganese oxides in the buried soil profile is similar to that described for other yellow duplex soils (see *Stace et al.*, 1968). In these soils, the

concentrations of Fe and Mn generally increase with depth with a marked peak at the junction of the A_2 and B horizons. The Fe peak in these samples is smaller than is typical for duplex soils (*Ian Willet*, 1993, *pers comm.*) but the general distribution is more or less typical.

The concentrations of iron and manganese present in the sediments may either have been deposited from the groundwater after deposition of the sediments or have been present on the sediments at the time of their deposition. The lack of a marked break in the percentage of extractable Mn_3O_4 (Figure 7.3c) between Unit 2 and the A_1 horizon of the duplex soil suggests that this is a post depositional feature. That is, the Fe and Mn were added to the sediments from the groundwater after the deposition of the sediments. This is further supported by the presence of iron mottling at the base of Unit 2. Mottling would not survive fluvial transport of disaggregated grains. This mottling was interpreted by *Talsma*, [1989] as being indicative of waterlogging in this horizon. Deposition of the iron and manganese probably ceased in the sediments when the gully incised, as the gully development would have locally lowered the groundwater table.

7.2.3 Mineralogy, particle size and chemistry summary

The soil block cut from the side of the Whiteheads Creek gully consists of three well defined units. The basal unit is a duplex soil profile which has formed in the valley fill. This was overlain by two sedimentary layers which were deposited prior to the gully incision.

The samples from throughout the profile consist of a three component mix; Si rich phase (quartz); Al rich phase (clay and feldspar); Fe_2O_3 rich component, dominated by poorly crystalline oxides. The sedimentary units are dominated by silt and sand consisting largely of quartz and feldspar. Clay is present in the B-horizon of the soil.

The distribution of iron and manganese in the duplex soil is considered to be the result of the soil formation. The peaks in Mn and Fe concentrations present in the sediment are considered to be the result of precipitation from groundwater after the deposition of the sediments. These sediments were deposited < 500 years ago.

7.2.4 Radiochemistry

The gamma and alpha spectrometry analyses of the bulk samples are presented in Appendix F, Table F3; the citrate-dithionite data are presented in Table F4.

7.2.4a Equilibrium conditions

The ^{228}Ra to ^{232}Th and ^{228}Th to ^{228}Ra concentration data are presented in Figures 7.4a and b respectively, and are all consistent with the equilibrium lines (solid lines). Within analytical uncertainties, there is no indication of disequilibrium within the ^{232}Th decay series.

In contrast, significant disequilibrium is present in the ^{238}U decay series. Figure 7.4c shows the ^{230}Th to ^{238}U concentration data. The data points are all individually consistent with the equilibrium line. However, there is a systematic tendency for ^{238}U to be in excess of its daughter. The ^{226}Ra to ^{230}Th plot (Figure 7.4d) indicates that ^{226}Ra is also generally in excess of ^{230}Th and that significant excess (>40%) occurs in samples S16, D3, D4, D6, D7 and D8. These samples are those in which peaks in the Mn and Fe concentration were also observed (this is examined further below). Concentrations of ^{226}Ra and ^{238}U are in apparent equilibrium (Figure 7.4e) in all the samples, except for those in which the ^{226}Ra concentrations were greatly in excess of ^{230}Th.

7.2.4b ^{230}Th and ^{232}Th

The concentrations of ^{230}Th and ^{232}Th and the ^{230}Th/^{232}Th ratios in the bulk samples (open symbols) are plotted against sampling depth in Figures 7.5a, b, and c respectively. As was shown in Chapter 4 the ^{230}Th/^{232}Th ratio in the soil profile is consistent with a uniform value of 0.532 $\pm$ 0.009, which is within analytical uncertainty of the parent-rock ratio of 0.55 $\pm$ 0.04. However, the ^{230}Th/^{232}Th ratio in the sediments (Units 1 and 2) varies from 0.26 to 0.4. Data presented in Chapters 4 and 5 indicated that the ^{230}Th/^{232}Th ratio of the sediments are dependent on the value of this ratio in the parent rock from which they were derived. The variations in the ^{230}Th/^{232}Th ratio evident in the Unit 1 and 2 sediments therefore suggests that these sediments were derived from a number of source areas.

The concentrations of ^{230}Th and ^{232}Th in the citrate-dithionite extracts are also plotted against depth in Figures 7.5a and b (closed symbols). In each case the concentration of extractable thorium increases with depth. The ^{230}Th/^{232}Th ratio of the citrate-dithionite extracts is also shown in Figure 7.5c. In Chapter 4 it was found that the ^{230}Th/^{232}Th ratio in

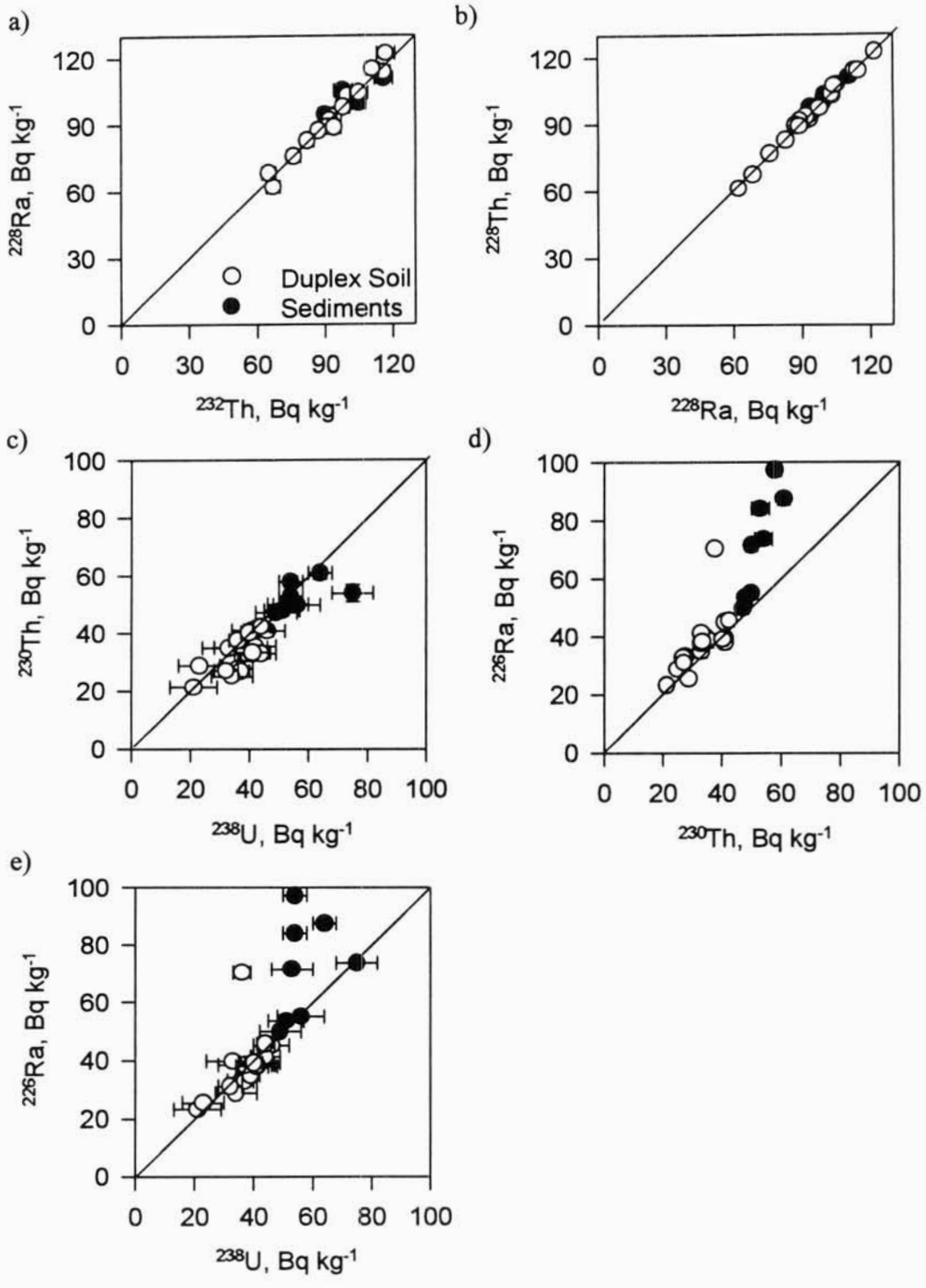

Figure 7.4: Radionuclide daughter to parent concentration plots for the Whiteheads Creek profile soil (closed circles) and sediment (open circles) samples; a) ^{228}Ra against ^{232}Th; b) ^{228}Th against ^{228}Ra; c) ^{230}Th against ^{238}U, d) ^{226}Ra against ^{230}Th, and ^{226}Ra against ^{238}U. In each case the solid line represents secular equilibrium. Error bars represent uncertainties equivalent to one standard error on the mean.

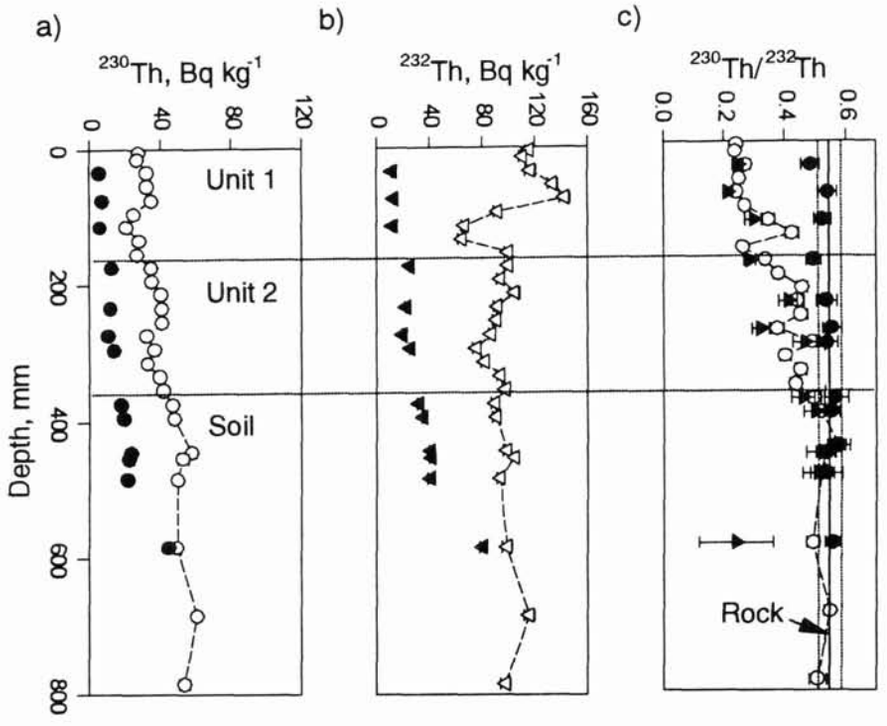

Figure 7.5: Concentrations of ^{230}Th (a) and ^{232}Th (b) in the bulk samples (open symbols) and citrate-dithionite extracts (closed symbols) with depth in samples from the Whiteheads Creek profile. (c) Variations in the ^{230}Th/^{232}Th ratio in the bulk samples (open circles), the citrate-dithionite extracts (closed circles) and in the residue (closed triangles) with depth. Error bars represent uncertainties equivalent to one standard error on the mean. The solid line in Figure 7.5c represents the rock ^{230}Th/^{232}Th ratio, the dashed lines correspond to the uncertainties on this ratio of one standard error.

the extracted fraction from the soil was the same as in the bulk soil. The ratio in the citrate-dithionite extracts from the sediments (Units 1 and 2) is also consistent with that of the soil. Citrate-dithionite primarily extracts the poorly crystalline iron and manganese oxides. It was shown in the previous section that iron and manganese have been deposited in the sediments probably from the groundwater. The above data suggest that ^{230}Th and ^{232}Th were deposited in the sediments (after they were laid down) in association with these iron and manganese oxides in the same ratio as they were present in the soil underlying profile. It is deduced that the ^{230}Th/^{232}Th ratio in the sediments at the time of deposition was overprinted by subsequent deposition of thorium isotopes in association with iron-manganese oxides.

If it is assumed that the citrate-dithionite extracted all of the thorium which had been added in association with the iron-manganese oxides then the inital ^{230}Th/^{232}Th ratio on the sediments can be calculated from the bulk sample and extraction concentration data (Figure 7.5c (closed triangles)). In this case these data show that while the addition of the ^{230}Th and

^{232}Th in association with the iron and manganese oxides has systematically increased the ratio in the sediments, it has not significantly altered the individual sample ratios. The variation in the $^{230}Th/^{232}Th$ ratios in the sediments is dominated by differences in the ratio of the material which was being deposited and has not been significantly altered by secondary overprinting following deposition. However, if the citrate-dithionite only extracted a small fraction of the thorium which has been added to the sediments, then the increase in the $^{230}Th/^{232}Th$ ratio with depth in the sediment could be due to overprinting by thorium from the groundwater. That is, the sediments could have been deposited with a uniform $^{230}Th/^{232}Th$ ratio of ~0.26, and the observed increase in the ratio with depth could be due to the deposition of thorium in the profile from the groundwater. However, given that the citrate-dithionte extracted up to 80% of the total thorium present in the soil samples, it is considered probable that it has extracted most of the secondary thorium from the sediments. It is therefore considered likely that the change in ratio observed in the sediments is dominated by differences in the ratio of the material which was being deposited.

7.2.4c ^{226}Ra

The discussion on equilibrium conditions showed that concentrations of ^{226}Ra were in excess of ^{230}Th concentrations in many of the samples examined. The ^{226}Ra excess is plotted (closed triangles) against depth of sampling in Figure 7.6. The extractable Mn_3O_4 data are shown as a dashed line on this plot. The peaks in the ^{226}Ra excess are clearly coincidental with the peaks in the extractable Mn_3O_4 concentrations. The Mn_3O_4 peak in the sediment was previously considered to have resulted from the deposition of Mn from groundwater. These data suggest that ^{226}Ra may have been deposited in association with the manganese either by coprecipitation or by sorbtion from the groundwater.

Concentrations of ^{226}Ra in the citrate-dithionite extractions from selected samples are also plotted in Figure 7.6. These data indicate that a large proportion of the ^{226}Ra excess was extracted by the citrate-dithionite, supporting the hypothesis that the ^{226}Ra excess was deposited in association with these oxides. In the 290 - 300 mm sample, which had the highest Mn_3O_4 peak, the concentration of ^{226}Ra was in excess of ^{230}Th by ~88% and ~60% of this excess ^{226}Ra was extracted. This radium addition would have altered the $^{226}Ra/^{232}Th$ ratio from 0.47 ± 0.05 to 0.93 ± 0.04 if it is assumed that initially the ^{226}Ra and ^{230}Th concentrations were at or near equilibrium.

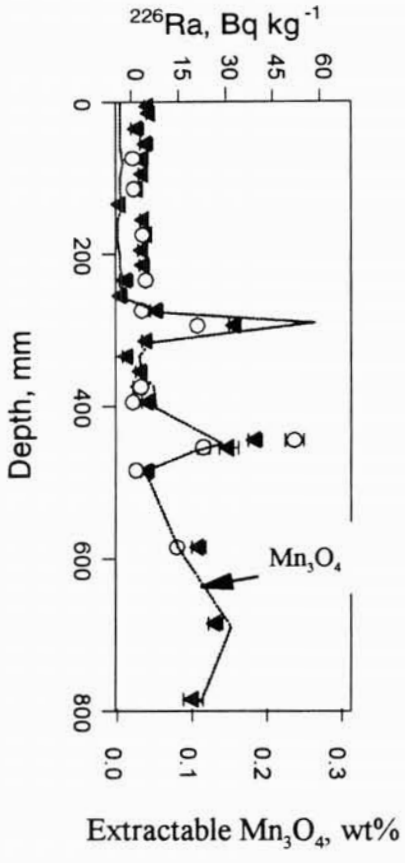

Figure 7.6: Concentrations of ^{226}Ra in excess of its parent ^{230}Th (closed triangles) and in the citrate-dithionite extracts (open circles) from samples from the Whiteheads Creek profile. The dashed line shows the extractable Mn_3O_4 concentrations. Error bars represent uncertainties equivalent to one standard error on the mean.

7.2.4d Timing of the deposition of the radionuclides in the sediments

The two sedimentary layers have been dated [*A.S. Murray pers. comm.* 1994] using optically stimulated luminescence (OSL) and are < 500 years old. Therefore ^{226}Ra, ^{230}Th and ^{232}Th have been deposited in the sediments in association with the iron-manganese oxides at sometime in the last 500 years.

7.3 Summary

Radionuclide and major element concentrations have been examined in alluvial sediments which were deposited < 500 years ago. These sediments overlie a duplex soil profile. It was shown that:

1. The $^{230}Th/^{232}Th$ ratio in the sediments varied with depth and was different to that of the soil. This suggests that they were derived from a number of sources.

2. Following the deposition of the sediments iron-manganese oxides were deposited in the sediments from groundwater.

3. Concentrations of ^{230}Th, ^{232}Th and ^{226}Ra were probably deposited from groundwater in association with these oxides. This indicates that these radionuclides are being significantly redistributed at this site on a time scale of < 500 years.

4. The $^{230}Th/^{232}Th$ ratio in the poorly crystalline, presumably recently deposited iron-manganese oxides in the sediments was the same as that of the soil which they overlie. It is deduced that the $^{230}Th/^{232}Th$ ratio in the sediments is being overprinted by the subsequent deposition of thorium isotopes from the local groundwater.

5. While the addition of ^{230}Th and ^{232}Th had on average increased the ratio in the sediments it has not significantly altered the individual sample ratios. The variation in the $^{230}Th/^{232}Th$ ratio in the sediments was considered to be dominated by differences in the ratio of the material which was deposited.

6. The addition of ^{226}Ra had significantly altered the $^{226}Ra/^{232}Th$ ratio in at least one of the sediment samples.

Chapter 8: General Discussion and Assessment of the Hypotheses

The aim of this thesis is to develop an understanding of the mechanisms which cause variability in nuclide concentrations and ratios in modern sediments, and to assess whether or not these variations can be used to trace the source of sediment. Chapters 4 to 7 have examined the behaviour and relationships between these radionuclides through the erosion cycle. This chapter (i) summarises and discusses the observations from chapters 4 to 7, (ii) assesses the hypotheses proposed in chapter 3 against these observations and (iii) develops a model of the mechanisms controlling the variability of radionuclide concentrations and ratios in modern sediment.

The effects of weathering and pedogenesis on the ^{238}U and ^{232}Th decay series nuclides are discussed first, followed by the effects of fluvial and post-depositional processes.

8.1 The Effects of Rock Weathering and Soil Formation

The weathering of rock to form soils involves many solution and precipitation reactions [*Krumbein and Sloss*, 1963]. Soluble elements such as Na, Ca, K and Mg are leached from the weathering profile [*Middelburg et al.*, 1988]. This results in an enrichment relative to the concentration in the rock of less mobile elements which are retained in the profile. Consequently the concentrations of elements which are not significantly mobilised during pedogenesis will be higher in the soils than in the parent rock. At many of the sites studied the concentrations of ^{238}U, ^{230}Th, ^{226}Ra, ^{232}Th and ^{228}Ra in the soils were either comparable or lower than those in the parent rock (Section 4.3.2). This implies that a significant fraction of these radionuclides including thorium are being mobilised during pedogenesis.

It was shown at Site A (Geebung Creek) that the movement of ^{230}Th and ^{232}Th could be occurring in association with colloids (Section 4.3.3b) as was suggested in Section 2.7. At a number of sites significant fractions (up to 80%) of the thorium isotopes retained in the soil were shown to be associated with secondary Fe-Mn oxides (Section 4.3.3). These oxides form as a result of precipitation reactions. The association of the thorium with these oxides implies that thorium is being either sorbed by these oxides or coprecipitated with them from

the soil water. These observations indicate that significant mobilisation and redistribution of thorium can occur during pedogenesis. Similar observations were made for ^{226}Ra, and the ^{238}U data presented in Chapter 4 are also consistent with uranium being significantly mobilised. It is concluded that significant mobilisation and redistribution of uranium, thorium and radium can occur during pedogenesis.

The ^{238}U and ^{232}Th decay series are expected to be in secular equilibrium in most unweathered rocks [*Iyengar*, 1990]. Data from soils (Section 4.3.1) showed that members of the ^{238}U decay series, particularly ^{230}Th and ^{226}Ra, were in many cases not in secular equilibrium. Given the degree of element mobilisation during pedogenesis, indicated by the results discussed above, this result is not surprising. Other workers have also reported similar disequilibrium in the ^{238}U decay series in soils [*Hansen and Stout*, 1968; *Megumi*, 1979; *Rosholt*, 1982; *Greeman and Rose*, 1990]. Disequilibrium was also observed between ^{228}Ra and ^{232}Th in the ^{232}Th decay series, with concentrations of ^{228}Ra in excess of its parent ^{232}Th in a number of soils (Section 4.3.1). The presence of disequilibrium in the soils indicates that differential mobilisation of decay series nuclides is occurring during pedogenesis.

While it is clear that thorium is being redistributed during soil formation, it was found that the ^{230}Th/^{232}Th ratio in all the soil samples examined was indistinguishable from the ^{238}U/^{232}Th ratio in the parent rock from which the soils were formed (Section 4.3.2a). This implies that no differential mobilisation of the thorium isotopes is occurring during pedogenesis. *Scott* [1968] and *Sarin et al.*, [1990] also observed that significant redistribution of thorium occurred during weathering with no significant differential mobilisation of the thorium isotopes. The similarity of the ^{230}Th/^{232}Th ratio in the soils and parent rock implies that either (a) no differential mobilisation of the uranium and thorium has occurred during pedogenesis or (b) any disequilibrium between ^{230}Th and ^{238}U in the soil is young compared to the half-life of ^{230}Th ($<<$ 75,200 years). Data presented in Section 4.3.1 showed that significant disequilibrium between ^{238}U over ^{230}Th were only evident in 5 of the 84 samples examined, although there was evidence of small systematic differences in concentrations in the samples from Sites B and E (Section 4.3.1). This suggests that in general uranium and thorium have behaved similarly during weathering at the sites examined. *Pliler and Adams* [1962b] in a study of the redistribution of uranium and thorium during granite weathering observed that in the early stages of rock weathering uranium was leached, but that as weathering proceeded the U/Th ratio in the weathered material became the same as that in the

parent rock. They noted that 'although the mechanisms of concentration were different, there is a striking parallel between the redistribution of uranium and thorium in the weathering profile'. Dr. B. Dickson (*pers. comm.* 1994) has also observed that the U/Th ratio in soils is comparable to those in the rock from which they were formed. These observations of parallel behaviour of uranium and thorium, at least during the later stages of weathering are consistent with the work presented in this study.

In contrast, to the uniformity of the $^{230}Th/^{232}Th$ ratio, the $^{226}Ra/^{232}Th$ ratio in soils was found in many cases to be highly variable (Section 4.3.2b) and typically not the same as the $^{238}U/^{232}Th$ ratio in the rock. This variability resulted largely from the presence of a ^{226}Ra excess over ^{230}Th in many of the samples. The excess ^{226}Ra was shown to be either surface sorbed (correlated with surrogates for grain surface area) or associated with the Fe-Mn secondary oxides (Section 5.3.1c). Excess ^{228}Ra over its parent ^{232}Th were also observed (Section 4.3.1). The presence of the disequilibrium between the radium and thorium in both of the decay series indicates that these nuclides are being differentially mobilised in the soil profile.

The ^{228}Ra excess over ^{232}Th indicates that these elements are in some instances being redistributed over a relatively short time period (<20 years). The data from Chapter 7 showed that ^{230}Th, ^{232}Th and ^{226}Ra had all been mobilised in the profile at Whiteheads Creek in less than the past 500 years. This redistribution was considered to have occurred in association with the iron and manganese oxides. *Middelburg et al.*, [1988] observed that iron and manganese oxides which are present both as amphorous phases or as surface coatings in soils are of major importance in controlling the behaviour of trace metals in weathering profiles. The data presented in this study suggest that these oxides are also important controls in the distribution of decay series nuclide concentrations.

8.2 The Effects Of Fluvial Processes

Fluvial transport produces changes in the characteristics of the material being transported as a result of sorting by particle size and density, and grain abrasion [*Krumbein and Sloss*, 1963; *Moss et al.*, 1973]. It was shown in Chapter 5 (Sections 5.3.1 and 5.3.2) that sorting soil material by density and by particle size produced fractions in which the concentration of the ^{238}U and ^{232}Th decay series nuclides differed, but these fractions had a constant $^{230}Th/^{232}Th$ ratio. This ratio was also found to be unaffected by grain abrasion (Section 5.3.3). It is thus confidently expected that fluvial transport of soil material will result

in sediments which have a uniform $^{230}Th/^{232}Th$ ratio, independent of which particle sizes or densities are sampled. The value of this ratio will be dependent on U/Th ratio of the rock from which the sediments are ultimately derived.

The $^{230}Th/^{232}Th$ ratio in the erosion cycle is unaffected by the transition from rock to soil or from soil to sediments. Consequently the variability of the $^{230}Th/^{232}Th$ ratio in sediment is therefore dependent only on the variability of the ratio in the rocks the sediments are derived from. The data from sediments presented in Chapter 6 were consistent with this statement. It is therefore expected that the $^{230}Th/^{232}Th$ ratio can be used to distinguish between sediments derived from different lithologies within a catchment, provided that the lithologies have distinctive $^{230}Th/^{232}Th$ ratios. (This is examined further in Chapter 10.)

The chemistry of thorium means that the $^{230}Th/^{232}Th$ ratio is likely to be stable in most fluvial environments. *Hancock* [1993] showed that this ratio was also stable in the estuarine environment. Data presented in Chapter 7 suggest that under conditions in which the sediments (following deposition) are exposed to local groundwaters with a different $^{230}Th/^{232}Th$ ratio, post-depositional alteration of this ratio on the sediments is possible, particularly in circumstances in which iron and manganese oxides are deposited in the sediments from the groundwater. Consequently, the use of this ratio in determining the origins of deposited sediments should be accompanied by an assessment of the degree to which post-depositonal redistribution and accumulation of the Fe-Mn oxides has occurred.

In soils in which the concentrations of ^{226}Ra and ^{230}Th were in secular equilibrium, the $^{226}Ra/^{232}Th$ ratio behaved similarly to that of $^{230}Th/^{232}Th$, and the $^{226}Ra/^{232}Th$ ratio in sediments derived from these soils will also have the same as the parent rock U/Th ratio. The $^{226}Ra/^{232}Th$ ratio on sediments is likely to be stable in most freshwater fluvial environments. However, *Hancock* [1993] showed that it is altered as a result of ^{226}Ra desorption in saline environments, and evidence presented in Chapter 7 showed that it is likely to be more susceptible to post-depositional alteration in situations in which Fe-Mn oxides are redistributed than the $^{230}Th/^{232}Th$ ratio.

It was noted in Chapter 2 (Section 2.1.4) that in the examples of nuclide concentrations and ratios in sediments given by *Murray et al.*, [1991] there was no significant disequilibrium between ^{238}U and ^{226}Ra. This suggests that in the sediments they examined the ^{238}U decay series was in equilibrium at least down to ^{226}Ra and that the ^{226}Ra and ^{232}Th correlations were in fact ^{238}U to ^{232}Th correlations. This is consistent with the above

discussion and suggests that in sediments in which the ^{238}U and ^{232}Th decay series are in equilibrium the ratio of any of the ^{238}U decay series nuclides to ^{232}Th decay series nuclides will be directly related to the parent rock U/Th ratio.

In soils which had large ^{226}Ra excess over ^{230}Th concentrations, sorting (by both particle size and density) and grain abrasion produced fractions which had variable $^{226}Ra/^{232}Th$ ratios. This was shown to be due to the thorium isotopes and the ^{226}Ra excess being differentially distributed on or in the soil grains. Sediment derived from these soils could be expected to have highly variable $^{226}Ra/^{232}Th$ ratios which will depend on particle size and density. These ratios will not easily be related to those of the soils, and may undergo further change as a function of fluvial processes. Consequently in sediments which have a ^{226}Ra excess, the $^{226}Ra/^{232}Th$ ratio is unlikely to be a useful indicator of sediment source in circumstances where particle size and density sorting are important.

Site A (Geebung Creek) is probably an exception to this observation. At this site the different particle size fractions from individual samples of this granitic soil were found to have a uniform $^{226}Ra/^{232}Th$ ratio which was generally the same as the ratio in the bulk soil sample (Section 5.3.1b). This was the case even in samples which had a large ^{226}Ra excess over ^{230}Th. It was shown that the ^{226}Ra excess and the thorium isotopes were all bound to the grain surfaces (Section 5.3.1c). That is, the radium and thorium were held in similar sites on the soil grains. While density fractions from these soils had variable $^{226}Ra/^{232}Th$ ratios these fractions were only a very small component (<1.5%) of the soils total weight and did not contribute significantly to the total activity of the sample. It is therefore expected that the $^{226}Ra/^{232}Th$ ratio in sediments derived from a point in the Geebung Creek catchment will have the same ratio as the bulk soil they are derived from (Section 5.3.1c). This suggests that the $^{226}Ra/^{232}Th$ ratio will be useful in distinguishing sediments derived from different points in this catchment despite the fact that some of these samples have a large ^{226}Ra excess. (This is examined further in Chapter 9).

While in general the presence of a ^{226}Ra excess in sediments means that the $^{226}Ra/^{232}Th$ ratio may not be a useful 'fingerprint' on the sediment, the excess itself may tell us something about sediment transport rates. Excesses of both ^{226}Ra and ^{228}Ra over their respective parents were observed in both soils (Section 4.3.1) and in sediments (Section 6.3.2) in this thesis. The concentrations of ^{228}Ra and its daughter ^{228}Th were found to be in secular equilibrium in both the soils and sediments examined (Sections 4.3.1 and 6.3.2), suggesting that the ^{228}Ra excesses

are old compared to the half-life of ^{228}Th (1.91 years). This implies that the ^{228}Ra excess has not been recently adsorbed or that the rate of sorption is slow compared to the half-life of ^{228}Th.

The ^{226}Ra and ^{228}Ra excesses in the sediments could have resulted from sorption of radium either; (i) in the soil profile, or (ii) in the fluvial system, or (iii) a combinations of both.

At this stage only (i) has been shown to occur, but there are no data to suggest which of these processes dominate. However, if the excesses are developed only in the soil profile then once the material is transported into the fluvial system they will begin to decay back to equilibrium. This being the case then a systematic decrease in the excesses would be expected as a function of distance from the source. Observation of a systematic decrease in the radium excesses in a river could therefore be interpreted in terms of sediment residence times and transport rates on the scales of 5,000 years (^{226}Ra) and 30 years (^{228}Ra), provided it can be demonstrated that these changes do not result from sediment mixing or fluvial sorting.

8.3 Summary

1. While the decay series are in secular equilibrium in unweathered rock this condition is not preserved during pedogenesis. Significant mobilisation of the decay series nuclides including the thorium isotopes occurs during this process and differential mobilisation of radium and thorium in particular results in disequilibrium in soils.

2. Although significant redistribution of thorium does occur during rock weathering no differential mobilisation of the isotopes occurs and the ^{230}Th/^{232}Th ratio present in the rocks are carried through to the soils developed on them. This implies that either no significant differential mobilisation of uranium and thorium occurs during pedogenesis (at these sites) or that any disequilibrium between ^{230}Th and ^{238}U concentrations in the soil is young (<<75,200 years).

3. The ^{230}Th/^{232}Th ratio is not effected by the transition from rock to soil, or by that from soil to sediment. The ^{230}Th/^{232}Th ratio in sediments is therefore dependent only on the ^{230}Th/^{232}Th ratio of the rocks from which they are ultimately derived.

4. Statement (3) above also applies to the ^{226}Ra/^{232}Th ratio when ^{226}Ra is in secular equilibrium with ^{230}Th (ie. ^{226}Ra/^{232}Th = ^{230}Th/^{232}Th)

5. In contrast to the uniformity of the $^{230}Th/^{232}Th$ ratio in soils developed from a uniform rock type, the $^{226}Ra/^{232}Th$ ratio was found to be variable and in many cases significantly different to the U/Th ratio in the rock. This variability was due largely to the presence of a ^{226}Ra excess over ^{230}Th. The effects of processes such as grain abrasion and sorting by particle size and density on the $^{226}Ra/^{232}Th$ ratio were shown to be dependent on two factors (i) the degree to which the ^{226}Ra concentration were in excess of ^{230}Th, and (ii) where the ^{226}Ra excess was bound on the particles in relation to the thorium. Where the ^{226}Ra and ^{232}Th were bound on similar sites on the soil grains and the ^{226}Ra excess over ^{230}Th varied throughout a catchment, it was found that the $^{226}Ra/^{232}Th$ in sediment derived from a point in the catchment would be uniform but this ratio could vary from point to point.

   In circumstances where the ^{226}Ra excess on the soil grains was not held in similar sites to the ^{232}Th, then grain abrasion and sorting (by particle-size and density) were found to produce fractions which had variable $^{226}Ra/^{232}Th$ ratios. This suggests that fluvial transport of soil material in which concentrations of ^{226}Ra are in excess of ^{230}Th concentrations and the radium and thorium are held in different sites will result in sediments which have a variable $^{226}Ra/^{232}Th$ ratio which cannot easily be related back to that of the source. Consequently, under circumstances in which these processes are important the $^{226}Ra/^{232}Th$ ratio is not considered to be a stable 'fingerprint' unless the ^{226}Ra and ^{232}Th are bound to similar sites on the grains or the ^{226}Ra excess is small.

6. Observation of changes in ^{226}Ra and ^{228}Ra excess on sediment in a fluvial system may provide information on sediment residence times and transport rates.

8.4 Assessment of the Hypotheses

Hypothesis 1 proposed that;

> Lithology is the dominant factor controlling the heterogeneity of ^{226}Ra and ^{232}Th across the landscape. Nuclide correlations present in the rock are carried through to the soils developed from them. The decay series are in secular equilibrium in soil material with the nuclides being present either on the grain surfaces or in primary resistate minerals. Erosion and sorting of the soil material results in sediments which have uranium to thorium series nuclide ratios equal to the uranium to thorium ratio of the parent material.

This hypothesis was not supported by the observations made in this thesis. Significant disequilibrium was observed between ^{230}Th and ^{226}Ra in soils and the $^{226}Ra/^{232}Th$ ratio was in many cases different to that of the parent rock. It was found, however, that the $^{230}Th/^{232}Th$ ratio in all the soil samples examined was the same as the $^{238}U/^{232}Th$ ratio in the parent rock (Section 4.3.2a). While the thorium isotopes ^{230}Th and ^{232}Th were redistributed during soil formation no differential mobilisation of the isotopes occurred at the sites examined (Sections 4.3.2a and 4.3.3). Consequently the $^{230}Th/^{232}Th$ ratio in the soils was inherited directly from the parent lithology. It was also shown that this ratio was unaltered by fluvial processes.

Hypothesis 2 stated:

> The heterogeneity observed in ^{226}Ra and ^{232}Th across the landscape is the result of soil forming processes. The ^{226}Ra distribution will not be correlated with ^{232}Th in soils, because of the differences in the relative mobility of these two nuclides. However, both ^{226}Ra and ^{232}Th are dominantly surface sorbed, either directly or in association with Fe/Mn oxide. Particle size separation during fluvial transport therefore results in the linear correlations observed in transported material. The $^{226}Ra/^{232}Th$ correlations in sediments are therefore related to soil formation effects.

This hypothesis was generally not supported by the evidence presented in this thesis. While it was found that the heterogeneity of $^{226}Ra/^{232}Th$ ratio across the landscape is the result of the soil forming process, sorting soil material by particle size often produced fractions with variable $^{226}Ra/^{232}Th$ ratios. However, this hypothesis was supported by data from Site A (Geebung Creek) at which all the decay series nuclides were found to be correlated with grain surface area. This suggests that in some catchments this hypothesis may hold true and $^{226}Ra/^{232}Th$ ratios would be a useful indicator of sediment source.

Hypothesis 3 stated that:

> In coarse grained material (sands) ^{226}Ra and ^{232}Th are primarily associated with resistate heavy minerals. Density separation of these minerals from the gangue results in the correlations observed in modern sediments.

This hypothesis (explicitly examined in Chapter 6) was not supported by the observations. It was found that the lithogenic radionuclide concentrations were probably primarily associated with the secondary iron oxides in the samples examined. These oxides

were present as surface coatings on the quartz and feldspar grains. These grains made up the bulk of the material, consequently even in these coarse grained (0.5 - 1.0 mm dia) sediments the radionuclides were associated with the bulk of the material and not some fluvially separable mineral fraction.

8.5 The Application of Lithogenic Radionuclides to the Sourcing of Sediments

The following model of the mechanisms which control the ^{238}U and ^{232}Th decay series radionuclides in modern sediments has been developed from observations made in this thesis. It particularly concerns the $^{226}Ra/^{232}Th$, $^{230}Th/^{232}Th$ and $^{228}Ra/^{232}Th$ ratios with respect to their application to the spatial sourcing of sediments and in determining sediment transport rates and residence times. Radionuclide distributions have been examined in each of the main compartments in the erosion process (shown diagrammatically in Figure 8.1).

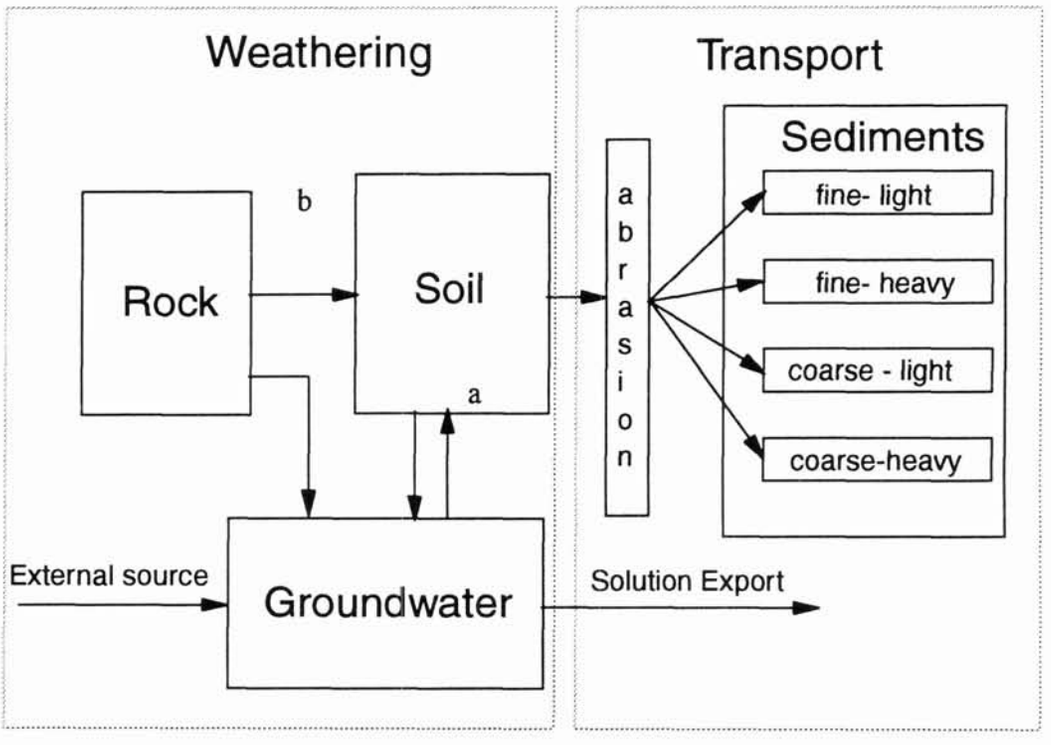

Figure 8.1: Diagram showing the links between the rock, soil and sediment compartments of the erosion process.

It is apparent from this figure that the radionuclide concentrations and ratios in the sediments are a function of the distribution of the nuclides in the soil, and the effects of the processes such as grain abrasion and sorting which occur during transport. The distribution of the radionuclides in the soils are a function of both the concentrations present in the rock, and the effects of the weathering on these concentrations. Significant redistribution of all of the radionuclides can occur during soil formation, and none of the nuclides (including thorium) are immobile during this process. However, while separation of both radium and thorium does

occur during weathering, differential mobilisation of the thorium isotopes ^{230}Th and ^{232}Th is not a significant process.

In the simplest terms a soil may be considered to consist of three main components; clay minerals, resistate rock minerals and secondary oxides (Fe-Mn). The secondary oxides are precipitated from the groundwater and consequently the radionuclide concentration in these oxides are related to those in the groundwater. In the circumstances when the input from external sources (to the groundwater) is small (Figure 8.1 arrow a) then, as no significant differential mobilisation of the thorium isotopes occur, the $^{230}Th/^{232}Th$ ratio in each of these components in soil will be the same and indistinguishable from that of the rock (Figure 8.1 arrow b). As all of the soil particles have a uniform $^{230}Th/^{232}Th$ ratio the processes which occur during transport will not effect this ratio, and the ratio in the sediments derived from this soil will be dependent only on the ratio in the rock from which it is derived. Under these conditions the $^{230}Th/^{232}Th$ ratio would be useful in distinguishing between sediments derived from different lithologies within a catchment, provide that the lithologies have distinctive $^{230}Th/^{232}Th$ ratios. An example of the possible application of $^{230}Th/^{232}Th$ ratios to determining the relative contribution from two catchments with distinctive lithologies which are supplying sediment from distributed sources to a drainage net is given in Figure 8.2.

The circumstance where the input of thorium from an external source into the groundwater is significant (Figure 8.1 arrow a) and the $^{230}Th/^{232}Th$ ratio in the groundwater is different to that in the parent rock, it is expected that the $^{230}Th/^{232}Th$ ratio in the different components of the soil may be different. The $^{230}Th/^{232}Th$ ratio of the secondary oxides would more closely resemble that of the groundwater, whereas the $^{230}Th/^{232}Th$ ratio in the resistate minerals would be closer to that of the parent rock. Then transport processes acting on the soil would produce sediments in which the $^{230}Th/^{232}Th$ ratios vary between that of the groundwater and that of the parent rock. Under such conditions interpreting the $^{230}Th/^{232}Th$ ratio in the sediments in terms of the spatial distribution of sediment source would be complicated.

As differential mobilisation of radium and thorium occurs during pedogenesis, it may be expected that the different components in the soil will have different $^{226}Ra/^{232}Th$ ratios, even if the system is closed. Consequently transport processes will be expected to produce sediments with variable $^{226}Ra/^{232}Th$ ratios which will not easily be related to the bulk ratio of the soil from which they were derived (Figure 8.2). This will be the case unless the

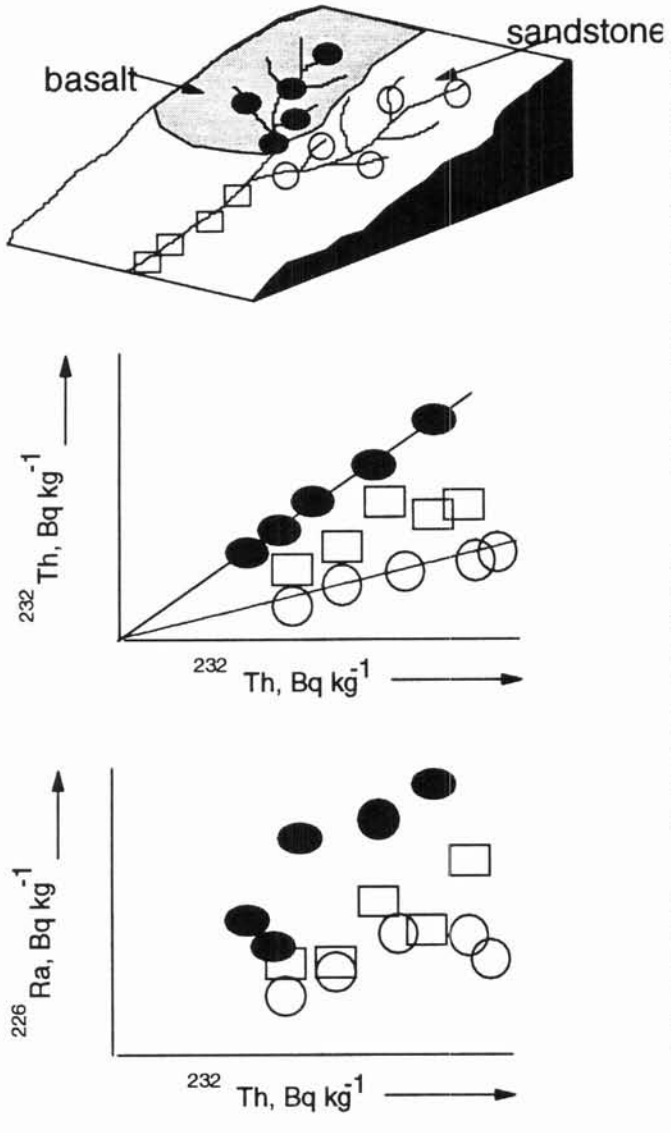

A diagram of a catchment containing two distinctive rock type (basalt and sandstone).

Sediments present in the channels within each of the lithologies are derived from those lithologies (open circles sandstone, closed circles basalt). The drainage nets from each of the lithologies combine to form a single channel. Sediments present in this channel (open squares) are a mixture of the sediments derived from the two lithologies

The basalt and the sandstone have distinctive $^{230}Th/^{232}Th$ ratios (solid and dashed lines respectively). The spread in concentration results from difference in grain characteristics (eg particle size and density)

Sediments derived from each of these lithologies have the same $^{230}Th/^{232}Th$ as the parent rock (symbols as above). Sediments from below the confluence are a mixture of the sediments derived from the two lithologies. The $^{230}Th/^{232}Th$ ratio on these sediments has to lie between the two source area ratios. The value of this ratio is dependent on the relative mix from the two sources and the way sediments with different concentration mix.

As the ^{226}Ra excess varies throughout the two source catchments each source area will produce sediments with a range of $^{226}Ra/^{232}Th$ ratios. Interpreting these data in terms of the relative contribution from each source area would be more complicated.

Figure 8.2: The expected behaviour of the $^{230}Th/^{232}Th$ and $^{226}Ra/^{232}Th$ ratios in fluvial sediments derived from two distributed source areas which have distinctive $^{230}Th/^{232}Th$ ratios and a heterogeneous distribution of ^{226}Ra excess.

distribution of both thorium and radium in the soil is controlled by the the same mechanism (e.g. both nuclides surface sorbed). Under such circumstances the transport related processes will produce fractions which have a uniform $^{226}Ra/^{232}Th$ ratio. If (i) the ^{226}Ra and ^{232}Th are bound on similar sites on the soil grains and (ii) the ^{226}Ra excess over ^{230}Th varied throughout a catchment, then the $^{226}Ra/^{232}Th$ could be used to distinguish sediments derived from different points in the catchment even if it had a uniform lithology and a uniform $^{230}Th/^{232}Th$ ratio. Figure 8.3 shows how, under these circumstances, the $^{226}Ra/^{232}Th$ ratio is likely to vary as a function of inputs from a series of point sources from within a uniform lithology.

The final element of this model does not relate to the spatial sourcing of sediment but deals with the problem of sediment transport rates and residence times. The differential mobilisation of radium and thorium in the soils means that both ^{228}Ra and ^{226}Ra excesses over their respective parents occur. If it is assumed that these excesses develop only in the soil profile, then once the material is transported into the fluvial system they may be expected to decay back to equilibrium with their respective parents. Changes in either the ^{228}Ra or ^{226}Ra excess in through a fluvial system can be interpreted in terms of the mean time since the sampled material entered the system if it is assumed that (i) the sediments entered with a constant excess, (ii) no fluvial separation of the material containing the excess has occurred, and (iii) that the system has remained geochemically closed since the sediments were detached from the soil profile. Figure 8.4 gives an idealised application of the ^{228}Ra excess to determining sediment residence times.

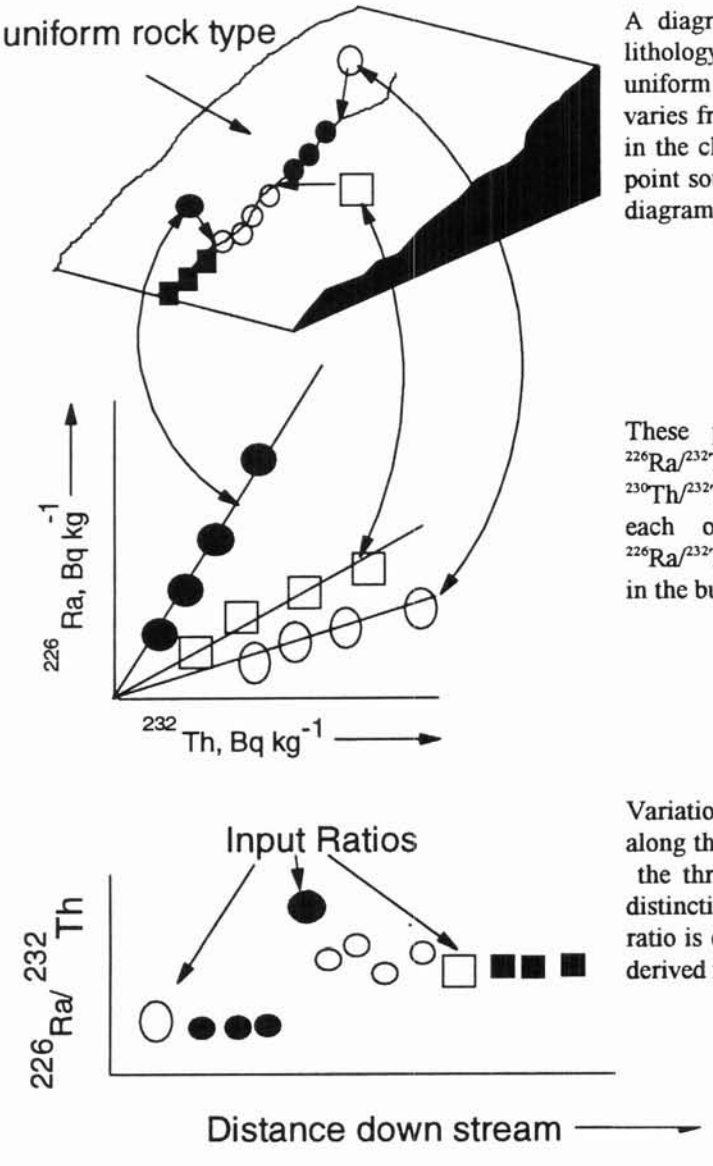

A diagram of a catchment with a uniform lithology, in which the $^{230}Th/^{232}Th$ ratio is uniform through out but the ^{226}Ra excess varies from point to point. Sediments present in the channel are derived from three distinct point sources (large symbols on the catchment diagram).

These point sources all have distinctive $^{226}Ra/^{232}Th$ ratios (solid lines), but a uniform $^{230}Th/^{232}Th$ ratio. Sediments derived from each of these sources have distinctive $^{226}Ra/^{232}Th$ ratios which are the same as those in the bulk soils (symbols as above).

Variations in the $^{226}Ra/^{232}Th$ ratio in sediments along the channel are the result of inputs from the three discrete point sources which have distinctive $^{226}Ra/^{232}Th$ ratios. The $^{230}Th/^{232}Th$ ratio is constant in all the samples as they are derived from a uniform lithogy

Figure 8.3: Example 2: a diagram showing the expected behaviour of the $^{226}Ra/^{232}Th$ and $^{230}Th/^{232}Th$ ratios in a catchment in which (i) the ^{226}Ra concentrations are in excess of ^{230}Th concentrations and the distribution of this excess is heterogeneous (ii) the radium and thorium distributions on the grains are contolled by the same mechanisms (iii) the catchment has a uniform lithology.

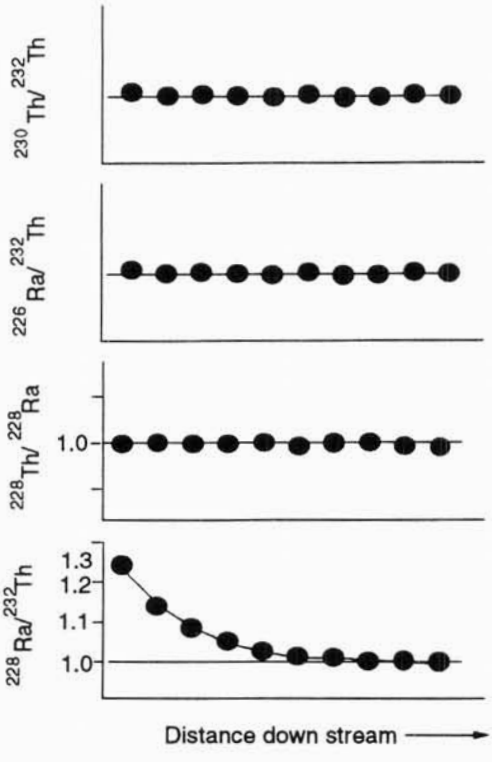

Observation of a uniform $^{230}Th/^{232}Th$ ratio or other source indicator along a fluvial channel suggests that the sediments sampled have been derived from a uniform source or mix of sources.

A uniform $^{226}Ra/^{232}Th$ ratio along the channel suggests that fluvial separation of the component containing the radium excess is not occurring as a function of distance.

A $^{228}Th/^{228}Ra$ ratio in these sediments of 1.0 suggests that any ^{228}Ra excesses on the sediments are old compared with the half-life of ^{228}Th, and that the system has been chemically closed at least over the last few years.

Given the above the systematic change in the ^{228}Ra excess along the channel can be interpreted in terms of sediment transport rates and residence times.

Figure 8.4: An idealised diagram of the application of ^{228}Ra excess to determining sediment transport rates and residence times

8.5.1 Model summary

It is considered that the $^{230}Th/^{232}Th$ ratio will provide a useful 'fingerprint' on sediments in catchments which contain a number of rock types which have distinctive $^{230}Th/^{232}Th$ ratios. However, it is unlikely to be useful in small catchments which have uniform lithologies. The heterogeneity of $^{226}Ra/^{232}Th$ ratio may in some circumstances provide a useful tracer 'signal' in small catchments which have a uniform lithology. Finally it is considered likely that the observation of systematic changes in the ^{228}Ra excess in sediments will prove to be a useful tool for examining sediment transport rates and residence times.

Part III

Three examples of the application of ^{238}U and ^{232}Th decay series nuclides to sediment tracing problems.

The model of lithogenic radionuclide behaviour in fluvial sediment described in chapter 8 has been applied to three distinct sites. In chapter 9 the model is applied to the Geebung Creek catchment. This catchment has a uniform lithology and the soils have a uniform $^{230}Th/^{232}Th$ ratio, but the $^{226}Ra/^{232}Th$ ratio is heterogeneous.

In chapter 10 $^{230}Th/^{232}Th$ ratios are used to examine the sources of sediment to the Jenolan Caves, New South Wales. McKeowns Valley is the main catchment area for the Jenolan Caves. These caves which are a major tourist attraction are filling with sediment. The sediment is being derived from McKeowns Valley. The NSW tourist commission which is concerned over the potential damage this sediment is doing to the caves would like to know where to target soil conservation works. The catchment contains two rock types which have distinctive $^{230}Th/^{232}Th$ ratios (section 4.3.2 sites B and C) this makes it an ideal site to examine the application of $^{230}Th/^{232}Th$ ratios to a sediment sourcing problem.

In chapter 11 the application of the ^{228}Ra excess to determining sediment transport rates and residence times for sediments from the Murrumbidgee Reach of Lake Burrinjuck, New South Wales, is examined.

Chapter 9: Identifying Sediment Sources in a Catchment with a Uniform Lithology

9.1 Introduction

The dry sclerophyll forests on the south-east coast of New South Wales (NSW) have been the subject of logging operations since the late 1960's. Most of the forested area is underlain by granite bedrock and the soils developed over these are generally considered to be easily erodible [*Moore et al.,* 1986a]. The public concern over the impact of these logging operations on water quality, sediment delivery and destruction of habitat, is described by *Routley and Routley* [1974]. In response to this concern six experimental catchments were established to provide data on the erosional behaviour of the granite soils within the wood chip concession [*Olive and Rieger*, 1987]. This chapter examines the sources of bedload sediment in one of these catchments over a two and a half year period following partial logging of the catchment.

Assessing the impact of logging operations on sediment delivery to stream-lines often entails intense monitoring programs which are expensive in terms of both time and resources. An alternative method is to trace sediments from within the stream-lines back to their source. This offers a direct method of determining whether the material is being derived primarily from the erosion of logged areas. Such an approach involves the measurement of some source specific label, such as clay mineralogy, sediment colour and major element chemistry [*e.g.;Woods,* 1978; *Grimshaw and Lewin,* 1980; *Walling and Kane,* 1984]. To be widely applicable, a tracer needs not only to be distributed throughout the bulk of the sediment, but also to have a high probability of providing a unique label for that sediment. Natural and anthropogenic radionuclide concentrations in sediments have been shown to provide such labels [*Wasson et al.,* 1987; *Sutherland and de Jong,* 1990; *Murray et al.,* 1993; *Olley et al., 1993*]. Correlations between ^{226}Ra and ^{232}Th have been used to characterise sediment sources where each source has a unique ^{226}Ra to ^{232}Th concentration ratio [*Murray et al.,* 1993; *Olley et al.*, 1993].

The purpose of this study was to use lithogenic and fallout radionuclides to test the hypothesis that sediments moving within a partially deforested catchment were derived primarily from the logged area. Radionuclide concentrations in sediment moving in the stream-lines within the catchment are studied both spatially and temporally,

and the likely effects of particle size and density separation during transport are examined. Variations in the radionuclide data are then interpreted in terms of sediment sources.

9.2: Catchment Description and Previous Studies.

The Geebung Creek catchment (site A in chapter 4 and 5) is situated in the Yambulla State Forest about 30 km inland from the south-east coast of NSW (Figure 8.1). The 76.9 ha catchment ranges in altitude from 157 m at the weir to 331 m on the highest ridge. Eighteen percent of the catchment has a slope of 0 - 5%; 32% has a slope of 6 - 10%; 27% has a slope of 11 - 15%; and 23% has a slope of 15% [*Moore et al.*, 1986b].

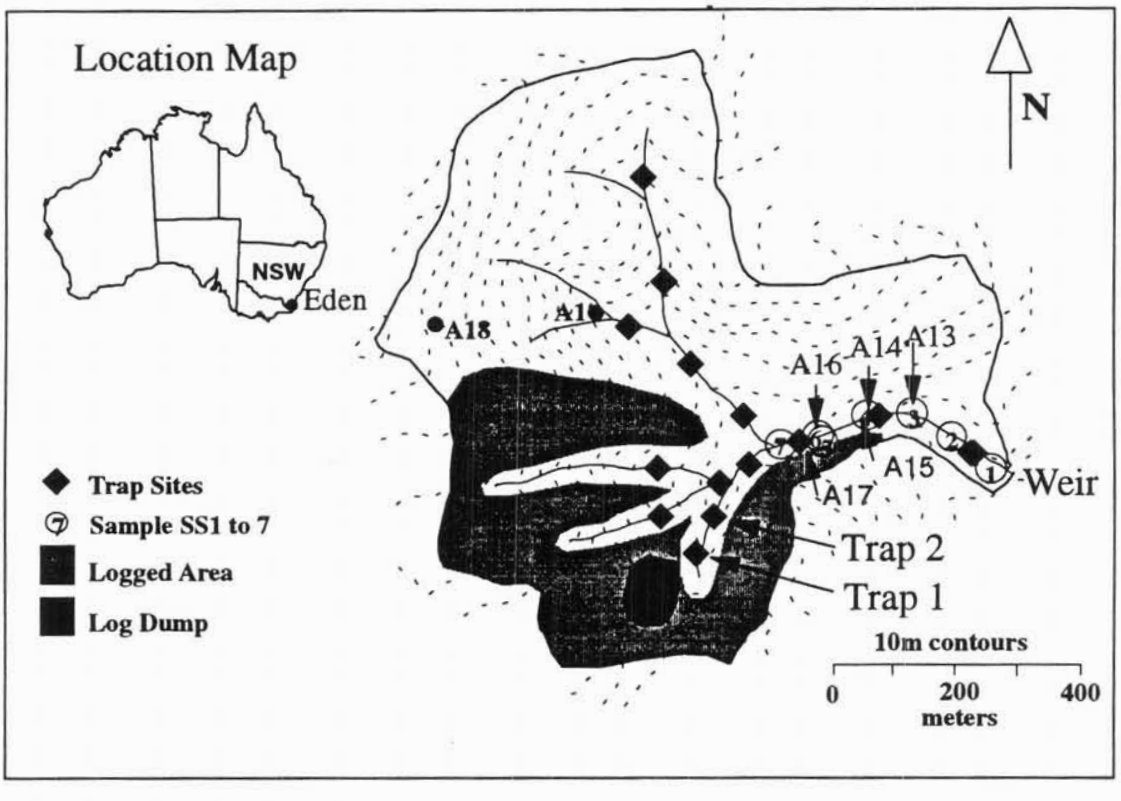

Figure 9.1: Map of the Geebung Creek catchment showing location and the sampling points

The catchment is underlain by the Yambulla granite pluton, part of the Bega Batholith, and outcrops occur throughout the catchment. The granite has uranium and thorium concentrations of 4.4 ppm (± 10%) and 24.0 ppm (± 5%) respectively

[*B.W.Chappell pers. comm.* 1992]. These correspond to activities of 54±5 Bq kg^{-1} for uranium and 97±5 Bq kg^{-1} for thorium giving an activity ratio of 0.56 ± 0.06.

The catchment soils have been described by *Moore et al.* [1986 a, b]. In summary, soils are generally less than a metre deep in the upslope areas, a somewhat greater depth in the lower-slope areas, and in all cases overlie weathered granite. They consist predominantly of coarse textured profiles (sandy loams and loamy sands) that are massive, have shallow A-horizons and grade sharply into decomposing rock at depths of 40 - 100 cm. The surface soils have high organic carbon contents (3 - 10%), low bulk densities (0.85 - 1.1 g cm^{-3}) and are considered to be highly erodible.

The stream channel is narrow, generally less than 2 m bank to bank. It is deeply incised in sections (down to ~1.5 m) in the lower catchment and in these areas local bank collapse is evident. The bedrock is exposed along most of the lower channel. The stream channels are less well defined in the upper catchment and are lined with native grasses and reeds. Sediment in the channel is not contiguous, but consists of a series of sediment lobes, usually located in slackwater areas. Observation suggests that sediments accumulate in the channel during low intensity rainfall events and that periodically a large proportion of this sediment is flushed out of the catchment during high intensity storms.

The entire catchment understorey was burnt in December 1972. In September 1979, a 140° V-notch weir was constructed at the outlet of the catchment (Figure 9.1). The southern part of the catchment was logged and then burnt (Figure 9.1) in June - July 1987 [*Mackay*, 1988]. The erosion mitigation and catchment protection procedures applied during logging included retention of 40 m buffer strips of vegetation on either side of the stream-lines for stream gradients greater than 18° and 20 m for lesser gradients; retention of seed trees; drainage of logging tracks, log landings and roads; and restrictions on the movement of logging equipment near sensitive areas.

The logging was followed by a 6 month period in which only low intensity rain events occurred. *Crapper et al.* [1989] in a study of the pre and post logging hydrology of the catchment noted that logging increased the water yield from the catchment. *Rieger et al.* [1979] and *Olive and Rieger* [1987] examined suspended sediment supply and concluded that logging and wildfires increase the supply of suspended sediment to the streams. This study is the first examination of the sources of bedload in the catchment.

9.3 Sampling Methods and Sample Treatment

Five groups of samples were collected. These are listed in Table 9.1 and are described below.

Table 9.1: Types of samples collected from the Geebung Creek Catchment

Type	Description
Point source :	Four samples A1, A13, A16 and A18 used to characterize the radionuclide signatures to be expected from point sources.
Stream Bank :	Five samples collected, from areas of localized bank collapse along the main channel below the confluence, to characterize the variability in the stream banks.
Sediment Trap:	Bedload samples collected using fixed passive sediment traps, during storm events over a 700 day period.
Sediment :	Seven bedload samples (SS1 to SS7) collected from the major sediment bodies present in the main channel below the confluence

9.3.1 Point source samples

Fluvial transportation results in sorting of soil material by particle size and to a lesser extent by density [*Krumbein and Sloss,* 1963]. In this study four samples were used to examine the types of relationships that might be expected between lithogenic radionuclides in sediments derived from point sources within the catchment. Samples A1 and A18 from the upper catchment (Figure 9.1) and samples A13 and A16 from the lower catchment.

Sub-samples of all the samples were separated by wet sieving into size fractions; <63 μm, 63-125 μm, 125-250 μm, 250-500 μm, 500-1400 μm, 1400-2000 μm, and >2000 μm. The <63μm fractions from samples A13 and A16 were additionally separated into <38μm and 38-63μm fractions. Heavy minerals (>2.95 g cm^{-3}) were also separated from samples A13 and A18. The particle size fractions and density separates were analysed to determine the type of radionuclide distribution to be expected from fluvially transported sediments derived from point sources within the catchment. The results of this work were discussed in chapter 5, sections 5.3.1 and 5.3.2.

9.3.2 Stream bank samples

Five samples (A13 to A17) were collected from the stream banks along the channel below the confluence (Figure 9.1) to characterise the variablity in the

radionuclide signature of the banks. In each case the samples were collected from areas of exposed bank in which bank collapse was evident.

9.3.3 Bedload samples

A sequence of event based samples was collected, using shallow steel traps fixed into stream beds, from both the logged and unlogged areas of the catchment and from the channel down stream of the junction (Figure 9.1). These traps (4cm deep x 20 x 40cm) were partially enclosed to ensure that bedload material which entered the trap did not escape. They were placed in the catchment after the post-logging burn in 1987. The logging operation was followed by a period of low rainfall and the first samples were collected 260 days after the post-logging burn, following an 80 mm rain event. Traps 1 and 2 were emptied six times in a 700 day period from the first sampling. The largest rain event during this period was 165mm (72 hours) which has a return period of ~2 years. The remaining traps were all emptied on at least 2 occasions in this period. Traps 1 and 2 were located in the stream-line directly below the area used as the log dump during logging (Figure 9.1).

In addition, seven 2kg samples (SS1 to SS7) were collected from the weir up the stream-line to the confluence of the logged and unlogged arms (Figure 9.1). Each sample consisted of up to 20 subsamples taken along a 10m section of the channel. They were all recently deposited, predominantly coarse grained sands. Samples SS5 and SS6 were collected from adjacent locations (Figure 9.1) in the channel. Sample SS5 came from a sediment bar onto which a new bedload material (SS6) was being deposited. The seven samples are representative of the major sediment bodies present in the downstream stream-line at the time of sampling. A 1kg sub-sample of each sample was particle size separated. Radionuclide concentrations were determined in the particle size fractions from samples SS2, SS3, SS6 and SS7.

9.4 Results and Discussion

All of the samples were analysed by gamma spectrometry, selected samples (26 out of 49) were analysed for thorium isotopes by alpha spectrometry. The analyses of samples used in this chapter are presented in Appendix G.

9.4.1 Equilibrium conditions

The parent/daughter activities for all the samples are plotted in Figures 8.2a,b and c. The concentrations of ^{228}Th and its parent ^{228}Ra are clearly consistent with equilibrium, (Figure 9.2a). This is similar to observations made at other study sites [*Murray et al.*, 1991; *Murray et al.*, 1993; *Olley et al.*, 1993]. In each study the authors assumed secular equilibrium in the ^{232}Th decay series and calculated the concentration of ^{232}Th from the weighted mean of the ^{228}Th and ^{228}Ra activities. The measured concentrations of ^{232}Th are plotted against ^{228}Ra concentrations in Figure 9.2b. All of the samples from Tray 2 have ^{228}Ra concentrations in excess of its ^{232}Th. However, the ^{232}Th decay series is in equilibrium in all the other sediment samples examined. Consequently, the ^{232}Th concentrations for those sediment samples (collected by traps other than Trap 2) for which thorium was not analysed have been calculated from the weighted mean of the ^{228}Th and ^{228}Ra activities, assuming secular equilibrium in the ^{232}Th decay series. This assumption is considered reasonable given the above data. A ^{228}Ra excess is also evident in one of the bank samples. All of the bank and point source samples were analysed by both gamma and alpha spectrometery. Concentrations of ^{226}Ra and ^{230}Th are typically not in equilibrium in all of the samples; ^{226}Ra is in excess of its parent by up to 40% (Figure 9.2c).

9.4.2 ^{230}Th to ^{232}Th and ^{226}Ra to ^{232}Th relationships

The concentrations of ^{230}Th in the sediment samples are plotted against ^{232}Th concentrations in Figure 9.3a. As expected from the uniform lithology the data are consistent with a single regression line pointing to the origin (r^2=0.98); the mean ^{230}Th/^{232}Th ratio is 0.582 $\pm$ 0.008 (n =26). This is consistent with the single activity ratio measurement for U/Th of 0.56 $\pm$ 0.06 (calculated from the concentration data) for the Yambulla Granite. This suggests that no differential loss of the thorium isotopes had occurred during weathering (as was shown in chapter 4 for the soil samples from this catchment). The uniformity of the ^{230}Th/^{232}Th ratio means that it is of little use in distinguishing sediments derived from different areas of the catchment.

In contrast, the ^{226}Ra to ^{232}Th concentrations show a wide scatter (Figure 9.3b), with ^{226}Ra/^{232}Th ratios ranging from 0.56 to 1.7. However there is considerable overlap between sediments collected from the different areas of the catchment. The spread in the

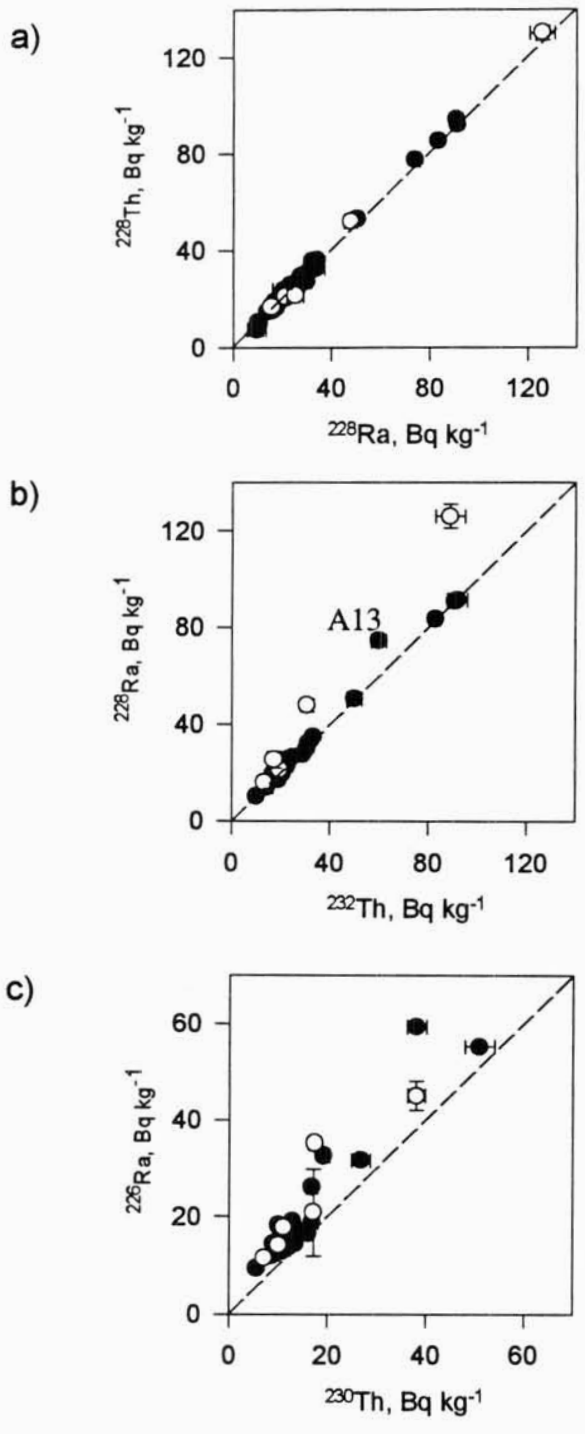

Figure 9.2: Parent/daughter activity plots for all sediment samples from the Geebung Creek Catchment. In each figure the dashed line represents the equilibrium condition. Data from Trap 2 saples shown as open symbols. Except where shown, analytical uncertainties equivalent to one standard error are smaller than the symbol size.

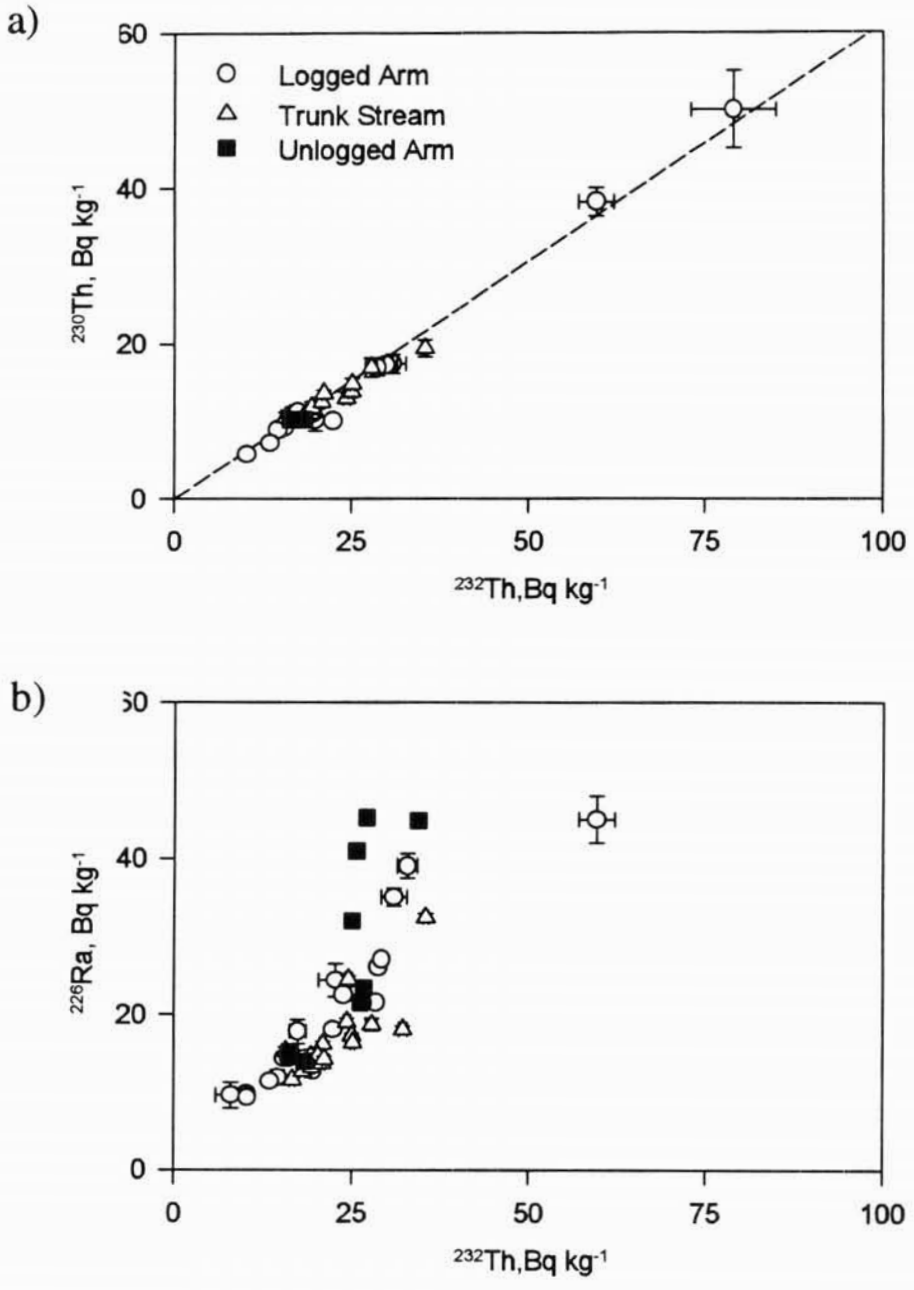

Figure 9.3: Concentrations of (a) ^{230}Th and ^{232}Th, and (b) ^{226}Ra and ^{232}Th in sediment samples from Geebung Creek. Except where shown, analytical uncertainties equivalent to one standard error are smaller than the symbol size.

$^{226}Ra/^{232}Th$ ratio indicates that it may be of use in distinguishing different sediment source areas within the catchment, but to proceed further, an understanding of the $^{226}Ra/^{232}Th$ relationships to be expected from erosion of sediment derived from point sources is needed.

9.4.3 Point sources

The four soil samples (A1, A18, A13 and A16) were used to examine the likely radionuclide distributions in material derived from point sources within the catchment. In chapter five it was shown that the particle size fractions of soils derived from points in this catchment have constant $^{226}Ra/^{232}Th$ activity ratios. While the >2.95 g cm^{-3} fractions were found to have variable $^{226}Ra/^{232}Th$ ratios this fraction was typically <1.5% of the samples by weight and did not significantly contribute to the total activity of the samples. This suggests that particle size separation will be the predominant fluvial process effecting the radionuclide concnetrations, and that sediments derived from a point source will have a uniform $^{226}Ra/^{232}Th$ ratio. It was shown in chapter 4 that the $^{226}Ra/^{232}Th$ ratio varies both horizontally and vertically in soils. In this context the term point source therefore refers to a small area constrained both vertically and horizonally.

9.4.4 Sediments collected from below the log dump

The $^{226}Ra/^{232}Th$ ratios have been calculated for the samples collected from Traps 1 and 2 and are plotted against time in days since first sampling in Figure 9.4. Trap 1 collected sediment with $^{226}Ra/^{232}Th$ ratios consistent with a uniform value (0.90 $\pm$0.02). This suggests that the sediments collected by this trap have been derived from a constant source or mix of sources over the 700 day sampling period. The $^{226}Ra/^{232}Th$ ratio data from the Tray 2 sediments is more variable (ranging from 1.13 $\pm$ 0.08 to 0.70 $\pm$ 0.07). This suggests that these Trap 2 sediments are derived from a number of point sources.

It was shown above that the concentrations of ^{228}Ra were in excess of ^{232}Th concentrations in the Trap 2 samples. The $^{226}Ra/^{228}Ra$ ratio has been calculated and is plotted against days since first sampling in Figure 9.5. This ratio in these sediments is consistent with a uniform value of 0.659 $\pm$ 0.014.

The ^{226}Ra and ^{228}Ra excesses have been calculated and are plotted in Figure 9.6. The ^{226}Ra and ^{228}Ra excesses are correlated (r^2=0.94) with an intercept close to zero.

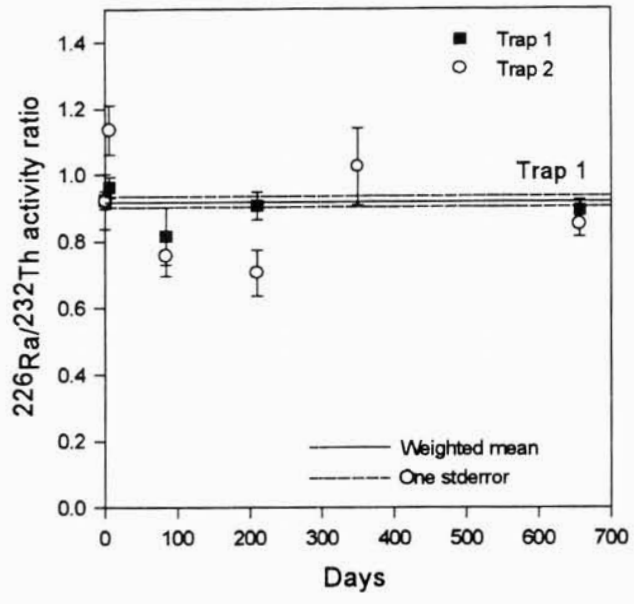

Figure 9.4: The $^{226}Ra/^{232}Th$ activity ratios in the sediments collected from Traps 1 and 2, Geebung Creek catchment against time of sampling. Except where shown, analytical uncertainties equivalent to one standard error are smaller than the symbol size.

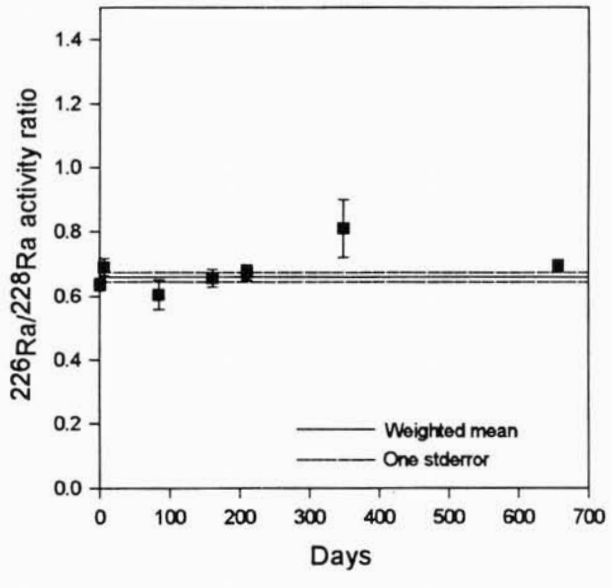

Figure 9.5: The $^{226}Ra/^{228}Ra$ activity ratio in the sediments collected from Trap 2, Geebung Creek catchment against time of sampling. Except where shown, analytical uncertainties equivalent to one standard error are smaller than the symbol size.

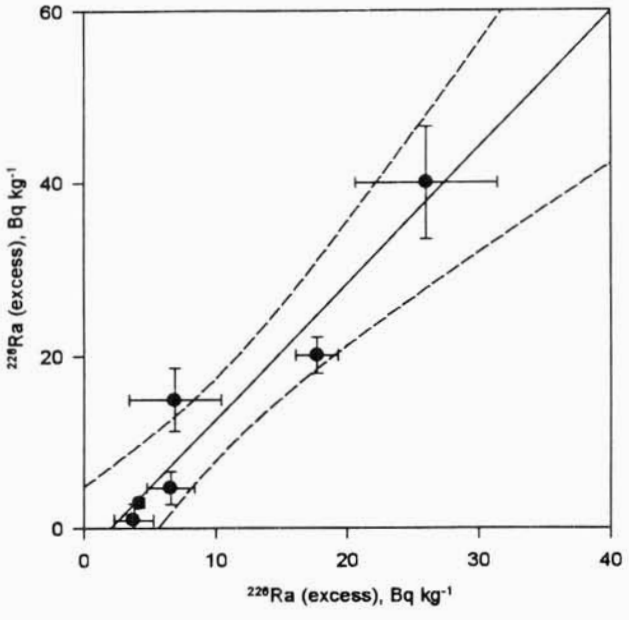

Figure 9.6: ^{228}Ra excess against ^{226}Ra excess in the sediments collected from Trap 2, Geebung Creek catchment. Error bars represent analytical uncertainties equivalent to one standard error. The regression line (solid) and 95% confidence limits (dashed lines) are shown.

This association of the two excesses explains the lower variability in the ^{226}Ra/^{228}Ra ratio compared to the ^{226}Ra/^{232}Th in the sediments. The correlation between the ^{226}Ra and ^{228}Ra excesses also indicates that both nuclides were co-deposited on the sediments either in the soil profile prior to transportation or from the stream waters. Given the low salinity of the surface waters in this catchment [*Gippel,* 1989] and particle reactive nature of radium (see chapter 2, section 2.4.3) it is considered that this deposition is most likely to have occurred in the soils prior to transportation. This assumption is supported by the fact that concentrations of ^{228}Ra in the sediments are in equilibrium with its daughter ^{228}Th. This indicates that the ^{228}Ra excess is old compared to the half-life of ^{228}Th (1.8 years) and that the excess ^{228}Ra has not been recently sorbed. Furthermore, the correlation between the radium excesses also implies that all the sediments were exposed to groundwater with a uniform ^{226}Ra/^{228}Ra activity ratio; they must also be of uniform age which must be less than a few half-lives of ^{228}Ra.

The presence of the ^{228}Ra excess on the sediments has the potential of providing information on sediment residence and transport times. Given the assumption that this excess was developed in the soil, then the excess can be expected to begin to decay back

to equilibrium following transportation. The short half-life of ^{228}Ra means that concentration of ^{228}Ra in excess of ^{232}Th can be used to examine sediment transport and storage on a time scale of up to a few ^{228}Ra half-lives (~30 years).

As the Tray 2 sediments were not derived from a common point source (evidenced by the variable $^{226}Ra/^{232}Th$ ratio), it is not valid to attempt to interpret the differences in ^{228}Ra excess in terms of different residence times or transport rates. Nevertheless, the presence of the ^{228}Ra excess does indicate that these samples have been in transport for a relatively short period of time (<<30years). It is considered that it would be possible to design experiments to study sediment transport rates or residence times using the ^{228}Ra excess in this catchment. When combined with indicators of sediment source such as $^{226}Ra/^{232}Th$ and $^{230}Th/^{232}Th$ ratios, observation of this excess should provide a useful new tool for examining bedload transport processes.

9.4.5 Stream bank samples

The $^{226}Ra/^{232}Th$ activity ratios of the stream bank samples collected from the lower channel are shown in Table 9.2.

TABLE 9.2: Sampling distance upstream of the weir, $^{226}Ra/^{232}Th$ ratios and ^{137}Cs concentrations (Bq kg^{-1}) for the stream bank samples collected from Geebung Creek. Uncertainties are equivalent to one standard error.

Sample	Distance (m)	$^{226}Ra/^{232}Th$	^{137}Cs
B1	200	0.79 ± 0.03	0.3 ± 0.2
B2	295	0.88 ± 0.02	-0.5 ± 0.4
B3	300	0.796 ± 0.019	0.6 ± 0.4
B4	380	1.80 ± 0.03	0.3 ± 0.2
B5	400	0.505 ± 0.006	0.04 ± 0.17

The $^{226}Ra/^{232}Th$ ratios vary markedly from sampling point to sampling point, ranging from 0.505 ± 0.006 to 1.80 ± 0.03. The ^{137}Cs concentrations in the samples are all low (within two standard errors of zero) and with a maximum value of 0.6 ± 0.4 Bq kg^{-1}.

Sediments derived from points along the stream banks could therefore be expected to have distinctive $^{226}Ra/^{232}Th$ ratios and low ^{137}Cs contents.

9.4.6 Sediment in the channel

The particle size distributions and mineralogy of samples SS1 to SS7 (Figure 9.1) showed that all were predominantly coarse grained (> 60% grains >500 μm) and consist largely of quartz and feldspar grains (iron oxide coats and staining were present on most of the grains). The downstream samples (SS1 to SS4) are coarser than those upstream (SS5 to SS7; 60% compared to 40% of the sample >2mm).

The $^{226}Ra/^{232}Th$ ratios for all the sediment samples collected are plotted against distance upstream from the weir in Figure 9.7. If a single well mixed source dominated the sediment present in the stream-lines, then a uniform $^{226}Ra/^{232}Th$ ratio would be expected in the sediments collected down the stream-line. However, the $^{226}Ra/^{232}Th$ ratios in the sediment varied markedly from one sampling point to the next, as was the case with the samples from Trap 1 and 2. Given that these ratios are unaffected by particle size separation (section 5.3.1b) which is the predominant fluvial sorting process [*Krumbein and Sloss,* 1963] these variations are unlikely to be the result of some transport related phenomena, and therefore the changes in ratio along the stream-line suggests that numerous small sources are supplying sediment to the stream-lines and no one source is dominating. Furthermore, these data suggest that longitudinal mixing in the channel is poor.

To test these conclusions, four of the trunk stream samples were separated into various particle sizes and each size fraction was analyzed . All these samples have similar $^{226}Ra/^{232}Th$ ratios of about 0.65. The ^{226}Ra and ^{232}Th concentrations for the size fractions analyzed from SS2 and SS3 (Figure 9.8) are consistent with a single regression line with a slope of 0.607 ± 0.007 and an intercept within analytical uncertainty of zero (1±2). The data from samples SS6 and SS7 are also consistent with a single regression line (intercept 0 ± 5) but with a slope of 0.679 ± 0.018. These data are clearly consistent with these groups of sediment being derived from separate source areas. Given that the sample locations for these two groups were less than 400 m apart, and that they were separated by SS4 and SS5, which have $^{226}Ra/^{232}Th$ ratios of 0.971 ± 0.005 and 0.97 ± 0.018 respectively, this supports the suggestion that sediments present in the stream-line are poorly mixed and derive from a large number of small source areas which have different radium ratios.

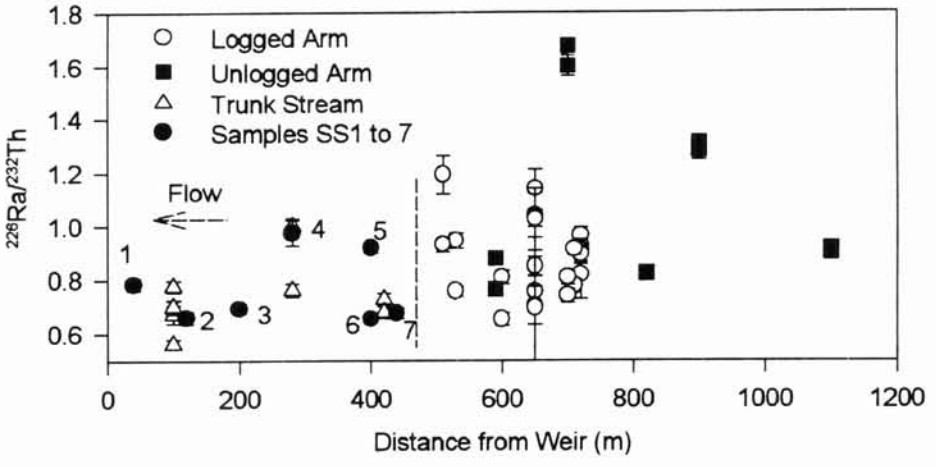

Figure 9.7: The activity ratio of $^{226}Ra/^{232}Th$ as a function of distance upstream from the weir, for sediment samples from the Geebung Creek catchment. Dashed line shows the location of the confluence. Except where shown, analytical uncertainties equivalent to one standard error are smaller than the symbol size.

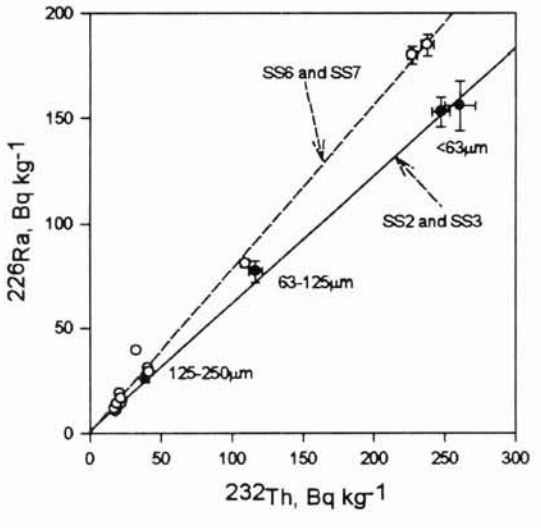

Figure 9.8: Concentrations of ^{226}Ra and ^{232}Th in the particle size fractions from sediment samples SS2, SS3, SS5 and SS7, Geebung Creek catchment. Except where shown, analytical uncertainties equivalent to one standard error are smaller than the symbol size.

9.4.7 Fallout nuclide data

The atmospherically derived radionuclide ^{137}Cs has been widely used in erosion studies [e.g. *Ritchie et al.,* 1974; *Burch et al.,* 1988; *Wallbrink and Murray,* 1993]. Concentrations in undisturbed soil profiles usually decrease exponentially with depth, with more than 90% of the total activity in the top 10-20 cm.

Concentrations of ^{137}Cs in sediments are known to be affected by the particle size distribution of the material [*Olley et al., 1991*]. ^{137}Cs tends to be sorbed onto particle surfaces and consequently tend to be in higher concentrations on the finer particles. It was shown previously that variation in the particle size distribution occur in the sediments present in the stream-line. Therefore to determine whether or not changes in ^{137}Cs concentrations in stream-channel sediment samples are the result of dilution by subsoil, or result from changes in particle size of the material, a method of minimising the effects of particle size variation is required.

The concentrations of ^{232}Th have been determined on the particle size fractions from six samples. The mean, standard deviation and standard error have been calculated for each particle size fraction and are presented in Table 9.3. The concentrations of ^{232}Th range from 234 $\pm$ 8 Bq kg^{-1} on the <63 μm to 17.7 $\pm$ 1.4 Bq kg^{-1} on the 1.4 - 2 mm fraction, a total range of more than 215 Bq kg^{-1}. In contrast, variations of the ^{232}Th concentration within an individual particle size fraction is small, as evidenced by the data in Table 9.3. Variations of the concentration of ^{232}Th in samples are clearly dominated by changes in the particle size of the samples.

Table 9.3. Variations in the concentration of ^{232}Th (Bq kg^{-1}) with particle size for samples from the Geebung Creek catchment.

	<63μm	63-125μm	125-250μm	250-500μm	0.5-1.4mm	1.4-2mm
n=	6	4	4	6	5	5
mean	234	100	37	21.4	17.8	17.7
std. dev.	19	16	7	2.0	1.6	3.2
std. err.	8	8	3	.8	.7	1.4

The ^{232}Th and ^{137}Cs concentrations and the $^{137}Cs/^{232}Th$ ratios for the particle size fractions from sample A18 have been plotted against particle size in Figure 9.9. The concentrations of ^{137}Cs range from 6.1 to 0.2 Bq kg^{-1}. Despite this, the $^{137}Cs/^{232}Th$ ratio in

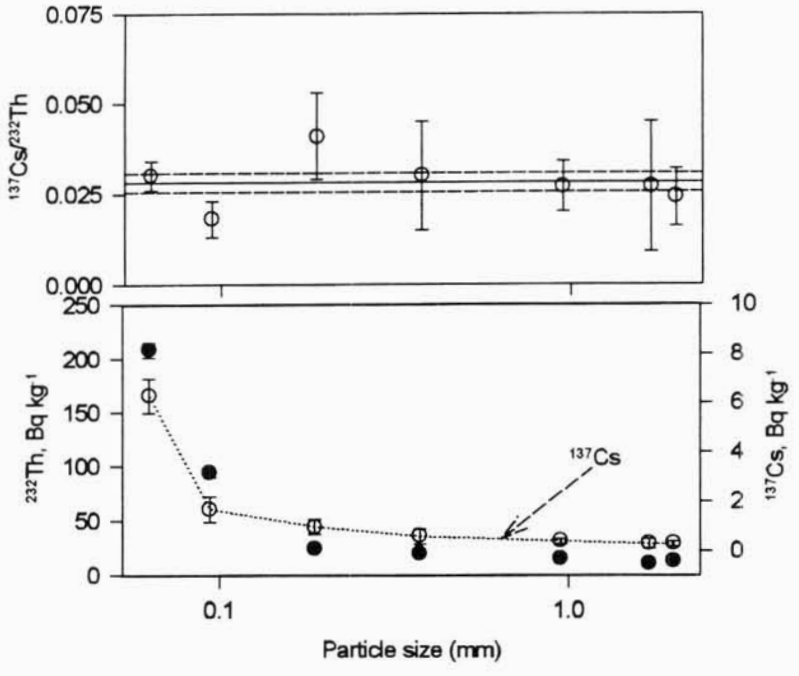

Figure 9.9: Concentrations of ^{137}Cs and ^{232}Th (bottom) and the $^{137}Cs/^{232}Th$ (top) in the particle size fractions from sample A18, Geebung Creek catchment. Except where shown, analytical uncertainties are smaller than the symbol size. The mean ratio and uncertainty (one standard error on the mean) are shown as solid and dashed lines respectively in the top figure. The ^{137}Cs axis has been offset for clarity.

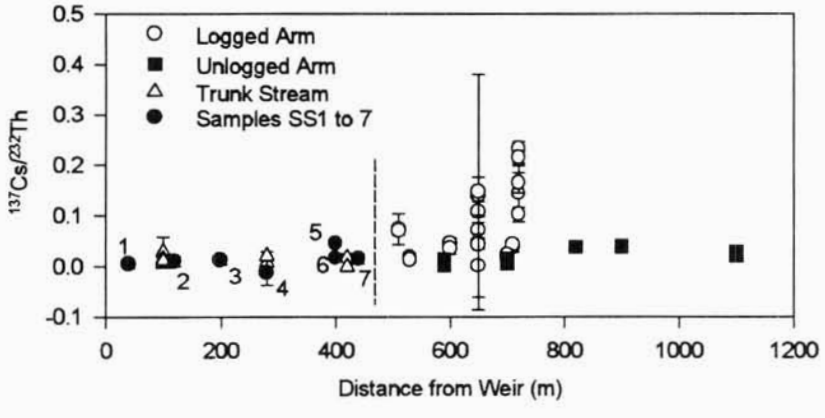

Figure 9.10: The $^{137}Cs/^{232}Th$ activity ratio against distance upstream from the weir, for sediment samples from the Geebung Creek catchment. Except where shown, analytical uncertainties equivalent to one standard error are smaller than the symbol size. The dashed line shows the position of the confluence.

each of the fractions are within analyctical uncertainty and are consistent with a uniform value. Thus dividing ^{137}Cs concentrations by ^{232}Th concentrations should remove the effects of particle size differences in this and in other samples.

The $^{137}Cs/^{232}Th$ ratio for the samples collected from the streamline have been calculated and are plotted against distance upstream of the weir in Figure 9.10. The $^{137}Cs/^{232}Th$ ratio is relatively high in the upper section of the stream-line draining the logged arm. However, while ^{137}Cs is still present in the downstream samples the ratio is significantly lower. This suggests that surface soil is entering the stream-line from the logged area, but that it is being diluted by ^{137}Cs poor subsoil, probably from the stream -banks, as the bedload moves downstream. These observations support the conclusion from the lithogenic radionuclide data that point sources along the streamline, rather than surface soil derived from overland flow, dominate the sources of bedload sediment in the catchment.

Note: Logging was followed by 6 months of dry weather, with only intermittent low intensity rainfalls. This allowed regrowth to occur in the logged catchment, favouring a low sediment yield from the logged areas. If the first 80 mm rain storm had occurred immediately after logging, the results of this study may well have been different. Furthermore, *Crapper et al.* [1989] demonstrated that logging significantly increased the water yield of the catchment and this may have also increased erosion of the stream banks.)

9.5 Summary

1. The $^{230}Th/^{232}Th$ ratio of samples from this catchment were very uniform and all within analytical uncertainty of the bedrock U/Th ratio. Consequently the $^{230}Th/^{232}Th$ ratio was not useful for distinguishing sediment sources within this catchment.

2. The $^{226}Ra/^{232}Th$ ratios on the sediments, which ranged from 0.52 to 1.8, proved to be useful in distinguishing different source areas. Point sources were found to have different $^{226}Ra/^{232}Th$ ratios. Variations in the $^{226}Ra/^{230}Th$ ratios in the sediments present in the drainage lines indicated that no single source dominated the sediment present in the Geebung Creek and these data were used to reject the hypothesis that the logged area was the dominant source of sediment in the

catchment. This conclusion was supported by the normalized ^{137}Cs data, which indicated that while some surface derived material had entered the channel below the logged area, it was diluted by subsoil sources along the drainage line, presumably from erosion of the stream banks. Bedload leaving the catchment is therefore dominated by material derived from the stream banks.

3. The presence of a ^{228}Ra excess over ^{232}Th concentrations on the sediments from Tray 2 indicates that these sediments have been in transport for less than 30 years. It is considered that observation of this excess, when combined with indicators of sediment source such as $^{226}Ra/^{232}Th$ and $^{230}Th/^{232}Th$ ratios, could provide a useful new tool for examining bedload transport processes.

Chapter 10: Sourcing Sediment in the McKeowns Valley Area NSW using $^{230}Th/^{232}Th$ ratios

In chapters 4 it was found that the $^{230}Th/^{232}Th$ ratios in soils formed on a uniform rock type were identical to the U/Th ratio of the rock. Evidence presented in chapter 5 showed that various particle size and density fractions derived from the soils have a constant $^{230}Th/^{232}Th$ activity ratio. This ratio was also shown to be unaffected by grain abrasion. This suggested that fluvial transport of material derived from a soil formed from a uniform rock type should result in sediments which have a uniform $^{230}Th/^{232}Th$ ratio, independent of which particle sizes or densities are sampled. From these observations the model proposed in Section 8.5 was developed. In summary this model poses that the $^{230}Th/^{232}Th$ ratio will be a good indicator of sediment source in catchments which contain rock types which have distinctive $^{230}Th/^{232}Th$ ratios. The application of this model to the spatial sourcing of sediment is examined in this chapter for the McKeowns Valley Area, NSW.

This valley is the main catchment area for the Jenolan Caves a major New South Wales tourist resort. Concerns over rising water levels and apparent increases in the sedimentation rate in the most popular tourist cave at Jenolan, Imperial Cave, led to an investigation of the sources of sediment in the cave system by *Murray et al.*, [1993]. Of primary concern was whether or not forestry disturbance in the catchment had caused the apparent increase in sedimentation. The study used empirically observed correlations between the lithogenic radionuclides ^{226}Ra and ^{232}Th (calculated from the weighted mean of ^{228}Ra and ^{228} Th concentration assuming secular equilibrium) to determine the sources of sediment entering the underground river system. In effect the study used ^{226}Ra to ^{228}Ra correlations to trace sediment. The sediment source areas defined in the sediment study had distinctive lithologies (described below) making it ideal for testing the application of $^{230}Th/^{232}Th$ ratios to the spatial sourcing of sediment (section 8.5).

The samples collected by *Murray et al.*, [1993] have been analysed for thorium isotopes. These results have been interpreted in terms of sediment source areas and then compared to the results of *Murray et al.*, [1993]. Decay series equilibrium conditions are also examined, particularly the assumption of secular equilibrium in the ^{232}Th decay series.

10.1 Catchment Description

The McKeowns valley is located within the Jenolan Plateau in the Oberon district of the NSW Eastern Highlands at about 1200m above sea level. The Jenolan caves are developed in Silurian limestone, part of a sequence of folded Paleozoic sediments and volcanics. A map of the catchment showing the drainage patterns and location of the major source areas as taken from *Murray et al.,* [1993] is shown in Figure 10.1 together with a diagram of the underground system.

The headwaters of the Jenolan river are a few hundred metres south of the divide between McKeowns valley and the Bindo catchment. The surface river flows to the east of the limestone belt for the first 6 km, and then through the limestone for the last 5 km to the Devils Coach House, where the underground river emerges.

Under normal flow conditions the river sinks through the sandy channel bed just downstream of the Terrace Creek confluence. The river bed is normally dry downstream of this point but with increasingly larger floods surface water flows progressively further southward. The only open connection between the underground system and the surface is the entrance to Bow Cave. This is level with the top of the river bank, 0.25m above the river channel. During flood events this entrance takes a significant volume of the river flow and provides the only direct entrance for surface derived sediment into the cave system.

Flow entering Bow Cave flows down Sand Passage to Lower River Cave where it joins the underground stream (Lower River). Flow in this underground channel is permanent and *Dunkley et al.,* [1988] suggested that this underground stream may receive water from as far north as the sinkhole terrain on the Bindo side of the Jenolan/Bindo divide. Lower River then flows into Imperial Cave, one of the prime tourist caves in the area.

Murray et al., [1993] divided the catchment into two main distinguishable potential source areas based on location, drainage, lithology and the ^{226}Ra to ^{228}Ra correlations (i) Western Ridge (WR), an area with shallow soils formed on steeply sloping interlain basalt and mudstone (Fig 9.1), and (ii) Terrace Ck/Bindo Divide catchments (Tck/JBD), characterised by deep soils formed on a sequence of volcanoclastic sediments, siltstones, sandstones and chert.

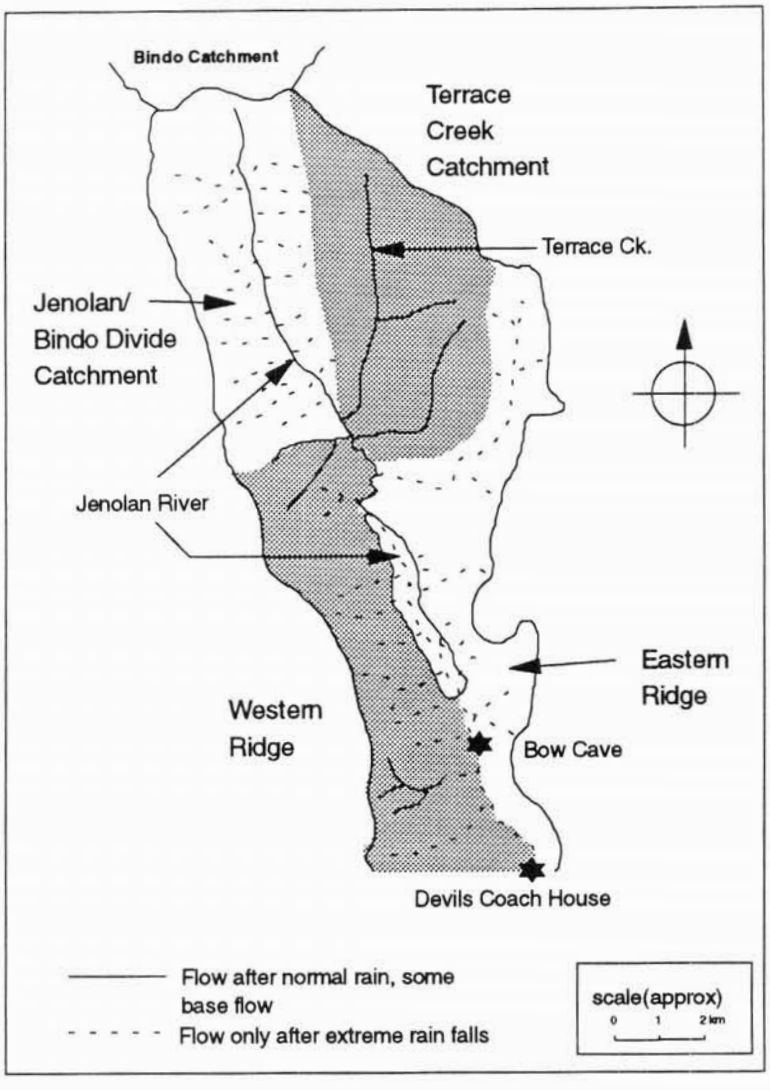

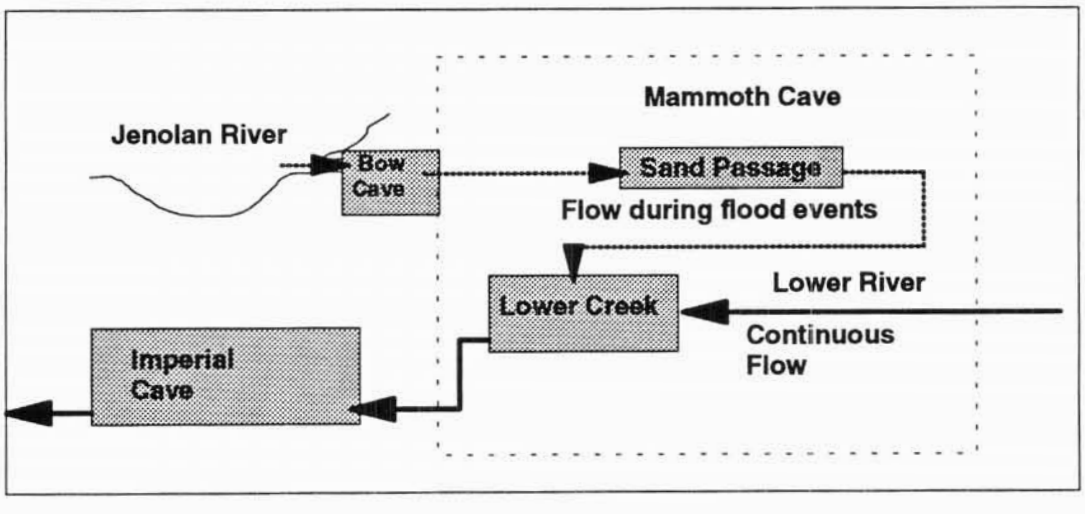

Figure 10.1: (Top) A map of the Jenolan catchment showing the drainage patterns and major source areas, and (bottom) a diagram of the underground cave system [after *Murray et al.*, 1993]

10.2 Sampling and Sample Treatment

The samples were analysed by alpha spectrometry for thorium isotopes. A list of the samples analysed is presented in Table 10.1.

Table 10.1: Number and type of samples from McKeowns Valley which have been analysed for major element concentrations and thorium isotopes.

Number	Sediment Source Area
	Terrace Creek
2	Composite samples each consisting of 50 soil cores 50mm dia. and 100mm deep collected on a grid pattern
2	samples from a small dam towards the outlet of the catchment
	Jenolan/Bindo Divide
3	composite soil samples similar to those from Terrace Creek
1	grab sample from the river bed above Terrace Creek
	Western Ridge
3	grab samples from the three large sediment fans
4	composite samples from sixteen soil samples collected from the lower third of Western Ridge
	Underground Sinks
	Sand Passage
11	samples from a sediment core collected from sand passage
	Lower Creek Cave
5	from a sediment core
1	grab sample from beneath the cobbled river bed
2	samples stratigraphically above the top of the core. The samples contained modern material as evidenced by germinating seeds on the top of the deposits and the presence of pine bark within the sediment.

The cores collected from the underground sinks are shown diagrammatically in Figure 10.2. The sedimentary correlations and chronologies are also shown in this figure. A full description of the sampling locations and procedures are given in *Murray et al.*, [1993].

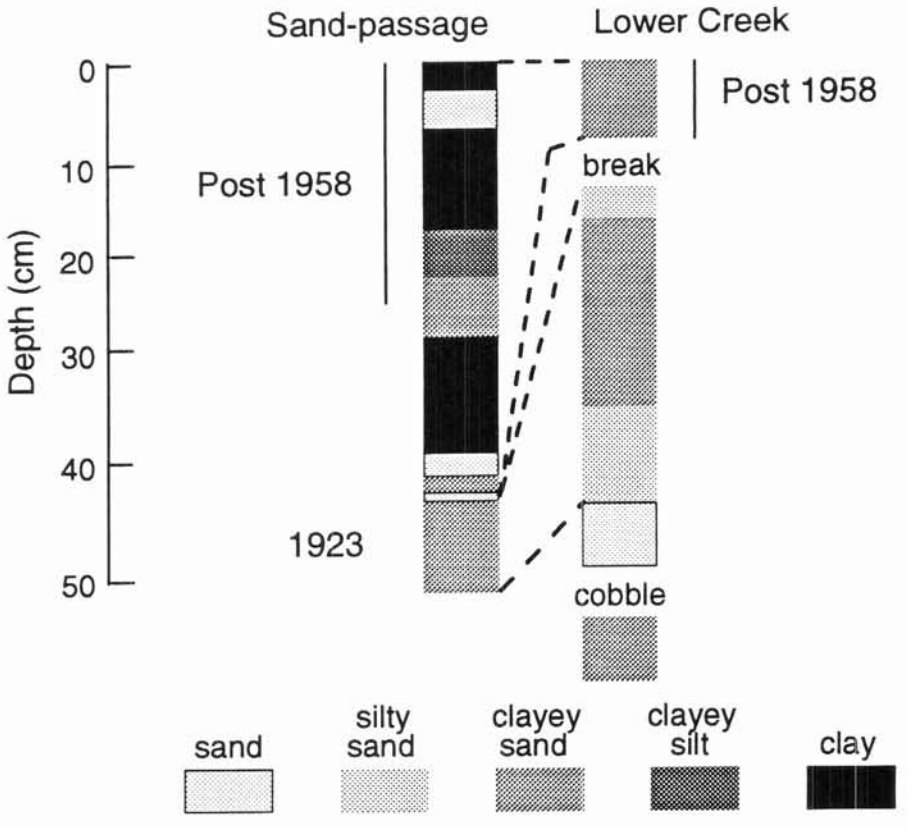

Figure 10.2: Diagram of the Lower Creek and Sand Passage Cores from the Jenolan Caves, showing sampling points, stratigraphic correlations and chronologies (after *Murray et al.,* [1993])

10.3 Results and Discussion

The gamma [*Murray et al.,* 1993] and alpha spectrometry analyses of the sample used to characterise the sediment source and those from the two major sediment sinks are presented in Appendix H.

10.3.1 Equilibrium conditions

The relevant parent/daughter concentrations are presented in Figure 10.3. The ^{228}Ra and ^{228}Th concentrations all plot on the equilibrium line (solid line Figure 10.3a) indicating that these nuclides are in equilibrium. *Murray et al.,* [1993] used this information as evidence that the ^{232}Th decay series was in secular equilibrium and then calculated the concentration of ^{232}Th from the weighted mean of the gamma spectrometry determination of the ^{228}Ra and ^{228}Th concentrations.

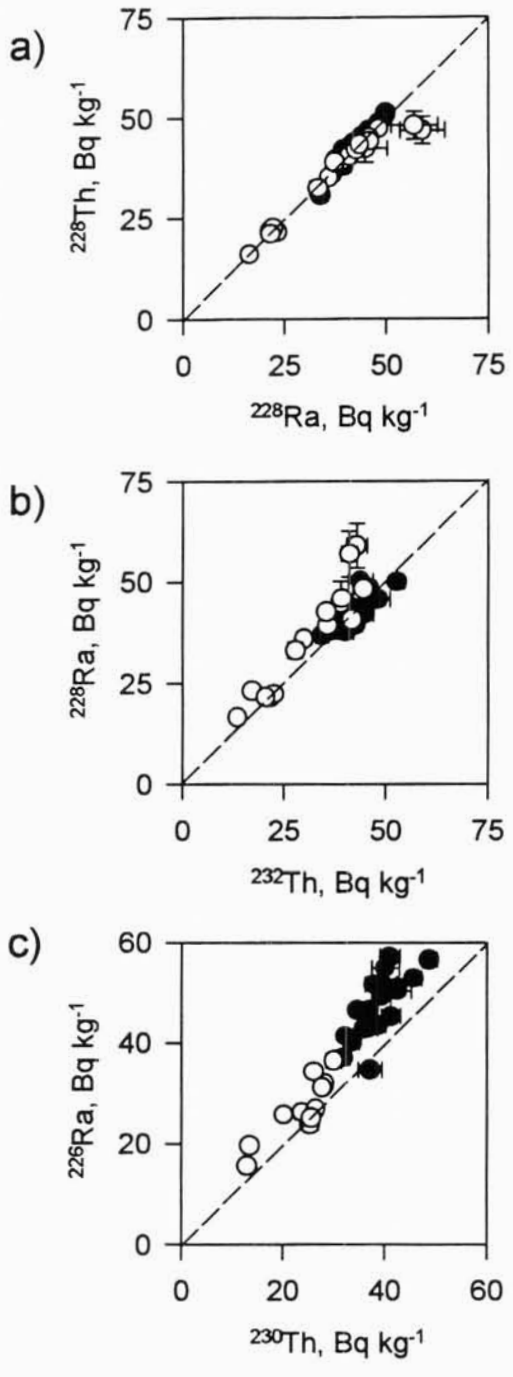

Figure 10.3: Parent/daughter concentrations for the Sink samples (closed circles) and Source area samples (open circles) from McKeowns Valley. (a) ^{228}Ra and ^{228}Th (b) ^{228}Ra and ^{232}Th (c) ^{226}Ra and ^{230}Th. The solid line in each figure indicates equilibrium. Error bars represent uncertainties equivalent to one standard error, in many cases these are smaller than the symbol size.

Figure 10.3b shows the ^{228}Ra to measured ^{232}Th concentrations. Whilst most of the samples collected from the sediment sinks lie on or close to the equilibrium line, most of the samples used to characterise the sediment sources have concentrations of ^{228}Ra in excess of its parent ^{232}Th (also see section 4.3.1). Clearly, the assumption of equilibrium in the ^{232}Th decay chain is incorrect for the samples from the source areas. This has serious implications for the *Murray et al.*, [1993] study. The presence of a ^{228}Ra excess on the source samples means that the $^{226}Ra/^{228}Ra$ ratio on these samples is not directly comparable to the $^{226}Ra/^{228}Ra$ ratio on the sink samples.

The concentrations of ^{226}Ra are also in excess of its parent ^{230}Th in most of the samples examined (Figure 10.3c).

10.3.2 ^{230}Th and ^{232}Th correlations

The concentration of ^{230}Th and ^{232}Th in the soil/colluvium samples from the two source areas are plotted in Figure 10.4. As discussed in chapter 4 the data from the basaltic soil samples from Western Ridge are all consistent with a single regression line (r^2=0.99) passing through the origin ($^{230}Th=(1.25 \pm 0.03)\,^{232}Th$). The data from the other two sources (Terrace Creek and the Jenolan Bindo Divide catchments) are also consistent with a single regression line passing through the origin. This line is distinct from the regression line fitted through the Western Ridge data, and has a much lower $^{230}Th/^{232}Th$ ratio (0.78 ± 0.04). However the data show much more spread about the line than was evident in the Western Ridge samples. Given the complexity and mixture of lithologies present in these source areas this is not surprising.

Evidence presented in chapter 5 indicates that sediments derived from these soils will also have the same distinctive ratios. Therefore, it should be possible to use the $^{230}Th/^{232}Th$ ratio to distinguish sediments derived from these respective areas.

The data from the cores from two sediment sinks, Sand Passage and Lower Creek Cave, are plotted in Figure 10.5. The regression lines from the two main source areas are also shown. The data plot as a poorly defined group between the two source area regression lines close to the Terrace Creek/Jenolan Bindo Divide line. This indicates that the sediments are a complex mixture of material from both source areas, but on average contain more material from the Terrace Creek/Jenolan Bindo Divide catchments.

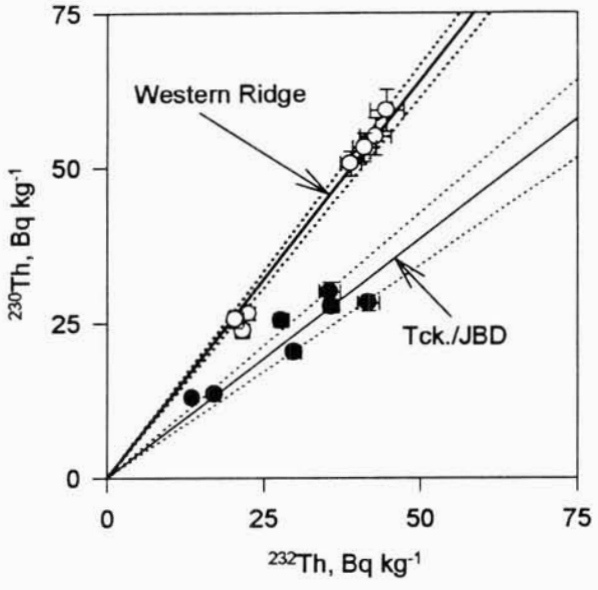

Figure 10.4: The concentration of ^{230}Th and ^{232}Th in the samples from the two main source areas in McKeowns Valley. Error bars represent uncertainties equivalent to one standard error, in many cases these are smaller than the symbol size.

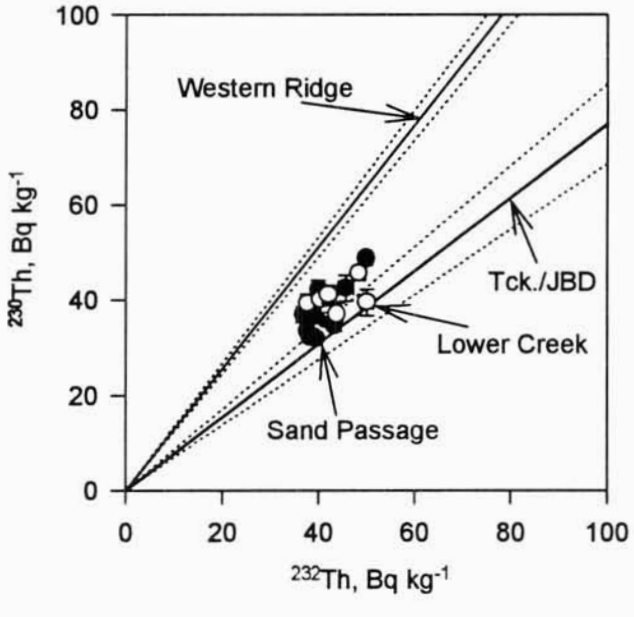

Figure 10.5: The concentration of ^{230}Th and ^{232}Th in the samples from the Lower Creek and Sand Passage sediment cores. Error bars represent uncertainties equivalent to one standard error, in many cases these are smaller than the

10.3.3 The relative contribution of the two sediment sources

The fractional contribution of sediments derived from the Western Ridge and Terrace Creek/Jenolan Bindo Divide catchments to each of the sedimentary layers analysed from the Sand Passage and Lower Creek Cores (Figure 10.2) has been calculated using a two component mixing model,

$$AX + BY = C \qquad (1)$$

where X and Y are the relative contributions from the two sources (Western Ridge and Terrace Creek/Jenolan Bindo Divide), so that X + Y=1, and A, B and C are the $^{230}Th/^{232}Th$ ratios of the two inputs and the output mix respectively. The model assumes a small angular separation between the two regression lines relating the two nuclides; this is satisfied by these data, and is described in more detail in *Murray et al.* [1993].

The calculated contributions to the sediments in Sand-passage and Lower Creek cores are plotted against depth in Figures 10.6 a and b respectively. The data indicate that the sediments in Sand-passage are dominated by material from Terrace Creek and Jenolan/Bindo Divide (mean 78%) with only the lower two samples showing any major input from Western

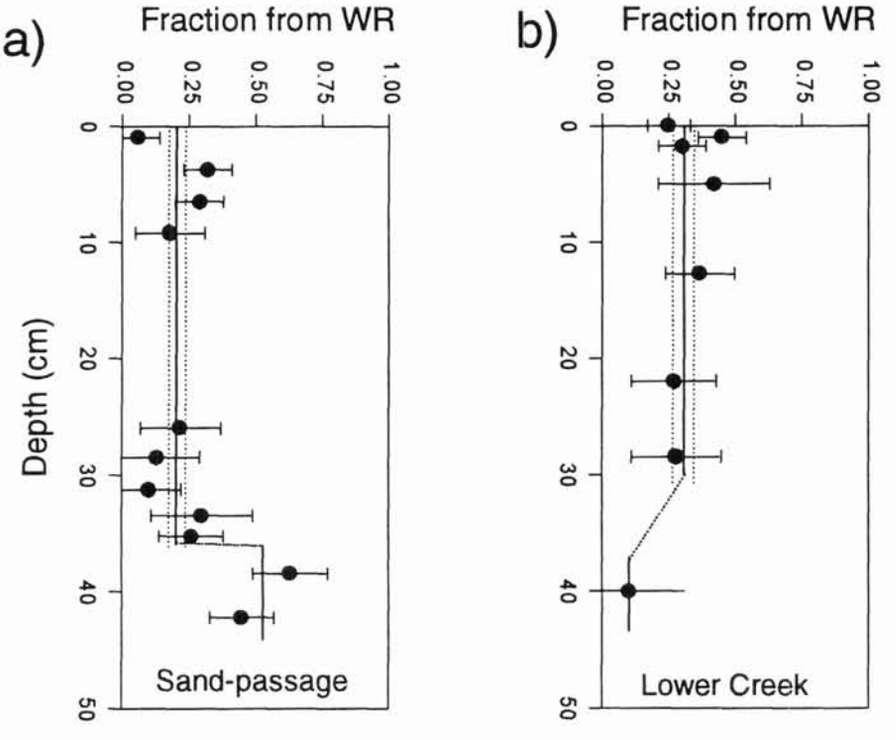

Figure 10.6: The calculated fractional contributions from the Western Ridge catchment to sediments from the a) Sand Passage Core and b) Lower Creek core. Error bars represent uncertainties equivalent to one standard error.

Ridge (~50%). The calculated contribution of the Western Ridge source area to that of the sediment present in Lower Creek core again indicates that the Terrace Creek/Jenolan Bindo Divide dominate the sediments in this core (mean ~68%). There is a systematic trend in the data with depth suggesting an increase in the contribution from Western Ridge with time.

10.3.4 History of sedimentation in the Jenolan Caves

The sedimentary correlations between the two core established by *Murray et al.,* [1993] are still valid as are their proposed chronologies (see Figure 10.2). However, the relative spatial sediment source contributions presented in that study are probably incorrect, because of the presence of a ^{228}Ra excess on the source samples.

The $^{230}Th/^{232}Th$ ratios indicate that most of the sediments in the earliest depositional (Lower Creek Bed Sample) phase were derived from the Terrace Creek/Jenolan Bindo Divide catchments. There was then a progressive increase in sediments derived from the Western Ridge catchments up to a maximum of ~50%. This is evident in both sediment cores. In the early 1950's there was a marked decrease in the fraction of sediment derived from Western Ridge (to <25% of the total). The core sediments from this point until the present are dominated by material from Terrace Creek/Jenolan Bindo Divide area.

The differences between these results and those of *Murray et al.,* [1993] are; (i) only three major phases of deposition can be distinguished, not four, (ii) Western Ridge has never supplied more than 50% (not 77%) of the sediment present in any of the layers evident in the cores, and (iii) since the 1950s the Terrace Creek/Jenolan Bindo Divide catchments have supplied 78% of the sediment present in the cores (not 50%). However, these differences probably do not invalidate the major conclusions of the *Murray et al.,* [1993] study, which were that (i) forestry practices in the 1950's had increased the supply of sediment from the Terrace Creek/Jenolan Bindo Divide catchments, and (ii) a higher yield from these areas has continued to the present day, perhaps due to the presence of forestry roads in the catchments.

10.3.5 Sediment transport rates

Concentrations of ^{226}Ra and ^{228}Ra are in excess of their respective parents in the samples collected from the two source areas (*in situ* soils $^{228}Ra/^{232}Th = 1.19 \pm 0.4$, $^{226}Ra/^{230}Th = 1.22 \pm 0.05$) . As in previous chapters the presence of this radium excess can be used to estimate sediment transport rates in the catchment. While the ^{226}Ra excess over ^{230}Th is still present in the recently deposited samples from the cores (13km downstream), the concentrations of ^{228}Ra are in equilibrium with ^{232}Th (mean ratio of 1.04 ± 0.03). The upper sediments in the Sand Passage core and the two grab samples from Lower Creek also contain ^{137}Cs, and must therefore have entered the cave system in the last 30 years. The absence of a ^{228}Ra excess shows that they must have been in transport for more than 9 (given an initial excess of $19 \pm 4\%$; an average activity of 40 $BqKg^{-1}$; and a detection limit of 5%). The combined ^{137}Cs and ^{228}Ra excess data indicates that the sediment in the caves took between 9 and 30 years from the time of detachment from the soil, to be deposited in the cave.

10.4 Summary

Evidence presented in this chapter demonstrated that the $^{230}Th/^{232}Th$ ratio can, as proposed in the model given in section 8.5, be successfully applied to sediment sourcing problems in catchments which have distinctive lithologies and it is concluded that:

1. The $^{230}Th/^{232}Th$ ratio was able to distinguish sediment source areas which had distinct lithologies.

2. The assumption by *Murray et al.*, [1993] of secular equilibrium in the ^{232}Th decay series was not valid for samples collected from the sediment source areas in this catchment. Nevertheless the major conclusions of the *Murray et al.*, [1993] study were supported by the $^{230}Th/^{232}Th$ data.

3. The presence of ^{137}Cs and the absence of a ^{228}Ra excess in the most recently deposited cave sediments indicates that these sediments took between 9 and 30 years from the time of detachment from the soil profile to reach the point of deposition.

Chapter 11: Sediment Residence Times in the Murrumbidgee Arm of Burrinjuck Reservoir

Sediment fluxes in river catchments have proved difficult to measure or model at time-scales relevant to land and water resource management decisions. Determining transport rates and residence times is complicated by the intermittent movement and temporary storage of sediments in natural streams [*Gomez,* 1991; *Mosley,* 1981; *Roberts and Church,* 1986]. This chapter presents a new tool for estimating the storage and transport times of river-borne sediments, based on the observed disequilibrium of the naturally occurring radionuclides ^{228}Ra and ^{232}Th in the thorium decay series, as outlined in the model (section 8.5). The short half-life of ^{228}Ra (5.75 years) enables this model to be applied to fluvial sediment transfers and alluvial storages over the past 30 years. When combined with indicators of sediment source, such as ^{226}Ra/^{232}Th and ^{230}Th/^{232}Th ratios, observation of this excess should provide a useful new tool for examining the transport rates and residence times of bedload and suspended load sediments in streams and lakes.

In this chapter radionuclide data from a sequence of samples collected from along the Murrumbidgee arm of Burrinjuck reservoir are examined and compared to data from a core collected from the end of this reach. Equilibrium conditions are examined and an attempt is made to determine the sediment residence times in the reach.

11.1 Site Description and Sampling Locations

Burrinjuck reservoir is a major irrigation water storage on the Murrumbidgee River, holding a maximum of 1.026 x 10^9 m^3 of water. It receives water from three major rivers, the Yass, the Murrumbidgee, and the Goodradigbee Rivers, and has a total catchment area of 13000km^2. The catchment receives between 500mm and 1000mm average rainfall per annum. The Murrumbidgee River drains an area of 8000km^2. Water and sediment from the catchment enter the main dam from the river via a long section of submerged river reach (Fig. 11.1) . Sediments deposited in this arm 13km below the point at which the river normally enters the ponded waters were sampled in 1983 when exposed during very dry conditions by Dr. R. J. Wasson (CSIRO). Sediment columns were collected from the walls of pits and then sub-sampled in the laboratory. The sampling location is shown in Figure 11.1. The stratigraphy in the sediment column is well defined and there is no evidence of iron

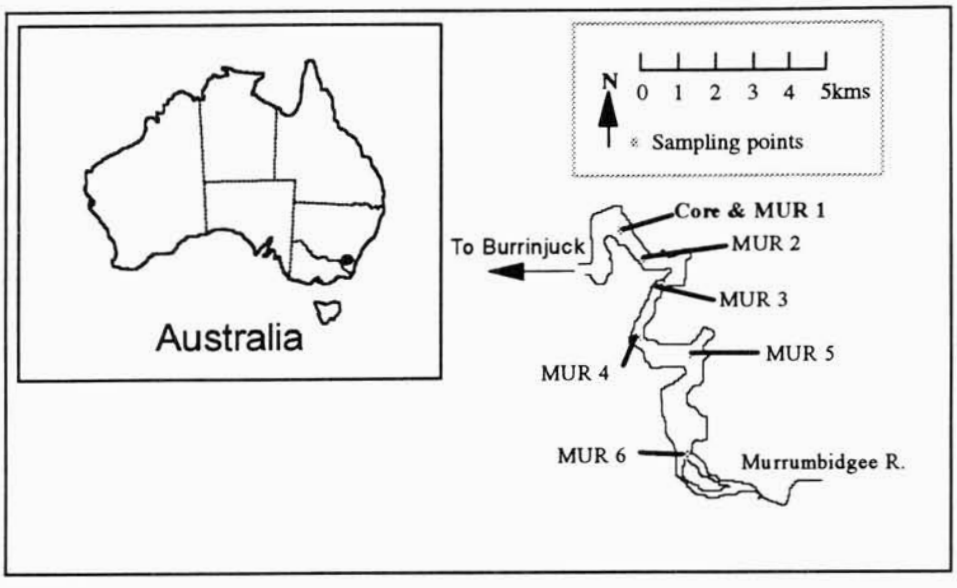

Figure 11.1: A map showing the location of the sampling points along the Murrumbidgee Arm of Burrinjuck Dam.

mottling, consequently it is considered that no significant redistribution of iron and manganese has occurred since deposition. The samples from the sediment column were all analysed using gamma spectrometry by *Murray et al.*, [1991] and by alpha spectrometry in this current study.

A sequence of 6 samples was collected from the 13 km reach of the Murrumbidgee arm of the reservoir above the point from which the sediment column was collected. Sampling locations are also shown in Figure 11.1. These samples were collected from a boat using an Eckman grab sampler which collected the upper ~3 cm of sediment. The sampling sequence began directly over the core sampling site and continued upstream to the point at which the river enters the still water of the reservoir. These samples were also analysed by gamma and alpha spectrometry. All of the samples consisted predominantly of fine clay and silt.

11.2 Results and Discussion

The gamma and alpha spectrometry analyses for the samples from the sediment column and those collected from the reach are presented in Appendix I.

11.2.1 Equilibrium conditions

The relevant parent/daughter concentration are plotted in Figure 11.2. In each plot the solid line represents equilibrium condition, the open circles are the core data and the closed circles the reach sediment data. The ^{238}U series nuclide data from the reach sediment

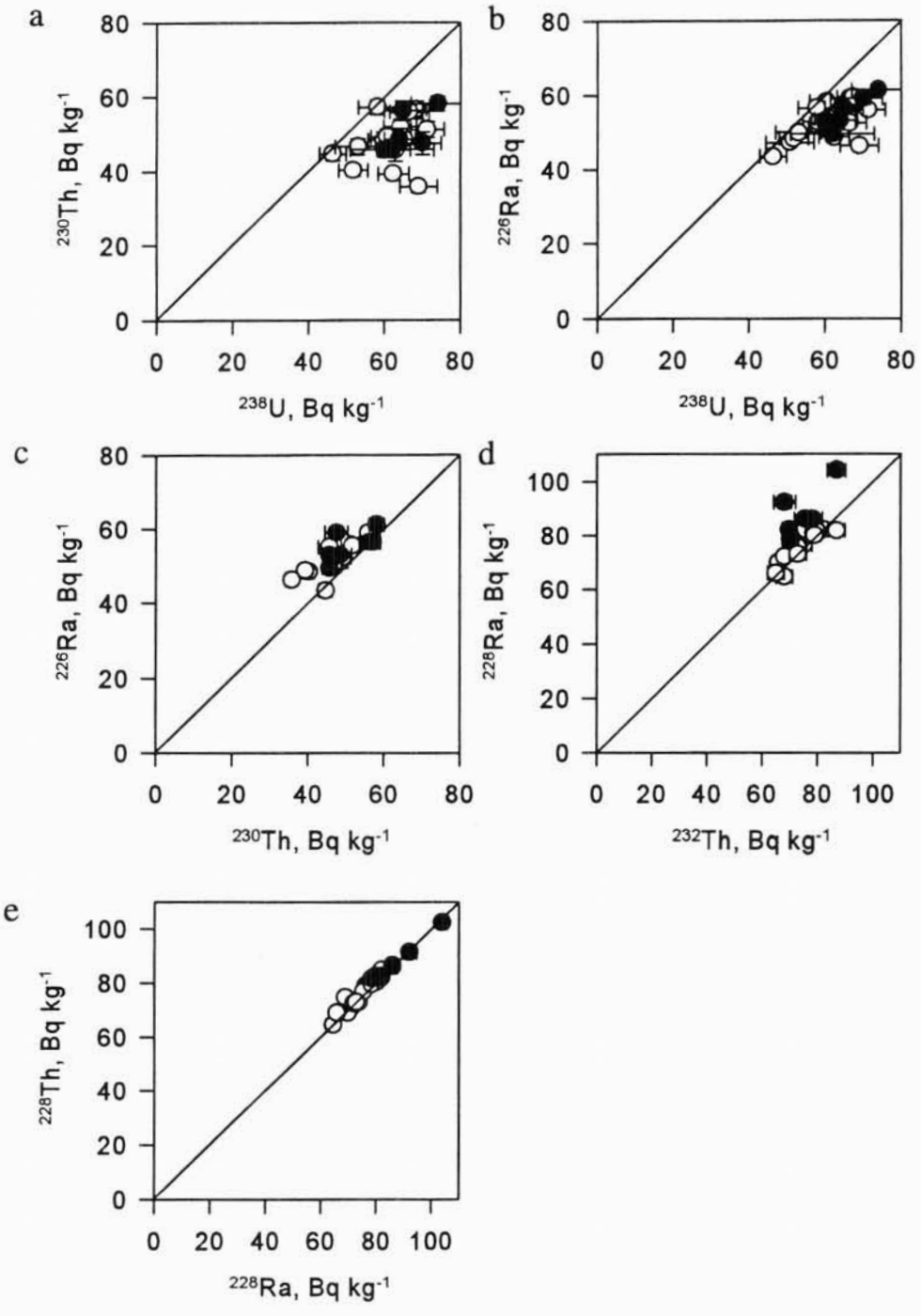

Figure 11.2: (a to e) Relevant parent/daughter equilibrium plots for reach samples (closed circles) and sediment column samples (open circles) collected from the Murrumbidgee Arm of Burrinjuck Dam. In each figure the solid line represents secular equilibrium. The error bars represent analytical uncertainties equivalent to one standard error on the mean.

samples generally lie within the concentration ranges of the sediment column data (Figure 11.2 a, b and c). Concentrations of ^{238}U are generally in excess of both ^{230}Th and ^{226}Ra concentrations (Figure 11.2 a and b). Concentrations of ^{226}Ra are also generally in excess of ^{230}Th concentrations (Figure 11.2c).

The concentration of ^{232}Th, ^{228}Ra and ^{228}Th are in equilibrium in samples from the sediment column (Figure 11.2 d and e). In contrast, the concentrations of ^{228}Ra are in excess of ^{232}Th concentrations in the reach sediment samples by up to $35 \pm 8\%$. The concentrations of ^{228}Th and ^{228}Ra in these samples are however in equilibrium. This indicates that the ^{228}Ra excess is old compared to the half-life of ^{228}Th. Consequently the ^{228}Ra excess is unlikely to have resulted from ^{228}Ra sorption from the water column. The presence of this excess implies that these sediments were eroded recently and has implications for the dating of sediment movement. This is examined further below.

11.2.2 ^{230}Th and ^{232}Th correlations

In chapter seven it was shown that $^{230}Th/^{232}Th$ ratios on sediments could be altered as a result of the redistribution and accumulation of Fe-Mn. There is no evidence of redistribution of Fe-Mn in the Murrumbidgee sediment column. It is therefore considered unlikely that the thorium isotope concentrations in the sediments have changed since the time of deposition.

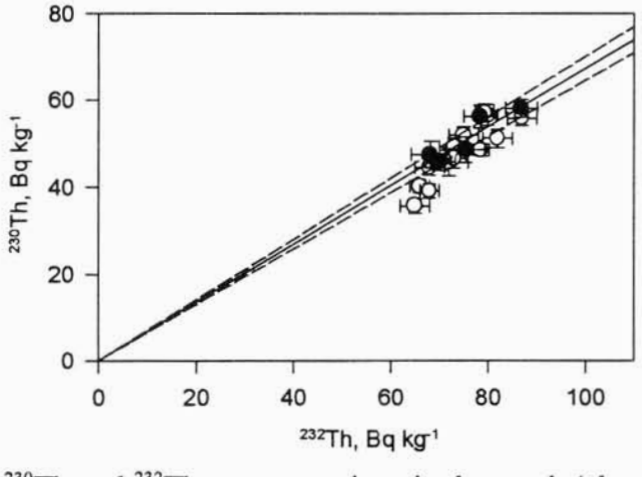

Figure 11.3: The ^{230}Th and ^{232}Th concentrations in the reach (closed circles) and sediment column samples (open circles) collected from the Murrumbidgee Arm of Burrinjuck Dam. The mean $^{230}Th/^{232}Th$ ratio of the reach samples and uncertainties corresponding to one standard error are shown as solid and dashed lines respectively. The error bars represent analytical uncertainties equivalent to one standard error on the mean.

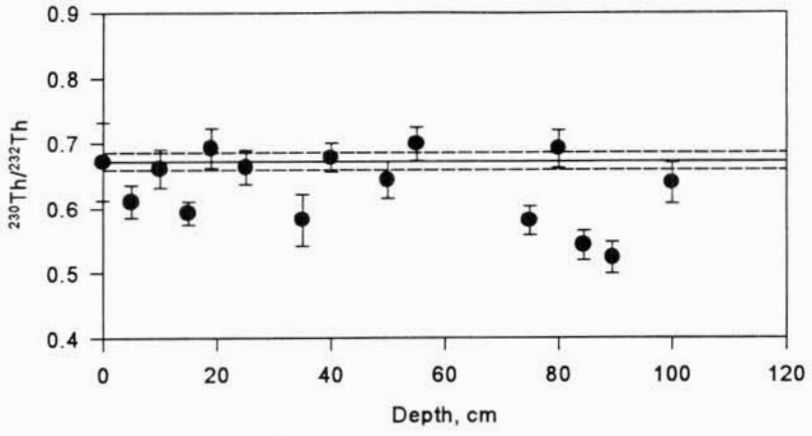

Figure 11.4: The $^{230}Th/^{232}Th$ ratio of the sediment column samples from the Murrumbidgee Arm of Burrinjuck Dam against depth. The mean $^{230}Th/^{232}Th$ ratio of the reach samples and uncertainties corresponding to one standard error are shown as solid and dashed lines respectively. The error bars represent analytical uncertainties equivalent to one standard error on the mean.

The ^{230}Th concentrations in the reach and sediment column samples have been plotted against ^{232}Th concentrations in Figure 11.3. All the reach sample data (closed circles) are consistent with a single regression line (solid line) passing through the origin (^{230}Th = 0.67 ^{232}Th). From previous work (chapters 4, 5 and 10) this suggests these sediments are derived from a uniform lithology, or a uniform mix of lithologies. Most of the sediment column data is also consistent with this regression line, falling within the 95% confidence limits (dotted lines) of the regression. However, a number of points do fall well outside this regression.

This is shown more clearly in Figure 11.4 in which the $^{230}Th/^{232}Th$ ratio of the sediment column samples are plotted against depth. The mean $^{230}Th/^{232}Th$ ratio and uncertainties corresponding to one standard error for the reach samples are shown as solid and dashed lines respectively. Most of the sediment column data have $^{230}Th/^{232}Th$ ratios consistent with the reach samples, however five samples lie outside two standard errors of the mean value of the reach samples. As there is no evidence of iron and manganese redistribution in the sediment column and given the low probability of differential mobilisation of the thorium isotopes, it is considered that these differences result from the sediment having been deposited with a different $^{230}Th/^{232}Th$ ratio. Consequently these four samples are considered to have been derived from a source or sources with a lower $^{230}Th/^{232}Th$ ratio than the sediment sampled in the reach.

The ^{230}Th and ^{232}Th concentrations in the samples from the sediment column are consistent with the sediment having been derived from at least two sources with distinctive $^{230}Th/^{232}Th$ ratios, one which supplied sediment similar to that currently present in the reach, with a $^{230}Th/^{232}Th$ ratio of ~0.67. The other source presumably supplied sediment with a $^{230}Th/^{232}Th$ ratio ≤ 0.52.

11.2.3 Sediment residence times

It was shown in the discussion on equilibrium conditions that ^{228}Ra was in excess of ^{232}Th concentrations in the samples collected from the reach. This excess varies systematically along the reach (Figure 11.5d) being highest at the point the river enters the ponded water of the reservoir ($^{228}Ra/^{232}Th = 1.35 \pm 0.08$) and decreasing down the reach (to 1.10 at the point the sediment core was taken). This systematic decrease in excess with distance downstream can be interpreted in terms of sediment residence time (Section 8.5) if (i) the sediments have been derived from a common source or mix of sources and had the same initial ^{228}Ra excess at the point of entry to the reservoir, (ii) no fluvial separation of the material containing the excess has occurred in the reach, and (iii) the system has remained geochemically closed.

The first of these criteria cannot be explicitly tested. However, the uniformity of the $^{230}Th/^{232}Th$ ratio in the reach sediments (Figure 11.5a) does suggest that they have been derived from a common source or mix of sources. The second criterion can be indirectly tested by studying the $^{226}Ra/^{232}Th$ ratio. In chapter 5 it was shown that fluvial sorting of material which had a ^{226}Ra excess can produce fractions which have variable $^{226}Ra/^{232}Th$ ratios. Concentrations of ^{226}Ra are in excess of ^{230}Th concentrations in the reach samples, and if fluvial separation, had occurred in the reach a change in the $^{226}Ra/^{232}Th$ ratio down the reach might be expected.

The $^{226}Ra/^{232}Th$ ratio in the reach samples (Figure 11.5b), because of the large uncertainties, can be interpreted in two ways: firstly, that the data are consistent with a uniform $^{226}Ra/^{232}Th$ ratio of ~0.75, this would suggest that no fluvial separation has occurred; or secondly, it could be argued that the $^{226}Ra/^{232}Th$ ratio is initially high and drops to a constant value at the second sampling point (down the reach), this would suggest that fluvial separation has occurred at the top of the reach.

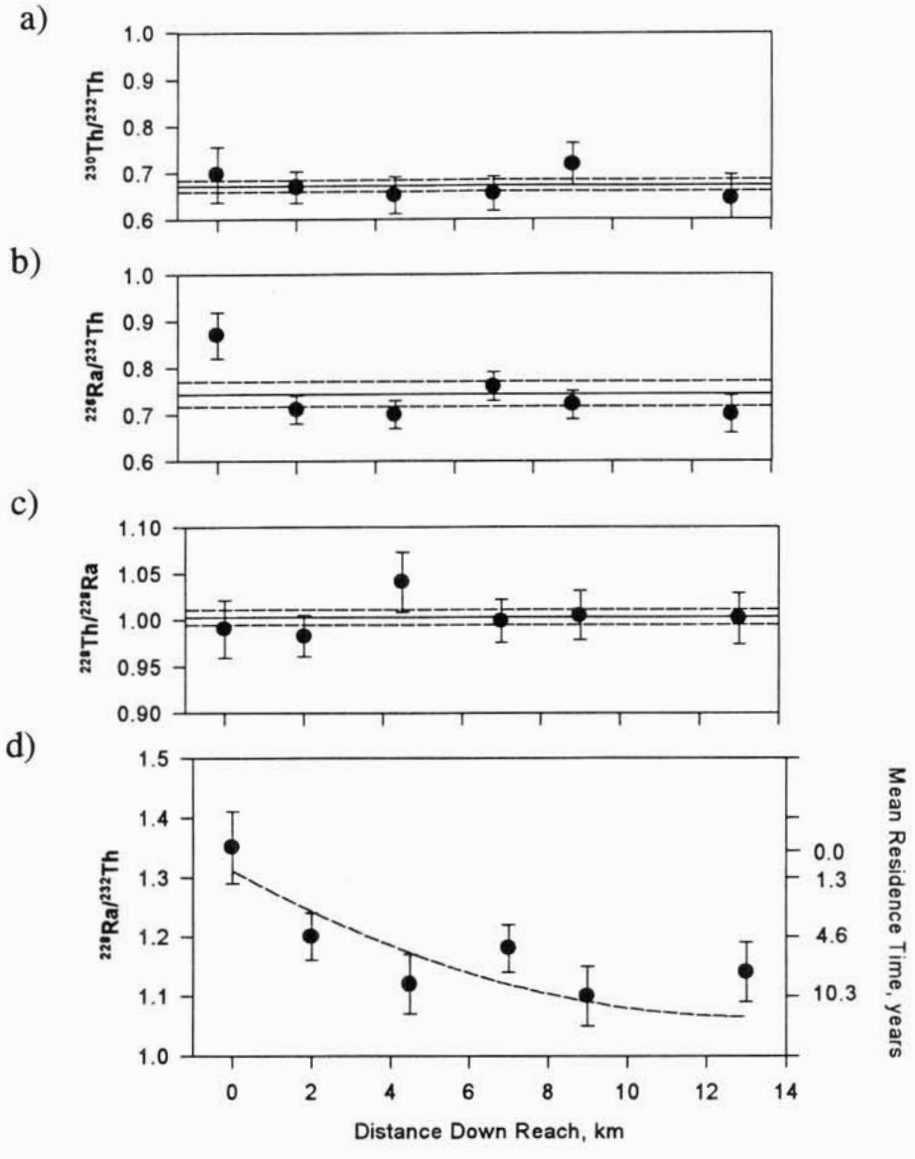

Figure 11.5: Radionuclide ratios for fine-grained samples from Murrumbidgee River arm of Burrinjuck Reservoir, Australia (a) Activity ratio of ^{230}Th to ^{232}Th suggesting a constant sediment source to the reach of the river; (b) ^{226}Ra to ^{232}Th ratio indicating the degree of fluvial sorting (c) activity ratio of ^{228}Th to ^{228}Ra demonstrating secular equilibrium and showing that the ^{228}Ra activity has been associated with the particles for a period which is long compared to the half-life of ^{228}Th (1.9y); (d) Activity ratio of ^{228}Ra to ^{232}Th showing that the average time since the sediment entered the reservoir increases with distance down-reach. Given the approximately constant sampling depth it is presumed that this pattern arises from decreasing sediment deposition rates along the reach. The right-hand axis shows the mean residence time calculated relative to that of the 0 km sample (assuming no fluvial separation, and a uniform ^{232}Th activity of 80 Bq kg^{-1}).

The assumption that the system is geochemically closed, at least on a time scale of a few years, is supported by the fact that for all the samples the concentration of ^{228}Ra is in equilibrium with its daughter ^{228}Th (Figure 11.5c) suggesting that the ^{228}Ra is unlikely to have been recently sorbed. Therefore, if it is assumed that no fluvial separation of material has occurred, then the changes in the ^{228}Ra excess down the reach can be interpreted in terms of the mean residence times of the sediments. Using this assumption the right-hand axis has been converted to time since deposition relative to the sample at the top of the reach (Figure 11.5 d). The sediments sampled at the lower end of the reach above the core site can be seen to have an apparent age of ~10 years older than the material at the point the river enters the ponded water of the reach. However, if fluvial separation has been an important process in the reach then the presence of the ^{228}Ra excess simply indicates that the sediments are young, and no interpretation (in terms of residence times) of the variation along the reach is possible.

11.3 Summary

1. The ^{230}Th/^{232}Th ratio in the sediment core varied with depth and indicated that the sediments were derived from a number of sources.

2. The reach samples were shown to have a uniform ^{230}Th/^{232}Th ratio, suggesting that they were derived from a common source. The concentrations of ^{228}Ra were in excess of ^{232}Th in the samples and this excess probably decreased systematically down the reach. The concentrations of ^{228}Ra and ^{228}Th were in equilibrium. This suggests that the system has been chemically closed at least over the last few years. Thus, the decrease in ^{228}Ra excess along the reach can be interpreted in terms of difference in sediment residence time, if it was assumed that no fluvial separation of the material containing the excess has occurred. On the other hand if fluvial separation is considered significant it is concluded that the sediments are young compared with the radium-228 half-life, but no detailed interpretation in terms of residence time is possible.

The data presented in this chapter clearly demonstrate the potential of applying ^{228}Ra excess to determining sediment residence time.

Chapter 12 : Concluding Remarks

The aim of this thesis was to develop an understanding of the behaviour and the causes of variability in ^{238}U and ^{232}Th decay series nuclides in modern sediments in order to provide a framework from which variations in the nuclide concentration and ratios in sediment could be used to trace sediment movement.

Decay series nuclide concentrations and ratios have been examined in rocks, soils and sediments (Chapters 4 to 7). The observed behaviour and distribution of the radionuclides in each of these compartments of the erosion cycle were summarised and used to develop a model for the application of ^{238}U and ^{232}Th nuclides to sediment tracing problems in Chapter 8. Elements of this model were successfully applied to three distinct sites in Chapters 9 to 11.

The major findings of this study in relation to the spatial sourcing of sediment are :

1. The $^{230}Th/^{232}Th$ ratio is in general not affected by the transition from rock to soil, or by that from soil to sediment. Consequently the $^{230}Th/^{232}Th$ ratios in sediments are likely to be largely dependent on the $^{230}Th/^{232}Th$ ratio of the rocks from which they are ultimately derived. This means that the $^{230}Th/^{232}Th$ ratios can be used to distinguish sediments derived from lithologies which have different $^{230}Th/^{232}Th$ ratios (as was demonstrated in Chapter 10). It is noted however that in circumstances where sediments are subsequently exposed to groundwaters in which the $^{230}Th/^{232}Th$ differs significantly from that of the sediment, the ratio of the sediment may be altered due to overprinting (see Chapter 7). Nevertheless this ratio was shown to provide a useful 'fingerprint' on sediments in catchments which contained a number of rock types of distinctive $^{230}Th/^{232}Th$ ratios (Chapter 10). It is, however, unlikely to be useful in small catchments which have uniform lithologies.

2. In contrast to the uniformity of the $^{230}Th/^{232}Th$ ratio during rock to soil to sediment transformations, the $^{226}Ra/^{232}Th$ ratio was found to be more variable. This variability was largely due to the presence of ^{226}Ra excess over ^{230}Th in many of the soils. While ^{226}Ra to ^{232}Th correlations have been previously applied in sediment tracing studies [*Olley et al.* 1993; *Murray et al.* 1993], work presented in this thesis has demonstrated that this ratio may alter as a function of fluvial processes and will only provide a useful

fingerprint on sediments under particular conditions. These are (1) if the ^{226}Ra concentrations are in equilibrium with ^{230}Th concentrations such that $^{226}Ra/^{232}Th$ ratio equals the $^{230}Th/^{232}Th$ ratio, or (2) in circumstances when the processes of fluvial sorting and grain abrasion are not important, or (3) when the ^{226}Ra and ^{232}Th are bound to similar sites (eg. on grain surfaces). It was shown in Chapter 9 that in circumstances where this latter criterion is fulfilled, the $^{226}Ra/^{232}Th$ ratios can provide sediment source information in catchments which had a uniform lithology and consequently a uniform $^{230}Th/^{232}Th$ ratio. It is therefore considered likely that the heterogeneity of $^{226}Ra/^{232}Th$ ratio may in some circumstances provide a useful tracer 'signal' in small catchments which have a uniform lithology.

3. While not conclusively demonstrated (Chapters 9, 10 & 11) it is likely that the observation of systematic changes in the ^{228}Ra excess in sediments will prove useful in examining sediment transport rates and residence times.

The results presented in this thesis have provided an understanding of the mechanisms which cause variability in ^{238}U and ^{232}Th decay series nuclides in modern sediments and demonstrate the applicability of nuclide ratios to providing information on the spatial distribution of sediment sources. Radionuclide tracing techniques offer a significant addition to the methods available for investigating sediment movement in the landscape. Such methods help to provide a better understanding of the sources of sediment, and facilitate more informed decisions concerning catchment management and the allocation of soil conservation resources.

12.1 Directions for Further Research

1. This study has developed a framework for applying decay series nuclide correlations and concentrations to sediment sourcing problems. The study has focused on particle size fractions generally >38 μm in diameter. Many Australian rivers carry significant loads of particles <38 μm in diameter. The few data presented from the <38 μm fractions in soils do suggest that the framework developed in this study still applies in these very fine fractions, however this does need to be explicitly tested.

2. The observation of a ^{228}Ra excess in soils and sediments in this study were in general serendipitous and the sampling strategies employed, with the exception of Chapter 11, were not specifically designed for the purpose of studying sediment transport rates or residence times. More specifically designed studies are required to demonstrate how useful observations of this excess will be to tackling problems of sediment transport rates and residence times.

3. The observation of a uniform $^{230}Th/^{232}Th$ ratio in the soils and parent rock implies parallel behaviour of uranium and thorium during the weathering (rock to soil). This is perhaps surprising given the differences in the element chemistry. Analysis of many more soil and parent rock pairs would be useful in determining how widespread this phenomenon is.

BIBLIOGRAPHY

Adams, J.A.S., Osmond J.K. and Rogers J.J.W. (1959). The geochemistry of thorium and uranium. In 'Physics and Chemistry of the Earth', ed. L.H. Ahrens, F. Press, K. Rankama and S.K. Runcorn, 3, 298-348.

Aitken, M.J. (1992). Optical dating. *Quaternary Science Re*views 11, 127-131

Allen, S.E., Grimshaw H.M., Parkinson J.A., and Quarinby C. (1974). 'Chemical Analysis of Ecological Materials', ed. S.E. Allen, [Blackwell Scientific Publications]

Anderson, R.F., Bacon M.P. and Brew P.G. (1982). Elevated concentrations of actinides in Mono Lake. *Science* 216, 514-516

Borovec, Z. (1981). The Adsorption of uranyl species by fine clay. *Chemical Geology* 32, 45 - 58

Burch, G.J., Barnes C.J., Moore I.D., Barling R.D., Mackenzie D.H. and Olley J.M. (1988). Detection and prediction of sediment sources in catchments: use of Be-7 and Cs-137. In 'Hydrology and Water Resources Symposium', Aust. Inst. Eng. National Conference Publication. No. 88/1, 146-151.

Caitcheon, G. (1993). Applying environmental magnetism to sediment tracing. Tracers in Hydrology (Proceedings of the Yokohama Symposium, July '93) *IAHS Publication No.* 215, 285-292

Caitcheon, G., Murray A.S., and Wasson R.L. (1991). The Snowy River sediment study : Sourcing sediment using environmental tracers. Division of Water Resources Report No. 80.

Callahan, J. (1987). A nontoxic heavy liquid and inexpensive filters for separation of mineral grains. *Journal of Sedimentary Petrology* 57, 765-766

Carpenter, R., Peterson M.L., Bennett J.T. and Somayajulu B.L.K. (1984). Mixing and cycling of uranium, thorium and ^{210}Pb in Puget Sound sediments. *Geochimica et Cosmochimica Acta* 48, 1949-1963

Chappell, B.W., English P.M., King P.L., White A.J.R., and Wyborn D. (1991). Granites and related rocks of the Lachlan Fold belt (1:1 250 000 scale map), Bureau of Mineral Resources, Geology and Geophysics, Canberra, Australia.

Clarke , S.P.Jr., Peterman Z.E. and Heier K.S. (1966). In 'Handbook of physical constants', ed. S.P. Clarke (Jr.) [Geological Society of America: New York]

Coffin, D.E. (1963). A Method for the determination of free iron in soils and clays. *Canadian Journal of Soil Science* 43, 7-17

Crapper, P.F., O'Loughlin E.M., and Mackay S.M. (1989). The hydrological effect of intensive logging operations on a small forested catchment near Eden, N.S.W. Hydrology and Water Resources Symposium, Christchurch, N.Z., 23-30 Nov. 1989.

Dearlove, J.P.L., Longworth G., Ivanovich M., Kim J., Delakowitz B. and Zeh P. (1991). A study of groundwater colloids and their geochemical interactions with natural radionuclides in the Gorleben aquifer systems. *Radiochimica Acta* 52-3, 83-89

Dickson, B.L., and Wheller G.E. (1992). Uranium series disequilibrium in exploration geology. In 'Uranium Series Disequilibrium: Applications to Environmental Problems', ed. M. Ivanovich and R.S. Harmon, second edition .[Clarendon Press: Oxford], 704-729

Dunkley, J.R., Kiernan K., and Hamilton-Smith E. (1988). Jenolan Caves and karst - the resources and their management. In 'Jenolan Caves Reserve Draft Plan of Management', Tourist Commission of New South Wales and Crown Lands Office, Vol. 2, Specialist papers 49pp.

Frissel, M.J. and Koster H.W. (1990). Radium in soil. In 'The environmental behaviour of radium'. IAEA Technical report series 310, vol. 1, 323-334.

Gaffney, J.S., Marley N.A., and Orlandini K.A. (1992). Evidence for thorium disequilibria due to organic complexation in natural waters. *Environmental Science and Technology* 26, 1248-1250

Gascoyne, M. (1992). The geochemistry of the actinides and their daughters. In 'Uranium Series Disequilibrium: Applications to Environmental Problems', ed. M. Ivanovich and R.S. Harmon, second edition. [Clarendon Press: Oxford], 34-58.

Gascoyne, M. (1989). High levels of uranium and radium in groundwaters at Canada's Underground Research Laboratory, Lac du Bonnet, Manitoba. *Applied Geochemistry* 4, 577-592

Gascoyne, M. (1982). The geochemistry of the actinides and their daughters. In 'Uranium Series Disequilibrium: Applications to Environmental Problems', ed. M. Ivanovich and R.S. Harmon, [Clarendon Press: Oxford], 33-55

Gippel, C.J. (1989). The use of turbidity instruments to measure stream water suspended sediment concentrations. Monograph Series No. 4, Dept. of Geography and Oceanography, UNSW, ADFA, Australia

Goldschmidt, V.H. (1954). 'Geochemistry'. [Clarendon Press: Oxford]

Gomez, B. (1991). Bedload transport. *Earth Science Reviews* 31, 89-132

Greeman, D.J., Rose A.W., and Jester W.A. (1990). Form and behavior of radium, uranium, and thorium in Central Pennsylvania soils derived from dolomite. *Geophysical Research Letters* 17, 833-836

Grimshaw, D.L., and Lewin J. (1980). Source identification for suspended sediments. *Journal of Hydrology* 47, 151-162

Hancock, G.J. (1993). The effects of salinity on the concentrations of radium and thorium in sediments. Unpublished MSc thesis. Geology Dept., Australian National University

Hancock, G.J., and Martin P. (1991). Determination of Ra in Environmental Samples by α-particle Spectrometry. *Applied Radiation Isotopes* 42, 63 - 69

Hansen, R.O., and Stout P.R. (1968). Isotopic distribution of uranium and thorium in soils. *Soil Science* 105, 44-50

Harmon R.S., and Rosholt J.N. (1982). Igneous Rocks. In 'Uranium Series Disequilibrium: Applications to Environmental Problems', ed. M. Ivanovich and R.S. Harmon, [Clarendon Press: Oxford], 145-164.

Harmsen, K., and de Haan F.A.M. (1980). Occurrence and behaviour of uranium and thorium in soil and water. *Netherlands Journal of Agricultural Science* 28, 40-62

Hart, D.M. (1988). A safe method for the extraction of plant opal from sediments. *Search* 19, 293-294

Hawtrey, K. (1987). Outlook for the rural economy. Proceedings Soil Conservation Service NSW Annual Conference, S.C.S., Sydney, Australia, 224-237

Henderson and Strusz (1971). Geological map of Canberra, Bureau of Mineral Resources, Geology and Geophysics, Canberra, ACT. [Mercury Walch Pty Ltd: Hobart, Australia]

Ivanovich, M. and Harmon R.S. (1992). 'Uranium Series Disequilibrium: Applications to Environmental Problems', second edition [Clarendon Press: Oxford].

Ivanovich, M. and Harmon R.S. (1982). 'Uranium Series Disequilibrium: Applications to Environmental Problems' [Clarendon Press: Oxford]

Iyengar, M.A.R. (1990). The natural distribution of radium. In 'The environmental behaviour of radium'. IAEA Technical report series 310, vol. 1, 59-70.

de Jesus, A.S.M., Malan J.J., and Basson J.K. (1980). Movement of radium from South African gold/uranium mine dumps into the aqueous environment. In 'Source distribution, movement and deposition of radium in inland waterways and aquifers', IAEA, Vienna

Kamel, A.M., and Johnson J.W. (1963). Tracing coastal sediment movement by naturally radioactive minerals. In 'Proceedings of the eighth conference on Coastal Engineering, Mexico city, Mexico', ed. J.W Johnson, Council on Wave Research, The Engineering Foundation, 324-330

Katzin, L.I. (1954). The chemistry of thorium. In 'The Actinide Elements', ed. G.T. Seaborg and J.J. Katz [McGraw-Hill: New York], 66-95

Krishnaswami, S., Bhushan R. and Baskaran M. (1991). Radium isotopes and ^{222}Rn in shallow brines, Kharaghoda (India). *Chemical Geology* 87, 125-136

Krishnaswami, S., Graustein W.C., Turekian K.K. and Dowd J.F. (1982). Radium, thorium and radioactive lead isotopes in groundwaters: application to the in-situ determination of adsorption-desorption rate constants and retardation factors. *Water Resources Research* 18, 1663-1675

Kronfeld, J., Ilani S. and Strull A. (1991). Radium precipitation and extreme ^{238}U-series disequilibrium along the Dead Sea coast, Israel. *Applied Geochemistry* 6, 355-361

Krumbein, W.C., and Sloss L.L. (1963). 'Stratigraphy and Sedimentation', second edition, [Freeman W.H. and Co.]

LaFlamme, B.D., and Murray J.W. (1987). Solid/solution interaction: The effect of carbonate alkalinity on absorbed thorium. *Geochimica et Cosmochimica Acta* 51, 243-250

Langmuir, D., and Herman J.S. (1980). The mobility of thorium in natural waters at low temperatures. *Geochimica et Cosmochimica Acta* 44, 1753-1766

Langmuir, D., and Reise A.C. (1985). The thermodynamic properties of radium. *Geochimica et Cosmochimica Acta* 49, 1593-1601

Larsen E.S., and Gottfried D. (1960). Uranium and thorium in selected suites of igneous rocks. *American Journal of Science* 258, 151-168

Leeder, M.R. (1982). 'Sedimentology: Process and Product', [George Allen & Unwin: London]

Levinson, A.A., Bland C.J. and Lively R.S. (1982). Exploration for U ore deposits. In 'Uranium Series Disequilibrium: Applications to Environmental Problems', ed. M. Ivanovich and R.S. Harmon, [Clarendon Press: Oxford], 351-381.

Lyons, J.B. (1964). Distribution of thorium and uranium in three early paleozoic plutonic series of New Hampshire. *U.S. Geological Survey Bulletin* 1144-F, F1-F43

Martin, P., and Hancock G. (1992). Routine analysis of naturally occurring radionuclides in environmental samples by alpha-particle spectrometry. Research report 7, Supervising Scientist for the Alligator Rivers Region, AGPS, Canberra.

Mackay, S.M. (1988). Hydrological studies in the Eden region. Forest Commission of New South Wales Internal Report, Research Meeting, Eden 1988.

Marley, N.A., Gaffney J.S., Orlandini K.A., and Cunningham M.A. (1993). Evidence for radionuclide transport and mobilization in a shallow, sandy aquifer. *Environmental Science and Technology* 27, 2456-2461

Megumi, K. (1979). Radioactive disequilibrium of uranium and actinium series nuclides in soil. *Journal of Geophysical Research* 84, 3677-3682

Megumi, K., Fan S.H, Kimura S., Tsujimoto T., Oka T. and Katsurayama K. (1986). Concentration of natural radioactive nuclides and mineral composition in soils in relation to their sizes. *Hoken Butsuri* 21, 155-160 (in Japanese, English abstract)

Megumi, K., and Mamuro T. (1977). Concentration of uranium series nuclides in soil particles in relation to their size. *Journal of Geophysical Research* 82, 353-356

Megumi, K., Oka T., Doi M., Kimura S., Tsujimoto T., Ishiyama T. and Katsurayama K. (1988). Relationships between the concentrations of natural radionuclides and the mineral composition of the surface soil. *Radiation Protection Dosimetry* 24, 69-72

Megumi, K., Oka T., Yaskawa K. and Sakanoue M. (1982). Contents of natural radioactive nuclides in soil in relation to their surface area. *Journal of Geophysical Research* 87, 10857-10860

Meijer, R.J., Put L.W., Schuiling R.D., de Reus J.H. and Weirsma J. (1988). Provenance of coastal sediments using natural radioactivity of heavy mineral sands. *Radiation Protection Dosimetry* 24, 55-58

Meijer, R.J., Put L.W., Schuiling R.D., de Reus J.H. and Weirsma J. (1987). Natural radioactivity of heavy-mineral sands: a tool for coastal sedimentology? In

'Proceedings of the International Symposium on Radioactivity and Oceanography', Cherbourg, France, 1987

Meriwether, J.R., Beck J.N., Keeley D.F., Langley M.P., Thompson R.H. and Young J.C. (1988). Radionuclides in Louisiana Soils. *Journal of Environmental Quality* 17, 562-568

Merrill, G.K. (1987). Cryogenic density separations of conodonts. In 'Conodonts: Investigative Techniques and applications', ed. R.L. Austin, [Ellis Horwood Ltd.], 63-66.

Michel, J. (1984). Redistribution of uranium and thorium series isotopes during isovolumetric weathering of granite. *Geochimica et Cosmochimica Acta* 48, 1249-1255

Middelburg, J.J., Van Der Weijden C.H. and Woittiez J.R.W. (1988). Chemical processes affecting the mobility of major, minor and trace elements during weathering of granitic rocks. *Chemical Geology* 68, 253-273

Moore, W.S. (1992). Radionuclides of the uranium and thorium decay series in estuarine environments. In 'Uranium Series Disequilibrium: Applications to Environmental Problems', ed. M. Ivanovich and R.S. Harmon, second edition, [Clarendon Press: Oxford], 145-164

Moore, I.D., Burch G.J., and Wallbrink P.J. (1986)a. Preferential flow and hydraulic conductivity of forest soils. *Soil Science Society of America Journal* 50, 876-881

Moore, I.D., Mackay S.M, Wallbrink P.J., Burch G.J. and O'Loughlin E.M. (1986)b. Hydrologic characteristics and modelling of a small forested catchment in southeastern NSW. Pre-logging condition. *Journal of Hydrology* 83, 307-335

Moreira-Nordemann, L.M. (1980). Use of $^{234}U/^{238}U$ disequilibrium in measuring chemical weathering rates of rocks. *Geochimica et Cosmochimica Acta* 44, 103-108

Mosley, M.P. (1981). The influence of organic debris on channel morphology and bedload transport in a New Zealand forest stream. *Earth Surface Processes and Landforms* 6, 571-579

Moss, A.J., Walker P.H., and Hutka J. (1973). Fragmentation of granitic quartz in water. *Sedimentology* 20, 489-511

Moss, A.J., and Walker P.H. (1978). Particle transport by continental water flows in relation to erosion, deposition, soils, and human activities. *Sedimentary Geology* 20, 81-139

Murray, A.S., Caitcheon G., Olley J.M. and Crockford H.(1990). Methods for determining the sources of sediment reaching reservoirs: Targeting soil conservation. *Ancold Bulletin* 85, 61-70

Murray, A.S., Marten R., Johnson A., and Martin P. (1987). Analysis for naturally occurring radionuclides at environmental concentrations by gamma spectrometry. *Journal of Radioanalytical and Nuclear Chemistry* 115, 263-288

Murray, A.S., Olley J.M., and Wallbrink P.J. (1992). Natural radionuclide behaviour in the fluvial environment. *Radiation Protection Dosimetry* 45, 285-288

Murray, A.S., Olley J.M., and Wallbrink P.J. (1991). Radionuclides for analysis of sediments in water supply catchments. CSIRO, Division of Water Resources Consultancy Report No. 91/8, Canberra

Murray, A.S., Stanton R., Olley J.M., and Morton R. (1993). Determining the origins and history of sedimentation in an underground river system using natural and fallout radionuclides. *Journal of Hydrology* 146, 341-359

Norrish, K., and Chappell B.W. (1977). X-ray fluorescence spectrometry. In 'Physical methods in determinative mineralogy', second edition, ed. J. Zussman [Academic Press: London], 201-272

Norrish, K., and Hutton J.T. (1969). An accurate X-ray spectrographic method for the analysis of a wide range of geological samples. *Geochimica et Cosmochimica Acta* 33, 431-453

Olive, L.J., and Rieger W.A. (1987). Eden catchment project: Sediment transport and catchment disturbance 1977-1983. Monograph Series No. 1, Dept. of Geography and Oceanography, UNSW, ADFA

Olley, J.M., Murray A.S., MacKenzie D.H., and Edwards K. (1993). Identifying sediment sources in a gullied catchment using natural and anthropogenic radioactivity. *Water Resources Research* 29, 1037-1043

Olley, J.M., Murray A.S., Wallbrink P.J., Caitcheon G., and Stanton R. (1991). The use of fallout nuclides as chronometers. Workshop on Quaternary Dating, Australian National University, Canberra 1991. pp 51-55

Orlandini, K.A., Penrose W.R., Harvey B.R., Lovett M.B., and Findlay M.W. (1990). Colloidal behavior of actinides in an oligotrophic lake. *Environmental Science and Technology* 24, 706-712

Osmond, J.K., and Cowart J.B. (1982). Groundwater. In 'Uranium Series Disequilibrium: Applications to Environmental Problems', ed. M. Ivanovich and R.S. Harmon, [Clarendon Press: Oxford], 202-245

Osmond, J.K., and Cowart J.B. (1976). The theory and uses of natural uranium isotopic variations in hydrology. *Atomic Energy Review* 14, 621-678

Osmond, J.K., and Ivanovich M. (1992). Uranium-series mobilisation and surface hydrology. In 'Uranium Series Disequilibrium: Applications to Environmental Problems', ed. M. Ivanovich and R.S. Harmon, second edition. [Clarendon Press: Oxford], 260-289

Paton, T.R. (1978). 'The formation of soil material'. [George Allen and Unwin: London.]

Pliler, R., and Adams J.A.S. (1962)a. The distribution of thorium, uranium and potassium in the Mancos shale. *Geochimica et Cosmochimica Acta* 26, 1115-1135

Pliler, R., and Adams J.A.S. (1962)b. The distribution of thorium and uranium in a Pennsylvanian weathering profile. *Geochimica et Cosmochimica Acta* 26, 1137-1146

Press, F., and Siever R. (1978). 'Earth', [Freeman W.H. and Co.: San Francisco].

Rieger, W.A., Olive L.J., and Burgess J.S. (1979). Sediment discharge response to clear-fell logging in selected small catchments, Eden, N.S.W. 10th. New Zealand Geography Conference 1979

Ritchie, J.C., Spraberry J.A., and McHenry J.R. (1974). Estimating soil loss from the redistribution of fallout ^{137}Cs. *Soil Society of America Proceedings* 38, 137-139

Roberts, R.G., and Church M. (1986). The sediment budget in severely disturbed watersheds, Queen Charlotte Ranges, British Columbia. *Canadian Journal of Forest Research* 16, 1096-1106

Rogers, J.J.W., and Adams J.A.S. (1969). Thorium. In the 'Handbook of Geochemistry', ed. K.H. Wedepohl, [Springer-Verlag: Berlin.]

Rosholt, J.N. (1983). Isotopic composition of uranium and thorium in crystalline rocks. *Journal of Geophysical Research* 88, 7315-7330

Rosholt, J.N. (1982). Mobilisation and weathering. In 'Uranium Series Disequilibrium: Applications to Environmental Problems', ed. M. Ivanovich and R.S. Harmon, [Clarendon Press: Oxford], 167-178

Routley, R., and Routley V. (1974). 'The Fight for the Forests', second edition [Australian National University Press: Canberra].

Sarin, M.M., Krishnaswami S., Somayajulu B.L.K., and Moore W.S. (1990). Chemistry of uranium, thorium, and radium isotopes in the Ganga-Brahmaputra river system: Weathering processes and fluxes to the Bay of Bengal. *Geochimica et Cosmochimica Acta* 54, 1387-1396

Scott, M.R. (1968). Thorium and uranium concentrations and isotopic ratios in river sediments. *Earth and Planetary Science Letters* 4, 245-252

Sheppard, J.C., Campbell M.J., Cheng T., and Kittrick J.A. (1980). Retention of radionuclides by mobile humic compounds and soil particles. *Environmental Science and Technology* 14, 1349-1353

Short, S.A., Lowson R.T., Ellis J., and Price D.M. (1989). Thorium-uranium disequilibrium dating of late Quaternary ferruginous concretions and rinds. *Geochimica et Cosmochimica Acta* 53, 1379-1389

Short, S.A., Lowson R.T., and Ellis J. (1988). $^{234}U/^{238}U$ and $^{230}Th/^{234}U$ activity ratios in colloidal phases of aquifers in lateritic weathered zones. *Geochimica et Cosmochimica Acta* 52, 2555-2563

Sill, C.W. (1987). Determination of radium-226 in ores, nuclear wastes and environmental samples by high-resolution alpha spectrometry. *Nuclear and Chemical Waste Management* 7, 239-256

Sill, C.W., and Olsen D.G. (1970). Sources and prevention of recoil contamination of solid-state alpha detectors. *Analytical Chemistry* 49, 618-621

Simpson, H.R., Olsen C.R., Hammond D.E., Fuller C., Ku T.L., Trier R.M., Toggweiler J.R., Mathieu G., and Deck B.L. (1982). Radionuclides in Mono Lake, California. *Science* 216, 512-514

Stace, H.C.T., Hubble G.D., Brewer R., Northcote K.H., Sleeman J.R., Mulcahy M.J., and Hallsworth E.G. (1968). 'A Handbook of Australian Soils' [Rellim Technical Publications: Glenside, South Australia]

Sutherland, R.A., and de Jong E. (1990). Estimation of sediment redistribution within agricultural fields using ^{137}Cs, Crystal Springs, Saskatchewan, Canada. *Applied Geography* 10, 205-221

Talsma, T. (1989). Soil survey of Whiteheads Creek study area. Unpublished consultant's report, CSIRO Division of Water Resources

Tipping, E., and Higgo J.J.W. (1992). The role of colloids in the release and transport of radionuclides in the near and far field. British Geol. Survey Technical Report WE/91/16

Vilkes, P., Crammer J.J., Shewchuk T.A., and Larocque J.P.A. (1988). Colloid and particulate matter studies in the Cigar Lake natural-anolog program. *Radiochimica Acta* 44-5, 305-310

Wallbrink, P.J., and Murray A.S. (1993). Use of fallout radionuclides as indicators of erosion processes. *Hydrological Processes* 7, 297-304

Walling, D.E., and Kane P. (1984). Suspended sediment properties and their geomorphological significance. In 'Catchment Experiments in Fluvial

Geomorphology', ed. T.P. Burt and D.E. Walling, [Geo Books: Norwich], 311-334

Wasson, R.J., Clarke R.L., Nanninga P.M., and Waters J. (1987). ^{210}Pb as a chronometer and tracer, Burrinjuck Reservoir, Australia. *Earth Surface Processes and Landforms* 12, 399-414

Wedepohl, G. (1969). 'Handbook of Geochemistry'. [Springer-Verlag: Berlin.]

White, A.J.R., Williams I.S., and Chappell B.W. (1976). The Jindabyne thrust and its tectonic, physiographic and petrographic significance. *Journal of the Geological Society of Australia* 23, 105-112

Woods, P.A. (1978). Fine sediment mineralogy of source rocks and suspended sediment , Rother catchment West Sussex. *Earth Surface Processes* 3, 255-263

Appendix A

Conversion Factors

1 ppm U = 12.450 Bq kg^{-1} , ^{238}U

1 ppm Th = 4.105 Bq kg^{-1}, ^{232}Th

Appendix B

Site and Sampling Descriptions

The sampling strategies used at each of the sites discussed in Chapters 4 and 5 are described in the following sections. The general location of each of the sites was given in Figure 4.1.

Site A : Geebung Creek 37°18' S and 149°40' E

The Geebung Creek catchment is a 76 ha forested catchment located within the Yambulla State forest NSW. It overlies the Yambulla Granite (a coarse grained adamellite). The soils consist dominantly of coarse textured profiles (sand loams and loamy sands) that are massive, have shallow A horizons and grade sharply into decomposing rock at depths of 40-100 cm. Soils in the upper catchment were sampled by digging four soil pits (down to bedrock) along an 150m transect (Figure A1). The pits were evenly spaced along the transect which ran downslope from the top of the hill to the saturated zone. Samples were collected from each of the soil horizons exposed, a total of 11 samples (A1 to A12) were collected (Figure A1). Soils in the lower catchment were sampled from along stream-banks (Figure A1). Five samples (A13 to A17) were collected along a 200m reach of stream. Sample A18 was collected from the upper catchment. The soil mineralogy is dominated by quartz and feldspar with many of these grains >55μm in diameter. Iron oxide coatings were present on grains from all the samples and discrete iron oxide grains were present in the samples collected from the lower catchment. No rock sample was collected from this site as the granite had been previously analysed by XRF (Dr. B.W. Chappell *pers comm.*) and the U and Th data from this analysis were used to characterise the bedrock.

Three 20 litre groundwater samples were collected from the downslope transect from two lower pits (AW1 and AW2) and from the spring zone directly below the transect (AW3). An additional 20 litre sample was collected from the stream directly above the weir (AW4). The pits were each bailed clear of water then allowed to refill. Water samples were then collected in 20 litre plastic buckets and the pH and EC were measured at the time of sampling. The pH and EC were measured again on return to the laboratory and the samples immediately filtered through 0.45μm millipore filter, and the filtrate was acidified with 2ml of concentrated HCl.

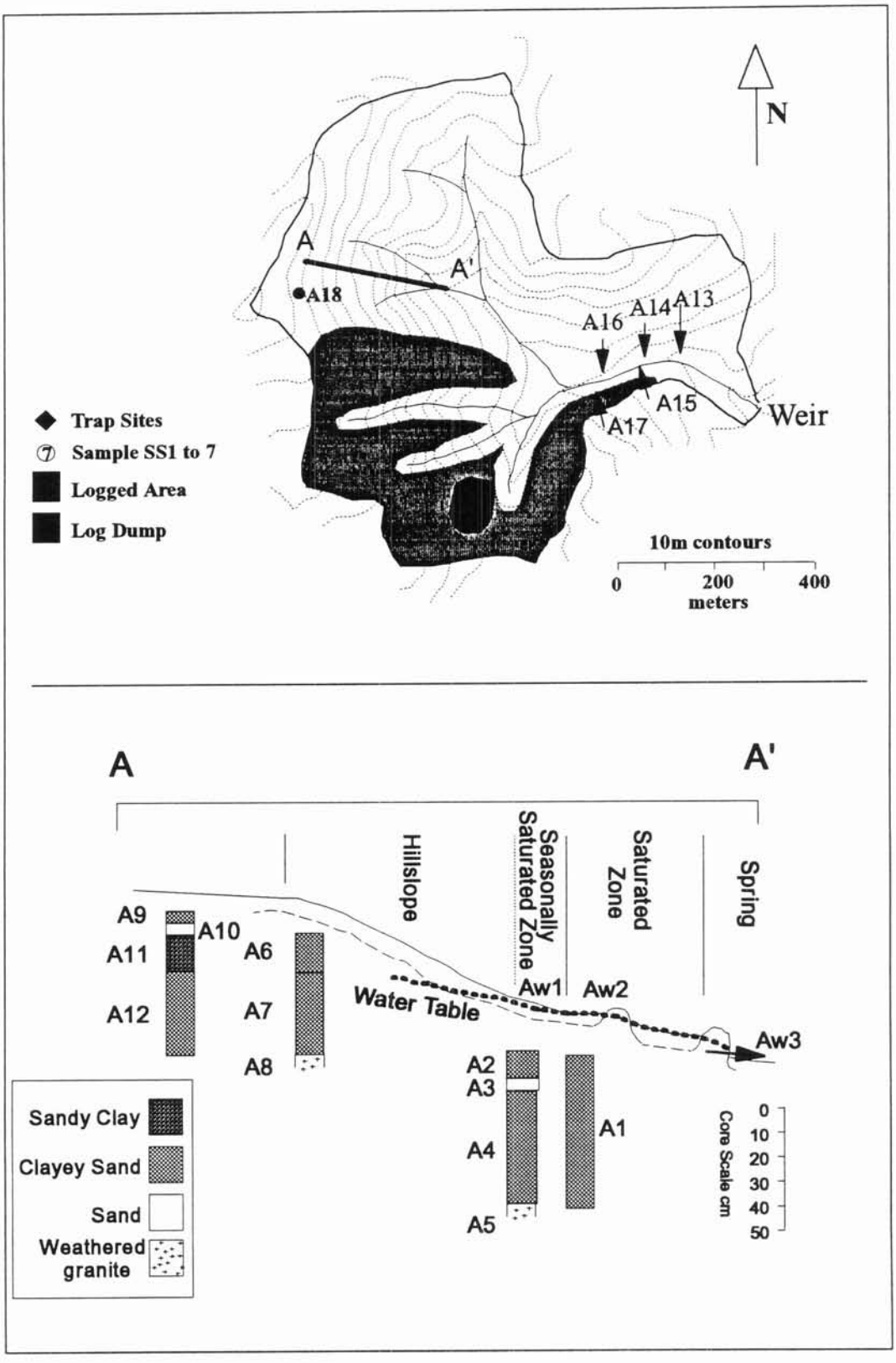

Figure A1: (Top) map of the Geebung Creek Catchment showing sampling locations. (Bottom) details of the soil pits and transect samples.

Sites B and C : McKeowns Valley 33°47' S and 150°02' E

The McKeowns Valley catchment is the main catchment area for the Jenolan Caves, NSW and is dominated by two major rock groups (see Figure 10.1); the first is a sequence of interlain sandstones and volcanoclastic sediments which cover about 3/4 of the catchment (Site C); the second is a basalt which occurs along the Western edge of the catchment and covers ~1/4 of the total catchment (Site B). Samples were collected from a large number of points within each rock type and combined to provide 13 samples from the basalt (B1 to B13) and 13 samples from the sediments (C1 to C13). Rock samples were collected along with the soil samples from each rock type. Weathered and secondary material was excluded. These rock samples were combined to provide one analysis from each rock group.

Site D : Whiteheads Creek 35°40' S and 149°36' E

Eight samples (D1 to D8) were collected from a duplex soil exposed in a gully wall at Whiteheads Creek (see Figure 7.1 for details). One from each of the A1 and A2 horizons, the rest from the B horizon down to bedrock (Figure A4 insert). The A1 horizon consists of fine sandy loam (quartz and feldspar). The A2 horizon is coarser grained, fine loamy sand (quartz and feldspar) with iron staining present. The transition to the B horizon (quartz, feldspar, clay and iron oxide) is marked by a sharp decrease in particle size. Bleaching and mottling increase down the profile and iron nodules are present in the lower profile. This soil is considered to have formed from sediments derived from the surrounding granite and deposited in the valley. An additional 2 kg sample D9 was collected from an adjacent site. This sample represents a uniform cut of material from the top to the base off the profile. Three samples of the coarse grained granite were collected to characterise the parent material.

Site E : Yarramundi Reach 35°17' S and 149°04' E

This site is located on the northern shore of Lake Burley Griffin (ACT) and slopes towards the lake. The bedrock is dacitic tuff with minor agglomerate and volcanoclastic sediments. The soils are yellow texture contrast soils with shallow A horizons. Fifty samples (E1 to E50) were collected in a regular grid pattern from a 100m x 100m plot on the slope. Rock samples were collected from 5 points within the 100m x 100m plot, these were then combined to provide a single rock sample. The soil samples were dominated by quartz and feldspar with only minor clay present.

Site F : Black Mountain 35°16' S and 149°06' E

The site bedrock is fine grained quartz sandstone; the soil has been formed on sand colluvium [*Henderson and Strusz*, 1971]. It is a yellow texture contrast soil with a shallow a horizon (5cm) of fine grey loam overlying a yellow silty clay loam (B horizon). Seven soil samples (F1 to F7) were collected from a 20cm x 20cm pit sampled to a depth of 25cm. A rock sample was collected from the base of the pit. The rock sample was fine grained red sandstone. The soil samples consisted predominantly of quartz with minor clay. Iron oxide coatings were evident on the coarser particles.

Twenty samples were collected (20 x 20 x 1cm deep) from within a 12m x 12m area at this site and combined to provide a representative sample of the surface soil (F8).

Sites G and H : Killimacat Creek 35°15' S and 148°15' E

Two soil samples were collected from the Killimacat Creek catchment. One from a fine grained sandstone bedrock, the other from rhyolitic bedrock. Each sample consisted of ~1kg of material collected from soil pits dug to bedrock. Rock samples were collected from each sampling site. The soil developed on the sediment consisted dominantly of quartz, minor feldspar and secondary iron oxides and clay.

Site I : Chaffey Dam 31°07' S and 150°57' E

Four soil samples were collected from a soil formed on upland basalt in the Chaffey Dam catchment. These samples were combined to provide a single sample of this basaltic soil. Three fresh rock samples were collected from the same location. These were combined to provide a single sample of the basalt rock.

Appendix C

Rock and Bulk Soil Sample Radionuclide Analyses. All data reported as Bq/kg. Uncertainies are equilvalent to one standard error on the mean.

Table C1: Rock Samples

Sample Code	Site	Rock Type	Th-230	Th-232	Th-230/Th-232
A	Geebung Creek	Granite	54.0 ± 5.0	97.0 ± 5.0	0.56 ± 0.06
B	McKeowns Valley	Basalt	12.5 ± 0.5	9.6 ± 0.5	1.30 ± 0.09
C	McKeowns Valley	Mixed Sediments	28.5 ± 0.9	40.9 ± 1.1	0.70 ± 0.03
D	Whiteheads Creek	Granite	52.0 ± 3.0	95.0 ± 5.0	0.55 ± 0.04
E	Yarramundi Reach	Dacite	33.5 ± 1.5	48.0 ± 2.0	0.70 ± 0.04
F	Black Mountain	Sandstone	27.2 ± 1.1	34.2 ± 1.2	0.80 ± 0.04
G	Killimacat Creek	Sandstone	47.5 ± 1.0	74.8 ± 2.0	0.64 ± 0.02
H	Killimacat Creek	Rhyolite	22.7 ± 0.8	23.7 ± 0.9	0.96 ± 0.05
I	Chaffee Dam	Basalt	11.7 ± 0.5	14.0 ± 0.4	0.84 ± 0.04

Table C2: Soil Samples

				Geebung Creek Granite				
	U-238	Th-230	Ra-226	Th-232	Ra-228	Th-228	K-40	Cs-137
A1	75 ± 3	51.0 ± 3.0	55.2 ± 0.5	92.0 ± 4.0	91.3 ± 1.1	92.1 ± 0.9	464 ± 7	0.7 ± 0.2
A2	44 ± 8	26.8 ± 1.9	31.5 ± 0.7	50.0 ± 3.0	50.5 ± 1.6	52.6 ± 1.3	432 ± 9	2.6 ± 0.4
A3	32 ± 8	25.1 ± 0.9	29.0 ± 0.6	47.1 ± 1.5	46.8 ± 1.4	49.3 ± 1.2	434 ± 9	0.4 ± 0.3
A4	27 ± 5	26.3 ± 1.7	25.1 ± 0.4	49.0 ± 3.0	44.9 ± 0.9	45.4 ± 0.5	378 ± 7	0.2 ± 0.2
A5	30 ± 5	21.9 ± 1.2	21.9 ± 0.4	40.2 ± 1.9	41.6 ± 0.9	41.4 ± 0.6	369 ± 7	0.1 ± 0.2
A6	37 ± 7	26.5 ± 1.3	28.2 ± 0.6	47.1 ± 2.0	45.4 ± 1.4	46.1 ± 1.2	335 ± 7	14.0 ± 0.5
A7	25 ± 2	23.0 ± 1.2	22.1 ± 0.3	41.0 ± 1.9	42.5 ± 0.7	42.5 ± 0.5	321 ± 6	0.6 ± 0.2
A8	36 ± 6	29.2 ± 1.5	30.3 ± 0.5	55.0 ± 2.0	59.4 ± 1.1	59.4 ± 0.7	658 ± 10	-0.1 ± 0.3
A9	32 ± 2	29.3 ± 2.0	33.2 ± 0.5	48.0 ± 3.0	56.4 ± 1.3	55.4 ± 0.9	512 ± 10	9.4 ± 0.4
A10	35 ± 1	29.9 ± 1.5	29.8 ± 0.4	51.0 ± 2.0	45.8 ± 1.1	46.9 ± 0.9	453 ± 9	1.1 ± 0.3
A11	34 ± 2	30.2 ± 2.0	31.9 ± 0.5	53.0 ± 3.0	56.0 ± 1.3	55.3 ± 0.9	527 ± 10	0.4 ± 0.3
A12	41 ± 3	49.0 ± 1.3	44 ± 0.3	86 ± 2	87.1 ± 0.9	88.2 ± 0.7	1119 ± 14	0.03 ± 0.2
A13	88 ± 4	38.2 ± 2	59.3 ± 0.6	60 ± 3	74.4 ± 1.6	77.1 ± 1.3	1050 ± 16	0.6 ± 0.5
A14	74 ± 4	51.9 ± 1.8	80.2 ± 0.7	91 ± 2	90.9 ± 1.7	94.1 ± 1.4	1110 ± 17	-0.5 ± 0.4
A15	20 ± 2	13.1 ± 1.3	18.1 ± 0.3	23 ± 2	23.1 ± 0.7	22.6 ± 0.4	589 ± 9	0.3 ± 0.2
A16	108 ± 3	47.3 ± 1.6	152 ± 1	83 ± 2	83.6 ± 1	85.2 ± 0.8	931 ± 12	0.3 ± 0.2
A17	18 ± 2	11.6 ± 0.9	17.7 ± 0.3	17.4 ± 1.2	19.4 ± 0.5	20.1 ± 0.3	640 ± 9	0.3 ± 0.1
A18		16.1 ± 0.6	16.3 ± 0.4	31.5 ± 0.9	31.9 ± 0.9	31.4 ± 0.5	672 ± 10	0.8 ± 0.2
				McKeown Valley Basalt				
B1	51 ± 5	59.2 ± 3.4	73.2 ± 1.1	44.6 ± 2.7	48.2 ± 1.1	47.2 ± 1	701 ± 17	9.2 ± 0.4
B2	43 ± 28	55 ± 3	71.6 ± 2.9	42.8 ± 2.5	58.9 ± 5.5	46.8 ± 3.4	748 ± 36	10.3 ± 1.7
B3	44 ± 27	50.6 ± 2	63.2 ± 2.8	38.9 ± 1.7	44.8 ± 5.4	42.3 ± 3.4	635 ± 34	6.7 ± 1.7
B4	39 ± 28	53.2 ± 2.3	78.3 ± 3	41 ± 1.9	56.9 ± 5.7	48 ± 3.4	811 ± 38	8.4 ± 1.8
B5	18 ± 3	23.7 ± 1.2	26.2 ± 0.4	21.6 ± 1.1	21.6 ± 0.6	21.8 ± 0.5	553 ± 13	4 ± 0.2
B6	23 ± 6	26.5 ± 1	26.9 ± 0.5	22.6 ± 0.9	22.3 ± 0.9	22.5 ± 0.6	639 ± 16	3.2 ± 0.3
B7	22 ± 5	25.6 ± 1.4	25.1 ± 0.5	20.5 ± 1.3	21.5 ± 0.9	21.1 ± 0.6	570 ± 15	3.9 ± 0.3
B8	51 ± 10	50.3 ± 1.6	54.1 ± 1.2	42.8 ± 1.5	45.4 ± 2.3	41.9 ± 1.1	737 ± 18	5.5 ± 0.8
B9	45 ± 12	56 ± 2	54.1 ± 1.3	42.3 ± 1.6	44.6 ± 2.5	43.9 ± 1.2	740 ± 19	6.1 ± 0.8
B10	51 ± 10	55.6 ± 2.1	51.9 ± 1.2	42.8 ± 1.6	45.2 ± 2.3	43.6 ± 1.2	751 ± 18	5.7 ± 0.8
B11	52 ± 10	53.2 ± 1.6	52.7 ± 1.2	44.9 ± 1.5	43.2 ± 2.4	43.3 ± 1.1	743 ± 18	6.3 ± 0.7
B12	55 ± 11	57 ± 2	58.4 ± 1.3	43 ± 2	45.1 ± 2.5	43.3 ± 1.2	757 ± 19	5.2 ± 0.8
B13	60 ± 10	55 ± 2	54.8 ± 1.1	47 ± 2	46.2 ± 2.0	45.4 ± 1.0	772 ± 17	6.0 ± 0.6
				McKeowns Valley Mixed Sediments				
C1	23 ± 5	20.2 ± 0.8	25.7 ± 0.6	29.9 ± 1.1	35.9 ± 1.1	35.1 ± 0.8	269 ± 9	10.4 ± 0.4
C2	21 ± 10	28.2 ± 1.3	31.9 ± 1	41.7 ± 1.7	40.7 ± 1.9	41.1 ± 1.2	362 ± 14	11.9 ± 0.7
C3	30 ± 11	25.4 ± 1.1	23.8 ± 1	27.8 ± 1.2	33.2 ± 2	32.4 ± 1.3	240 ± 12	10.2 ± 0.7
C4	30 ± 9	27.7 ± 1.1	31.2 ± 1	35.8 ± 1.3	39.3 ± 1.8	39.3 ± 1.1	226 ± 11	12.7 ± 0.7
C5	21 ± 7	30 ± 1.5	36.4 ± 0.8	35.5 ± 1.7	42.6 ± 1.4	42.1 ± 1	273 ± 10	13.6 ± 0.6
C6	11 ± 3	13 ± 0.6	15.6 ± 0.3	13.6 ± 0.6	16.4 ± 0.5	16.1 ± 0.4	198 ± 6	1.9 ± 0.1
C7	15 ± 3	13.5 ± 0.4	19.6 ± 0.4	17.2 ± 0.5	23.1 ± 0.6	21.6 ± 0.5	153 ± 5	3.9 ± 0.2
C8	24 ± 10	37.7 ± 1.7	40.1 ± 0.9	46 ± 2	41 ± 1.5	43.2 ± 1	510 ± 15	8.9 ± 0.5
C9	48 ± 12	36.9 ± 1.7	35.2 ± 0.9	56 ± 1.9	55.3 ± 1.8	54.8 ± 1.1	379 ± 11	3 ± 0.5
C10	39 ± 6	36 ± 1.6	31.3 ± 0.4	52 ± 1.9	52.2 ± 1	53.2 ± 0.7	609 ± 10	5.2 ± 0.3
C11	40 ± 6	45 ± 1.7	44.2 ± 0.5	66 ± 2	68.5 ± 1.1	68.9 ± 0.8	732 ± 11	4.9 ± 0.3
C12	30 ± 4	33.2 ± 1.5	30 ± 0.7	48.6 ± 1.8	47.7 ± 1.6	48.8 ± 0.8	646 ± 15	5.5 ± 0.5
C13	42 ± 5	43.4 ± 1.7	47.5 ± 0.8	65 ± 2	64.9 ± 1.8	66.7 ± 0.9	739 ± 16	7.5 ± 0.6

Table C2: Soil Samples (cont.)

	U-238	Th-230	Ra-226	Th-232	Ra-228	Th-228	K-40	Cs-137
Whiteheads Creek Granite								
D1	49 ± 7	47.1 ± 1.9	49.8 ± 0.8	90 ± 3	94.9 ± 1.6	94.5 ± 1.6	418 ± 11	-0.1 ± 0.3
D2	51 ± 6	48 ± 2	53.5 ± 0.8	91 ± 3	91.8 ± 1.5	92.3 ± 1.5	408 ± 10	0.0 ± 0.2
D3	54 ± 4	58 ± 2	97.2 ± 0.8	99 ± 3	99.8 ± 1	100 ± 0.9	423 ± 7	-0.2 ± 0.2
D4	54 ± 4	53 ± 2	84.1 ± 0.7	105 ± 3	99.6 ± 1.2	99.7 ± 1	415 ± 7	-0.0 ± 0.3
D5	56 ± 8	49.9 ± 1.8	55.1 ± 0.9	94 ± 3	93.8 ± 1.8	97.3 ± 1.6	404 ± 11	0.0 ± 0.3
D6	53 ± 7	50 ± 2	71.5 ± 1.1	99 ± 3	100 ± 1.8	103 ± 1.7	422 ± 11	-0.2 ± 0.3
D7	64 ± 4	61 ± 3	87.5 ± 0.8	116 ± 4	111 ± 1.5	111 ± 1.1	418 ± 8	0.1 ± 0.2
D8	75 ± 7	54 ± 3	73.7 ± 1.1	98 ± 4	105 ± 1.7	108 ± 1.7	398 ± 11	-0.0 ± 0.3
D9	60 ± 4	53.1 ± 1.6	65.9 ± 0.8	97 ± 2	96.9 ± 1.9	98.0 ± 1.2	413 ± 11	0.0 ± 0.5
Yarramundi Reach Dacite								
E1	27 ± 9		34.0 ± 0.7		50.0 ± 1.3	51.1 ± 1.0	297 ± 10	2.3 ± 0.3
E2	35 ± 8		33.5 ± 0.6		48.7 ± 1.2	49.3 ± 0.9	330 ± 9	2.2 ± 0.3
E3	33 ± 12		33.0 ± 0.6		50.4 ± 1.2	49.9 ± 0.9	324 ± 9	1.6 ± 0.3
E4	35 ± 8		33.5 ± 0.6		52.2 ± 1.1	52.6 ± 1.0	327 ± 9	1.2 ± 0.2
E5			33.1 ± 0.4		48.0 ± 0.8	48.9 ± 0.6	293 ± 6	1.4 ± 0.2
E6	17 ± 7		27.6 ± 0.4		45.1 ± 0.8	46.0 ± 0.8	304 ± 8	2.6 ± 0.2
E7	26 ± 6	35.5 ± 1.5	33.6 ± 0.6	49.0 ± 2.0	47.9 ± 0.9	49.5 ± 0.8	335 ± 9	1.1 ± 0.2
E8			31.1 ± 0.6		47.1 ± 1.1	46.0 ± 0.9	329 ± 10	1.8 ± 0.3
E9	30 ± 4		33.6 ± 0.5		47.3 ± 0.9	47.4 ± 0.6	314 ± 6	2.2 ± 0.2
E10	25 ± 7		28.9 ± 0.5		44.7 ± 0.9	45.4 ± 0.8	236 ± 7	1.7 ± 0.2
E11	25 ± 5	32.0 ± 1.5	32.5 ± 0.5	48.0 ± 2.0	47.6 ± 0.9	49.6 ± 0.8	301 ± 8	3.0 ± 0.2
E12	31 ± 4		34.5 ± 0.5		50.2 ± 0.8	50.8 ± 0.8	342 ± 8	1.9 ± 0.1
E13	30 ± 8	40.0 ± 3.0	35.7 ± 0.6	57.0 ± 4.0	52.2 ± 1.2	51.9 ± 1.0	339 ± 10	2.2 ± 0.3
E14	34 ± 7		33.3 ± 0.6		49.3 ± 1.1	50.9 ± 0.9	353 ± 10	2.0 ± 0.2
E15	38 ± 10	38.1 ± 1.7	32.2 ± 0.6	50.6 ± 2.1	51.3 ± 1.0	51.7 ± 0.9	294 ± 8	2.2 ± 0.2
E16	30 ± 3		30.2 ± 0.4		47.5 ± 0.8	47.4 ± 0.6	321 ± 6	1.7 ± 0.2
E17	28 ± 7	32.1 ± 1.5	28.4 ± 0.6	45.0 ± 1.9	43.0 ± 1.0	43.9 ± 0.8	296 ± 9	2.3 ± 0.2
E18	33 ± 3		32.7 ± 0.4		51.2 ± 0.8	50.6 ± 0.6	318 ± 6	0.9 ± 0.2
E19	28 ± 8		35.2 ± 0.6		50.1 ± 1.2	50.5 ± 1.0	322 ± 9	1.8 ± 0.2
E20	17 ± 12	35.0 ± 2.0	30.7 ± 0.6	50.0 ± 3.0	49.3 ± 1.2	49.6 ± 1.0	236 ± 7	1.5 ± 0.2
E21	38 ± 9	35.0 ± 4.0	30.3 ± 0.5	45.0 ± 5.0	45.0 ± 0.9	46.7 ± 0.8	311 ± 8	3.5 ± 0.2
E22	28 ± 5		34.9 ± 0.6		50.5 ± 1.2	51.8 ± 1.0	334 ± 10	2.5 ± 0.3
E23		33.5 ± 1.5	33.9 ± 0.6	55.0 ± 2.0	53.1 ± 1.1	53.8 ± 1.0	333 ± 9	1.4 ± 0.2
E24	27 ± 9	36.7 ± 1.5	34.9 ± 0.6	56.0 ± 2.0	56.9 ± 1.3	58.8 ± 1.1	320 ± 9	2.1 ± 0.3
E25	32 ± 3	36.0 ± 3.0	35.4 ± 0.4	52.0 ± 3.0	51.1 ± 0.8	52.4 ± 0.6	321 ± 6	2.6 ± 0.2
E26	26 ± 14	36.2 ± 1.5	32.7 ± 0.7	47.0 ± 2.0	46.3 ± 1.3	47.9 ± 1.0	328 ± 10	2.2 ± 0.3
E27	28 ± 12	39.8 ± 1.7	34.9 ± 0.6	61.0 ± 2.0	63.9 ± 1.3	63.5 ± 1.1	397 ± 11	2.7 ± 0.3
E28	56 ± 5		33.8 ± 0.4		60.9 ± 1.0	61.4 ± 0.7	390 ± 7	2.8 ± 0.2
E29			38.3 ± 0.4		61.4 ± 0.9	61.6 ± 0.6	406 ± 7	1.9 ± 0.2
E30	39 ± 11		34.5 ± 0.6		59.4 ± 1.2	61.2 ± 1.1	252 ± 8	2.7 ± 0.3
E31	36 ± 5	32.8 ± 1.1	33.0 ± 0.5	48.3 ± 1.6	48.1 ± 0.9	48.9 ± 0.8	341 ± 8	3.8 ± 0.2
E32			33.0 ± 0.6		57.0 ± 1.2	58.8 ± 1.0	401 ± 11	2.0 ± 0.3
E33	22 ± 8		33.8 ± 0.6		63.1 ± 1.4	63.6 ± 1.2	432 ± 12	1.1 ± 0.3
E34	24 ± 8	38.2 ± 1.5	34.2 ± 0.6	58.0 ± 2.0	59.6 ± 1.3	60.2 ± 1.0	530 ± 14	3.4 ± 0.3
E35	34 ± 4		37.0 ± 0.5		57.5 ± 0.9	58.1 ± 0.9	435 ± 10	1.5 ± 0.1
E36	33 ± 13	37.6 ± 1.6	27.4 ± 0.3	53.0 ± 2.0	56.6 ± 1.3	56.6 ± 1.0	437 ± 12	2.7 ± 0.3
E37	35 ± 5		31.4 ± 0.6		57.2 ± 1.3	58.0 ± 1.1	482 ± 13	1.5 ± 0.3
E38	37 ± 8		36.9 ± 0.7		61.8 ± 1.3	64.4 ± 1.1	685 ± 17	1.9 ± 0.3
E39	39 ± 8		35.1 ± 0.6		58.2 ± 1.3	60.2 ± 1.0	644 ± 16	2.3 ± 0.2
E40	49 ± 11		33.6 ± 0.6		53.6 ± 1.2	55.3 ± 1.0	449 ± 13	1.5 ± 0.3
E41	36 ± 7	35.1 ± 1.4	32.6 ± 0.5	50.0 ± 2.0	52.5 ± 0.9	52.6 ± 0.8	438 ± 11	4.8 ± 0.2
E42			32.6 ± 0.4		56.4 ± 1.0	56.8 ± 0.7	499 ± 8	1.7 ± 0.2
E43			31.2 ± 0.3		58.2 ± 0.7	57.7 ± 0.6	565 ± 8	1.6 ± 0.2
E44	27 ± 8	42.5 ± 3.0	32.8 ± 0.6	62.0 ± 3.0	59.4 ± 1.3	61.1 ± 1.1	742 ± 19	2.2 ± 0.3
E45		39.0 ± 3.0	39.9 ± 0.9	57.0 ± 3.0	56.9 ± 1.2	57.9 ± 1.0	582 ± 15	2.0 ± 0.3
E46			37.2 ± 0.7		59.0 ± 1.4	61.7 ± 1.1	532 ± 14	1.6 ± 0.3
E47		32.8 ± 1.4	32.9 ± 0.6	52.0 ± 2.0	51.6 ± 1.3	52.9 ± 1.0	449 ± 13	2.8 ± 0.3
E48	19 ± 10	43.1 ± 1.4	35.8 ± 0.7	61.0 ± 2.0	59.5 ± 1.4	61.6 ± 1.2	685 ± 18	3.1 ± 0.3
E49	54 ± 13		41.9 ± 0.7		56.6 ± 1.3	58.5 ± 1.1	661 ± 17	1.7 ± 0.3
E50	33 ± 3		33.3 ± 0.4		55.0 ± 0.9	54.4 ± 0.6	365 ± 6	1.5 ± 2.0
Black Mountain Sandstone								
F1	31.4 ± 1.8	30.5 ± 1.6	29.82 ± 0.66	41 ± 2	41.4 ± 1.5	41.2 ± 0.83	181.5 ± 11.5	4.69 ± 2.26
F2	29.8 ± 2	30.2 ± 1.7	29.09 ± 0.31	41 ± 2	40.4 ± 0.6	40.8 ± 0.43	161 ± 3	0.75 ± 0.14
F3	33 ± 2	31.2 ± 1.7	30.1 ± 0.3	41 ± 2	41.7 ± 0.5	41.3 ± 0.4	165 ± 3	0.9 ± 0.1
F4	30 ± 3	30.1 ± 1.7	30.8 ± 0.4	40 ± 2	41 ± 0.7	42 ± 0.5	161 ± 4	0.7 ± 0.2
F5	30 ± 3	30.2 ± 1.6	30.6 ± 0.4	41.1 ± 1.8	42.8 ± 0.8	42 ± 0.5	165 ± 4	0.4 ± 0.2
F6	29.9 ± 2.6	29.9 ± 1.6	29.46 ± 0.38	40.5 ± 1.7	41 ± 0.8	41.2 ± 0.5	156 ± 4	0.4 ± 0.18
F7	33.8 ± 2.4	29.5 ± 1.7	28.36 ± 0.35	40 ± 2	40.3 ± 0.7	39.8 ± 0.47	158 ± 4	0.05 ± 0.17
F8	30 ± 3	33.5 ± 1.5	32.4 ± 0.6	43.1 ± 1.8	42.1 ± 1.5	42.3 ± 0.9	265 ± 9	5.9 ± 0.5

Table C2: Soil Samples (cont.)

	U-238	Th-230	Ra-226	Th-232	Ra-228	Th-228	K-40	Cs-137
				Killimacat Creek Sandstone				
G1	48 ± 4	50 ± 1	49.3 ± 0.4	76 ± 1.6	75.4 ± 1.2	75.8 ± 1.1	615 ± 9.3	0.49 ± 0.3
				Killimacat Creek Rhyolite				
H1	23 ± 3	23 ± 1	21.9 ± 0.6	24.2 ± 1	26.1 ± 1.2	23.9 ± 0.6	392 ± 10	0.4 ± 0.4
				Chaffee Basalt				
I1		18.4 ± 1	16.9 ± 0.3	20.1 ± 0.8	20.9 ± 0.3			

Table C3:Bulk Soil Citrate Dithonite Extraction Radionuclide Analyses.

	Th-230	Ra-226	Th-232	Th-228
		Geebung Creek Granite		
A1	27.7 ± 1.1	18.4 ± 0.7	42.7 ± 1.5	35.9 ± 1.3
A2	3 ± 0.3	7.2 ± 0.3	7.3 ± 0.5	8.5 ± 0.6
A3	1.6 ± 0.3	5.7 ± 0.4	4.5 ± 1.6	9 ± 0.6
A4	1.9 ± 0.2	5.7 ± 0.3	4.6 ± 0.2	7.8 ± 0.3
A5	1.5 ± 0.2	4.9 ± 0.3	3.2 ± 0.2	7.8 ± 0.3
A6	0.6 ± 0.2	5.6 ± 0.5	11.7 ± 0.6	6 ± 0.3
A7	0.3 ± 0.1	5.5 ± 0.8	1.4 ± 0.2	6.5 ± 0.4
A8	1.2 ± 0.1	4.7 ± 0.3	5.5 ± 0.3	11.7 ± 0.4
A9	0.7 ± 0.6	4.5 ± 0.4	9.5 ± 1.1	10.3 ± 1.3
A10	1.6 ± 0.2	5 ± 0.8	6.4 ± 0.3	9.9 ± 0.4
A11	2.1 ± 0.2	4.9 ± 0.8	8.1 ± 0.4	15.5 ± 0.6
A12	19.0 ± 1.1		34 ± 1.5	34 ± 1.4
A13	5.5 ± 0.2		11 ± 0.6	6 ± 0.3
A14	21.1 ± 1.3		37 ± 1.4	32 ± 1.4
A15	3.1 ± 0.2		5.5 ± 0.3	7 ± 0.3
A16	11.4 ± 1.6		20 ± 1.1	17 ± 1.1
A17	0.3 ± 0.1		1.5 ± 0.2	5 ± 0.3
		McKeowns Valley Mixed Sediments		
C8	9.3 ± 0.5		14.4 ± 0.6	11.7 ± 0.6
C9	11.1 ± 0.4		16 ± 0.5	15.2 ± 0.5
C10	12.2 ± 0.5		16.9 ± 0.6	15 ± 0.6
C11	7.5 ± 0.3		10.7 ± 0.4	11.5 ± 0.5
C12	14.1 ± 0.6		19.5 ± 0.7	18.3 ± 0.7
		Whiteheads Creek		
D1	18.5 ± 1.0	3.0 ± 0.3	32.5 ± 1.5	24.8 ± 1.2
D2	19.7 ± 1.0	0.5 ± 0.1	35.6 ± 1.1	25 ± 0.8
D3	23.9 ± 1.0	52.0 ± 3.0	41.5 ± 1.6	39.3 ± 1.5
D4	22.5 ± 1.0	23.0 ± 2.0	41.9 ± 1.6	41.3 ± 1.5
D5	22.1 ± 1.6	1.7 ± 0.2	41.2 ± 2.7	15.7 ± 1.3
D6	45.0 ± 1.4	14.6 ± 0.5	80.7 ± 2.7	40 ± 1.3

Table C4:Soil Particle Size Fraction Radionuclide Analyses.

	U-238	Th-230	Ra-226	Th-232	Ra-228	Th-228	K-40	Cs-137
				Sample A1				
<63um	174 ± 3	132 ± 1	137.5 ± 1	234 ± 1.3	228 ± 1.8	237 ± 0.2	900 ± 12	1.5 ± 0.3
63-125um		42 ± 0.8	42.9 ± 0.8	74 ± 1.4	73.2 ± 1.9	74.1 ± 1.1	525 ± 14	0.2 ± 0.6
125-250um		15 ± 1	14.7 ± 0.5	26 ± 1.8	27 ± 1	25.1 ± 0.5	310 ± 7	-0.4 ± 0.3
250-500um		9.3 ± 0.7	10.7 ± 0.4	20.3 ± 1.3	20.3 ± 1	21 ± 0.5	730 ± 9	0.4 ± 0.1
500-1.4mm		7.2 ± 0.4	7.2 ± 0.2	15 ± 0.4	15.2 ± 0.4	14.3 ± 0.2	400 ± 7	0.3 ± 0.2
1.4-2mm		4.3 ± 0.2	6.1 ± 0.3	11 ± 0.5	11.4 ± 0.6	11.4 ± 0.3	320 ± 6	0.3 ± 0.1
>2mm		5.7 ± 0.2	8.3 ± 0.2	10.1 ± 0.4	10.3 ± 0.5	10.2 ± 0.3	350 ± 7	-0.1 ± 0.3
				Sample A13				
<38um	235 ± 7		204.1 ± 1.5		272 ± 4	265 ± 4	1277 ± 22	0.6 ± 0.7
38-63um			84 ± 2		107 ± 5	121 ± 4	1490 ± 40	-0.2 ± 1.3
63-125um			57.5 ± 1.7		73 ± 3	83 ± 2	1016 ± 25	-0.1 ± 0.9
125-250um	70 ± 5		35.1 ± 1.2		48 ± 3	56.7 ± 1.2	1747 ± 35	0.5 ± 0.8
250-500um			27.4 ± 1.9		39 ± 5	39.9 ± 1.6	1697 ± 53	-0.1 ± 1.5
500-1.4mm			21.5 ± 0.7		26.9 ± 1.8	28.1 ± 0.7	1176 ± 24	-0.3 ± 0.6
1.4-2mm			24.9 ± 0.6		31.3 ± 1.2	31.5 ± 0.6	862 ± 15	-0.1 ± 0.3
>2mm			111.7 ± 0.9		42.9 ± 1.1	43.6 ± 0.6	640 ± 10	0.2 ± 0.3

Table C4:Soil Particle Size Fractions (cont.)

	U-238	Th-230	Ra-226	Th-232	Ra-228	Th-228	K-40	Cs-137
Sample A16								
<38um			406 ± 3		218 ± 2	227 ± 2	885 ± 15	0.6 ± 0.4
38-63um			242 ± 4		145 ± 6	136 ± 3	860 ± 35	1.1 ± 1.6
63-125um			155 ± 2		92 ± 3	86.7 ± 1.7	1160 ± 26	0.6 ± 0.9
125-250um			111.6 ± 1.7		66.4 ± 2.7	64.5 ± 1.1	1211 ± 25	0.2 ± 0.7
250-500um			72.6 ± 0.9		44.4 ± 1.5	42.8 ± 0.7	1155 ± 18	0.2 ± 0.4
500-1.4mm			77.1 ± 0.6		42.1 ± 0.8	41.5 ± 0.5	944 ± 13	-0.1 ± 0.2
1.4-2mm			78 ± 1.2		46 ± 2	44.5 ± 1	645 ± 20	0.2 ± 0.6
>2mm			91.7 ± 1		46.3 ± 1.3	46.7 ± 0.7	783 ± 13	0 ± 0.4
Sample A18								
<63um		116 ± 5	109.7 ± 1.5	208 ± 7	199 ± 3.3	201 ± 2.3	1055 ± 20	6.3 ± 0.7
63-125um		50 ± 3	50.6 ± 2	94 ± 4	101 ± 2.3	98.7 ± 1.4	1172 ± 21	1.7 ± 0.5
125-250um		9.8 ± 0.5	13.2 ± 0.5	24.4 ± 0.9	26.3 ± 1.2	25.1 ± 0.6	1190 ± 19	1 ± 0.3
250-500um		9.1 ± 0.7	9.4 ± 0.4	20.3 ± 1.3	20.3 ± 1	21 ± 0.5	1066 ± 16	0.6 ± 0.3
500-1.4mm		7 ± 0.4	6.6 ± 0.2	14.9 ± 0.4	15.3 ± 0.4	14.7 ± 0.2	728 ± 9	0.4 ± 0.1
1.4-2mm		4.5 ± 0.2	5.9 ± 0.3	11 ± 0.5	11.4 ± 0.6	11.5 ± 0.3	385 ± 7	0.3 ± 0.2
>2mm		8.5 ± 0.2	8.1 ± 0.2	12.6 ± 0.4	12.4 ± 0.5	12.8 ± 0.3	342 ± 6	0.3 ± 0.1
Sample B8								
<63um	51 ± 16		90.7 ± 2.4		53.3 ± 4.5	47.2 ± 2	652 ± 29	17.7 ± 1.7
<63-250um	36 ± 14		80.2 ± 2.1		41.6 ± 3.9	42.8 ± 1.7	488 ± 23	12.1 ± 1.4
~250-500um	54 ± 18		67.7 ± 2.5		44.7 ± 5.2	39.5 ± 2.3	600 ± 30.4	7.6 ± 1.7
~500-1.4mm	41 ± 10		52.5 ± 1.4		42 ± 2.8	36.1 ± 1.3	623 ± 20.3	5.7 ± 0.9
~1.4-2mm	43 ± 27		48.9 ± 3.5		46.6 ± 7.4	33.3 ± 3.2	700 ± 43.5	1.7 ± 2.5
>2mm	56 ± 7		44.7 ± 0.6		45.7 ± 1.1	43.3 ± 0.6	827 ± 13	2.8 ± 0.3
Sample B9								
<63um	44 ± 21		91.7 ± 3		42.1 ± 5.6	48.1 ± 2.5	577 ± 33.8	16 ± 2
63-250um	39 ± 13		75 ± 1.8		45.9 ± 3.4	44.8 ± 1.6	507 ± 20.9	12.1 ± 1.2
250-500um	40 ± 19		67.5 ± 2.6		39 ± 5.2	41.2 ± 2.3	598 ± 32	9.5 ± 1.8
500-1.4mm	28 ± 16		56.9 ± 1.3		45.7 ± 2.4	42.1 ± 1.2	680 ± 19	6.7 ± 0.7
1.4-2mm	52 ± 19		55.1 ± 2.5		45.3 ± 5.3	36.2 ± 2.3	694 ± 31.4	3.7 ± 1.8
>2mm	51 ± 8		42.3 ± 0.7		45.1 ± 1.3	44.6 ± 0.7	844 ± 14	3.1 ± 0.3
Sample B10								
<63um	55 ± 18		98.9 ± 2.6		47.6 ± 4.8	50.4 ± 2.2	614 ± 28.4	16.3 ± 1.8
63-250um	39 ± 14		74.9 ± 2		40.7 ± 3.9	39.9 ± 1.7	511 ± 23.4	14.1 ± 1.4
250-500um	38 ± 20		66.3 ± 2.7		38.2 ± 5.4	38.8 ± 2.4	575 ± 31.2	9.9 ± 1.9
500-1.4mm	33 ± 15		55.5 ± 1.9		45.7 ± 3.9	42 ± 1.8	634 ± 26.1	5.6 ± 1.3
1.4-2mm	47 ± 18		49.9 ± 2.2		42.5 ± 4.8	40.4 ± 2.1	649 ± 27	4.7 ± 1.6
>2mm	58 ± 7		41.5 ± 0.6		46.2 ± 1.1	44.3 ± 0.7	845 ± 13	3.1 ± 0.3
Sample B11								
<63um	51 ± 14		93.2 ± 2.1		57.5 ± 3.9	49.4 ± 1.7	620 ± 23.2	17.2 ± 1.4
63-250um	29 ± 18		80.8 ± 2.6		36.6 ± 5	42 ± 2.2	534 ± 28.7	12.5 ± 1.8
250-500um	74 ± 18		66.4 ± 2.4		41.1 ± 4.9	39.6 ± 2.2	551 ± 28.7	11.5 ± 1.7
500-1.4mm	56 ± 12		58.2 ± 1.6		42 ± 3.3	40.7 ± 1.5	647 ± 22.6	7.6 ± 1.1
1.4-2mm	51 ± 31		54.1 ± 4		37.4 ± 8.5	38.2 ± 3.7	746 ± 49.9	6.5 ± 3
>2mm	52 ± 7		42.8 ± 0.6		43.4 ± 1.1	44.1 ± 0.6	819 ± 12	3.7 ± 0.2
Sample B12								
<63um	46 ± 22	54.5 ± 1.9	126.7 ± 3.3	34.9 ± 1.4	52.5 ± 6	44.7 ± 2.6	567 ± 34.4	13.1 ± 2.2
63-250um	39 ± 10	51.2 ± 1.6	82.1 ± 1.5	38.5 ± 1.3	41.2 ± 2.8	40.2 ± 1.3	553 ± 17.2	10.3 ± 1
250-500um	61 ± 26	54 ± 2	69.5 ± 3.5	34 ± 2	49.2 ± 7.2	36 ± 3.1	589 ± 39.8	6.4 ± 2.5
500-1.4mm	70 ± 13	52 ± 3	63.3 ± 1.8	40 ± 3	41.8 ± 3.5	44.2 ± 1.6	702 ± 24.3	6.4 ± 1.2
1.4-2mm	57 ± 38		59.5 ± 4.8		39.2 ± 10	33.4 ± 4.4	683 ± 55.4	4.3 ± 3.5
>2mm	54 ± 7	68 ± 3	46 ± 0.6	51 ± 2	45.3 ± 1.1	44.4 ± 0.7	832 ± 13	3.4 ± 0.3
Sample B13								
<63um	38 ± 15		95.4 ± 2.2		56.1 ± 4.1	49.9 ± 1.8	638 ± 25.5	17.8 ± 1.5
63-250um	48 ± 11		73.9 ± 1.6		45.3 ± 3.1	39.2 ± 1.4	474 ± 18.2	13.4 ± 1.1
250-500um	35 ± 19		69.2 ± 2.7		40.7 ± 5.4	42.1 ± 2.4	597 ± 32.5	11.5 ± 1.9
500-1.4mm	36 ± 11		57.5 ± 0.9		46 ± 1.7	43.9 ± 0.9	668 ± 14	7.9 ± 0.5
1.4-2mm	95 ± 30		53.4 ± 3.8		49.8 ± 8.2	41.3 ± 3.6	710 ± 47.1	2.3 ± 2.8
>2mm	67 ± 8		48.2 ± 0.7		45.7 ± 1.2	46.3 ± 0.7	843 ± 14	3.8 ± 0.3
Sample C13								
<63um	48 ± 7	47 ± 3	59.5 ± 1.2	79 ± 4	74 ± 3	78.6 ± 1.3	620 ± 20	10.5 ± 1
63-125um	60 ± 34	33.1 ± 1.4	72 ± 5	52 ± 2	90 ± 10	63 ± 4	478 ± 48	8 ± 3
125-250um		41.1 ± 1.3	55 ± 3	62 ± 2	77 ± 7	76 ± 3	680 ± 39	5 ± 3
250 - 500	54 ± 11	42.6 ± 1.8	55.2 ± 0.5	67 ± 3	69.1 ± 1.1	68.8 ± 0.6	590 ± 20	2 ± 0.5
500-1.4	35 ± 7	33.5 ± 1.3	38.5 ± 0.6	50 ± 1.7	53.2 ± 1	52.9 ± 0.6	680 ± 16	2 ± 0.6

Table C4:Soil Particle Size Fractions (cont.)

				Sample D1				
<63	52 ± 11	63 ± 3	64.7 ± 0.9	126 ± 4	124 ± 2	124 ± 1.4	367 ± 9	0.5 ± 0.4
63-125	30 ± 30	46 ± 2	32 ± 2	95 ± 3	90 ± 5	98 ± 3	467 ± 26	-1 ± 1
125-250	70 ± 70	22 ± 2	30 ± 5	43 ± 3	56 ± 10	45 ± 4	965 ± 60	-5 ± 3
250-500	30 ± 50	12 ± 1.8	25 ± 3	30 ± 2	36 ± 7	35 ± 3	682 ± 43	-1 ± 2
>500		12 ± 3	26 ± 4	32 ± 4	30 ± 8	24 ± 5	280 ± 60	0 ± 2
				Sample D9				
<38um	68 ± 5	74 ± 3	71.8 ± 0.8	127 ± 4	130 ± 2	129 ± 1.3	373 ± 10	-0.4 ± 0.5
250-500um	25 ± 2	17.6 ± 1.9	23.3 ± 0.8	36 ± 3	40.3 ± 1.8	40.5 ± 0.9	948 ± 18	-0.4 ± 0.5
500-1.4mm	47 ± 3	31 ± 2	35.3 ± 0.5	56 ± 3	55.6 ± 1	54.7 ± 0.7	473 ± 9	-0.3 ± 0.2
1.4-2mm	83 ± 6	34.5 ± 1.7	109 ± 1.6	69 ± 3	75 ± 2	75.2 ± 1.3	249 ± 10	0.1 ± 0.5
>2mm	75 ± 4	47 ± 3	275.8 ± 1.9	84 ± 4	91 ± 2	92.6 ± 1.3	307 ± 12	-0.1 ± 0.7
				Sample F8				
<63um	47 ± 3	44 ± 3	41.9 ± 0.5	56 ± 3	53.6 ± 0.9	56.6 ± 0.6	284 ± 6	11.3 ± 0.3
63-125um	14.6 ± 13	17.2 ± 0.9	15.8 ± 0.3	24.6 ± 1.1	20.8 ± 0.7	21.4 ± 0.4	134 ± 4	4 ± 0.2
125-250um	15 ± 3	15.5 ± 1.1	13.9 ± 0.6	18.8 ± 1.2	18.3 ± 1.4	19.8 ± 0.7	190 ± 10	3.9 ± 0.5
250-500um	9 ± 3	10.1 ± 1.5	11.8 ± 0.6	16.2 ± 1.7	17.5 ± 1.4	15.9 ± 0.6	344 ± 11	2.6 ± 0.5
>500um	4 ± 6	8.5 ± 1.5	8.1 ± 0.7	10 ± 1.7	11.2 ± 0.6	9.3 ± 0.6	55 ± 20	0.4 ± 0.3
				Sample G1				
<2		53 ± 3		96 ± 5		120 ± 6		
2-63	45 ± 5	50 ± 1.2	49.4 ± 0.5	77 ± 2	77.2 ± 0.9	78.1 ± 0.8	630 ± 8	0.6 ± 0.2
63-125	43 ± 6	38.6 ± 1.8	38.6 ± 1.6	61 ± 2	61 ± 4	62.9 ± 1.6	519 ± 25	0.6 ± 1
125-250		40 ± 2		65 ± 3			±	±
250-500	61 ± 14	47 ± 2	47 ± 3	66 ± 2	66 ± 8	66 ± 3	298 ± 17	2 ± 2
0.5-1.4	47 ± 14	46.5 ± 1.9	49 ± 3	70 ± 3	82 ± 8	70 ± 3	328 ± 17	3 ± 2
vol				**Sample H1**				
<2		23.7 ± 0.9	25 ± 2	27.6 ± 0.8		25.1 ± 1.9		
63-125		23.4 ± 1		25.1 ± 1		25 ± 1		
125-250	23 3	23 ± 1	22.1 ± 0.6	24 ± 1	24 ± 1.2	23 ± 0.6	392 ± 10	0.4 0.4
250-500	20 4	21.2 ± 0.7	20.3 ± 0.7	23.05 ± 0.8	23.6 ± 1.6	22.5 ± 0.7	424 ± 14	0 0.5
0.5-1.4		17.8 ± 0.8		19.4 ± 0.7		22.8 ± 0.8		

				Sample I1				
	U-238	**Th-230**	**Ra-226**	**Th-232**	**Ra-228**	**Th-228**	**K-40**	**Cs-137**
2-10um		17 ± 2	16.5 ± 0.5	20 ± 2	19.9 ± 1.1	20.9 0.5	211 ± 8	13.3 ± 0.5
10-20um		22.1 ± 1.2	17.7 ± 0.4	22.6 ± 1.2	22.4 ± 1	21.7 0.5	241 ± 7	7.1 ± 0.4
20-38um		19 ± 1.2	16 ± 0.3	18.3 ± 1.1	18.5 ± 0.5	18.4 0.4	213 ± 5	9.6 ± 0.3
38-63um		13.7 ± 0.7	11.8 ± 0.2	15.2 ± 0.8	14.7 ± 0.5	14.6 0.3	204 ± 4	8.2 ± 0.2
63-125um		18.4 ± 1	16.9 ± 0.3	20.1 ± 1	20.7 ± 0.5	20.9 0.3	192 ± 4	9.9 ± 0.3
125-250um		21.4 ± 1.9	23.1 ± 0.4	24 ± 2	26.6 ± 0.8	26.2 0.4	214 ± 6	10.3 ± 0.4
250-500um		23 ± 1.1	24.9 ± 0.3	28.9 ± 1.2	29.3 ± 0.6	28.8 0.4	139 ± 4	9.1 ± 0.2
>500um		19 ± 1.2	22.2 ± 0.3	22.8 ± 1.4	27.9 ± 0.5	27.2 0.3	140 ± 3	9.4 ± 0.2

Table C5:Site F Sediment Radionuclide Analyses.

	Sediment Samples				
	Ra-226	**Ra-228**	**Th-228**	**K-40**	**Cs-137**
CFC1	41 ± 4	72 ± 10	57 ± 4	290 ± 47	14 ± 4
CFC2	37 ± 2	54 ± 6	53 ± 2	250 ± 31	10 ± 2
CFC3	38 ± 2	49 ± 6	50 ± 2	285 ± 31	11 ± 2
CFC4	29 ± 4	38 ± 9	48 ± 4	197 ± 42	22 ± 3
CFC5	35 ± 3	43 ± 8	39 ± 9	288 ± 41	11 ± 3
CFC7	32 ± 3	44 ± 6	47 ± 3	235 ± 30	25 ± 2
CFC8	28 ± 3	47 ± 7	45 ± 3	227 ± 35	11 ± 3
CFC9	31 ± 5	44 ± 11	43 ± 4	230 ± 58	11 ± 4
CFC10	33 ± 2	35 ± 6	45 ± 2	187 ± 29	9 ± 2
CFC11	36 ± 4	48 ± 8	42 ± 3	236 ± 36	29 ± 3
CFC12	28 ± 1.8	35 ± 5	32.5 ± 1.8	139 ± 22	5.5 ± 1.6
BED1	13.6 ± 0.5	15.1 ± 1.1	17.2 ± 0.6	203 ± 7	3.7 ± 0.4

Appendix D

Bulk Soil Sample Chemical Analyses. All data reported as wt% oxide.

SAMPLE	Na2O	MgO	Al2O3	SiO2	P2O5	K2O	CaO	TiO2	Mn3O4	Fe2O3
A1	0.31	0.15	5.91	90.79	0.05	1.66	0.05	0.50	0.001	0.50
A2	0.30	0.10	4.05	93.03	0.06	1.55	0.07	0.34	0.004	0.42
A3	0.24	0.06	3.38	93.99	0.05	1.20	0.03	0.56	0.003	0.44
A4	0.30	0.05	3.26	94.18	0.06	1.41	0.02	0.27	0.012	0.39
A5	0.14	0.07	3.08	94.72	0.05	1.32	0.02	0.26	0.005	0.30
A6	0.15	0.14	3.13	94.42	0.06	1.10	0.10	0.36	0.004	0.47
A7	0.18	0.11	3.51	94.05	0.05	1.15	0.02	0.40	0.005	0.47
A8	0.30	0.20	8.06	87.60	0.05	2.18	0.02	0.35	0.008	1.19
A9	0.27	0.12	6.58	90.11	0.05	1.95	0.08	0.24	0.006	0.54
A10	0.32	0.12	6.39	90.28	0.05	1.94	0.04	0.23	0.006	0.59
A11	0.25	0.14	7.19	89.45	0.05	1.67	0.02	0.61	0.001	0.59
A12	1.02	0.08	7.25	87.47	0.00	3.35	0.07	0.17	0.001	0.63
A13	0.70	0.15	11.83	80.66	0.00	4.53	0.08	0.22	0.007	1.84
A14	0.62	0.06	9.78	84.42	0.00	4.00	0.06	0.23	0.005	0.86
A15	0.83	0.03	5.45	90.67	0.00	2.28	0.05	0.09	0.006	0.64
A16	1.11	0.21	10.97	82.03	0.00	3.61	0.23	0.24	0.042	1.57
A17	0.84	0.03	5.01	91.08	0.00	2.34	0.06	0.06	0.002	0.62
B1	0.19	0.55	15.99	70.00	0.34	2.50	0.54	0.83	0.181	8.82
B2	0.15	0.44	15.29	70.99	0.29	2.77	0.35	0.70	0.131	8.86
B3	0.19	0.46	15.16	71.49	0.29	2.79	0.35	0.71	0.134	8.39
B4	0.12	0.49	15.34	71.00	0.30	2.68	0.39	0.74	0.139	8.76
B5	0.62	1.46	15.09	70.93	0.24	2.63	0.52	0.65	0.142	7.68
B6	0.55	1.41	15.05	70.98	0.23	2.62	0.50	0.64	0.149	7.86
B7	0.63	1.43	14.77	71.45	0.21	2.68	0.38	0.63	0.121	7.68
B8	0.26	0.41	32.37	57.27	0.19	2.15	0.26	0.60	0.081	6.39
B9	0.29	0.51	20.48	67.40	0.24	2.83	0.28	0.67	0.073	7.22
B10	0.32	0.45	16.96	70.08	0.22	3.17	0.21	0.64	0.084	7.87
B11	0.32	0.39	15.93	71.61	0.22	3.19	0.20	0.62	0.081	7.44
B12	0.33	0.38	14.87	70.40	0.24	3.12	0.12	0.61	0.053	9.87
B13	0.32	0.45	15.50	71.15	0.24	3.14	0.25	0.68	0.087	8.17
C1	0.16	0.48	12.74	78.94	0.18	1.51	0.29	0.94	0.111	4.61
C2	0.16	0.54	12.98	78.29	0.18	1.65	0.27	0.94	0.107	4.84
C3	0.18	0.51	12.21	79.73	0.14	1.52	0.28	0.91	0.096	4.39
C4	0.12	0.33	13.72	77.45	0.15	1.18	0.37	1.12	0.276	5.20
C5	0.06	0.32	13.87	77.62	0.14	1.19	0.30	1.02	0.269	5.19
C6	0.22	0.42	8.62	84.25	0.09	1.48	0.46	1.09	0.061	3.26
C7	0.32	0.79	16.58	73.14	0.22	1.83	1.21	1.08	0.066	4.62
C8	0.14	0.36	11.22			1.52	0.30		0.189	3.49
C9	0.19	0.40	12.10			2.27	0.20		0.136	4.59
C10	0.09	0.61	14.16			2.55	0.30		0.207	4.78
C11	0.10	0.41	11.66			0.86	0.60		0.088	4.54
C12	0.10	0.59	14.11			2.69	0.30		0.207	5.38

Appendix D (cont.)

SAMPLE	Na2O	MgO	Al2O3	SiO2	P2O5	K2O	CaO	TiO2	Mn3O4	Fe2O3
D1	1.15	0.13	7.04	87.14		1.63	0.33		0.018	2.52
D2	1.11	0.13	6.90	87.36		1.57	0.28		0.020	2.59
D3	1.19	0.14	7.26	86.47		1.64	0.25		0.049	2.90
D4	1.20	0.13	7.27	86.70		1.68	0.30		0.035	2.61
D5	1.15	0.12	7.25	86.89		1.66	0.26		0.015	2.61
D6	1.15	0.11	7.05	86.13		1.67	0.22		0.030	3.58
D7	1.11	0.13	7.92	83.84		1.66	0.18		0.050	5.00
D8	1.04	0.14	8.15	83.08		1.66	0.20		0.040	5.60
E1	0.32	0.16	5.62	89.21		1.03	0.11		0.036	3.45
E2	0.30	0.16	5.35	89.56		1.09	0.06		0.028	3.40
E3	0.31	0.17	5.92	88.92		1.19	0.06		0.033	3.33
E4	0.29	0.18	6.56	88.40		1.13	0.05		0.030	3.30
E5	0.17	0.09	3.24	95.66		0.51	0.09		0.021	0.18
E6	0.33	0.16	5.37	90.03		1.11	0.07		0.032	2.85
E7	0.34	0.16	5.29	90.37		1.14	0.05		0.024	2.58
E8	0.34	0.18	5.43	89.72		1.19	0.09		0.030	2.96
E9	0.32	0.16	5.46	90.07		1.09	0.06		0.048	2.69
E10	0.24	0.19	6.75	87.82		0.91	0.04		0.022	3.99
E11	0.33	0.18	6.02	88.78		1.04	0.06		0.028	3.50
E12	0.33	0.16	5.31	89.90		1.12	0.06		0.026	3.04
E13	0.34	0.19	6.32	88.07		1.20	0.04		0.032	3.74
E14	0.32	0.16	5.75	88.92		1.23	0.05		0.034	3.47
E15	0.32	0.19	6.72	87.99		1.09	0.07		0.026	3.54
E16	0.31	0.33	5.29	89.10		1.14	0.05		0.024	3.70
E17	0.33	0.20	6.11	88.19		1.17	0.07		0.031	3.85
E18	0.30	0.17	5.46	88.74		1.10	0.03		0.026	4.12
E19	0.32	0.18	5.96	89.05		1.09	0.10		0.026	3.22
E20	0.26	0.17	5.99	90.23		0.90	0.07		0.030	2.28
E21	0.35	0.16	5.18	90.26		1.19	0.06		0.021	2.74
E22	0.32	0.17	5.57	89.29		1.15	0.05		0.028	3.36
E23	0.31	0.18	5.75	88.73		1.11	0.04		0.018	3.83
E24	0.29	0.22	8.95	84.59		1.12	0.03		0.022	4.74
E25	0.36	0.24	6.17	87.37		1.14	0.07		0.043	4.51
E26	0.35	0.09	5.31	89.76		1.18	0.05		0.020	3.20
E27	0.39	0.47	15.55	76.88		1.26	0.07		0.017	5.32
E28	0.47	0.38	11.53	81.36		1.47	0.08		0.016	4.67
E29	0.54	0.40	11.88	80.79		1.57	0.08		0.015	4.71
E30	0.21	0.24	9.10	80.76		0.91	0.03		0.040	8.64
E31	0.33	0.19	5.68	89.98		1.21	0.08		0.024	2.45
E32	0.97	0.88	24.01	60.95		3.46	0.16		0.028	9.48
E33	0.58	0.44	10.10	82.81		1.62	0.08		0.011	4.33
E34	0.83	0.76	10.52	81.58		2.06	0.08		0.023	4.10
E35	0.62	0.39	8.24	84.98		1.55	0.08		0.018	4.08
E36	0.32	0.31	8.21	85.72		1.64	0.05		0.019	3.70
E37	0.55	0.41	7.76	86.20		1.68	0.09		0.015	3.28
E38	1.16	0.97	11.16	79.83		2.67	0.11		0.025	4.02

Appendix D (cont.)

SAMPLE	Na2O	MgO	Al2O3	SiO2	P2O5	K2O	CaO	TiO2	Mn3O4	Fe2O3
E39	1.14	0.89	9.00	82.31		2.39	0.13		0.025	4.06
E40	0.70	0.58	8.87	83.75		1.90	0.10		0.032	4.00
E41	0.40	0.32	7.54	86.55		1.70	0.05		0.041	3.31
E42	0.61	0.46	8.75	85.00		1.60	0.08		0.012	3.46
E43	0.81	0.67	9.35	82.92		2.25	0.08		0.012	3.88
E44	1.30	0.96	11.23	79.41		2.77	0.14		0.034	4.10
E45	0.73	0.46	7.95	85.43		1.94	0.07		0.040	3.31
E46	0.67	0.51	9.52	83.47		2.08	0.09		0.023	3.60
E47	0.54	0.30	6.97	86.90		1.64	0.08		0.040	3.45
E48	1.11	0.67	10.41	81.00		2.64	0.11		0.053	3.90
E49	0.79	0.51	10.70	81.21		2.64	0.11		0.062	3.85
E50	0.54	0.41	11.59	81.82		1.32	0.06		0.015	4.22
F1	0.49	0.14	14.14	81.87	0.00	0.64	0.06	0.63	0.025	2.00
F2										
F3	0.36	0.12	8.90	87.33	0.00	0.58	0.04	0.64	0.026	2.00
F4	0.41	0.10	7.89	88.28	0.00	0.64	0.03	0.65	0.033	1.98
F5	0.45	0.10	5.59	90.47	0.00	0.58	0.02	0.66	0.023	2.12
F6	0.34	0.09	3.84	92.51	0.00	0.60	0.14	0.60	0.009	1.88
F7	0.33	0.10	4.52	91.99	0.00	0.57	0.04	0.71	0.006	1.76

Appendix E

Table E1: Snowy River-Wullwye Creek Sediment Sample Radionuclide Analyses. All data reported as Bq/kg. Uncertainies are equilvalent to one standard error on the mean.

SAMPLE	U-238	Th-230	Ra-226	Th-232	Ra-228	Th-228	K-40
WUS1	17 ± 10	9.5 ± 0.8	10.0 ± 1.2	17.9 ± 1.0	15.5 ± 1.1	16.5 ± 1.0	786 ± 23
WUS2	4 ± 7	7.7 ± 0.8	11.8 ± 1.0	18.2 ± 1.1	16.4 ± 0.9	15.8 ± 1.1	849 ± 26
WUS3	13 ± 10	9.5 ± 0.6	8.4 ± 1.2	17.1 ± 0.8	14.5 ± 1.1	14.4 ± 0.8	778 ± 24
WUS4	8 ± 9	7.6 ± 0.7	10.1 ± 1.1	19.8 ± 1.1	16.4 ± 1.0	16.8 ± 1.0	873 ± 24
WUS5	14 ± 5	13.0 ± 0.7	9.1 ± 0.7	25.6 ± 1.0	23.8 ± 0.7	23.8 ± 1.0	971 ± 22
SUW1	47 ± 9	37.7 ± 1.9	46.7 ± 1.4	90.0 ± 4.0	95.4 ± 1.6	92.0 ± 4.0	779 ± 26
SUW2	18 ± 13	16.3 ± 0.8	20.1 ± 1.7	35.3 ± 1.4	38.2 ± 1.5	35.0 ± 1.4	916 ± 29
SUW3	17 ± 5	11.9 ± 0.8	10.6 ± 0.4	19.6 ± 1.0	17.8 ± 0.4	20.0 ± 1.1	678 ± 12
SUW4	41 ± 4	33.6 ± 1.9	36.4 ± 0.6	71.0 ± 3.0	74.2 ± 0.8	71.0 ± 3.0	934 ± 15
SUW5	49 ± 5	37.0 ± 2.0	43.4 ± 0.7	77.0 ± 4.0	83.0 ± 0.8	81.0 ± 4.0	782 ± 13
SDW1	30 ± 6	32.2 ± 2.2	31.0 ± 0.8	55.7 ± 3.0	59.5 ± 0.9	55.0 ± 3.0	847 ± 17
SDW2	41 ± 6	31.4 ± 1.8	31.5 ± 1.0	45.0 ± 2.7	51.9 ± 1.0	51.3 ± 2.7	775 ± 21
SDW3	54 ± 5	47.0 ± 3.0	57.3 ± 0.7	86.0 ± 4.0	97.9 ± 0.9	96.0 ± 5.0	738 ± 13
SDW4	30 ± 7	24.6 ± 1.2	24.2 ± 1.1	37.6 ± 1.5	40.4 ± 1.1	41.0 ± 1.6	747 ± 25
SDW5	14 ± 15	16.8 ± 1.1	20.6 ± 1.9	39.8 ± 1.8	39.3 ± 1.8	38.0 ± 1.8	788 ± 31

Table E2: Snowy River-Wullwye Creek Sediment Sample Chemical Data.
All Data Reported as Wt% Oxide

SAMPLE	Na20 %	MgO %	Al2O3 %	SiO2 %	P2O5 %	K2O %	CaO %	TiO2 %	Mn3O4 %	Fe2O3 %
WUS1	1.33	0.26	8.48	84.22	0.05	3.53	0.59	0.10	0.022	1.40
WUS2	1.31	0.22	8.47	83.92	0.06	3.98	0.58	0.13	0.015	1.28
WUS3	1.29	0.23	8.30	84.68	0.05	3.41	0.58	0.14	0.019	1.29
WUS4	1.24	0.21	8.41	84.46	0.06	3.47	0.61	0.11	0.020	1.41
WUS5	1.42	0.27	9.13	83.18	0.05	3.92	0.60	0.10	0.018	1.31
SUW1	1.33	0.82	12.69	76.56	0.14	3.27	0.93	0.54	0.108	3.57
SUW2	1.32	0.50	10.84	80.36	0.10	3.52	0.72	0.31	0.065	2.25
SUW3	1.17	0.27	7.54	86.55	0.05	2.64	0.52	0.12	0.022	1.12
SUW4	1.23	0.79	12.36	77.08	0.13	3.51	0.87	0.46	0.109	3.43
SUW5	1.26	0.93	13.09	76.03	0.12	3.19	0.95	0.58	0.107	3.67
SDW1	1.44	0.66	11.47	78.54	0.11	3.42	0.96	0.41	0.077	2.86
SDW2	1.25	0.64	11.52	78.62	0.14	3.21	0.95	0.44	0.093	3.07
SDW3	1.35	1.13	14.82	72.65	0.19	2.86	1.05	0.88	0.157	4.85
SDW4	1.35	0.52	10.70	80.06	0.13	3.09	0.80	0.37	0.065	2.86
SDW5	1.30	0.40	9.22	82.70	0.08	3.09	0.75	0.24	0.047	2.16

Table E3: Catchment Granite U and Th data (Dr B.W.Chappell unpublished data)
All Data Reported Bq kg-1

Wullwye Creek Catchment		Snowy River Catchment 'upstream of'Wullwye Creek	
U-238	Th-232	U-238	Th-232
114	68	32	62
17	60	49	67
49	69	54	55
52	81	27	66
32	64	27	64
49	77	44	62
22	81	44	81
25	76	47	72
47	73	47	78
32	81	47	48
52	77	57	81
67	94	44	81
72	77	35	77
32	76	35	73
57	81	37	75
52	73	40	78
74	58	42	67
		49	80
		42	77
		40	75
		40	78
		40	77
		37	81
		47	76
		40	86
		25	83
		44	73
		67	68
		27	81
		30	94
		54	76
		49	66
		44	71
		27	68

Appendix F

Table F1: Whiteheads Creek Deposited Sediment Particle Size Data. All Results as Fractions of the Total.

	<63um	63-125um	125-250um	250-500um	0.5-1.4mm	1.4-2mm	>2mm
S1							
S2	0.29	0.25	0.17	0.11	0.13	0.02	0.03
S3	0.26	0.31	0.18	0.10	0.10	0.01	0.03
S4	0.24	0.30	0.22	0.08	0.13	0.01	0.01
S5	0.28	0.18	0.12	0.11	0.17	0.08	0.06
S6	0.30	0.16	0.07	0.09	0.26	0.07	0.05
S7	0.22	0.11	0.09	0.11	0.26	0.13	0.08
S8	0.22	0.13	0.09	0.09	0.25	0.07	0.15
S9	0.25	0.14	0.11	0.13	0.17	0.11	0.10
S10	0.47	0.29	0.11	0.06	0.06	0.01	0.01
S11	0.51	0.29	0.08	0.06	0.05	0.01	0.00
S12	0.57	0.18	0.10	0.06	0.07	0.00	0.01
S13	0.62	0.19	0.08	0.05	0.05	0.00	0.00
S14	0.61	0.10	0.12	0.08	0.08	0.00	0.00
S15	0.41	0.15	0.10	0.10	0.17	0.03	0.04
S16	0.32	0.12	0.08	0.09	0.13	0.03	0.23
S17	0.34	0.15	0.07	0.10	0.18	0.03	0.11
S18	0.45	0.14	0.08	0.08	0.16	0.03	0.06
S19	0.58	0.15	0.08	0.07	0.10	0.01	0.01

Table F2: Whiteheads Creek Deposited Sediment Chemical Data. All results as wt% oxide.

	SiO2	Al2O3	Fe2O3	CaO	MgO	Na2O	K2O	Mn3O4	Fe% ex	Mn% ex
S1	87.31	7.10	1.36	0.39	0.09	1.44	2.29	0.018	43	44
S2	88.34	6.80	1.12	0.21	0.08	1.35	2.09	0.015	31	30
S3	87.05	7.47	1.39	0.23	0.08	1.52	2.24	0.016	62	61
S4	88.64	6.57	1.37	0.21	0.08	1.26	1.86	0.014	57	57
S5	87.77	6.76	1.50	0.37	0.11	1.40	2.08	0.016	65	53
S6	90.01	5.80	1.61	0.20	0.07	0.49	1.81	0.010	65	43
S7	90.56	4.81	1.70	0.16	0.06	1.01	1.70	0.010	82	56
S8	88.86	5.80	2.16	0.14	0.07	1.12	1.83	0.014	100	76
S9	88.89	5.91	1.72	0.18	0.05	1.24	2.00	0.011	88	49
S10	87.43	6.95	1.94	0.33	0.11	1.31	1.92	0.011	74	32
S11	89.25	6.54	1.61	0.22	0.09	0.51	1.76	0.013	72	35
S12	88.33	6.39	1.61	0.39	0.10	1.32	1.85	0.015	70	41
S13	88.32	6.42	1.59	0.35	0.09	1.32	1.89	0.017	62	40
S14	87.63	6.95	1.75	0.35	0.11	1.35	1.85	0.012	58	70
S15	88.40	5.68	2.51	0.26	0.08	1.16	1.84	0.061	69	102
S16	83.90	6.89	5.79	0.22	0.11	1.07	1.76	0.263	61	101
S17	87.03	6.21	3.52	0.22	0.09	1.12	1.75	0.054	73	90
S18	87.45	6.34	2.93	0.26	0.10	1.15	1.73	0.040	57	102
S19	87.67	7.06	1.96	0.20	0.08	1.23	1.75	0.040	100	97

Table F3: Whiteheads Creek Deposited Sediment Sample Radionuclide Analyses. All data reported as Bq/kg. Uncertainies are equilvalent to one standard error on the mean.

	U-238	Th-230	Ra-226	Th-232	Ra-228	Th-228	K-40	Cs-137
S1	36 ± 5	27.7 ± 1.2	33.2 ± 0.6	116 ± 3	113.4 ± 1.8	114.1 ± 1.3	598 ± 12	7.3 ± 0.5
S2	37 ± 3	26.9 ± 1	32.8 ± 0.4	111 ± 3	114.9 ± 1.3	113.9 ± 1.1	610 ± 9	8.5 ± 0.3
S3	39 ± 3	33 ± 2	34.9 ± 0.3	117 ± 4	122.1 ± 0.9	122.2 ± 1	621 ± 7	5.1 ± 0.2
S4	41 ± 4	33 ± 2	37.8 ± 0.4	134 ± 4	132.1 ± 1.1	131.3 ± 1.1	572 ± 8	2 ± 0.2
S5	37 ± 9	35 ± 2	38.3 ± 0.7	143 ± 4	144.1 ± 2.4	142.6 ± 2.3	538 ± 14	0.5 ± 0.3
S6	34 ± 7	25.0 ± 1.4	28.8 ± 0.6	92 ± 3	93.3 ± 1.7	92.1 ± 1.5	499 ± 13	0.3 ± 0.3
S7	21 ± 8	21.2 ± 1.4	23.2 ± 0.6	67 ± 3	62 ± 1.4	61.1 ± 1.1	483 ± 13	0.1 ± 0.3
S8	23 ± 7	28.8 ± 1.4	25.4 ± 0.6	65 ± 3	68.2 ± 1.4	67.4 ± 1.2	508 ± 14	-0.2 ± 0.3
S9	32 ± 4	27.0 ± 1.1	31 ± 0.5	100 ± 3	103.4 ± 1.5	102.7 ± 1.5	539 ± 13	0.2 ± 0.2
S10	33 ± 9	34.8 ± 1.3	39.7 ± 0.7	100 ± 3	103 ± 1.9	103.3 ± 1.7	502 ± 14	-0.4 ± 0.3
S11	42 ± 7	35.4 ± 1.3	39.1 ± 0.7	94 ± 3	93.4 ± 1.7	94 ± 1.6	493 ± 13	0.05 ± 0.3
S12	46 ± 6	40.9 ± 1.4	45.1 ± 0.7	105 ± 4	104.3 ± 1.6	107.1 ± 1.6	480 ± 13	-0.2 ± 0.2
S13	41 ± 3	41 ± 2	39.4 ± 0.5	92 ± 3	91.8 ± 1.1	93.3 ± 0.9	507 ± 8	-0.1 ± 0.2
S14	41 ± 7	41.0 ± 1.7	37.9 ± 0.7	91 ± 3	89 ± 1.7	91.4 ± 1.5	494 ± 13	-0.1 ± 0.3
S15	44 ± 5	33.0 ± 1.9	41.2 ± 0.6	87 ± 2	87.2 ± 1.7	89.2 ± 1.3	498 ± 11	0.09 ± 0.2
S16	36 ± 3	37.5 ± 1.8	70.5 ± 0.6	76 ± 3	75.7 ± 1	76.8 ± 0.8	345 ± 8	-0.1 ± 0.1
S17	41 ± 6	33.4 ± 1.4	38.4 ± 0.7	82 ± 3	82.9 ± 1.5	82.9 ± 1.4	456 ± 12	-0.2 ± 0.25
S18	40 ± 3	40.3 ± 1.5	39.1 ± 0.5	94 ± 3	88.8 ± 1.3	89.1 ± 1.33	438 ± 10	0.06 ± 0.13
S19	44 ± 3	42.4 ± 1.8	45.6 ± 0.5	98 ± 3	97.9 ± 1.1	97 ± 0.9	466 ± 11	0.1 ± 0.2

Table F4: Whiteheads Creek Citrate Dithionite extraction Radionuclide Analyses. All data reported as Bq/kg. Uncertainies are equilvalent to one standard error on the mean.

	Th-230	Ra-226	Th-232	Ra-228	Th-228
S3	6.0 ± 0.3	0.4 ± 0.2	12.4 ± 0.5		11.1 ± 0.5
S5	7.3 ± 0.3	0.9 ± 0.1	13.5 ± 0.5		14.7 ± 0.5
S7	6.7 ± 0.3	0.9 ± 0.2	12.8 ± 0.4		11.1 ± 0.4
S10	12.6 ± 0.6	3.5 ± 0.4	25.5 ± 0.1		21.9 ± 0.9
S13	12.3 ± 0.6	4.6 ± 0.4	22.9 ± 0.9		16.5 ± 0.7
S15	11.2 ± 0.5	3.4 ± 0.3	20.2 ± 0.7		15.2 ± 0.5
S16	14.0 ± 0.7	21.0 ± 1.0	26.0 ± 1.0	23.7 ± 1.3	23.0 ± 1.0

Appendix G

Geebung Creek Sediment Sample Radionuclide Analyses. All data reported as Bq/kg.
Uncertainies are equilvalent to one standard error on the mean.

Date	Trap	U-238	Th-230	Ra-226	Th-232	Ra-228	Th-228	K-40	Cs-137
				Trap Sediment Samples					
27-Apr-88	**1**	9 ± 4	9.2 ± 0.6	14.3 ± 0.3	14.7 ± 0.9	15.9 ± 0.5	15.2 ± 0.4	652 ± 15	3.6 ± 0.2
03-May-88	**1**	5 ± 3		9.8 ± 0.2		10.7 ± 0.5	10 ± 0.3	424 ± 10	2.2 ± 0.1
20-Jul-88	**1**	11 ± 10	8.9 ± 0.6	11.9 ± 1	14.3 ± 0.9	14 ± 2.4	14.7 ± 1.0	557 ± 18	2.1 ± 0.8
05-Oct-88	**1**	13 ± 25		9.6 ± 1.7		9.7 ± 3.9	7.3 ± 2.5	292 ± 23	2.5 ± 1.2
23-Nov-88	**1**	11 ± 4	5.8 ± 0.5	9.3 ± 0.3	10.4 ± 0.7	10.4 ± 0.6	10.2 ± 0.4	447 ± 12	1.7 ± 0.2
11-Apr-89	**1**	22 ± 27		24.4 ± 2.1		21 ± 4.8	23.3 ± 2.7	552 ± 28	1.9 ± 1.5
13-Feb-90	**1**	10 ± 4		14.4 ± 0.4		15.5 ± 0.8	16.4 ± 0.5	509 ± 14	1.7 ± 0.2
27-Apr-88	**2**	89 ± 18	56 ± 5	82 ± 2	89 ± 6	126 ± 5	130 ± 3.0	711 ± 27	8.5 ± 1.5
03-May-88	**2**	33 ± 8	17.4 ± 1.2	35.1 ± 1.1	30.9 ± 1.8	47.9 ± 2.6	51.6 ± 1.3	820 ± 21	2.2 ± 0.8
20-Jul-88	**2**	36 ± 34	38.1 ± 1.8	45 ± 3	59.6 ± 2.5	77 ± 7	74 ± 3.0	733 ± 44	8.3 ± 2.2
05-Oct-88	**2**	18 ± 5		14.5 ± 0.5		21.4 ± 0.9	21.3 ± 0.6	700 ± 18	0.5 ± 0.2
23-Nov-88	**2**	11 ± 5	10.2 ± 1.4	14 ± 0.4	19.9 ± 1.9	21.3 ± 0.9	20.6 ± 0.5	735 ± 19	0.9 ± 0.2
11-Apr-89	**2**	14 ± 14	11.2 ± 0.9	17.8 ± 1.6	17.4 ± 1.2	25.4 ± 3.4	21.2 ± 1.6	759 ± 26	0.0 ± 1.1
13-Feb-90	**2**	9 ± 2	7.2 ± 0.3	11.4 ± 0.21	13.5 ± 0.5	15.8 ± 0.4	16.8 ± 0.3	536 ± 13	0.6 ± 0.1
03-May-88	**3**	70 ± 72	17.2 ± 1	20.8 ± 8.9	29.9 ± 1.5	28.1 ± 24	30.6 ± 12.3	881 ± 92	4.4 ± 7.0
20-Jul-88	**3**	329 ± 325		35.3 ± 21		55 ± 45	23 ± 28.0	1251 ± 243	21 ± 21
11-Apr-89	**3**	13 ± 3		14.3 ± 0.3		18.7 ± 0.7	18.3 ± 0.5	771 ± 19	0.7 ± 0.2
13-Feb-90	**3**	27.3 ± 3.4	16.9 ± 1.1	26.12 ± 0.45	29.1 ± 1.5	27.5 ± 0.8	29.3 ± 0.6	810 ± 19	1.2 ± 0.2
11-Apr-89	**11**	21 ± 5		22.5 ± 0.5		23.7 ± 0.8	23.9 ± 0.6	752 ± 19	0.4 ± 0.2
13-Feb-90	**11**	24 ± 3		21.51 ± 0.39		27.6 ± 0.7	29 ± 0.6	625 ± 15	0.4 ± 0.2
11-Apr-89	**12**	12 ± 5	10.1 ± 0.5	18.1 ± 0.4	20.1 ± 0.8	21.1 ± 0.8	23.2 ± 0.6	948 ± 23	0.4 ± 0.2
13-Feb-90	**12**	11 ± 3		13.81 ± 0.36		18.6 ± 0.8	18.7 ± 0.5	609 ± 16	0.4 ± 0.2
11-Apr-89	**13**	22 ± 6		21.5 ± 0.5		27.5 ± 1	26.2 ± 0.7	795 ± 20	1.2 ± 0.3
13-Feb-90	**13**	10 ± 4	11 ± 0.5	12.76 ± 0.37	20 ± 0.8	19.6 ± 0.8	19.6 ± 0.5	648 ± 17	0.7 ± 0.2
11-Apr-89	**14**	23 ± 12		39.1 ± 1.6		34.1 ± 3.2	32.5 ± 1.6	474 ± 20	2.4 ± 1.0
13-Feb-90	**14**	14 ± 4		27.1 ± 0.55		28.6 ± 1	29.4 ± 0.7	514 ± 14	2.0 ± 0.3
27-Apr-88	**4**	14 ± 8		18.1 ± 0.5		31.6 ± 1	32.5 ± 0.7	1060 ± 26	0.5 ± 0.2
05-Oct-88	**4**	26 ± 11	16.9 ± 1.2	18.7 ± 0.8	30.9 ± 1.6	30.1 ± 1.7	27.1 ± 0.9	925 ± 26	0.8 ± 0.8
23-Nov-88	**4**	20 ± 14		11.6 ± 0.3		17.4 ± 0.7	16.2 ± 0.5	350 ± 10	0.1 ± 0.1
11-Apr-89	**4**	16 ± 3		16.2 ± 0.3		19.8 ± 0.7	21.4 ± 0.5	698 ± 17	0.3 ± 0.2
13-Feb-90	**4**	22 ± 4	10.4 ± 0.5	12.7 ± 0.36	19.1 ± 0.8	17 ± 0.8	18.5 ± 0.5	501 ± 13	0.2 ± 0.2
11-Apr-89	**5**	20 ± 5		24.5 ± 0.5		24.6 ± 0.8	24.4 ± 0.6	698 ± 18	0.2 ± 0.2
13-Feb-90	**5**	11 ± 3	11.1 ± 0.5	14.63 ± 0.34	18.9 ± 0.7	18.6 ± 0.7	19.4 ± 0.4	520 ± 13	0.4 ± 0.2
11-Apr-89	**6**	14 ± 3		14.7 ± 0.3		19.3 ± 0.7	20.6 ± 0.5	731 ± 18	0.3 ± 0.2
13-Feb-90	**6**	12 ± 3	11.8 ± 0.7	13.21 ± 0.34	20.6 ± 0.7	19.5 ± 0.8	19.4 ± 0.5	535 ± 14	-0.0 ± 0.2
11-Apr-89	**7**	19 ± 2		23.4 ± 0.3		26.4 ± 0.6	26.8 ± 0.4	933 ± 12	0.1 ± 0.2
13-Feb-90	**7**	12 ± 3	10.3 ± 0.5	13.95 ± 0.32	17.1 ± 0.8	18.5 ± 0.7	18.1 ± 0.4	572 ± 14	0.3 ± 0.2
11-Apr-89	**8**	20 ± 2		45.2 ± 0.4		26.7 ± 0.6	27.1 ± 0.4	647 ± 9	0.4 ± 0.2
13-Feb-90	**8**	16 ± 4		40.92 ± 0.63		25.2 ± 0.8	25.7 ± 0.5	594 ± 15	0.1 ± 0.2
11-Apr-89	**9**	34 ± 6		44.8 ± 0.7		32.5 ± 1	35.4 ± 0.8	790 ± 20	1.3 ± 0.3
13-Feb-90	**9**	14 ± 5		32.02 ± 0.61		23.6 ± 1	25.5 ± 0.6	575 ± 15	1.0 ± 0.2
11-Apr-89	**10**	26 ± 5		21.5 ± 0.4		25.9 ± 0.8	26.3 ± 0.6	642 ± 16	1.0 ± 0.2
11-Apr-89	**15**	11 ± 3	10.3 ± 0.5	15 ± 0.3	17.2 ± 0.8	16.9 ± 0.6	16.2 ± 0.4	665 ± 16	0.5 ± 0.2
13-Feb-90	**15**	9 ± 3		14.59 ± 0.34		15.7 ± 0.7	16.4 ± 0.4	563 ± 14	0.3 ± 0.2
				Sediment Grab Samples					
	SS1		13.0 ± 0.7	19.1 ± 0.4	24.0 ± 1.0	25.8 ± 0.9	23.7 ± 0.6	797 ± 11	0.1 ± 0.2
	SS2		12.5 ± 0.7	13.7 ± 0.4	21.6 ± 1.0	21.9 ± 0.9	20.4 ± 0.5	620 ± 11	0.2 ± 0.2
	SS3		13.8 ± 0.7	17.3 ± 0.3	25.0 ± 1.1	26.3 ± 0.8	24.7 ± 0.4	763 ± 11	0.3 ± 0.2
	SS4		10.6 ± 0.6	15.3 ± 0.5	16.6 ± 0.8	16.8 ± 1.4	15.5 ± 0.6	671 ± 12	-0.2 ± 0.4
	SS5		19.4 ± 1.1	32.5 ± 0.5	33.5 ± 1.4	34.5 ± 0.9	35.7 ± 0.5	807 ± 12	1.6 ± 0.2
	SS6		14.8 ± 0.7	16.4 ± 0.2	24.0 ± 0.9	25.2 ± 0.5	25.0 ± 0.3	623 ± 8	0.4 ± 0.1
	SS7		13.6 ± 0.4	14.3 ± 0.3	21.1 ± 0.4	22.2 ± 0.7	20.8 ± 0.4	702 ± 11	0.3 ± 0.2

Appendix G (cont.)

Sediment Particle Size Fractions

Fraction	U-238	Th-230	Ra-226	Th-232	Ra-228	Th-228	K-40	Cs-137
				SS2				
<63um			156 ± 12		268 ± 25	259 ± 12.0	679 ± 110	17.0 ± 8.0
250-500um			13.9 ± 1.6		24 ± 4	19.4 ± 1.5	788 ± 28	-1.0 ± 1.1
500-1.4mm			10.3 ± 0.3		19 ± 0.7	18.2 ± 0.4	534 ± 9	0.0 ± 0.2
1.4-2mm			12.1 ± 0.2		18.8 ± 0.5	18.5 ± 0.3	523 ± 7	0.3 ± 0.1
>2mm			15.3 ± 0.3		23 ± 0.7	22.5 ± 0.4	645 ± 10	0.2 ± 0.2
				SS3				
<63um			153 ± 7		248 ± 15	247 ± 7.0	665 ± 68	10.0 ± 5.0
63-125um			77 ± 5		124 ± 11	115 ± 5.0	1008 ± 62	3.0 ± 4.0
125-250um			25.8 ± 1.6		43.4 ± 3.7	38.5 ± 1.6	1026 ± 29	1.3 ± 1.1
250-500um			13.3 ± 1		21 ± 2	20.2 ± 1.0	837 ± 22	0.7 ± 0.7
500-1.4mm			10.3 ± 0.5		17.5 ± 1.3	18.4 ± 0.7	576 ± 11	0.2 ± 0.4
1.4-2mm			11.8 ± 0.4		19.3 ± 0.8	18.5 ± 0.4	555 ± 10	0.1 ± 0.2
>2mm			15.3 ± 0.3		23 ± 0.6	22.4 ± 0.4	750 ± 10	0.1 ± 0.2
				SS5				
<63um			180 ± 4		212 ± 7	232 ± 4.0	832 ± 37	1.8 ± 0.2
125-250um			30.8 ± 1.6		43 ± 4	40.1 ± 1.6	1036 ± 29	1.3 ± 1.1
250-500um			16.5 ± 0.7		23.4 ± 1.8	21.2 ± 0.7	8 ± 2	0.6 ± 0.6
500-1.4mm			14.3 ± 0.4		21.5 ± 0.8	19.3 ± 0.4	779 ± 12	0.4 ± 0.2
1.4-2mm			18.9 ± 0.6		19.9 ± 1.2	20.8 ± 0.6	685 ± 13	0.2 ± 0.3
>2mm			39.4 ± 0.5		32.2 ± 1	32.7 ± 0.5	735 ± 12	0.6 ± 0.2
				SS7				
<63um		152 ± 6	185 ± 5	223 ± 8	221 ± 10	242 ± 5.0	864 ± 48	4.0 ± 3.0
63-125um		60 ± 3	81 ± 2	105 ± 4	104 ± 5	111 ± 3.0	1040 ± 35	6.6 ± 1.6
125-250um		24 ± 2	29 ± 1.4	42 ± 3	42 ± 3	41.4 ± 1.5	1004 ± 27	1.0 ± 1.0
250-500um		12 ± 1.8	13.8 ± 0.7	21 ± 0.2	21.7 ± 1.6	21.8 ± 0.8	812 ± 17	0.0 ± 0.3
500-1.4mm		9 ± 1	11.4 ± 0.2	15 ± 1.8	18.9 ± 0.5	17.3 ± 0.3	680 ± 9	0.2 ± 0.1
1.4-2mm			14.2 ± 0.3		20.5 ± 0.7	18.9 ± 0.4	706 ± 7	0.5 ± 0.2
>2mm			16.6 ± 0.3		22 ± 0.7	21.9 ± 0.4	759 ± 11	0.3 ± 0.2

Appendix H

Jenolan Caves Radionuclide Data. All data reported as Bq/kg.

Uncertainties are equilivalent to one standard error on the mean.

Sources	Th-230	Ra-226	Th-232	Ra-228	Th-228
		Western Ridge			
	23.7 ± 1.2	26.2 ±0.4	21.6 ±1.1	21.6 ±0.6	21.8 ±0.5
	26.5 ± 1.0	26.9 ±0.5	22.6 ±0.9	22.3 ±0.9	22.5 ±0.6
	25.6 ± 1.4	25.1 ±0.5	20.5 ±1.3	21.5 ±0.9	21.1 ±0.6
	59.2 ± 3.4	73.2 ±1.1	44.6 ±2.7	48.2 ±1.1	47.2 ±1.0
	55.0 ± 3.0	71.6 ±2.9	42.8 ±2.5	58.9 ±5.5	46.8 ±3.4
	50.6 ± 2.0	63.2 ±2.8	38.9 ±1.7	44.8 ±5.4	42.3 ±3.4
	53.2 ± 2.3	78.3 ±3.0	41.0 ±1.9	56.9 ±5.7	48.0 ±3.4
		Terrace Creek			
	27.7 ± 1.1	31.2 ±1.0	35.8 ±1.3	39.3 ±1.8	39.3 ±1.1
	30.0 ± 1.5	36.4 ±0.8	35.5 ±1.7	42.6 ±1.4	42.1 ±1.0
	13.0 ± 0.6	15.6 ±0.3	13.6 ±0.6	16.4 ±0.5	16.1 ±0.4
	13.5 ± 0.4	19.6 ±0.4	17.2 ±0.5	23.1 ±0.6	21.6 ±0.5
		Jenolan/Bindo Divide			
	20.2 ± 0.8	25.7 ±0.6	29.9 ±1.1	35.9 ±1.1	35.1 ±0.8
	28.2 ± 1.3	31.9 ±1.0	41.7 ±1.7	40.7 ±1.9	41.1 ±1.2
	25.4 ± 1.1	23.8 ±1.0	27.8 ±1.2	33.2 ±2.0	32.4 ±1.3
	26.1 ± 1.1	34.3 ±0.8	39.2 ±1.5	45.9 ±1.4	44.9 ±1.0
Sinks: Depth		**Sand Passage**			
1	31.9 ± 1.3	37.0 ±0.5	39.3 ±1.5	39.5 ±0.9	38.0 ±0.6
3.75	33.6 ± 1.4	40.1 ±0.6	35.9 ±1.5	37.8 ±0.9	39.1 ±0.8
6.5	36.8 ± 1.8	42.9 ±0.7	40.0 ±2.0	39.9 ±1.1	40.1 ±0.9
9.25	32.3 ± 1.1	41.3 ±0.5	37.2 ±1.2	38.2 ±0.9	39.1 ±0.6
26	42.5 ± 2.7	50.4 ±1.0	48.0 ±3.0	45.7 ±1.6	46.8 ±1.2
28.5	35.8 ± 1.2	42.7 ±0.6	42.2 ±1.4	41.7 ±1.1	41.8 ±0.7
31.25	34.7 ± 1.3	46.5 ±0.8	41.8 ±1.5	43.4 ±0.9	43.5 ±0.9
33.5	48.8 ± 1.4	56.5 ±0.9	52.8 ±1.5	49.9 ±1.3	51.2 ±1.1
35.25	38.6 ± 1.6	43.5 ±0.7	42.5 ±1.7	39.5 ±1.1	42.1 ±0.9
38.5	36.9 ± 1.7	46.5 ±0.8	34.3 ±1.6	36.8 ±1.2	36.0 ±0.8
42.25	42.4 ± 1.7	51.1 ±0.8	42.7 ±1.8	40.0 ±1.1	39.5 ±0.9
		Lower Creek			
0	39.5 ± 2.8	51.9 ±0.9	43.8 ±3.0	50.1 ±1.3	50.8 ±1.0
1	45.7 ± 1.5	52.9 ±0.9	46.0 ±1.5	48.4 ±1.3	48.8 ±1.0
1.75	38.0 ± 1.8	51.6 ±0.7	41.0 ±1.8	42.2 ±0.8	42.5 ±0.8
5	39.3 ± 1.9	49.1 ±0.8	40.2 ±1.9	37.7 ±1.1	39.6 ±0.8
12.75	40.1 ± 2.7	54.9 ±0.9	42.0 ±2.8	40.5 ±1.2	41.5 ±0.9
22	41.0 ± 2.0	57.1 ±0.9	45.0 ±2.0	42.3 ±1.1	42.6 ±0.9
28.5	41.2 ± 1.9	45.3 ±0.8	45.0 ±2.0	42.1 ±1.2	43.7 ±0.9
40	37.1 ± 2.3	34.6 ±0.6	44.5 ±2.6	43.9 ±1.1	45.2 ±1.0

Appendix I

Burrinjuck Dam Radionuclide Data. All data reported as Bq/kg. Uncertainies are equilvalent. to one standard error on the mean.

Murrumbidgee Sediment Core

DEPTH (cm)	U-238	Th-230	Ra-226	Pb-210	Th-232	Ra-228	Th-228	K-40	Cs-137
5.0	71.4 ±4.4	51.2 ±2.1	56.0 ± 0.7	61.6 ± 5.2	82.0 ± 3.0	82.3 ± 1.4	84.7 ± 1.0	713 ±12	4.6 ± 0.4
10.0	59.7 ±4.1	48.4 ±2.1	51.1 ± 0.6	55.8 ± 4.8	73.0 ± 3.0	73.6 ± 1.3	73.1 ± 0.9	645 ±11	4.8 ± 0.3
15.0	65.3 ±4.1	48.5 ±1.4	57.6 ± 0.6	62.9 ± 4.8	78.6 ± 1.7	80.9 ± 1.3	82.3 ± 0.9	712 ±11	6.3 ± 0.4
19.0	68.5 ±2.5	56.5 ±2.4	58.8 ± 0.5	59.4 ± 3.0	80.0 ± 2.0	81.3 ± 0.9	81.9 ± 0.8	763 ± 9	5.1 ± 0.2
25.0	64.1 ±4.3	51.9 ±2.0	55.5 ± 0.7	56.1 ± 5.0	75.0 ± 3.0	76.2 ± 1.4	79.2 ± 0.9	729 ±12	2.5 ± 0.3
30.0	60.5 ±4.5		58.3 ± 0.7	53.4 ± 5.1		80.3 ± 1.4	80.5 ± 1.0	763 ±12	2.8 ± 0.3
35.0	62.9 ±3.9	45.7 ±3.1	55.1 ± 0.6	53.4 ± 4.4	72.0 ± 4.0	77.2 ± 1.2	79.4 ± 0.9	716 ±11	1.4 ± 0.3
40.0	66.6 ±5.2	55.8 ±1.7	59.0 ± 0.8	53.5 ± 6.1	87.0 ± 3.0	81.8 ± 1.6	82.6 ± 1.1	834 ±14	0.4 ± 0.4
41.0	67.5 ±4.4		59.4 ± 0.7	47.5 ± 5.2		77.7 ± 1.4	79.6 ± 1.0	784 ±13	0.2 ± 0.3
45.0	58.2 ±4.0		52.7 ± 0.6	44.2 ± 4.7		73.8 ± 1.3	73.5 ± 0.9	690 ±11	0.3 ± 0.3
50.0	60.6 ±4.2	49.2 ±2.1	52.2 ± 0.6	48.4 ± 4.9	73.0 ± 3.0	75.4 ± 1.3	77.0 ± 0.9	688 ±11	0.3 ± 0.3
55.0	58.0 ±5.0	57.1 ±2.0	56.4 ± 0.7	51.3 ± 5.6	79.3 ± 1.9	80.0 ± 1.5	82.6 ± 1.0	781 ±13	0.3 ± 0.4
60.0	61.8 ±4.5		53.5 ± 0.7	48.6 ± 5.5		78.4 ± 1.4	79.6 ± 1.0	753 ±13	0.3 ± 0.4
65.0	50.8 ±6.3		47.2 ± 0.8	48.9 ±		71.7 ± 1.6	71.6 ± 1.4	669 ±18	0.2 ± 0.3
70.0	66.6 ±4.2		52.4 ± 0.6	47.0 ± 4.9		68.9 ± 1.3	74.7 ± 0.9	638 ±11	0.5 ± 0.5
75.0	51.8 ±3.8	40.2 ±1.5	48.4 ± 0.6	42.1 ± 4.4	66.0 ± 2.0	69.9 ± 1.2	69.0 ± 0.9	593 ±10	0.3 ± 0.3
80.0	46.4 ±3.5	44.6 ±1.8	43.5 ± 0.5	41.0 ± 4.1	68.0 ± 3.0	64.5 ± 1.1	64.6 ± 0.8	520 ± 9	0.6 ± 0.3
84.5	62.4 ±4.0	39.2 ±1.6	48.7 ± 0.6	47.4 ± 4.6	68.0 ± 2.0	71.9 ± 1.3	72.5 ± 0.9	663 ±11	0.2 ± 0.3
89.5	69.0 ±5.0	35.7 ±1.6	46.4 ± 0.7	47.3 ± 6.1	65.0 ± 3.0	65.9 ± 1.6	69.2 ± 1.0	566 ±12	0.2 ± 0.4
100.0	53.0 ±6.0	46.6 ±2.2	50.0 ± 0.9	41.9 ± 7.5	73.0 ± 3.0	72.9 ± 1.9	73.1 ± 1.2	605 ±13	0.3 ± 0.5

Murrumbidgee Distance Samples

Distanc (km)	U-238	Th-230	Ra-226	Pb-210	Th-232	Ra-228	Th-228	K-40	Cs-137
0.0	64 ± 4	48.6 ±2.9	53.1 ± 0.7	72 ± 4	75.5 ± 3.9	85.9 ± 1.9	86 ± 1.4	692 ±14	2.8 ± 0.5
2.0	65 ± 5	56.2 ±2.6	56.4 ± 0.6	83 ± 4	78.4 ± 3.4	86.1 ± 1.7	86.5 ± 1.5	672 ±11	2.8 ± 0.4
4.5	60 ± 2	45.7 ±1.9	53.1 ± 0.6	67 ± 3	69.9 ± 2.6	82.3 ± 1.5	82.2 ± 1.2	644 ±11	3.7 ± 0.3
7.0	62 ±11	45.8 ± 2	49.5 ± 0.8		70.3 ± 3	78.5 ± 1.8	81.7 ± 1.7	671 ±11	2.6 ± 0.4
9.0	74 ± 7	58.1 ± 2	61.3 ± 0.9		86.9 ± 3.3	104 ± 1.9	102 ± 1.3	648 ±12	2.5 ± 0.5
13.0	70 ± 5	47.5 ± 3	59.1 ± 0.9	83 ± 7	68.2 ± 4	92.3 ± 2.3	91.4 ± 1.7	612 ±15	2.4 ± 0.6